The Design, Synthesis and Study of Mixed-Metal Ru,Rh and Os,Rh Complexes with Biologically Relevant Reactivity

Jing Wang

Dissertation submitted to the faculty of the Virginia Polytechnic Institute and State University in partial fulfillment of the requirements for the degree of

Doctor of Philosophy

In

Chemistry

Karen J. Brewer, Chair

Brenda S. J. Winkel

Brian M. Tissue

Louis A. Madsen

November 30, 2012

Blacksburg, VA

Keywords: photodynamic therapy, mixed-metal, polyazine, DNA photocleavage, DNA photobinding, rhodium

The Design, Synthesis and Study of Mixed-Metal Ru,Rh and Os,Rh Complexes with Biologically Relevant Reactivity

Jing Wang

ABSTRACT

A series of mixed-metal bimetallic complexes $[(TL)_2M(dpp)RhCl_2(TL')]^{3+}$ (M = Ru and Os, terminal ligands (TL) = phen, Ph_2phen, Me_2phen and bpy, terminal ligands (TL′) = phen, bpy and Me_2bpy), which couple one Ru or Os polyazine light absorber (LA) to a *cis*-$Rh^{III}Cl_2$ center through a dpp bridging ligand (BL), were synthesized using a building block method. These are related to previously studied trimetallic systems $[\{(TL)_2M(dpp)_2RhCl_2]^{5+}$, but the bimetallics are synthetically more complex to prepare due to the tendency of Rh^{III} halide starting materials to react with diimine ligands to form *cis*-$[Rh(NN)_2Cl_2]^+$ motifs. The bimetallic complexes, $[(phen)_2Ru(dpp)RhCl_2(bpy)]^{3+}$, $[(phen)_2Ru(dpp)RhCl_2(phen)]^{3+}$, $[(Ph_2phen)_2Ru(dpp)RhCl_2(phen)]^{3+}$, $[(Me_2phen)_2Ru(dpp)RhCl_2(phen)]^{3+}$, $[(bpy)_2Ru(dpp)RhCl_2(bpy)]^{3+}$, $[(bpy)_2Ru(dpp)RhCl_2(Me_2bpy)]^{3+}$ and $[(bpy)_2Os(dpp)RhCl_2(phen)]^{3+}$, were characterized and studied by electrochemistry, electronic absorption spectroscopy, ESI-mass spectrometry, steady-state and time-resolved emission spectroscopy.

The electrochemical properties of bimetallic complexes with polyazine ligands exhibit a reversible one-electron metal-based oxidation, a quasi-reversible $Rh^{III/II}Cl_2$ overlapped with a small amount of $Rh^{II/I}Cl$ and an irreversible $Rh^{II/I}Cl_2$ reductions prior to the reversible bridging ligand $dpp^{0/-}$ reduction. The energetically close Rh ($d\sigma^*$) orbital and the bridging ligand dpp (π^*) orbitals in this motif complicate analysis.

The title bimetallic complexes are efficient light absorbers due to the $[(TL)_2M^{II}(dpp)]$ light absorber subunit. The bimetallics display ligand-based $\pi\rightarrow\pi^*$ transitions in the UV region and metal-to-ligand charge transfer (MLCT) transitions in the visible region of the spectrum with approximately half the absorption extinction coefficient values relative to the trimetallics in the spectrum. The Os,Rh bimetallic complex, $[(bpy)_2Os(dpp)RhCl_2(phen)]^{3+}$, displays $Os(d\pi)\rightarrow dpp(\pi^*)$ CT transition at 521 nm ($\varepsilon = 1.8 \times 10^4\ M^{-1}cm^{-1}$) and a low energy absorption band at 750 nm ($\varepsilon = 2.9 \times 10^3\ M^{-1}cm^{-1}$) in the near-infrared region representing direct $^1GS\rightarrow{}^3MLCT$ excitation due to the high degree of spin orbital coupling in Os complexes. The bimetallic complexes $[(phen)_2Ru(dpp)RhCl_2(bpy)]^{3+}$, $[(phen)_2Ru(dpp)RhCl_2(phen)]^{3+}$, $[(Ph_2phen)_2Ru(dpp)RhCl_2(phen)]^{3+}$, $[(Me_2phen)_2Ru(dpp)RhCl_2(phen)]^{3+}$, $[(bpy)_2Ru(dpp)RhCl_2(bpy)]^{3+}$ and $[(bpy)_2Ru(dpp)RhCl_2(Me_2bpy)]^{3+}$ display $Ru(d\pi)\rightarrow dpp(\pi^*)$ MLCT transitions centered at 505, 508, 515, 516, 510 and 506 nm, respectively. The bimetallic complex $[(Ph_2phen)_2Ru(dpp)RhCl_2(phen)]^{3+}$ displays enhanced absorption ($\varepsilon = 1.8 \times 10^4\ M^{-1}cm^{-1}$ at 426 nm) compared to the absorption of $[(phen)_2Ru(dpp)RhCl_2(phen)]^{3+}$ ($\varepsilon = 1.0 \times 10^4\ M^{-1}cm^{-1}$ at 426 nm).

The photophysical properties of Ru,Rh bimetallic complexes are close to those of trimetallic analogues. In room temperature acetonitrile, both bimetallic and trimetallic complexes display a weak and short-lived emission from the $Ru(d\pi)\rightarrow dpp(\pi^*)$ ^{3}MLCT excited state. For example, the bimetallic complex $[(phen)_2Ru(dpp)RhCl_2(bpy)]^{3+}$ emits at 766 nm with $\Phi^{em} = 1.5 \times 10^{-4}$ (τ = 42 ns) and the trimetallic complex $[\{(phen)_2Ru(dpp)\}_2RhCl_2]^{5+}$ emits at 760 nm ($\Phi^{em} = 2.2 \times 10^{-4}$, τ = 35 ns). At 77 K in 4:1 ethanol/methanol glass, the bimetallics, as well as trimetallics, exhibit a more intense blue-shifted emission with a longer lifetime, which is from the same ^{3}MLCT excited state. At 77 K, the low temperature emission from the same ^{3}MLCT state of

$[\{(phen)_2Ru(dpp)\}_2RhCl_2]^{5+}$ blue-shifts to 706 nm with the emission lifetime of 1.8 μs and the bimetallic $[(phen)_2Ru(dpp)RhCl_2(bpy)]^{3+}$ emits at 706 nm (τ = 1.8 μs). The Ru,Rh complexes ^{3}MLCT excited states can populate Ru(dπ)→Rh(dσ*) triplet metal-to-metal charge transfer (^{3}MMCT) excited states through intramolecular electron transfer at room temperature, which is impeded in the rigid matrice at 77 K due to the large reorganizational energy and restricted molecular motion. The emission of Os,Rh bimetallic complex $[(bpy)_2Os(dpp)RhCl_2(phen)]^{3+}$ could not be detected by our instruments likely due to its expected red-shifted emission which lies outside our detector window.

The Ru,Rh bimetallics display interesting and efficient photo-reactivity with DNA activated by visible light. The DNA gel shift assay, selective precipitation, ESI-mass spectrometry and polymerase chain reaction (PCR) studies suggest that Ru,Rh bimetallic complexes photobind to DNA following visible light excitation. This reactivity is not observed for analogous Ru,Rh,Ru trimetallics due to the steric protection of the Rh site in that motif. The bimetallic $[(TL)_2Ru(dpp)RhCl_2(TL')]^{3+}$ systems have Ru (dπ) based the highest occupied molecular orbitals (HOMOs) and Rh (dσ*) based the lowest unoccupied molecular orbitals (LUMOs), and can photobind and photocleave DNA through low-lying ^{3}MMCT excited states when excited by the low energy visible light, with or without molecular oxygen. This is unusual but desirable reactivity for photodynamic therapy (PDT) drug development. The Os,Rh bimetallic complex $[(bpy)_2Os(dpp)RhCl_2(phen)]^{3+}$ photobinds and photocleaves DNA under red therapeutic light excitation without molecular oxygen, an unprecedented result. Polymerase chain reaction experiments were used to evaluate the impact on DNA amplification of the DNA photo-modification and photo-damage induced by $[(bpy)_2Os(dpp)RhCl_2(phen)]^{3+}$ under red light irradiation. Either photobinding or photocleavage induced by red light excitation of

$[(bpy)_2Os(dpp)RhCl_2(phen)]^{3+}$ on DNA inhibits amplification via PCR methods, a model for *in vivo* replication. Moreover, significant thermal stability of DNA photo-modification over 90 °C is required for PCR. A red light-activated drug that acts in an oxygen-independent mechanism to impede DNA amplification is unique in this field and desirable for study as a new class of PDT drugs.

Thesis Statement

The goal of this research is to design, synthesize and characterize Ru,Rh and Os,Rh bimetallic complexes and understand the effect of component modification on the electrochemical, spectroscopic, photophysical properties and DNA interactions of the bimetallic complexes with comparison to known trimetallic Ru,Rh,Ru and Os,Rh,Os systems.

Acknowledgements

I wish to give special thanks to Profs. Brenda S. J. Winkel, Brian M. Tissue, Robert B. Moore, and Louis A. Madsen for taking time to serve in my committee and review my work with their helpful discussions and comments. I would like to express my sincerest appreciation to my advisor, Prof. Karen J. Brewer, for her guidance, support, and encouragement throughout my PhD research.

I also thank the Brewer group, especially Dr. Samatha Lake Hopkins Higgins, Jessica D. Knoll, Dr. Travis A. White, Rongwei Zhou, Dr. David F. Zigler, Dr. Avijita Jain, Dr. Shamindri M. Arachchige and Dr. Jerry Manbeck for the good suggestions and helpful discussions.

I especially thank the undergraduates I worked with, including Norm Hurst, Harjot Othee, Kyle Mullins, Giovanni Schiano-Moriello, Jerelle Downing, Vien Truong, Reece Prussin, Shashwat Sinha, Kaitlyn M. Brewer and a high school student, Jerry Newman, Jr.

I want to give my special thanks to Prof. Y. A. Liu and his wife for their encouragement and support through my study at Virginia Tech, and to the Chinese Bible Study brothers and sisters for their comfort and support.

Finally, I would like to express my gratitude to all my family members, especially my parents who always encourage me to learn new things and my husband, Xiang, who always encourages and supports me to pursue my dreams.

Table of Contents

List of Figures

List of Tables

List of Abbreviations

BAS= bioactive sites
BL = bridging ligand
bpy = 2,2'-bipyridine
CV = cyclic voltammetry
CT-DNA = Calf thymus DNA
DNA= deoxyribonucleic acid
DMF = dimethylformamide
dpp = 2,3-bis(2-pyridyl)pyrazine
dppz = dipyrido[3,2-a;2′,3′-c]phenazine
dppn = benzo[i]dipyrido[3,2-a:2′, 3′-h]quinoxaline
dpq = 2,3-bis(2-pyridyl)quinoxaline
et = excited state energy transfer
et = excited state electron transfer
$E_{1/2}$ = half-wave potential in voltammetry
E_p^a = anodic peak potential
E_p^c = cathodic peak potential
ES = excited state
ESI-ms = electrospray ionization-mass spectrometry
F = Faraday constant
GS = ground state
h = hours
HOMO = highest occupied molecular orbital
HpD = hematoporphyrin
ic = internal conversion
IL = internal ligand
i_p^a = anodic peak current
i_p^c = cathodic peak current
ivr = intramolecular vibrational relaxation
isc = intersystem crossing
k_x = rate constant of process "x"
LA = ground state light absorber
*LA = excited state light absorber
LED = light emitting diode
LF = ligand field
LMCT = ligand-to-metal charge transfer
LUMO = lowest unoccupied molecular orbital
MC:BP = metal complex to base pairs ratio
Me_2phen = 4,7-dimethyl-1,10-phenanthroline
Me_2bpy = 4,4′-dimethyl-2,2'-bipyridine
min = minutes
MLCT = metal-to-ligand charge transfer
MMCT = metal-to-metal charge transfer
m/z = mass to charge
NHE = normal hydrogen electrode

nr = non-radiative decay
$^1O_2$ = singlet oxygen
$^3O_2$ = molecular oxygen
PDT= photodynamic therapy
phen = 1,10-phenanthroline
Ph_2phen = 4,7-diphenyl-1,10-phenanthroline
PPh_3 = triphenylphosphine
py = pyridine
Q = quencher
rxn = photochemical reaction
ROS = reactive oxygen species
RT = room temperature
SCE = saturated calomel electrode
TB = tris base
TBAH = tetrabutylammonium hexafluorophosphate
$^tBu_2$bpy = 4,4'-di-tert-butyl-2,2'-bipyridine
TL, TL′ = terminal ligand
tppz = 2, 3, 5, 6-tetrakis(2-pyridyl)pyrazine
tpy = 2, 2′:6′, 2″-terpyridine
UV = ultraviolet
τ = electronic excited state lifetime
Φ = quantum yield
λ_{max}^{abs} = absorption maximum
λ_{max}^{em} = emission maximum

Preface

During my graduate study at Virginia Tech, I have also been involved with several projects, resulting in other publications, which are beyond the scope of this dissertation. Following is the list of publications to date from my graduate work at Virginia Tech.

1. Wang, J.; Newman, J; Higgins, S. L. H.; Brewer, K. M.; Winkel, B. S. J.; Brewer, K. J. "Therapeutic Window Red Light Induced Inhibition of DNA Replication and Amplification in PCR Using a Os,Rh Supramolecule" *Angew. Chem. Int. Ed. Engl.* **2012,** in press.

2. Wang, J.; Zigler, D. F.; Hurst, N.; Othee, H.; Winkel, B. S. J.; Brewer, K. J. "A new, bioactive structural motif: Visible light induced DNA photobinding and oxygen independent photocleavage by Ru^{II},Rh^{III} bimetallics" *J. Inorg. Biochem*. **2012**, *116*, 135-139.

3. Wang, J.; Higgins, S. L. H.; Winkel, B. S. J.; Brewer, K. J. "A new Os,Rh bimetallic with O_2 Independent DNA cleavage and DNA photobinding with red therapeutic light excitation." *Chem. Comm.* **2011**, *47*, 9786-9788.

4. Wang, J.; White, T. A.; Arachchige, S. M.; Brewer, K. J. "A new structural motif for photoinitiated electron collection: Ru,Rh bimetallics providing insight into H_2 production via photocatalysis of water reduction by Ru,Rh,Ru supramolecules." *Chem. Comm.* **2011,** *47*, 4451-4453.

5. Wang, J.; Arachchige, S. M.; Brewer, K. J. "Supramolecular complex design and function for photodynamic therapy and solar energy conversion via hydrogen production: common requirements for molecular architectures for varied light activated processes." *Applications of supramolecular chemistry Taylor& Francis* **2012**, 255-300. *(Invited Book chapter)*

6. Jain, A; Wang, J.; Mashack, E.; Winkel, B. J; Brewer, K. J. "Multifunctional DNA interactions of Ru-Pt mixed metal supramolecular complexes with substituted terpyridine ligands." *Inorg. Chem.* **2009**, *48*, 9077-9084.

7. Zigler, D. F.; Wang, J.; Brewer, K. J. "Ruthenium(II)-polyazine light absorbers bridged to reactive *cis*-dichlororhodium(III) centers in bimetallic molecular architecture." *Inorg. Chem.* **2008**, *47*, 11342-11350.

Chapter 1. Introduction

1.1. Cancer

Cancer, a large group of diseases, is caused by a group of cells that grow uncontrollably invading surrounding healthy tissues.[1,2] Accounting for 571,950 deaths in the United States in 2011 based on the report of the American Cancer Society, it was the second killer for Americans under 85.[3] Cancer diseases have common traits which Hanahan and Weinberg summarized as six hallmarks including self-sufficient growth signals, evading apoptosis, evasion of growth inhibitory signals, unlimited replicative potential, angiogenesis and invasion.[4]

The development of cancer is a multi-step process.[5,6] The first step is initiation which involves DNA mutation[7-9] caused by genotoxic radiation, viruses, or carcinogenic chemicals.[10,11] The second step is promotion, at which the initiated cells with DNA mutation evolve to origin cells such as nodules, papillomas and polyps. These cells have the potential to become malignant cells or to exist as benignant cells. The third step is progression, whereby some origin cells become cancer cells. In the further steps, cancer cells can also break away from the original tumor and spread through the blood and lymph in the body, then colonize distant organs including liver, bone, lung and brain, and form new tumors.[12,13] This process is called metastasis.[14] Metastasis causes 90% of deaths among patients who have solid tumors.[14] Cancer can be treated by surgery, chemotherapy, radiation therapy, or other methods.[1]

1.2. Chemotherapy

Chemotherapy treats cancer with drugs that can limit cell growth by blocking DNA synthesis, eventually leading to cell death.[15] Cancer chemotherapy was started by Goodman and Gilman to treat a patient with lymphoma in 1946.[16] In the trials of chemotherapy in acute childhood

leukemia, researchers first found that a combination of different drugs is more effective than a single-agent treatment.[17] Then they learned that this combination chemotherapy could be applied to other cancers. In the efforts of developing more chemotherapeutic drugs, seven drugs (i.e., cyclophosphamide, methotrexate, vincristine, 5-fluorouacil, adriamycin, cisplatin, tamoxifen) are most used.[18,19]

Chemotherapy has two common limitations in clinical practice.[17] First, antitumor drugs can produce significant toxicity in normal tissues. Patients will experience side effects such as intense nausea, ulcers and hair loss. The second problem is drug resistance. During clinical cancer chemotherapy, the sensitive tumor will often cease to respond to the treatment as effectively as the initial therapy.[20]

1.3. Photodynamic Therapy

Photodynamic therapy (PDT) is a promising cancer treatment that uses visible non-thermal light to excite a photosensitizer.[21,22] The photosensitizer subsequently generates cytotoxic species to kill tumor cells.[23] This approach allows the local delivery of active drug to reduce systemic toxicity and the use of highly active drugs. These unique properties of PDT lead to potential applications in the treatment of localized tumors and non-malignant lesions.[22]

Oscar Raab reported the first photodynamic action in 1900.[24] He observed that the lethal effects of an acridine orange solution on paramecia were influenced by light intensity. Schwartz and Lipson discovered that the acid product of hematoporphyrin named hematoporphyrin derivative (HpD) can be used to image tumors and has PDT functions.[25,26] Diamond and coworkers reported that 100% cell death of rat glioma cells was caused by the exposure to white light for 50 minutes after using hematoporphyrin (HpD).[21] Dougherty and coworkers first

successfully used HpD and red light to treat animal tumors.[27] The first human clinic trial of PDT was performed by Kelly and Snell in 1976 using HpD to treat five patients with bladder cancer.[28] Sibille and coworkers reported that 123 patients with esophageal cancer were treated by PDT from 1983 to 1991.[29] The tumors were irradiated with 630 nm laser irradiation 72 hours after injection of 2-3 mg/kg HpD. The 5-year disease-specific survival rate is 74% ± 5%. Now in the clinic, photosensitizers are administered by injection or on the skin surface, followed by a 5 minutes to 24 hours drug-light interval, then irradiated by the low energy visible light (600-900 nm).[22]

Since the 1990s, PDT has been successfully employed in treating a variety of cancers including oral, skin, breast, and bladder cancer. PDT has particular advantages in the treatment of cancer with few toxic effects such as nausea and ulcers over other common treatments involving traditional radiation and chemotherapies.[22,30,31] Currently, the mechanisms of PDT have also been investigated and three different types of mechanism, which are involved in the PDT process, have been proposed and shown in Figure 1.1.[32,33] When illuminated by low energy visible light (600-900 nm)[34], a photosensitizer (PS) in the singlet ground state (^{1}GS) is excited to its singlet excited state (^{1}ES). The photosensitizer in the ^{1}ES decays back to ^{1}GS by emitting fluorescence light, or by non-radiative processes. It also can undergo intersystem crossing to the triplet excited state (^{3}ES). The photosensitizer in the ^{3}ES can undergo non-radiative decay, radiative decay (emitting phosphorescence), or a reaction to the ground state (^{1}GS). The excited state of the photosensitizer can undergo reactions of three different types dictating the mechanism of PDT.[35] In type I reaction, the photosensitizer directly reacts with water molecule or oxygen and generates reactive oxygen species (ROS) including $HO^{\cdot}$ and $O_2^{-\cdot}$ radicals through electron transfer. The radicals cause biomolecules, such as protein and DNA, oxidative damage

by chain reactions leading to cell death. In the type II reaction, photosensitizer converts molecular oxygen, which has triplet ground state spin multiplicity, to singlet oxygen ($^1O_2$) excited through energy transfer quenching. The highly reactive $^1O_2$ can cause cell apoptosis or necrosis. The lifetime of $^1O_2$ in biological environment is short. It can only function locally, with a special diffusion radius of 20 nm.[33,36] In the type III reactions, the excited photosensitizer directly reacts with cellular targets, such as protein, RNA and DNA, without molecular oxygen and causes cell death.[32]

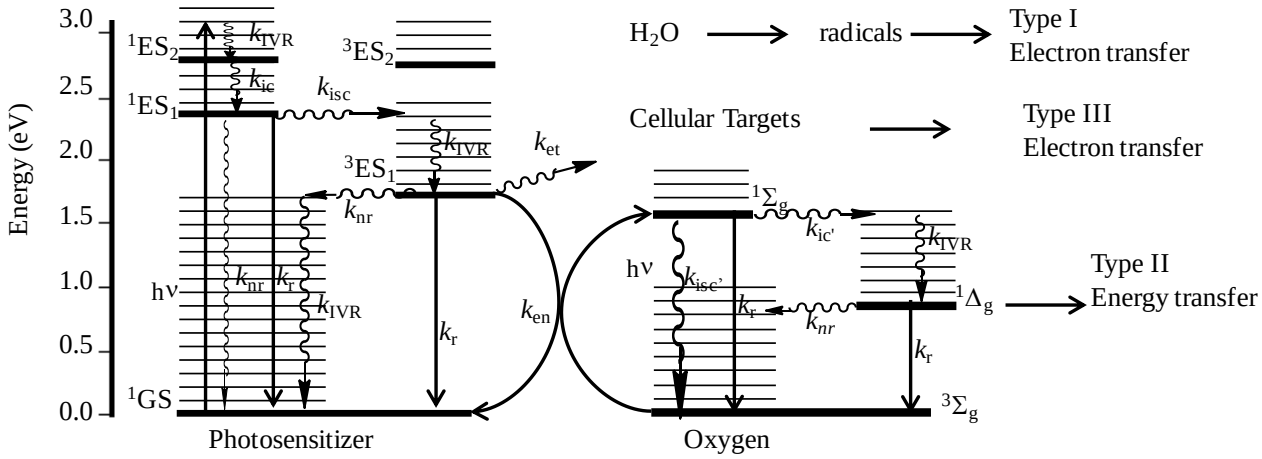

Figure 1.1. State diagram for a photosensitizer undergoing photochemical reactions in three types of photodynamic mechanism with different energy levels, ^{1}ES = singlet excited state, ^{3}ES = triplet excited state, ^{1}GS = singlet ground state, k_r = rate constant for radiative decay, k_{nr} = rate constant for non-radiative decay, k_{IVR} = intramolecular vibrational relaxation, k_{ic} = rate constant for internal conversion, k_{isc} = rate constant for intersystem crossing non-radiative decay, k_{en} = rate constant for energy transfer, and k_{et} = rate constant for electron transfer, and modified from Allison, R.; Moghissi, K.; Downie, G.; and Dixon, K. "Photodynamic therapy (PDT) for lung cancer" *Photodiagnosis and Photodynamic Therapy* **2011**, *8*, 231-239.[32]

1.3.1. DNA as a Target for PDT

Deoxyribonucleic acid (DNA) contains the inherited information of cells.[37] It is a polymeric chain of nucleotides, which consist of a nucleobase (guanine, cytosine, adenine and thymine), a sugar molecule (deoxyribose), and a phosphate group. DNA has a double helix structure composed of two polynucleotide strands with nucleobases at the core of the helix and sugar-phosphate chains outside as shown in Figure 1.2. Each base is hydrogen bonded to a complementary base on the opposite polynucleotide chain.[38] The double helix structure forms a major groove and a minor groove on the DNA surface. DNA plays a central role in the cellular life, controlling cell structure and functions, especially the replication and transcription process. Most carcinogen agents change the DNA sequence or induce DNA mutations in the cell. The mutations will not pass to the next generation of offspring, but are passed to the daughter cells through cell division.[39] In addition, DNA provides several target sites for PDT agents to function including electron-rich nucleotides, anionic phosphate backbone and sugars. DNA emerges as an ideal target in PDT.[40,41] DNA may be targeted in many ways. Cations bind ionically to the polyanionic DNA. Metal complexes with vacant or labile sites can form coordinate covalent bonds to the Lewis basic sites of DNA.[42,43] Molecules with appropriate shape and lipophilicity can groove bind to DNA.[44] Finally planar organic aromatics can insert between DNA bases, an interaction that is termed intercalation.[45]

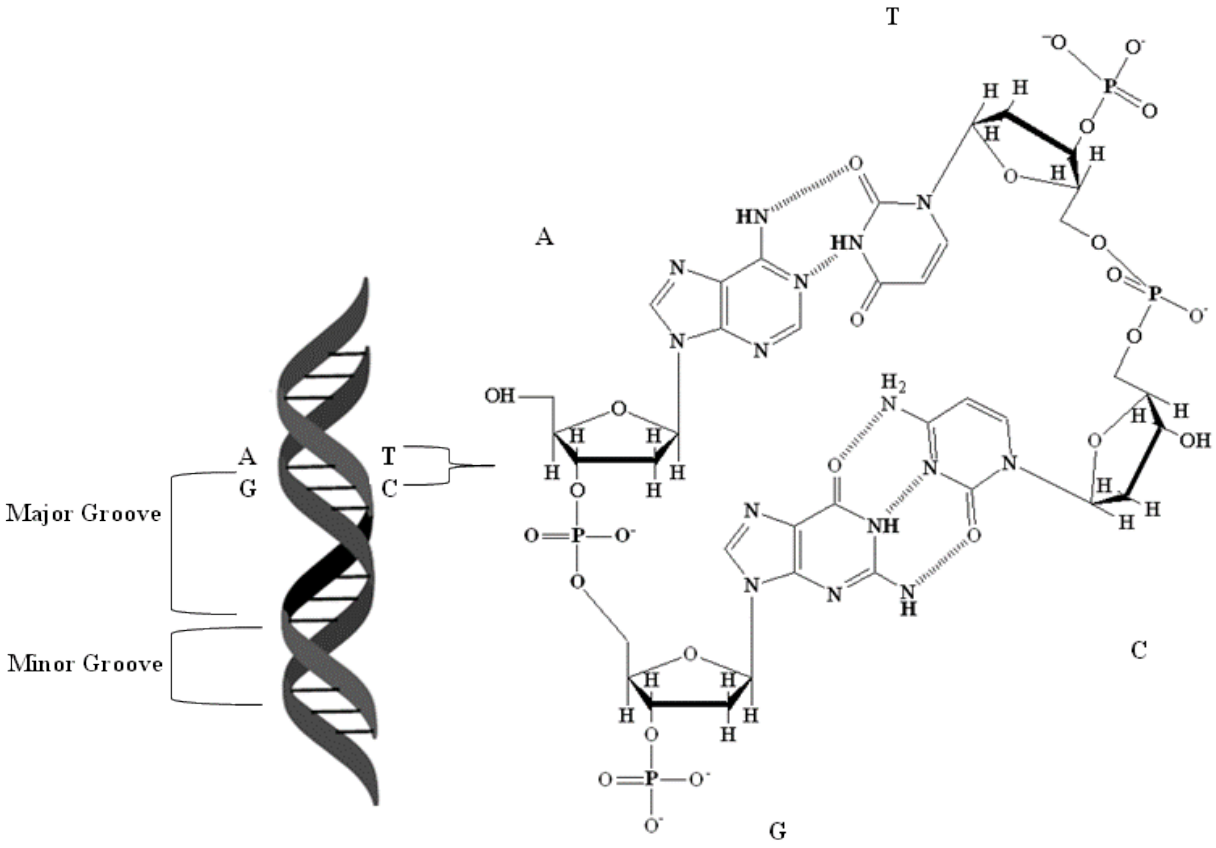

Figure 1.2. The structural picture of deoxyribonucleic acid (DNA).

1.3.2. The Development of Photodynamic Therapy Drugs

Requirements for drugs to be used in PDT applications include being non-toxic and stable in the dark, absorbing light within the "phototherapeutic window" (600-900 nm, where light can efficiently penetrate body tissues[34]) and generating reactive, toxic species following light excitation.[32,46]

Great effort has been devoted to developing PDT drugs that meet these requirements over the past 30 year. Some of the drugs are organic photosensitizers including porphyrins, chlorins and phthalocyanines. The first photosensitizer family discovered was the hematoporphyrin and its derivatives, HpD. Its commercial product, Photofrin® (Figure 1.3) is composed of different porphyrins including monomers, dimers and oligomers.[47] Photofrin® was approved for use in

PDT in 1995.[48] Tetraphenylchlorin (Foscan® as shown in Figure 1.3) belongs to the chlorin family, and can effectively control tumors.[49,50] Phthalocyanines and their derivatives including chloroaluminium and zinc complexes are also clinical photosensitizers.[51,52]

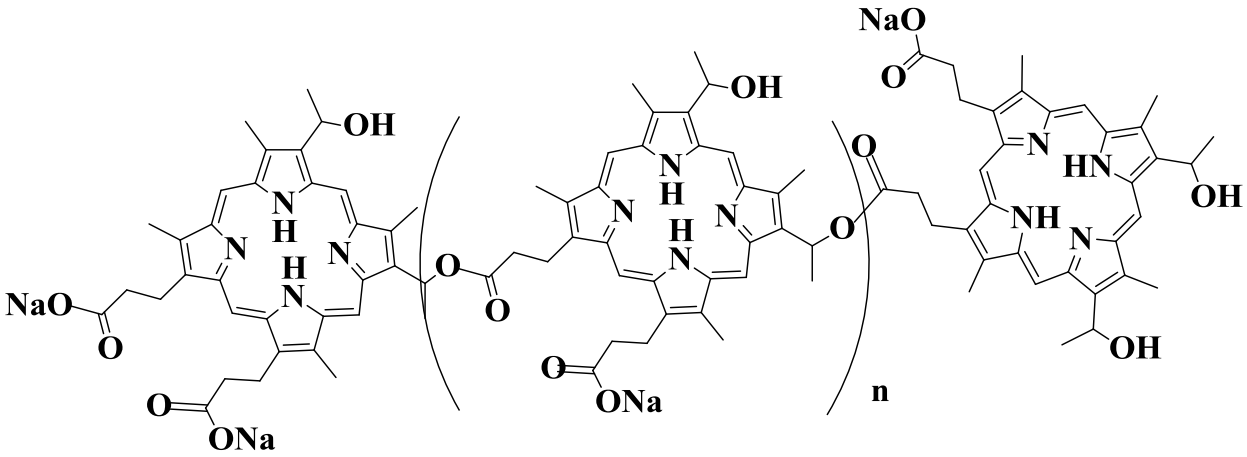

Photofrin

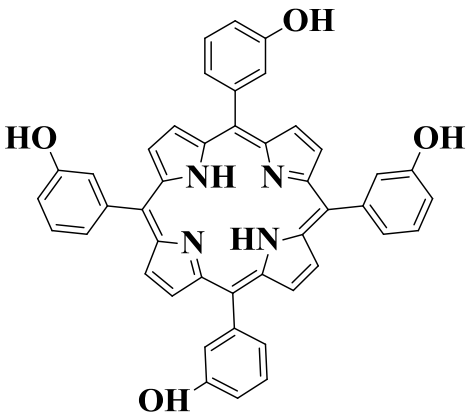

Foscan

Figure 1.3. The structure of Photofrin® and Foscan®.

Transition metal complexes with porphyrin,[53] phthalocyanine,[54] naphthalocyanine[55] or polypyridine ligands have interesting excited state light absorber properties, which may lead to a new generation of potential PDT drugs.[52,56,57]

1.3.3. Supramolecular Complexes Coupling Ru(II), Os(II) Polyazine Light Absorbers to Rh(III) Centers for PDT

Metal-based chromophores, such as the prototypical $[Ru(bpy)_3]^{2+}$ or $[Os(bpy)_3]^{2+}$ (bpy = 2,2′-bipyridine), are efficient light absorbers (LAs) with high extinction coefficients in the ultraviolet (UV) and visible spectral regions. They have an emissive MLCT excited state, allowing a probe into excited state reactivity and the generation of a charge separation with excited state. The chromophores are photo-stable and their redox and spectroscopic properties are tunable by using different ligands. The ruthenium polyazine complex, $[Ru(bpy)_3]^{2+}$, is well studied and shown to display interesting photophysical and photochemical properties which will be discussed thoroughly in this dissertation.[58-60]

A photodynamic reaction to produce ROS may happen with a photosensitizer, light energy and oxygen.[24] However, most aggressive cancer cells exist in low-oxygen environments.[61] Recent emphasis has therefore been placed on developing potential oxygen-independent PDT agents including metal complexes. Among these new complexes, rhodium complexes have demonstrated the ability to photocleave DNA which will be described in the later section.[62-65]

As defined by Balzani, the supramolecular complexes couple several molecular components that typically retain individual properties to provide one or more whole-system functions from the incorporated subunits.[66] The supramolecular complexes discussed herein are composed of sub-units connected via coordinate covalent bonds. The sub-units incorporated in our systems include light absorbers (LAs), bridging ligands (BLs), and bioactive metal centers (BAS). The light absorbers, which contain polyazine terminal ligands (TLs) and the metal center, are used to harness UV and visible light energy.[67] The bridging ligands form coordinate covalent bonds between the light absorbers and metal centers, and mediate intercomponent communications.

The coupling of Ru or Os metal-to-ligand charge transfer (MLCT) light absorbers to Rh centers provides trimetallic assemblies a function as photosensitizers for PDT. Supramolecular trimetallic complexes such as $[\{(bpy)_2Ru(dpp)\}_2RhCl_2]^{5+}$, $[\{(bpy)_2Os(dpp)\}_2RhCl_2]^{5+}$ and $[\{(tpy)RuCl(dpp)\}_2RhCl_2]^{3+}$ (dpp = 2,3-bis(2-pyridyl)pyrazine, tpy = 2, 2′:6′, 2″-terpyridine) consist of two Ru or Os polyazine light absorbers coupled to a *cis*-$Rh^{III}Cl_2$ reactive metal center through dpp bridging ligands.[15,68-73] These supramolecular complexes display O_2-independent reactivities, which include photocleaving DNA under visible light ($\lambda \geq 475$ nm) irradiation without molecular oxygen in contrast to Ru and Os polyazine monometalic light absorbers.[68,72] The trimetallic complexes, $[\{(bpy)_2Ru(dpp)\}_2RhCl_2]^{5+}$ and $[\{(bpy)_2Os(dpp)\}_2RhCl_2]^{5+}$, can also inhibit African green monkey kidney epithelial (Vero) cell growth *in vitro* after exposure to visible light ($\lambda > 460$ nm) and hold promise as future PDT agents via a novel mechanism of action.[68,69,72]

1.4. Redox Properties of Mixed-Metal Polyazine Complexes

1.4.1. Electrochemistry Theory and Application

1.4.1.1. Cyclic Voltammetry

Electrochemistry is one of several useful methods to characterize electroactive metal complexes. Cyclic voltammetry (CV), a form of linear sweep voltammetry, is a static and non-destructive method with a three electrode system including a working electrode, a counter electrode and a reference electrode. The experimental configuration has a platinum disc or glassy carbon working electrode, a platinum wire auxiliary electrode and a reference electrode system with the analyte in a solvent/electrolyte solution. The choice of solvent, electrolyte and electrode

material is important to the observation of the electrochemistry of analytes. Solvents and electrolytes are important to provide a sufficient electrochemical window to observe the redox behaviors of analytes. A reference electrode is used to provide a constant potential to the system. The normal hydrogen electrode (NHE) which is a platinum electrode with hydrogen gas bubbling in an acidic solution has all components at unit activity and is applied as a basis for comparison with all other reference electrodes. However, NHE is difficult to operate. Some reference electrodes listed in Table 1.1 are easy to operate and commonly used including saturated calomel electrode (SCE), sodium saturated calomel electrode (SSCE), normal calomel electrode (NCE) and silver/silver chloride electrode (Ag/AgCl).[74]

Table 1.1. Common reference electrodes and their potentials relative to the normal hydrogen electrode.[74]

Electrode	Composition	Potential (V vs. NHE)
Norma hydrogen electrode (NHE)	Pt/H_2 (a = 1), H^+ (a = 1)	0
Saturated calomel electrode (SCE)	Hg/Hg_2Cl_2, KCl (saturated)	0.2412
Sodium saturated calomel electrode (SSCE)	Hg/Hg_2Cl_2, NaCl (saturated)	0.2360
Normal calomel electrode (NCE)	Hg/Hg_2Cl_2, KCl (1 M)	0.2801
Silver/silver chloride	Ag/AgCl, NaCl (3 M)	0.2860
	Ag/AgCl, NaCl (saturated)	0.1940
	Ag/AgCl, KCl (saturated)	0.1970

Cyclic voltammetry monitors the change of the working electrode current at fixed potential change versus time, or varying scan rate. During the cyclic voltammetry measurement, the potentiostat applies a potential ramp then reverses the direction of potential change, returning to

the initial potential (Figure 1.4). Ideally, the initial potential is the rest potential where no current flows. As the potential is scanned in the positive-going direction, the analyte is oxidized at the electrode surface. At the switching potential, the scan direction is reversed and the oxidized analyte is reduced. Once the potential is returned to the initial value, the experiment is typically terminated.[75] The cathodic or anodic peak current (i_p^c or i_p^a) can be related by the Randles-Sevcik equation 1.1.

$$i_p^c, i_p^a = (2.69 \times 10^5) n^{\frac{3}{2}} A D^{\frac{1}{2}} [A] \upsilon^{\frac{1}{2}} \quad (1.1)$$

Where *n* is the number of electrons passed per mole of the analyte, A is the active area of the working electrode (m^2). D is the diffusion coefficient of the analyte (m^2/s), [*A*] is the concentration of the analyte (mole/L) and υ is the potential scan rate (V/s). Figure 1.5 is a typical cyclic voltammogram in which the current of the working electrode changes with the scanning potential. If an electrochemical process does not involve any chemical bond forming or breaking and electron transfer kinetics are fast at the interferer, the cyclic voltammogram would be reversible with $i_p^a / i_p^c = 1$. The potential separation between the cathodic peak potential and the anodic peak potential (ΔE_p) will be independent of the potential scan rate and is related by the equation 1.2.

$$\Delta E_p = E_p^c - E_p^a = \frac{59\ mV}{n} (at\ 25℃) \quad (1.2)$$

Where n is the number of electrons passed in the redox process.

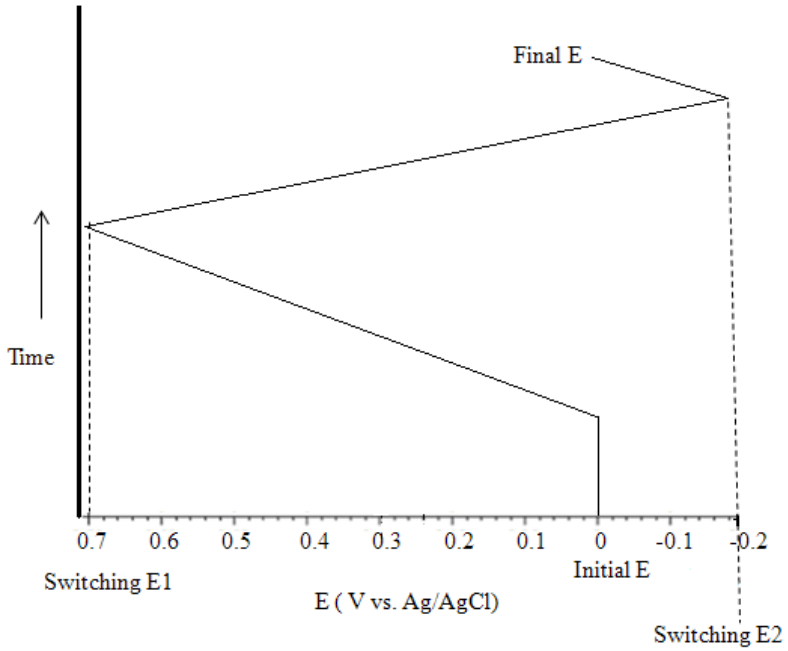

Figure 1.4. The potential sweep function applied in a cyclic voltammetry experiment at a scan rate (υ) of 100 mV/s.[76]

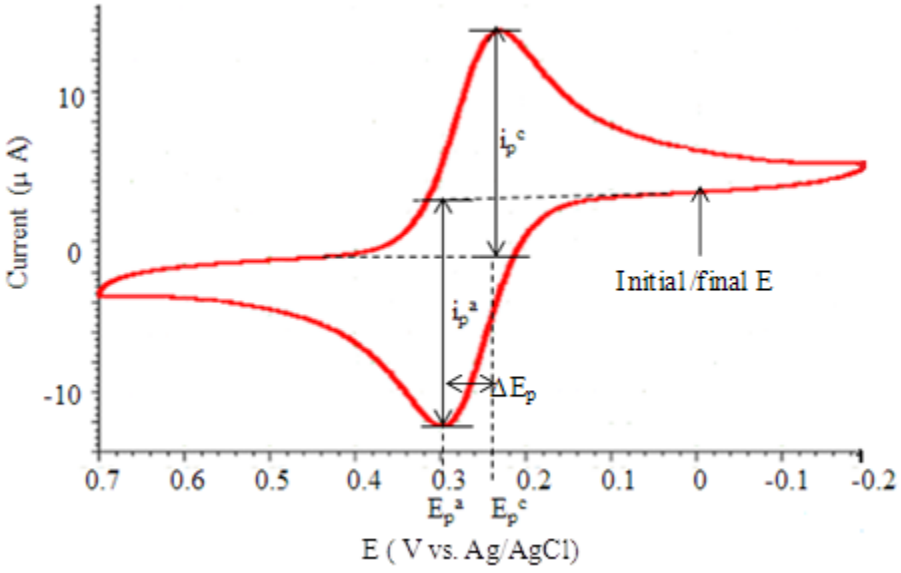

Figure 1.5. Cyclic voltammogram of $Fe(CN)_6^{3-}/Fe(CN)_6^{4-}$ couple that follows Nernstian reversible behavior, where cathodic and anodic peak potentials are E_p^c and E_p^a respectively, and the analogous peak currents are i_p^c and i_p^a at a scan rate of 100 mV/s.[76]

The half wave potential ($E_{1/2}$) is reported for the reversible redox couple and related by the equation 1.3.

$$E_{1/2} = \frac{E_{\mathrm{p}}^{\mathrm{c}} + E_{\mathrm{p}}^{\mathrm{a}}}{2} \tag{1.3}$$

If $i_{\mathrm{p}}^{\mathrm{c}}$ or $i_{\mathrm{p}}^{\mathrm{a}} = 0$, the redox process is irreversible. And if $i_{\mathrm{p}}^{\mathrm{c}}$ or $i_{\mathrm{p}}^{\mathrm{a}} > 0$ and $i_{\mathrm{p}}^{\mathrm{a}} / i_{\mathrm{p}}^{\mathrm{c}} \neq 1$, the cyclic voltammogram would be quasi-reversible. CV is a useful method to investigate electroactive redox properties and allows evaluation of the analyte frontier orbital energetics. CV provides information about stability and reactivity of oxidized or reduced analytes and differentiates reversible and irreversible electrochemical couples. Other merits of CV are its high precision and sensitivity.[76]

1.4.1.2. Bulk Electrolytic Technique

Another useful electrochemical technique is controlled potential bulk electrolysis. It is often used to change the redox state of the entire analyte in the bulk solution and investigate the electron stoichiometry of the electrochemical process. The instrument applies a steady potential at the working electrode to a stirring solution. The method is based on converting a bulk analyte sample into a redox modified product and measuring the amount of charge required. Faraday's Law shows the relationship between charge consumed and amount of analyte and number of e^- transferred, seen in equation 1.4[77]:

$$Q = n\mathrm{F}VC = n\mathrm{F}W/M \tag{1.4}$$

where Q is the consumed charge, n is the number of equivalents of charge required per mole of reaction (equivalents/mole), F is Faraday's constant (96,486 Coulomb/mol), V is the volume of the electrolytic solution (L), C is the concentration of the analyte (mole/L), W is the mass of the analyte used, and M is the analyte molecular weight. The current decreases exponentially, and

the experiment is considered completed when the current drops to a background non-Faradic current. Charge is obtained by integration of the current passed over time.[77]

1.4.2. Electrochemical Properties of Ru(II) Monometallic, Bimetallic and Os(II) Monometallic Complexes

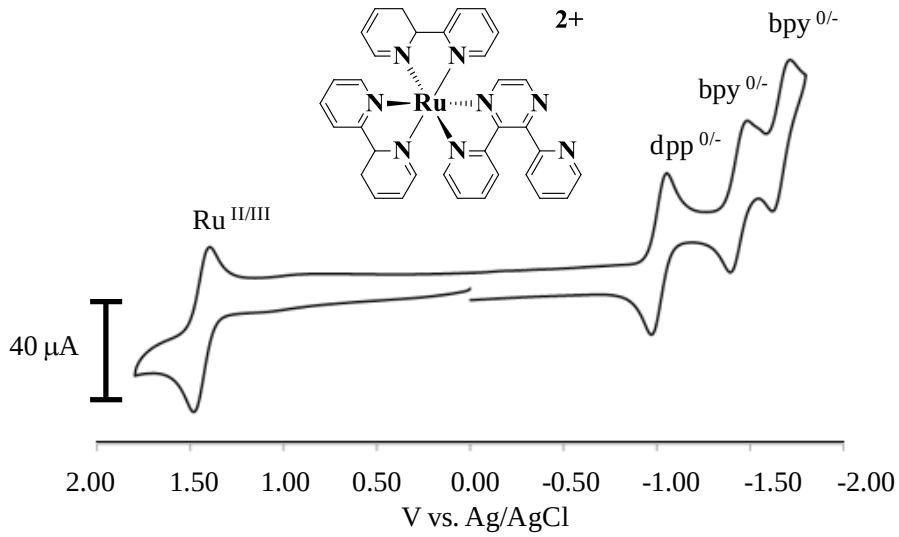

Figure 1.6. Cyclic voltammogram of ruthenium monometallic complex $[(bpy)_2Ru(dpp)]^{2+}$ in 0.1 M Bu_4PF_6 in acetonitrile at room temperature using Ag/AgCl reference electrode with bpy = 2,2′-bipyridine, dpp = 2,3-bis(2-pyridyl)pyrazine.[78]

The electrochemical properties of Ru(II) monometallic, bimetallic and Os(II) monometallic complexes are reviewed herein and summarized in Table A-1 (A-11). The CV of the ruthenium monometallic complex $[(bpy)_2Ru(dpp)]^{2+}$ is shown in Figure 1.6. The complex oxidizes reversibly at 1.38 V vs. Ag/AgCl assigned to $Ru^{II/III}$ oxidation, and reduces reversibly at –1.02 V vs. Ag/AgCl attributed to $dpp^{0/-}$ couple, followed by two reversible $bpy^{0/-}$ reductions at –1.44 and –1.76 V vs. Ag/AgCl.[78,79] The electrochemistry of ruthenium monometallic complexes $[(TL)_2Ru(dpp)]^{2+}$ (TL = phen, and Ph_2phen, phen = 1,10-phenanthroline, Ph_2phen = 4,7-diphenyl-1,10-phenanthroline) consists of a reversible one-electron $Ru^{II/III}$ oxidation at 1.45 and

1.39 V vs. Ag/AgCl and a reversible $dpp^{0/-}$ reduction at −1.02 and −1.04 V vs. Ag/AgCl prior to terminal ligand reduction at −1.45 and −1.38 V vs. Ag/AgCl, respectively.[80-82] The electrochemistry data shows that the highest occupied molecular orbital (HOMO) of ruthenium monometallics is Ru (dπ)-based, while the lowest unoccupied molecular orbital (LUMO) is dpp (π*)-based.[80]

The electrochemistry of ruthenium bimetallic complex $[(bpy)_2Ru(dpp)Ru(bpy)_2]^{4+}$ comprises two reversible one-electron $Ru^{II/III}$ oxidations and two reversible dpp based reductions.[83,84] The first $Ru^{II/III}$ oxidation occurs at 1.43 V vs. Ag/AgCl, while the second $Ru^{II/III}$ oxidation occurs at 1.60 V vs. Ag/AgCl. The two $Ru^{II/III}$ oxidations occur at different oxidative potentials, indicating significant electronic coupling between two Ru centers bridged by a dpp ligand. Two reversible one-electron reductions occur at −0.62 and −1.10 V vs. Ag/AgCl assigned to the first and second dpp bridging ligand reductions. The $BL^{0/-}$ and $BL^{-/2-}$ couples occurring prior to $TL^{0/-}$ couples is indicative of μ-dpp bound to two electropositive metals.[83] The result of electrochemistry suggests that the HOMO of $[(bpy)_2Ru(dpp)Ru(bpy)_2]^{4+}$ is Ru (dπ)-based, while the LUMO is dpp (π*)-based.

The electrochemistry of osmium monometallic complex $[(bpy)_2Os(dpp)]^{2+}$ is similar to that of the ruthenium monometallic analog.[85,86] The $[(bpy)_2Os(dpp)]^{2+}$ oxidizes at 0.94 V vs. Ag/AgCl, 0.43 V easier than the Ru monometallic, indicative of the higher energy dπ orbitals on Os compared to Ru 4d orbitals. Reductively, a reversible one-electron reduction occurs at −1.02 V vs. Ag/AgCl assigned to $dpp^{0/-}$ couple, followed by two reversible $bpy^{0/-}$ reductions at −1.38 and −1.58 V vs. Ag/AgCl.[85] The electrochemistry data indicate that the HOMO of $[(bpy)_2Os(dpp)]^{2+}$ is Os(dπ)-based, while LUMO of $[(bpy)_2Os(dpp)]^{2+}$ is dpp (π*)-based.

1.4.3. Electrochemical Properties of Rh(III) Monometallic Complexes

The electrochemical mechanisms of rhodium complexes such as $[Rh(phen)_3]^{3+}$, $[Rh(bpy)_3]^{3+}$, $[Rh(bpy)_2Cl_2]^+$ were investigated by DeArmond and coworkers.[87,88] Electrochemical reduction of $[Rh(phen)_3]^{3+}$ was found to follow an ECECEE mechanism (E: electron transfer process, C: chemical reaction process.).[88] The first reductive wave of $[Rh(phen)_3]^{3+}$, shown in Figure 1.7 A, is reversible with one-electron transfer, followed by a slow chemical reaction. The forward rate constant of this slow chemical reaction, $(k_f)_I = 0.12 \pm 0.04\ s^{-1}$, was calculated using a method described by Nicholson.[89,90] The luminescence spectra support the presence of free phen ligand in the bulk electrolyzed $[Rh(phen)_3]^{3+}$ solution. The second reduction is a one-electron transfer followed by a very fast chemical reaction, as shown in Figure 1.7 B. The whole CV of $[Rh(phen)_3]^{3+}$ reductions are shown in Figure 1.7 C. The electrochemical potentials of $[Rh(phen)_3]^{3+}$ are listed in Table 1.2 and the electrochemical mechanism for $[Rh(phen)_3]^{3+}$ is proposed as shown in Figure 1.8.

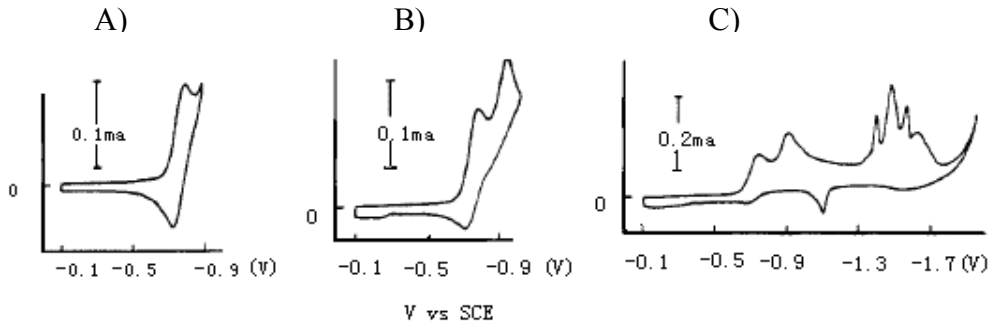

Figure 1.7. Cyclic voltammograms of $[Rh(phen)_3]^{3+}$, at a concentration of 5.90×10^{-4} M, using a scan rate of υ = 0.10 V/sec, (SCE: the saturated calomel reference electrode), phen = 1,10-phenanthroline. Reprinted with permission from Kew, G.; Hanck, K.; DeArmond, K. *Phys. Chem.* **1975**, *79*, 1828-1835. Copyright 1975 American Chemical Society.[88]

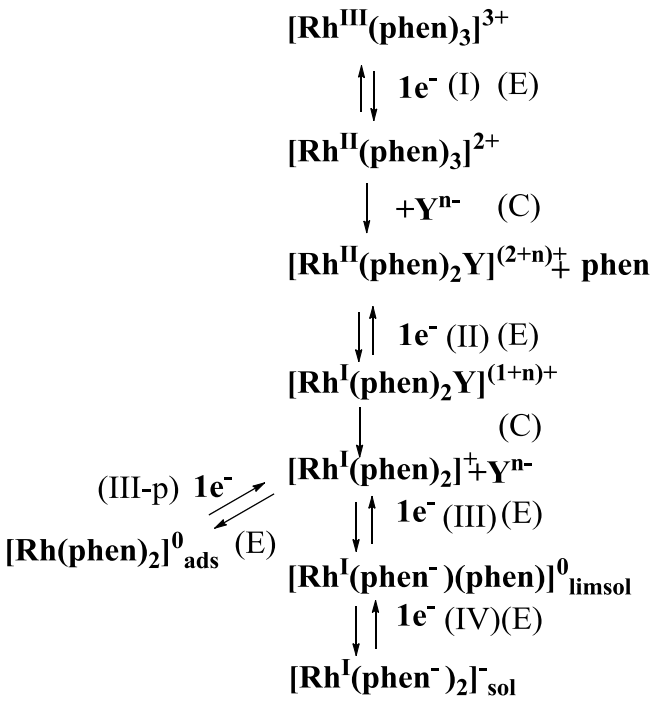

Figure 1.8. Proposed electrochemical mechanism for $[Rh(phen)_3]^{3+}$ (Y is Cl^- or CH_3CN in the solution.), phen = phenanthroline. Reprinted with permission from Kew, G.; Hanck, K.; DeArmond, K. *Phys. Chem.* **1975**, *79*, 1828-1835. Copyright 1975 American Chemical Society.[88]

Electrochemical reductions of $[Rh(bpy)_3]^{3+}$ occur by an ECECEE mechanism. Since the rate of the chemical reaction following one-electron transfer is much faster than the phen analog, two consecutive one-electron transfers overlap in one reduction wave at scan rates below 1-2 V/sec, as shown in Figure 1.9 A.[87] These two reduction processes will separate at higher scan rates, as shown in Figure 1.9 B. The free bpy ligand is detected by luminescence spectroscopy in the bulk electrolyzed $[Rh(bpy)_3]^{3+}$ solution. There is one electron involved in the third reduction couple ($(E_p^c)_{III}$ = −1.46 V vs. SCE (SCE: the saturated calomel electrode)) and the forth reduction couple ($(E_p^c)_{IV}$ = −1.67 V vs. SCE). The electrochemical potentials of $[Rh(bpy)_3]^{3+}$ are summarized in Table 1.2 and the proposed electrochemical mechanism of $[Rh(bpy)_3]^{3+}$ is shown in Figure 1.10.

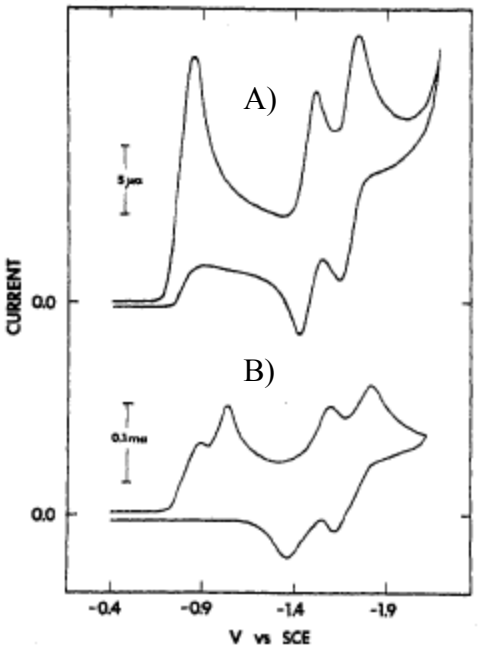

Figure 1.9. Cyclic voltammograms of $[Rh(bpy)_3]^{3+}$, 1.08×10^{-4} M: A) υ = 0.10 V/sec; B) υ = 31.2 V/sec, (SCE: the saturated calomel reference electrode), bpy = 2,2′-bipyridine. Reprinted with permission from Kew, G.; DeArmond, K.; Hanck, K. *Phys. Chem.* **1974**, *78*, 727-734. Copyright 1974 American Chemical Society.[87]

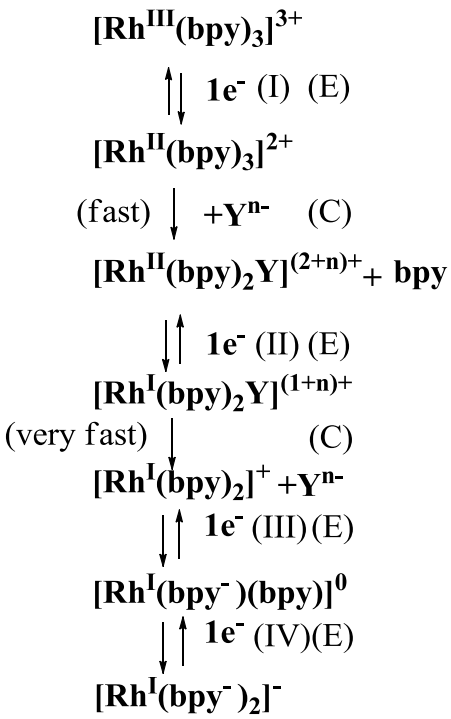

Figure 1.10. Proposed electrochemical mechanism for $[Rh(bpy)_3]^{3+}$, bpy = 2,2′-bipyridine. (Y is Cl^- or CH_3CN in the solution.) Reprinted with permission from Kew, G.; DeArmond, K.; Hanck, K. *Phys. Chem.* **1974**, *78*, 727-734. Copyright 1974 American Chemical Society.[87]

The CV of $[Rh(bpy)_2Cl_2]^+$ at the scan rate of 0.10 V/s (Figure 1.11 A) is similar to that of $[Rh(bpy)_3]^{3+}$ at the same scan rate (Figure 1.9 A). The CV of this bis-complex at the scan rate of 32.2 V/s (Figure 1.11 B) looks similar to its CV at 0.1 V/s (Figure 1.11 A), but is different from the CV of the tris-complex $[Rh(bpy)_3]^{3+}$ at the scan rate of 31.2 V/s, which has an additional wave at –0.8 V vs. SCE (Figure 1.9 B). No other waves can be detected for bis-complex $[Rh(bpy)_2Cl_2]^+$ by increasing the potential scan rate. This observation suggests that the rate constant $(k_f)_I$ of the first chemical reaction in $[Rh(bpy)_2Cl_2]^+$ system, which is chloride ligand elimination, is larger than the $(k_f)_I$ in $[Rh(bpy)_3]^{3+}$ system. It also suggests that $(k_f)_I$ and $(k_f)_{II}$ are close in $[Rh(bpy)_2Cl_2]^+$ system and much different in $[Rh(bpy)_3]^{3+}$ system.

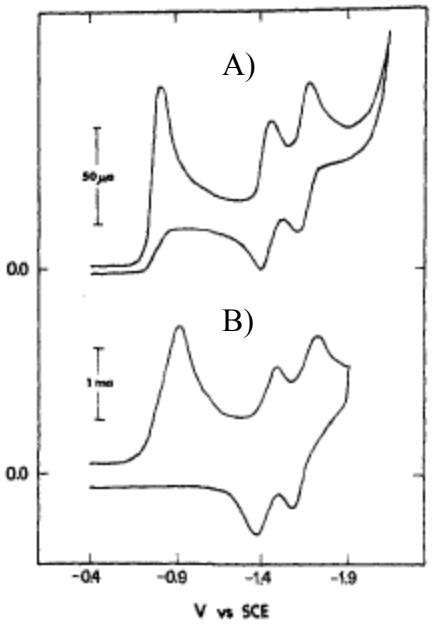

Figure 1.11. Cyclic voltammograms of $[Rh(bpy)_2Cl_2]^+$, 5.16×10^{-4} M: A) υ = 0.10 V/sec; B) υ = 32.2 V/sec, (SCE: the saturated coalomel reference electrode), bpy = 2,2′-bipyridine. Reprinted with permission from Kew, G.; DeArmond, K.; Hanck, K. *Phys. Chem.* **1974**, *78*, 727-734. Copyright 1974 American Chemical Society.[87]

The complex $[Rh(bpy)_2Cl_2]^+$ has an ECECEE electrochemical mechanism. The first one-electron reduction of the complex is followed by a very fast chemical reaction of a chloride ligand elimination which is supported by the chloride oxidation peak at 1.40 V vs. SCE. This first chemical reaction rate is much faster than the rate of the loss of the bpy ligand from the complex $[Rh(bpy)_3]^{3+}$ expected due to the chelate effect present in bpy. The second one-electron reduction of $[Rh(bpy)_2Cl_2]^+$ is also followed by a very fast chloride ligand elimination. The third reduction ($(E_p^c)_{III}$ = −1.46 V vs. SCE) is one-electron reversible couple and the forth reduction ($(E_p^c)_{IV}$ = −1.67 V vs. SCE) is also reversible. The third and forth reductions are attributed to bpy ligand reductions. The electrochemical potentials of $[Rh(bpy)_2Cl_2]^+$ are summarized in Table 1.2 and the electrochemical mechanism of $[Rh(bpy)_2Cl_2]^+$ is proposed in Figure 1.12.

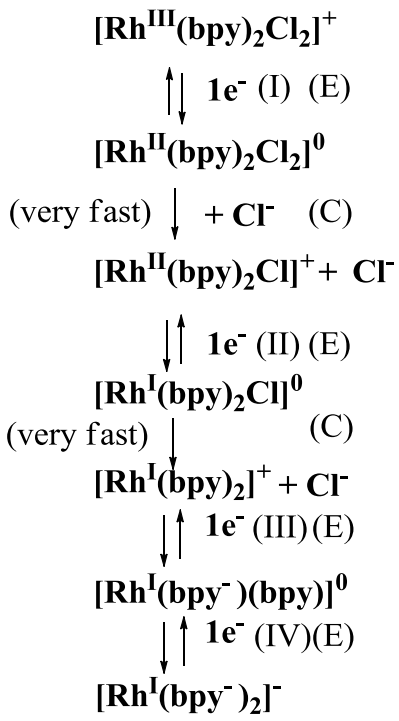

Figure 1.12. Proposed electrochemical mechanism for $[Rh(bpy)_2Cl_2]^+$, bpy = 2,2′-bipyridine. (Y is Cl^- or CH_3CN in the solution.) Reprinted with permission from Kew, G.; DeArmond, K.; Hanck, K. *Phys. Chem.* **1974**, *78*, 727-734. Copyright 1974 American Chemical Society.[87]

The complexes $[Rh(BL)_2Br_2]^+$ (BL = bpm, dpp, dpq, dpb and bpm = 2,2′-bipyrimidine, dpq = 2,3-bis(2-pyridyl)quinoxaline, dpb = 2,3-bis(2-pyridyl)benzoquinoxaline) reported by Brewer and coworkers have the similar electrochemical properties to $[Rh(bpy)_2Cl_2]^+$ and electrochemical potentials are listed in Table 1.2.[91] The electrochemical mechanism of complexes $[Rh(BL)_2Br_2]^+$ is proposed as ECECEE as the bpy analog.

Table 1.2. Electrochemical properties of RhIII complexes.

Complexes[a, b]	$Rh^{III/II}$	$Rh^{II/I}$	$Rh^{III/II/I}$	$L_1^{0/-}$	$L_2^{0/-}$	Reference
	E_p^c (V)	E_p^c (V)	E_p^c (V)	$E_{1/2}$ (V)	$E_{1/2}$ (V)	
$[Rh(phen)_3](ClO_4)_3$	–0.79[c]	–0.96[c]	--	–1.49	–1.64	[88]
$[Rh(bpy)_3](ClO_4)_3$	–0.83[c]	–0.96[c]	--	–1.46	–1.67	[87]
$[Rh(bpy)_2Cl_2](ClO_4)$	--	--	–0.84[c]	–1.46	–1.67	[87]
$[Rh(bpy)_2Br_2](PF_6)$	--	--	–0.83[c]	–1.37	–1.58	[91]
$[Rh(bpm)_2Br_2](PF_6)$	--	--	–0.66[c]	–1.38	–1.74	[91]
$[Rh(dpp)_2Br_2](PF_6)$	--	--	–0.64[c]	–1.14	–1.27	[91]
$[Rh(dpq)_2Br_2](PF_6)$	--	--	–0.48[c]	–1.00	–1.64	[91]
$[Rh(dpb)_2Br_2](PF_6)$	--	--	–0.43[c]	–0.81	–1.34	[91]

[a]Potentials are reported in CH_3CN at υ = 100 mV/s versus SCE (SCE: the saturated calomel electrode) vs. NHE (NHE: the normal hydrogen electrode) 0.241 V.
[b]bpy = 2,2′-bipyridine, phen = 1,10-phenanthroline, bpm = 2,2′-bipyrimidine, dpp = 2,3-bis(2-pyridyl)pyrazine, dpq = 2,3-bis(2-pyridyl)quinoxaline and dpb = 2,3-bis(2-pyridyl)benzoquinoxaline.
[c]Electron transfer followed by a chemical reaction.

1.4.4. Electrochemical Properties of Bimetallic Complexes

The first electrochemical reduction of the bimetallic complex $[(bpy)_2Ru(dpp)Rh(bpy)_2]^{5+}$ is an irreversible couple at –0.65 V vs. SCE assigned to rhodium center reduction,[92] while the first reduction couple of $[(bpy)_2Ru(dpp)Ru(bpy)_2]^{4+}$ is reversible at –0.70 V vs. SCE attributed to dpp ligand reduction.[83]

1.4.5. Electrochemical Properties of Trimetallic Complexes

The oxidative electrochemistry of trimetallic complex $[\{(bpy)_2Ru(dpp)\}_2RhCl_2]^{5+}$ shows two overlapping one-electron reversible $Ru^{II/III}$ oxidations at 1.60 V vs. Ag/AgCl due to nearly simultaneous oxidation of the two equivalent Ru centers that are weakly coupled in this motif providing ΔE_p = ca. 100 mV in these systems. Reductively, two overlapping irreversible one-electron reductions occur at –0.39 V vs. Ag/AgCl corresponding to $Rh^{III/II/I}$ couple, followed by two reversible reductions at –0.79 and –1.02 V vs. Ag/AgCl attributed to two $dpp^{0/-}$ couples.[68,72] The reductive electrochemistry is described as an ECECEE mechanism as the $[Rh(bpy)_2Cl_2]^+$. The electrochemistry data show that the HOMO of $[\{(bpy)_2Ru(dpp)\}_2RhCl_2]^{5+}$ is Ru(dπ)-based, while the LUMO of $[\{(bpy)_2Ru(dpp)\}_2RhCl_2]^{5+}$ is Rh(dσ*)-based. The electrochemistry of $[\{(bpy)_2Os(dpp)\}_2RhCl_2]^{5+}$ is similar to that of the ruthenium trimetallic complex $[\{(bpy)_2Ru(dpp)\}_2RhCl_2]^{5+}$.[68] The osmium trimetallic complex $[\{(bpy)_2Os(dpp)\}_2RhCl_2]^{5+}$ displays two overlapping one-electron reversible $Os^{II/III}$ oxidations at 1.21 V vs. Ag/AgCl, 0.39 V negative relative to Ru analogue, indicating that the energy of the Os trimetallic dπ orbitals are destabilized relative to the Ru analogue. The reductive electrochemistry of trimetallic complex $[\{(bpy)_2Os(dpp)\}_2RhCl_2]^{5+}$ shows two overlapping irreversible one-electron $Rh^{III/II/I}$ reductions at –0.39 V vs. Ag/AgCl, followed by two reversible $dpp^{0/-}$ reductions at –0.76 and –1.00 V vs. Ag/AgCl.[68] The electrochemistry result of $[\{(bpy)_2Os(dpp)\}_2RhCl_2]^{5+}$ suggests that the HOMO is Os(dπ)-based and the LUMO is Rh(dσ*)-based, these Ru or Os based HOMOs and Rh based LUMOs indicate a lowest lying triplet Os(dπ)→Rh(σ*) MMCT excited state.[68]

1.5. Photophysical Properties

1.5.1. Electronic Excited States

In order to understand photochemical and photophysical properties, the excited states of mixed-metal polyazine complexes need to be considered. Upon the irradiation with visible light, the electrons of the complex in occupied low energy orbitals are promoted to unoccupied high energy orbitals due to absorption of the energy from the photons of absorbed light. Such excitation leads to the population of an electronic excited state (Figure 1.13).

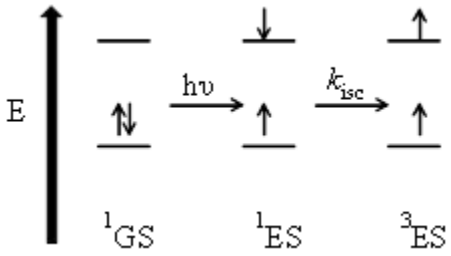

Figure 1.13. The electron configuration of a singlet ground state, a singlet excited state and a triplet excited state.

Allowed electronic transitions that meet the symmetry and spin selection rules will display intense bands in the electronic absorption spectrum.[93] The symmetry rule allows the transitions, when the direct product of three factors, which are the ground state and excited state wave functions and electronic dipole moment operator, contains the total symmetric representation or when a change in dipole from the GS to the ES occours. The symmetry rule governs the Laporte allowance of transitions between ground and excited electronic states.[93] The intensity of an electronic transition, which is determined by the symmetry selective rule, is related by equation 1.5.

$$f \propto \int \Psi_{el}^{ES} \boldsymbol{\mu} \Psi_{el}^{GS} d\upsilon \qquad (1.5)$$

Where *f* is the oscillator strength, which is proportional to the integral of the product of Ψ_{el}^{ES} (the excited state wave function) and Ψ_{el}^{GS} (the grounde state wave function). $\boldsymbol{\mu}$ is the electronic dipole moment operator defined in equation 1.6.

$$\boldsymbol{\mu} = -e\sum_i r_i + \sum_j q_j R_j \tag{1.6}$$

Where *e* is the electron charge, r_i is the vector position, q_j is the nuclear charge, R_j is the nuclear position. The spin selection rule states that electronic transitions are spin allowed, when the system does not change its spin multiplicity during the excitation.[93] Figure 1.13 shows a two orbital diagram illustrating excitation and intersystem crossing for a simple two orbital system. In the excited state, when two orbitals are singly occupied, it is lowest energy for spins to be aligned. This suggests the singlet excited state moves down in energy via intersystem crossing to produce this spin aligned triplet excited state. The electronic transitions allowed by the symmetry and spin selection rules are the most intense transitions with extinction coefficient (ε) larger than 10^3 $M^{-1}cm^{-1}$. The transitions allowed by spin selection rule, but forbidden by the symmetry selection rule, are low intense bands with ε between 1 to10^2 $M^{-1}cm^{-1}$. Some formally forbidden transitions may still be observed due to the relaxation of the selection rules, most commonly via spin orbital coupling or vibronic coupling.

Figure 1.14 shows the block molecular orbital diagram of an octahedral metal complex with some common electronic transitions. The block molecular orbital diagram is made by a linear combination of atomic orbitals (LCAO) using a localized orbital approach. In this approach, each molecular orbital is a combination of one or more atomic orbitals. Orbitals are labeled metal, if the metal atomic orbitals (AOs) contribute more to the molecular orbital (MO) than the ligand. The orbitals are labeled ligand, if the ligand orbitals contribute more to the MO at interest. Each

box in the diagram represents a set of orbitals with close energy. The shaded boxes show the filled orbitals and unshaded boxes represent unfilled orbitals. Several transitions are involved in spectroscopy and excited states in photochemistry. Internal ligand (IL) transitions involve optically promoting electrons from a formally occupied ligand-based orbital to an unoccupied ligand-based orbital. Ligand field transitions (LF) are attributed to the process of electrons being optically promoted from formally occupied metal-based orbitals to unoccupied metal-based orbitals that are d or f in nature. Ligand-to-metal charge transfer transitions (LMCT) are associated with the process of electrons being optically promoted from formally occupied ligand-based π orbital to unoccupied metal-based orbitals. Metal-to-ligand charge transfer transitions (MLCT) are associated with the process of electrons being promoted from formally occupied metal-based orbitals to unoccupied ligand-based orbitals. The electronic transitions shown in the diagram including IL, LMCT and MLCT are allowed by the symmetry selection rule. These electronic transitions will be discussed in the following sections on each individual complex.

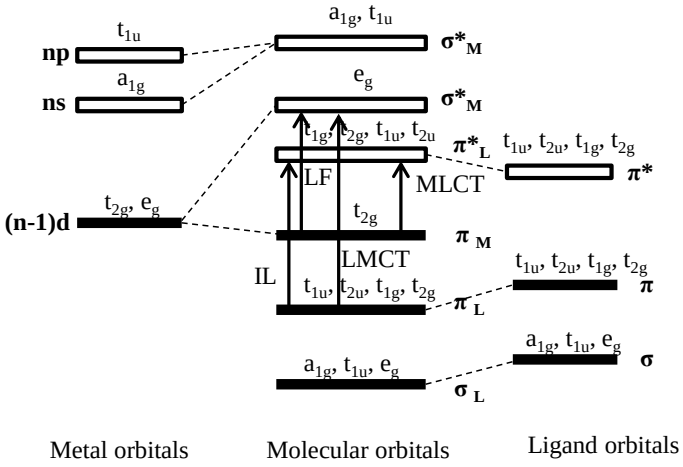

Figure 1.14. Block molecular orbital diagram of an octahedral metal complex with some common electronic transitions. (IL = intraligand, LF = ligand field, LMCT = ligand-to-metal charge transfer and MLCT = metal-to-ligand charge transfer). Shaded blocks show electron filled orbitals and unshade blocks represent electron unfilled orbitals.[94]

Electronic transitions are generally accompanied with significant vibrational excitation. The conversion between electronic energy surfaces are controlled by the Franck-Condon principle which states that electronic transitions occur in the absence of nuclear motion.[93] Figure 1.15 shows Morse energy surface diagram of electronic states (^{1}GS, ^{1}ES, ^{3}ES) and vibrational states of $[Ru(bpy)_3]^{2+}$. When $[Ru(bpy)_3]^{2+}$ absorbs photons from the light, it is excited from ground state (^{1}GS) to its lowest-lying singlet excited state (^{1}ES). $[Ru(bpy)_3]^{2+}$ at the ^{1}ES undergoes intersystem crossing to the triplet excited state (^{3}ES) with unit efficiency. The ^{3}ES excited state can undergo non-radiative decay (knr), radiative decay (emitting phosphorescence), or a photochemical reaction to the ground state (^{1}GS). Radiative processes providing conversion between states by absorption or emission of light are represented by straight arrows. Non-radiative processes not involving light but rather vibrational movement for conversion between states are shown as wavy arrows. Radiative processes are vertical, with the intensities proportional to the square of the overlap integral between the vibration wavefuction of the two states.[93] The non-radiative conversion between vibrational states of the same spin multiplicity is termed intramolecular vibrational relaxation (k_{ivr}) and that between states of differing spin multiplicity is called intersystem crossing (k_{isc}). The radiative relaxation without spin change gives fluorescence (k_f) and with spin change provides phosphorescence (k_p). The electronic states of molecules are often represented using Jablonski (Figure 1.16) or simplified state diagrams (Figure 1.17). $[Ru(bpy)_3]^{2+}$, as shown in Figure 1.15, 1.16 and 1.17, possesses a lowest-lying ^{3}MLCT excited state populated with unit efficiency that is long lived (τ = 860 ns) at room temperature with λ_{max}^{em} = 605 nm in the visible region of the spectrum (Figure 1.17). [58,80] State diagrams are often simplified for complex molecules to exclude vibronic excitation although it occurs, illustrated in Figure 1.17.

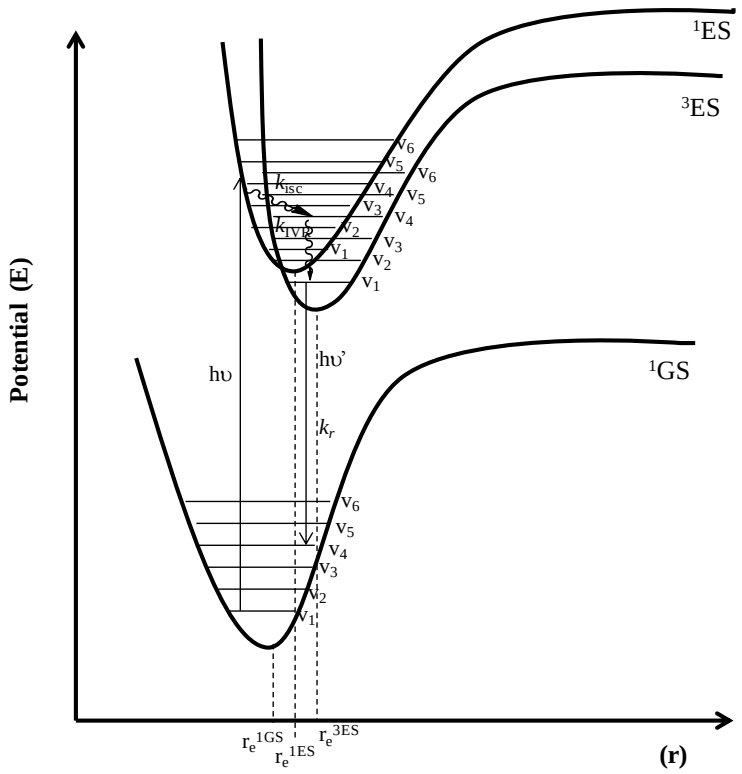

Figure 1.15. Morse potential energy surface for electronic states (^{1}GS, ^{1}ES and ^{3}ES) of $[Ru(bpy)_3]^{2+}$. bpy = 2,2′-bipyridine, ^{1}GS = singlet ground state, ^{1}ES = singlet excited state, ^{3}ES = triplet excited state, k_r = rate constant for radiative decay, k_{nr} = rate constant for non-radiative decay, k_{IVR} = rate constant for intramolecular vibrational relaxation, k_{isc} = rate constant for intersystem crossing non-radiative decay.[93]

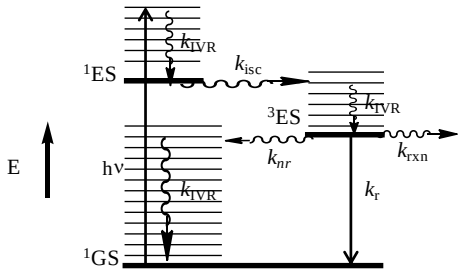

Figure 1.16. Jablonski diagram for $[Ru(bpy)_3]^{2+}$ with energy levels for the ^{1}GS, ^{1}ES and ^{3}ES. bpy = 2,2′-bipyridine, ^{1}GS = singlet ground state, ^{1}ES = singlet excited state, ^{3}ES = triplet excited state, k_{IVR} = rate constant for intramolecular vibrational relaxation, k_r = rate constant for radiative decay, k_{nr} = rate constant for non-radiative decay, k_{isc} = rate constant for intersystem crossing non-radiative decay, k_{ic} = rate constant for internal conversion non-radiative decay, and k_{rxn} = rate constant for reaction decay.

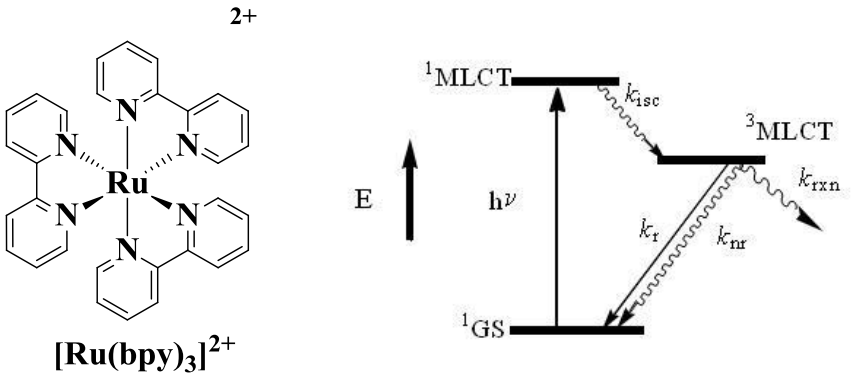

Figure 1.17. State diagram for $[Ru(bpy)_3]^{2+}$ with energy levels for the ^{1}MLCT and ^{3}MLCT excited state. bpy = 2,2′-bipyridine, ^{1}GS = singlet ground state, ^{1}MLCT = singlet metal-to-ligand charge transfer excited state, ^{3}MLCT = triplet metal-to-ligand charge transfer excited state, k_r = rate constant for radiative decay, k_{nr} = rate constant for non-radiative decay, k_{isc} = rate constant for intersystem crossing non-radiative decay, and k_{rxn}= rate constant for reaction decay.

The quantification of light activated processes is typically described in terms of quantum yields, Φ, and excited state lifetimes, τ, and studied using steady-state and time-resolved spectroscopy. These quantities can be related to the rates of reactions and conversions between states. The quantum yield is a measurement of the efficiency of a process, expressed as a ratio of a particular process divided by the sum of all rates for deactivation of the excited state. For indirectly populated states, the quantum yield is calculated by the efficiency of the process multiplied by the efficiency for population of that excited state, with the maximum efficiency being 1. The Φ for emission is defined as k_r divided by the sum of the rate constants of all pathways depopulating that state, $\sum k$ ($\sum k = k_r + k_{nr} + k_{rxn}$) times the quantum yield for population of that state. For emission by $[Ru(bpy)_3]^{2+}$ from the ^{3}MLCT state, Φ is given by equation 1.7.

$$\Phi^{em} = \Phi^{pop}_{^3MLCT} \frac{k_r}{k_r + k_{nr} + k_{rxn}} \qquad (1.7)$$

Given $\Phi^{pop}_{^3\mathrm{MLCT}}$ = 1, the equation is simplified to $\Phi^{\mathrm{em}} = \frac{k_r}{k_r+k_{nr}+k_{rxn}}$. The excited state lifetime of any state, τ, is defined as the inverse of the sum the rate constants of all pathways quenching that state, $\sum k^{-1}$. For the ^{3}MLCT state of $[Ru(bpy)_3]^{2+}$, the lifetime is provided by equation 1.8.

$$\tau = \frac{1}{k_r + k_{nr} + k_{rxn}} \tag{1.8}$$

1.5.2. Electronic Excited States and Photophysical Properties of Ru(II) Monometallic, Bimetallic and Os(II) Monometallic Complexes

The photophysical properties of Ru(II) monometallic, bimetallic and Os(II) monometallic complexes in literature are reviewed herein and summarized in Table A-1 (A-11). The electronic absorption spectra of Ru monometallic complexes $[(TL)_2Ru(dpp)]^{2+}$ (TL = bpy, phen, and Ph_2phen) display ligand-based π→π* IL transitions in the UV and metal-to-ligand charge transfer (MLCT) transitions in the visible region of the electronic absorption spectrum. The ruthenium monometallic complex $[(bpy)_2Ru(dpp)]^{2+}$ strongly absorbs at 284 nm in the UV region due to bpy-based π→π* IL transition. The Ru-based MLCT transitions of $[(bpy)_2Ru(dpp)]^{2+}$ in the visible region of the spectrum consist of the Ru(dπ)→bpy(π*) MLCT transition (λ_{max}^{abs} = 441 nm) at the higher energy region and the Ru(dπ)→dpp(π*) MLCT transition (λ_{max}^{abs} = 464 nm, ε = 1.2 × 10^4 $M^{-1}cm^{-1}$) at the lower energy region.[80] The complex $[(bpy)_2Ru(dpp)]^{2+}$ emits at 680 nm (Φ^{em} = 0.012, τ = 380 ns) from ^{3}MLCT excited state in acetonitrile solution, and emits at 692 nm from the same state in aqueous solution at room temperature.[81,95,96] The electronic absorption spectrum of monometallic complex $[(phen)_2Ru(dpp)]^{2+}$ displays phen-based π→π* IL transition at 262 nm in the UV region, with a shoulder at 387 nm assigned to dpp-based π→π* IL transition.[83,97,98] The complex

$[(phen)_2Ru(dpp)]^{2+}$ shows the Ru(dπ)→phen(π*) MLCT transition (λ_{max}^{abs} = 434 nm) and the Ru(dπ)→dpp(π*) MLCT transition (λ_{max}^{abs} = 465 nm, $\varepsilon = 1.4 \times 10^4$ $M^{-1}cm^{-1}$) in the visible region. The room temperature emission of $[(phen)_2Ru(dpp)]^{2+}$ shows at 660 nm (Φ^{em} = 0.027) with a longer lifetime (τ = 460 ns) in acetonitrile solution and red-shifts at 690 nm in aqueous solution also from the ^{3}MLCT excited state.[81,95,96] The monometallic complex $[(Ph_2phen)_2Ru(dpp)]^{2+}$ displays typical Ph_2phen-based π→π* IL transition at 274 nm in the UV region, with a shoulder at 310 nm assigned to dpp-based π→π* IL transition.[99] The Ru(dπ)→Ph_2phen(π*) MLCT transition of $[(Ph_2phen)_2Ru(dpp)]^{2+}$ displays at 424 nm and the Ru(dπ)→dpp(π*) MLCT transition occurs at 474 nm with $\varepsilon = 1.6 \times 10^4$ $M^{-1}cm^{-1}$ in the visible region of the spectrum.[99] A long-lived room temperature emission of $[(Ph_2phen)_2Ru(dpp)]^{2+}$ in acetonitrile solution shows at 697 nm (Φ^{em} = 0.032, τ = 1000 ns) from the ^{3}MLCT excited state and the same emission displays at 698 nm from the aqueous solution.[82,96,99] Since Ru monometallic complexes $[(TL)_2Ru(dpp)]^{2+}$ (TL = bpy, phen, and Ph_2phen) strongly absorb the light in the UV and visible region of the spectrum and display room temperature emission from the ^{3}MLCT excited state, they are suitable to be used as light absorbers in the proposed Ru,Rh bimetallic systems which are designed for the photodynamic therapy applications.

The Ru bimetallic complex $[(bpy)_2Ru(dpp)Ru(bpy)_2]^{4+}$ will be used as a model system to investigate the excited states of the new Ru,Rh bimetallic systems. It is important to review the photophysical properties of $[(bpy)_2Ru(dpp)Ru(bpy)_2]^{4+}$ (summarized in Table A-1). The electronic absorption spectra of the Ru bimetallic complex $[(bpy)_2Ru(dpp)Ru(bpy)_2]^{4+}$ are similar to those of the ruthenium monometallics, displaying ligand-based π→π* IL transitions in the UV and MLCT transitions in the visible region of the spectrum.[83,84,95] $[(bpy)_2Ru(dpp)Ru(bpy)_2]^{4+}$ shows a bpy-based π→π* IL transition at 284 nm in the UV region,

and displays the Ru(dπ)→bpy(π*) MLCT transition (ε = 2.0 × 10^4 $M^{-1}cm^{-1}$) at 425 nm and the Ru(dπ)→dpp(π*) MLCT transition at 526 nm (ε = 2.4 × 10^4 $M^{-1}cm^{-1}$) in the visible region of the spectrum. The electronic absorption data of $[(bpy)_2Ru(dpp)Ru(bpy)_2]^{4+}$ suggest that coupling $Ru(bpy)_2$ to $[(bpy)_2Ru(dpp)]^{2+}$ decreases the energy of the dpp ligand π* acceptor orbital by 1600 cm^{-1} and shifts the Ru(dπ)→dpp(π*) MLCT transition to lower energy region compared to the Ru monometallics.[83] This property is used herein to design Ru,Rh bimetallic complexes with dpp bridging ligand for photodynamic therapy applications.The Ru bimetallic complex $[(bpy)_2Ru(dpp)Ru(bpy)_2]^{4+}$ emits at 752 nm (Φ^{em} = 9.8 x 10^{-4} and τ = 126 ns) from Ru(dπ)→dpp(π*) ^{3}MLCT excited state in room temperature CH_3CN solution.[81] At 77 K, the low temperature emission of $[(bpy)_2Ru(dpp)Ru(bpy)_2]^{4+}$ in 4:1 v/v ethanol/methanol glass blue-shifts at 715 nm with a longer lifetime 2.0 μs.[95] Since $[(bpy)_2Ru(dpp)Ru(bpy)_2]^{4+}$ has the similar nature and energy of the emissive Ru(dπ)→dpp(π*) ^{3}MLCT excited states as those of Ru,Rh bimetallic and trimetallic systems explored herein, the Ru,Ru bimetallic complex $[(bpy)_2Ru(dpp)Ru(bpy)_2]^{4+}$ will be used as a model system for a Ru→μ-dpp ^{3}MLCT emission.

The photophysical properties of Os(II) monometallic complexes in literature are described herein and summarized in Table A-1 (A-11). The Os monometallic complex $[(bpy)_2Os(dpp)]^{2+}$ displays an intense absorption band at 290 nm in the UV region assigned to bpy-based π→π* IL transition. The Os-based MLCT transitions of $[(bpy)_2Os(dpp)]^{2+}$ in the visible region of the spectrum include the Os(dπ)→bpy(π*) CT transition (λ_{max}^{abs} = 432 nm) at the higher energy region and the Os(dπ)→dpp(π*) CT transition (λ_{max}^{abs} = 486 nm, ε = 1.3 ×10^4 $M^{-1}cm^{-1}$) at the lower energy region.[85] The complex $[(bpy)_2Os(dpp)]^{2+}$ also shows the weak absorption displayed as a tail in the near-infrared region of the electronic absorption spectrum due to enhanced spin-

orbital coupling in Os, providing $^1GS \rightarrow {}^3MLCT$ absorption with $\varepsilon = 3 \times 10^3\ M^{-1}cm^{-1}$.[86] The fact that Os complexes optically populate the ^3MLCT excited state from the ^1GS made possiblely significant spin-orbital coupling is used herein to design an Os,Rh bimetallic complex which performs PDT function in red therapeutic region. A room temperature emission of $[(bpy)_2Os(dpp)]^{2+}$ was shown at 778 nm from the triplet $Os(d\pi) \rightarrow dpp(\pi^*)$ CT excited state with $\tau = 60$ ns.[86,100] Compared to the room temperature emission of Ru monometallic complexes, the room temperature emission of $[(bpy)_2Os(dpp)]^{2+}$ at 778 nm is red-shifted and has shorter emission lifetime consistent with the energy gap law and enhanced spin orbital coupling in Os.

1.5.3. Photochemical Properties of Ru(II) and Os(II) Monometallic Complexes

The Ru monometallic complexes $[(TL)_2Ru(dpp)]^{2+}$ (TL = bpy, phen, and Ph_2phen) all emit from $Ru(d\pi) \rightarrow dpp(\pi^*)$ ^3MLCT excited state in aqueous solution and are reported to photocleave DNA via a singlet oxygen ($^1O_2$) generation energy transfer mechanism shown in Figure 1.18.[72,96] Using $[(bpy)_2Ru(dpp)]^{2+}$ as an example, when the ground state $[(bpy)_2Ru(dpp)]^{2+}$ absorbs photons from the visible light, it is excited to $Ru(d\pi) \rightarrow dpp(\pi^*)$ ^1MLCT excited state and converted to $Ru(d\pi) \rightarrow dpp(\pi^*)$ ^3MLCT excited state with unit efficiency through intersystem crossing. The ^3MLCT excited states of the monometallic system decay to the ground state by energy transfer to the molecular oxygen ($^3O_2$) to generate $^1O_2$ with the quenching rate constant $k_q = 1.1 \times 10^9\ dm^3\ mol^{-1}\ s^{-1}$ and singlet oxygen quantum yield $\Phi_\Delta = 0.31 \pm 0.2$. The reactive $^1O_2$ species cleave DNA.[101,102] The Figure 1.19 shows that the efficiency of DNA Photocleavage by Ru monometallic complexes increases in the order $[(bpy)_2Ru(dpp)]^{2+} < [(phen)_2Ru(dpp)]^{2+} < [(Ph_2phen)_2Ru(dpp)]^{2+}$.[96] The authors have attributed the different DNA photocleavage efficiency to the varied abilities to generate $^1O_2$.[103]

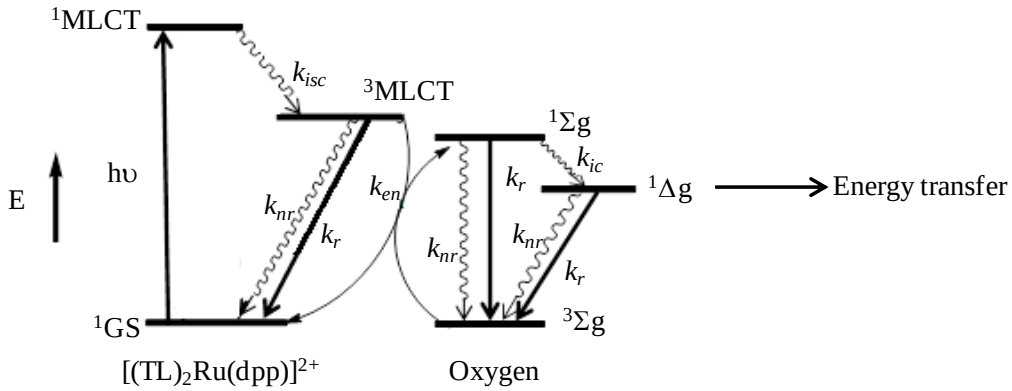

Figure 1.18. State diagram for a ruthenium monometallic complex undergoing photochemical reactions in energy transfer mechanism with different energy levels, TL = bpy, phen, and Ph_2phen, bpy = 2,2′-bipyridine, phen = 1,10-phenanthroline, Ph_2phen = 4,7-diphenyl-1,10-phenanthroline and dpp = 2,3-bis(2-pyridyl)pyrazine, ^{1}MLCT = singlet metal-to-ligand excited state, ^{3}MLCT = triplet metal-to-ligand excited state, ^{1}GS = singlet ground state, k_r = rate constant for radiative decay, k_{nr} = rate constant for non-radiative decay, k_{ic} = rate constant for internal conversion, k_{isc} = rate constant for intersystem crossing non-radiative decay, k_{en} = rate constant for energy transfer.

The ^{3}MLCT excited state of $[(bpy)_2Os(dpp)]^{2+}$ is also quenched by the molecular oxygen ($^3O_2$) to generate $^1O_2$ with singlet oxygen quantum yield Φ_Δ, which is equal to 0.05 ± 0.01.[103] Since the Os monometallic complexes have a shorter excited state lifetime compared to the Ru monometallics, the energy transfer process of the excited Os complex is not as favorable as the excited state Ru complexes. The interactions of $[(bpy)_2Os(dpp)]^{2+}$ with DNA have not been reported in the literature.

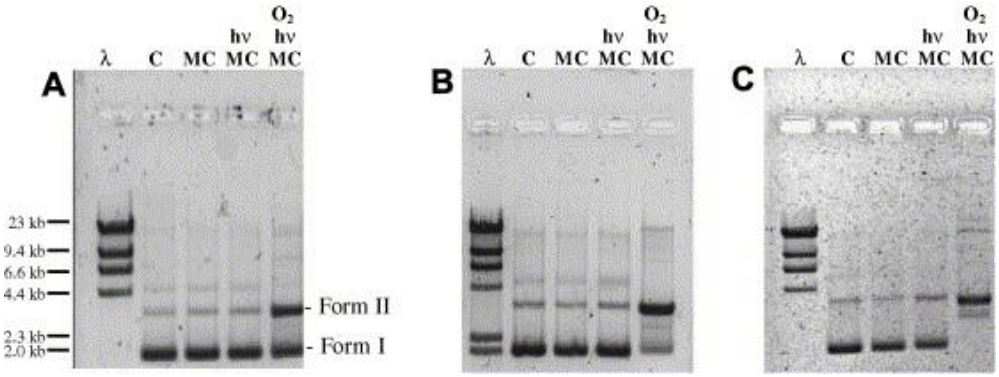

Figure 1.19. DNA photocleavage assay for the complexes $[(bpy)_2Ru(dpp)]^{2+}$ (A), $[(phen)_2Ru(dpp)]^{2+}$ (B), and $[(Ph_2phen)_2Ru(dpp)]^{2+}$ (C) using pUC18 circular plasmid DNA, 0.8% agarose gel electrophoresis, imaged with ethidium bromide staining, bpy = 2,2′-bipyridine, phen = 1,10-phenanthroline, Ph_2phen = 4,7-diphenyl-1,10-phenanthroline, and dpp = 2,3-bis(2-pyridyl)pyrazine. Lane λ is the λ molecular weight standard. Lane C is the DNA control showing pUC18 occurs in primarily the supercoiled (Form I) with minor nicked (Form II) components. Lane MC is 5:1 base pair (BP):metal complex (MC) dark control illustrating no dark modification of pUC18 by these metal complexes. Lane MC, hυ is 5:1 BP:MC photolyzed in the absence of molecular oxygen. Lane MC, hυ, O_2 is 5:1 BP:MC photolyzed in the presence of molecular oxygen illustrating that all three complexes photocleave DNA through an oxygen-mediated pathway. Reprinted from Mongelli, M. T.; Heinecke, J.; Mayfield, S; Okyere, B.; Winkel, B. S. J.; Brewer, K. J. *Journal of Inorganic Biochemistry* **2006**, *100*, 1983-1987, copyright 2006 with permission from ELSEVIER.[96]

1.5.4. Electronic Excited States and Photophysical Properties of Rh (III) Monometallic Complexes

Since the Rh(III) complex will be used herein as a reactive metal center to design Ru,Rh and Os,Rh bimetallic complexes which perform PDT function without molecular oxygen, it will be helpful to review the photophysical properties of Rh (III) monometallic complexes in literature (summarized in Table A-1). The Rh(III) monometallic complex *cis*-$[Rh(bpy)_2Cl_2]^+$ in aqueous solution displays two intense electronic absorption transitions at 300 nm ($\varepsilon = 2.3 \times 10^4\ M^{-1}cm^{-1}$) and 311 nm ($\varepsilon = 2.9 \times 10^4\ M^{-1}cm^{-1}$) assigned to bpy-based $\pi \rightarrow \pi^*$ Intraligand (IL) transitions, and a weak transition at 384 nm ($\varepsilon = 0.1 \times 10^3\ M^{-1}cm^{-1}$) attributed to Rh-based ligand field (LF) transition. No room temperature emission of $[Rh(bpy)_2Cl_2]^+$ is observed, while a 77 K emission

of $[Rh(bpy)_2Cl_2]^+$ displays at 704 nm with 27.2 μs lifetime from the d,d LF excited state.[92,104] The complex $[Rh(dpp)_2Cl_2]^+$ in CH_3CN solution shows two broad electronic absorption bands at 286 nm ($\varepsilon = 1.3 \times 10^3$ $M^{-1}cm^{-1}$) and 326 nm ($\varepsilon = 110$ $M^{-1}cm^{-1}$). No room temperature emission of $[Rh(dpp)_2Cl_2]^+$ is observed, but a 77 K emission of $[Rh(dpp)_2Cl_2]^+$ is shown at 704 nm with 19.6 μs lifetime from the LF excited state.[92]

The complex *cis*-$[Rh(phen)_2Cl_2]^+$ in aqueous solution displays several phen-based IL transitions at 273 nm ($\varepsilon = 6.5 \times 10^4$ $M^{-1}cm^{-1}$), 336 nm ($\varepsilon = 2.9 \times 10^3$ $M^{-1}cm^{-1}$) and 352 nm ($\varepsilon = 2.7 \times 10^3$ $M^{-1}cm^{-1}$). The complex also shows a weak transition at 385 nm ($\varepsilon = 110$ $M^{-1}cm^{-1}$) due to Rh-based LF transition. No room temperature emission of $[Rh(phen)_2Cl_2]^+$ is observed. However, $[Rh(phen)_2Cl_2]^+$ emits at 709 nm with 41.5 μs lifetime from the LF excited state at 77 K.[105-107] The *cis*-$[Rh(dppz)(phen)Cl_2]^+$ in 50 mM phosphate buffer solution shows two ligand-based IL transitions at 277 nm ($\varepsilon = 7.7 \times 10^4$ $M^{-1}cm^{-1}$), and 362 nm ($\varepsilon = 1.3 \times 10^4$ $M^{-1}cm^{-1}$) and a metal-based transition at 380 nm (1.4×10^3 $M^{-1}cm^{-1}$) assigned to Rh-based LF transition.[108] According to the steady-state emission spectroscopy of *cis*-$[Rh(dppz)(phen)Cl_2]^+$, no emission is observed at room temperatue, while, two emission bands emerge from two excited states at 77 K. One is a short-lived, structureless emission at 710 nm assigned to the ^{3}LF excited state, and the other is a long-lived structured emission at 554 nm due to the ^{3}IL excited state.[108] The Rh(III) monometallic complexes strongly absorb light in the UV region of the spectrum, but weakly absorb in visible region of the spectrum, and emit from the LF excited state. These photophysical properties will be considered to design Ru,Rh and Os,Rh bimetallic systems which perform PDT function in the visible light region.

1.5.5. Photochemical Properties of Rh (III) Monometallic Complexes

Morrison and coworkers reported that *cis*-$[Rh(phen)_2Cl_2]^+$ can covalently photobind to calf thymus DNA when it is excited by UV light.[107,109,110] The *cis*-$[Rh(phen)_2Cl_2]^+$ in the aqueous solution is excited to ^{3}LF excited state under the UV light irradiation, then loses photolabile chloride ligands[106] and coordinates to Lewis basic sites in DNA such as the bases and phosphate groups.[107] The proposed photobinding mechanism is illustrated in Figure 1.20. The ^{3}LF excited state of *cis*-$[Rh(phen)_2Cl_2]^+$ is quenched by the guanosine and adenosine bases in DNA and forms the rhodium bond without the presence of oxygen. Morrison and coworkers also observed that *cis*-$[Rh(dppz)(phen)Cl_2]^+$ could photobind to calf thymus DNA and photocleave supercoiled plasmid DNA in the presence of UV light.[108] The *cis*-$[Rh(dppz)(phen)Cl_2]^+$ accociates with DNA through the dppz ligand intercalating between DNA base pairs at the ground state. The complex photobinds to DNA by the photoaquation under the near UV light.[108] When *cis*-$[Rh(dppz)(phen)Cl_2]^+$ is excited by visible light, a dppz radical is formed, which abstracts hydrogen from the DNA backbone, causing DNA photocleavage. The result of irradiating *cis*-$[Rh(dppz)(phen)Cl_2]^+$ in the presence of supercoiled plasmid DNA suggests that the complex photocleaves DNA into relatively small (< 36 base pairs) fragments.[108] The Rh(III) monometallic complexes display photobinding and photocleavage interactions with DNA without molecular oxygen under the UV light irradiation, which are consistent with their photophysical properties.

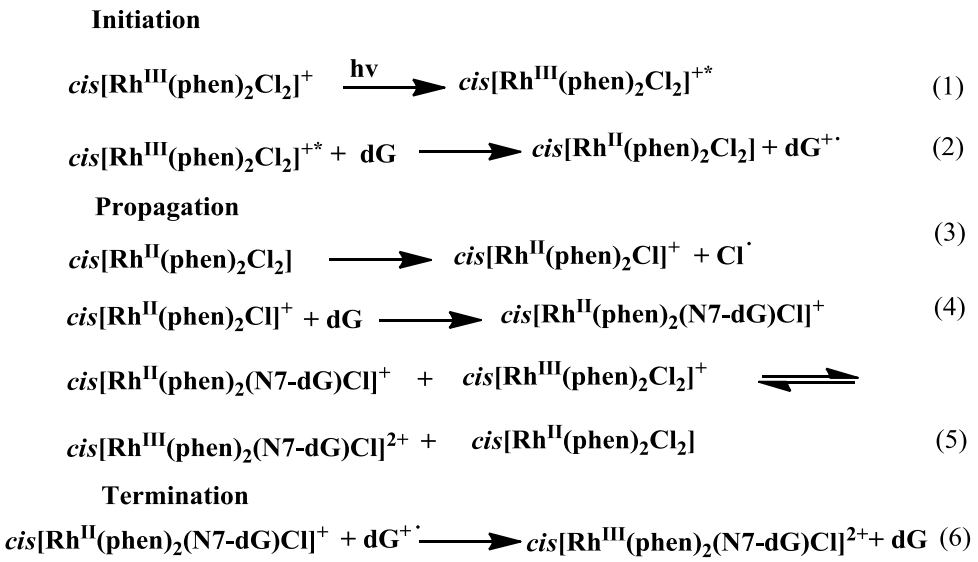

Figure 1.20. Proposed mechanism for the photo-induced binding of *cis*-$[Rh(phen)_2Cl_2]^+$ to DNA in the absence of molecular oxygen.[110] (dG is the guanosine base in DNA.)

1.5.6. Electronic Excited States and Photophysical Properties of Ru,Rh bimetallic Complex

The bimetallic complex $[(bpy)_2Ru(dpp)Rh(bpy)_2]^{5+}$ displays several intense electronic absorption transitions in the UV and visible region of the spectrum (Table A-1).[92] One (λ_{max}^{abs} = 295 nm, $\varepsilon = 1.2 \times 10^5\ M^{-1}cm^{-1}$) of two principal absorption bands in the UV region has been assigned to $\pi \rightarrow \pi^*$ IL transition on dpp and bpy ligands. The other band (λ_{max}^{abs} = 312 nm, $\varepsilon = 5.0 \times 10^4\ M^{-1}cm^{-1}$) is due to bpy based $\pi \rightarrow \pi^*$ transition for the bpy ligands bound to the Rh. The complex $[(bpy)_2Ru(dpp)Rh(bpy)_2]^{5+}$ displays a Ru→dpp CT transition at 514 nm ($\varepsilon = 1.4 \times 10^4\ M^{-1}cm^{-1}$) and a Ru→bpy CT transition at 351 nm ($\varepsilon = 1.7 \times 10^4\ M^{-1}cm^{-1}$) in the visible region. The complex $[(bpy)_2Ru(dpp)Rh(bpy)_2]^{5+}$ emits at 778 nm (τ = 37 ns) from room temperature acetonitrile complex solution. The 77 K emission of $[(bpy)_2Ru(dpp)Rh(bpy)]^{5+}$ in 4:1 v/v ethanol/methanol glass blue-shifts to 687 nm with a longer lifetime (τ = 1.7 μs). The MLCT absorption and emission of Ru,Rh bimetallic complex shift to the red region compared with

those of Ru(II) mononuclear analog. The excited-state lifetime is much shorter than that of mono and binuclear complexes of Ru(II), indicating that Ru(II)-polypyridyl excited states are quenched by the Rh(III) center efficiently.[92,111] When the light absorber $[(bpy)_2Ru(dpp)]^{2+}$coordinates to the Rh(III) center, the bimetallic system $[(bpy)_2Ru(dpp)Rh(bpy)_2]^{5+}$ strongly absorbs light in the UV and visible region of the spectrum, which is different from the Rh(III) monometallic complexes and will be used herein to design Ru,Rh bimetallic complexes which perform PDT function in the visible light region.

1.5.7. Electronic Excited States and Photophysical and Photochemical Properties of Trimetallic Complexes

Emission spectroscopy and excited state lifetime measurements are used to investigate the excited state dynamics of the trimetallic systems that motivated the studies herein (Table A-1).[15,112] The emission spectra of $[\{(bpy)_2Ru(dpp)\}_2RhCl_2]^{5+}$ were observed from room temperature acetonitrile solution and from 4:1 ethanol/ methanol glass at 77 K.[15] At room temperature, a weak ($\Phi^{em} = 1.9 \times 10^{-4}$) emission is shown ($\lambda_{RT}{}^{em} = 786$ nm, $\tau = 32$ ns), which is attributed to Ru→μ-dpp ^{3}MLCT emission. At 77 K, the emission displays a longer lifetime ($\tau =$ 1.8 μs) and blue-shifts to 730 nm also from the Ru→μ-dpp ^{3}MLCT excited state based on its similarity in energy and band shape to the model $[(bpy)_2Ru(dpp)Ru(bpy)_2]^{4+}$. The decreased τ and Φ^{em} at room temperature and the similarity at 77 K compared to the model system $[(bpy)_2Ru(dpp)Ru(bpy)_2]^{4+}$ are due to quenching of the ^{3}MLCT state through dpp to Rh through intramolecular electron transfer to populate the Ru→Rh ^{3}MMCT excited state at room temperature (Figure 1.21). The intramolecular electron transfer is allowed at room temperature in fluid media, and inhibited at 77 K in a rigid media due to large reorganization energy to

accommodate electrons transfer providing the trimetallic a similarity to the model system $[(bpy)_2Ru(dpp)Ru(bpy)_2]^{4+}$.[112]

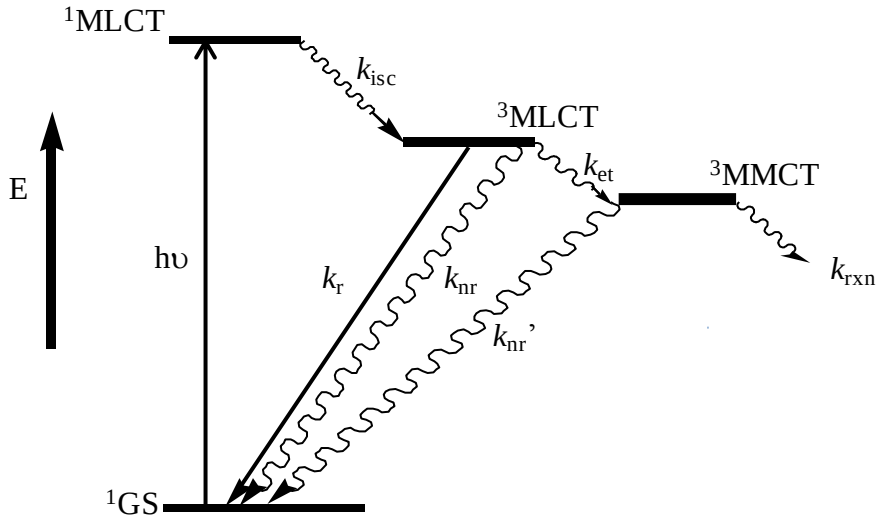

Figure 1.21. State diagram of trimetallic complex $[\{(bpy)_2Ru(dpp)\}_2RhCl_2]^{5+}$, ^{1}GS = singlet ground state, ^{1}MLCT = singlet metal-to-ligand charge transfer excited state, ^{3}MLCT = triplet metal-to-ligand charge transfer excited state, k_r = rate constant for radiative decay, k_{nr} = rate constant for non-radiative decay, k_{isc} = rate constant for intersystem crossing non-radiative decay, k_{et} = rate constant for electron transfer and k_{rxn} = rate constant for reaction decay. bpy = 2,2′-bipyridine, and dpp = 2,3-bis(2-pyridyl)pyrazine.

The trimetallic complex $[\{(bpy)_2Ru(dpp)\}_2RhCl_2]^{5+}$ is the first system which cleaves DNA via a Ru(dπ)→Rh(σ*) ^{3}MMCT excited state and this cleavage occurs via a novel oxygen independent mechanism using low energy visible light.[68,72] The effect on DNA photolysis in the presence of $[\{(bpy)_2Ru(dpp)\}_2RhCl_2]^{5+}$ was investigated by the agarose gel electrophoresis gel shift assays. The agarose gel electrophoresis is a common method to study the DNA modification. It can separate biological macromolecules including DNA, RNA and proteins according to their molecular size, shape, mass and charges by applying a potential to an agarose gel matrix. The electric field causes the charged biomolecule to migrate through a porous matrix. When a potential is applied, the negatively charged DNA moves toward the positive potential

electrode side with migration rate determined by the molecular size and shape of the DNA as well as the potential applied. The compact, supercoiled form DNA moves faster than open-circular relaxed form (Figure 1.22).[113] The agarose gel image in Figure 1.22 shows a molecular weight marker (lane λ), a DNA control (lane C), a complex/DNA solution at 1:5 metal complex: base pairs ratio in dark (lane MC) and a complex/DNA solution at 1:5 metal complex: base pairs ratio irradiated for 20 min under argon (lane hυ MC). The $[\{(bpy)_2Ru(dpp)\}_2RhCl_2]^{5+}$ complex photocleavage of pUC18 plasmid DNA was observed in an oxygen independent environment irradiated by light at $\lambda \geq 475$ nm in the complex/DNA solution at 1:5 metal complex: base pairs ratio for 20 min (lane hυ MC). The DNA photocleavage is supported by converting supercoiled pUC18 DNA (lane C) to its nicked open-circular relaxed form.[101] Since the open-circular relaxed form has a large size, it migrates more slowly than the native supercoiled DNA. The function of $[\{(bpy)_2Ru(dpp)\}_2RhCl_2]^{5+}$ complex, which photocleaves DNA with or without molecular oxygen via visible light excitation, is unusual. This complex is excited by low energy visible light into a Ru→μ-dpp ^{3}MLCT state, and then populates the ^{3}MMCT excited state via intramolecular electron transfer. The trimetallic complex $[\{(bpy)_2Ru(dpp)\}_2RhCl_2]^{5+}$ at the ^{3}MMCT excited state has a formally Ru^{III} and Rh^{II} center, both reactive centers; DNA cleavage likely occurs at the Rh^{II} site.[68]

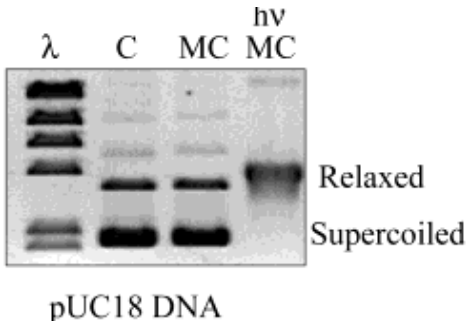

Figure 1.22. The imaged agarose gel showing the photocleavage of pUC18 plasmid DNA by $[\{(bpy)_2Ru(dpp)\}_2RhCl_2]^{5+}$. Lane λ is the molecular weight marker and lane C is the DNA control with no metal complex. Lane MC is a complex/DNA solution at 1:5 metal complex: base pairs ratio in dark and lane hυ MC is a complex DNA solution at 1:5 metal complex: base pairs ratio irradiated by light at $\lambda \geq 475$ nm for 20 min under argon, bpy = 2,2′-bipyridine, and dpp = 2,3-bis(2-pyridyl)pyrazine. Reprinted with permission from Holder, A. A.; Swavey, S.; Brewer, K. J. *Inorg. Chem.* **2004**, *43*, 303-308. Copyright 2004 American Chemical Society.[68]

The photodynamic therapy functions of $[\{(bpy)_2Ru(dpp)\}_2RhCl_2]^{5+}$ were further observed in African green monkey kidney epithelial (Vero) cell cultures, where Vero cells replicate rapidly doubling the cell population in 24 hours. The trimetallic complex, $[\{(bpy)_2Ru(dpp)\}_2RhCl_2]^{5+}$ can inhibit Vero cell growth *in vitro* after exposure to visible light ($\lambda > 460$ nm).[69] Vero cells were treated by 3.0-120 μM $[\{(bpy)_2Ru(dpp)\}_2RhCl_2]^{5+}$ with growth media solutions for 48 hours, Then the media was removed, and cells were treated with light for 4 minutes (light samples) or kept in dark (dark controls). After that the cells were incubated with fresh media for another 48 hours. The dark control (cells treated with metal complex but no light) and light control (cells treated with no metal complex but with light) showed normal growth, while Vero cells treated by different concentrations of $[\{(bpy)_2Ru(dpp)\}_2RhCl_2]^{5+}$, then exposed to light, show increased inhibition of cell replication as the complex concentration increased. The cell death was observed as shown in Figure 1.23, when the complex concentration is higher than 10 μM. The $[\{(bpy)_2Ru(dpp)\}_2RhCl_2]^{5+}$ displays high photo-toxicity and low dark-cytotoxicity to Vero cells further indication of an effective PDT agent.

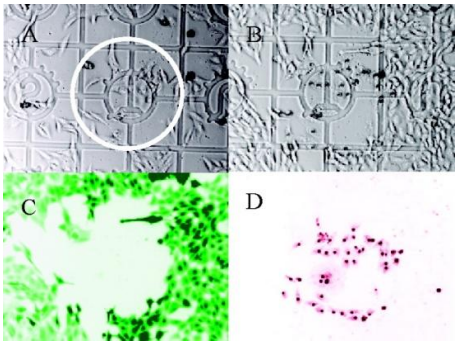

Figure 1.23. The micrographs of Vero cells after treatment of 122 μM $[\{(bpy)_2Ru(dpp)\}_2RhCl_2]^{5+}$, rinsing with a clean medium, irradiated by visible light ($\lambda > 460$ nm) for 4 min: (A) immediately after photolysis (the circle shows the border of the irradiation spot); (B) after a 48 h growth period in the dark; (C) after a 48 h growth period with live cell (green) visualization with calcein AM fluorescence; (D) after a 48 h growth period with dead cell (red) visualization with ethidium homodimer-1 fluorescence, bpy = 2,2′-bipyridine, and dpp = 2,3-bis(2-pyridyl)pyrazine. Reprinted with permission from Holder, A. A.; Zigler, D. F.; Tarrago-Trani, M. T.; Storrie, B.; Brewer, K. J. *Inorg. Chem.* **2007**, *46*, 4760-4762. Copyright 2007 American Chemical Societ.[69]

Other trimetallic complexes including $[\{(bpy)_2Os(dpp)\}_2RhCl_2]^{5+}$ and $[\{(tpy)_2RuCl(dpp)\}_2RhCl_2]^{3+}$ photocleave DNA under visible irradiation via an oxygen independent mechanism.[68]

1.6. Statement of Problem and Proposed Bimetallic Complex Structure

Ru,Rh,Ru and Os,Rh,Os trimetallic complexes couple two ruthenium polyazine light absorbers or two osmium polyazine light absorbers to a *cis*-$Rh^{III}Cl_2$ center through two dpp bridging ligands. They are good light absorbers and easily populate reactive ^{3}MMCT excited states and photocleave DNA under visible light irradiation via an oxygen independent mechanism. My research has focused on understanding of DNA interactions with new mixed-metal complexes such as Ru,Rh and Os,Rh bimetallic complexes, which are a new kind of molecular architecture. The bimetallic complexes which are designed based on the photolysical and photochemical properties of Ru(II), Os(II) and Rh(III) monometallic and trimetallic

complexes. The Ru and Os monometallic complexes strongly absorb visible light and photocleave DNA through $^1O_2$ generation via an energy transfer mechanism.[96] While, Rh(III) monometallic complexes display photobinding and photocleavage interactions with DNA without molecular oxygen under the UV light irradiation.[107,109,110] When the light absorber $[(bpy)_2Ru(dpp)]^{2+}$coordinates to the Rh(III) center, the bimetallic system $[(bpy)_2Ru(dpp)Rh(bpy)_2]^{5+}$ strongly absorbs light in the UV and visible region of the spectrum.[92]

The bimetallic complexes are designed to have only one light absorber attached to a *cis*-$Rh^{III}Cl_2$ center through a dpp bridging ligand, strongly absorb visible light, populate non-emissive ^{3}MMCT excited states and display efficient DNA photo-modifications without molecular oxygen as their trimetallic analogues. However, they have a sterically accessible Rh reactive center, and independently variable terminal ligand on the light absorbers and attached to Rh center. A series of bimetallic complexes $[(TL)_2M(dpp)RhCl_2(TL')]^{3+}$ (M = Ru and Os, TL = phen, Ph_2phen, Me_2phen and bpy, TL′ = phen, bpy and Me_2bpy, Me_2phen = 4,7-dimethyl-1,10-phenanthroline and Me_2bpy = 4,4′-dimethyl-2,2′-dipyridyl), as shown in Figure 1.24, are proposed to be synthesized and studied. The study of bimetallic complex DNA interactions will provide important information to understand mixed-metal complex DNA photo-modification process and to evaluate the effect of DNA modification by varying the complex structural subunits, which are useful for making a new generation PDT agent.

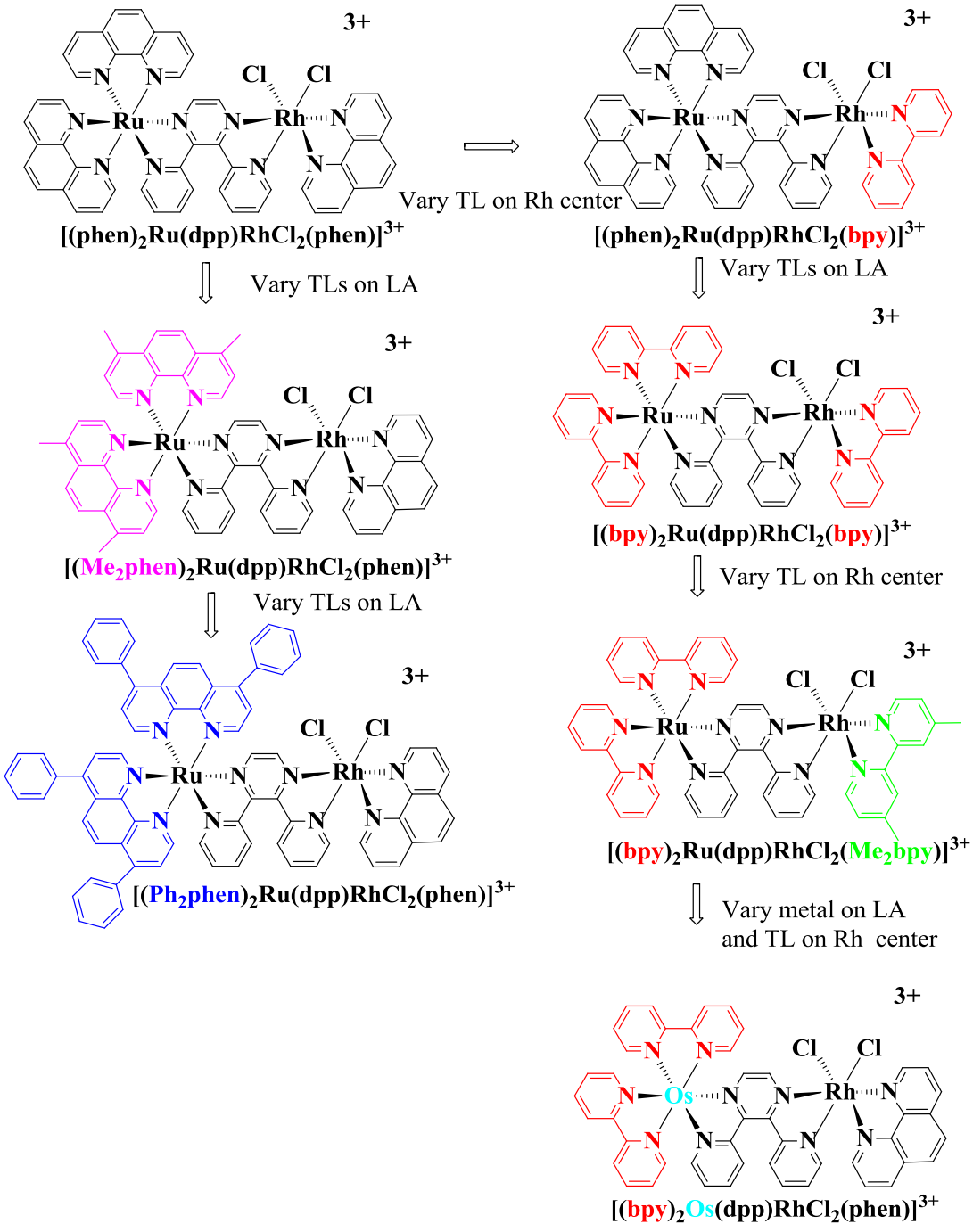

Figure 1.24. The structures of proposed bimetallic complexes $[(TL)_2M(dpp)RhCl_2(TL')]^{3+}$ (M = Ru and Os, TL = phen, Ph_2phen, Me_2phen and bpy, TL′ = phen, bpy and Me_2bpy).

Chapter 2. Experimental

2.1. Materials

All materials were used as received. The terminal ligand 4,4′-dimethyl-2,2′-dipyridyl (Me_2bpy), the bridging ligand 2,3-bis(2-pyridyl)pyrazine, and KPF_6 were purchased from Sigma-Aldrich (St. Louis, MO). Other terminal ligands including 2,2′-bipyridine (bpy), 1,10-phenanthroline (phen), 4,7-diphenyl-1,10-phenanthroline (Ph_2phen) and 4,7-dimethyl-1,10-phenanthroline (Me_2phen) and starting materials such as $RhCl_3 \cdot xH_2O$, $RuCl_3 \cdot xH_2O$ and LiCl were obtained from Alfa-Aesar (Ward Hill, MA). The starting material *cis*-dichlorobis(2,2′-bipyridine)ruthenium(II) dihydate $[(bpy)_2RuCl_2] \cdot 2H_2O$ was purchased from Strem Chemicals (Newburyport, MA). Adsorption alumina, HPLC grade acetone, toluene, HPLC grade methylene chloride, and anhydrous diethyl ether were purchased from Fisher (Fair Lawn, NJ). Other solvents including HPLC grade acetonitrile, spectrophotometric grade acetonitrile and ethylene glycol were purchased from Alfa-Aesar (Ward Hill, MA). *N*,*N*-dimethylformamide was obtained from Burdick & Jackson (Muskegon, MI). Electrochemical grade tetrabutylammonium hexafluorophosphate was purchased from Fluka (St. Louis, MO).

Electrophoresis grade agarose was obtained from Fisher Scientific (Fair Lawn, New Jersey). *Lambda* DNA/*HindIII* molecular weight marker, molecular biology grade boric acid and tri(hydroxymethyl)aminomethane (tris base) were purchased from Promega (Madison, WI). Plasmid pUC18 DNA was obtained from Bayou Biolabs (Harahan, LA) and calf thymus DNA

was purchased from Rockland. Ethidium bromide (10 mg/mL) solution was obtained from Biotium, Inc. Sodium phosphate buffer was obtained from Medicago (Uppsala, Sweden).

2.2. Synthesis

2.2.1. Monometallic Complexes

2.2.1.1. Synthesis of $[(bpy)_2Ru(dpp)](PF_6)_2$

A modified method developed by Gafney and coworkers was used to synthesize this monometallic complex.[83] 2.0 g (4.1 mmol) of $[(bpy)_2RuCl_2] \cdot 2H_2O$ and 1.5 g (6.4 mmol) of dpp were added to 90 mL 2:1 v/v ethanol/water in a 250 mL round bottom flask and heated at reflux for 3 hours. 20 mL of saturated KPF_6 aqueous solution (Aq.) was added to the room temperature reaction mixture to induce precipitation and stirred for 30 min. The crude product was collected via vacuum filtration and purified by column chromatography. The column chromatography was performed by using 30 cm methanol deactivated adsorption alumina column (2.5 cm diameter) with a 3:2 v/v toluene/acetonitrile as eluent. The methanol deactivated adsorption alumina was prepared beforehand by mixing 1000 g of adsorption alumina with 500 mL HPLC grade methanol and dried in air overnight. The crude product was dissolved in 10 mL eluent, filtered, and loaded on the column. The leading orange band was collected, using rotary evaporation to remove the solvent. A minimal amount of acetonitrile was added to the flask to dissolve the product which was added to 600 mL stirring anhydrous diethyl ether to induce precipitation. The bright orange color product (2.5 g, 2.7 mmol, 66% yield) was collected by vacuum filtration and dried under vacuum. The final product was checked by the electrochemistry. If any impurity was found, the product would be purified by the second time column chromatography. ESI-MS:

$[M-PF_6]^+$, m/z = 793.10. UV/vis (CH_3CN): λ^{abs}_{max} = 464 nm ($\varepsilon = 1.2 \times 10^4\ M^{-1}cm^{-1}$) and λ^{em}_{max} = 675 nm.

2.2.1.2. Synthesis of $[(phen)_2RuCl_2](PF_6)_2$

The synthetic procedure used to make starting material $[(phen)_2RuCl_2]$ is modified from the method of Meyer et al.[114] 3.0 g (11.5 mmol) of $RuCl_3 \cdot xH_2O$, 4.18 g (23.2 mmol) of phen and 6.15 g (145 mmol) of LiCl were combined in 30 mL dimethylformamide in a 100 mL round bottom flask. The mixture was heated at reflux with stirring for 8 hours. After being cooled, the mixture was added to ca. 200 mL acetone and placed in the freezer overnight. The mixture was added to 400 mL LiCl saturated aqueous solution stirring for 3 hours. The product was collected via vacuum filtration and rinsed with 400 mL water followed by 100 mL of anhydrous diethyl ether. The product of $[(phen)_2RuCl_2]$ (3.2 g, 6 mmol, 52% yield) was produced after drying in a desiccator overnight.

2.2.1.3. Synthesis of $[(phen)_2Ru(dpp)](PF_6)_2$

The synthesis of $[(phen)_2Ru(dpp)](PF_6)_2$ monometallic complex followed the method reported by Petersen et al.[80] 1.5 g (2.8 mmol) of $[(phen)_2RuCl_2]$ and 1.0 g (4.3 mmol) of dpp were combined with 60 mL 2:1 v/v ethanol/water in a 100 mL round bottom flask and heated to reflux for 3 hours. After being cooled, the product was flash precipitated by the addition of the reaction mixture to 20 mL of saturated KPF_6 (Aq.). The crude product was isolated by vacuum filtration and dried in a vacuum desiccator. The crude product was purified by column chromatography using 15 cm methanol deactivated adsorption alumina (4.0 cm diameter) with 3:2 v/v toluene/acetonitrile eluent. The desired product is an orange band, which elutes first. Rotary evaporation was used to remove the solvent. Column chromatography was repeated twice to

ensure purity. A minimal amount of acetonitrile ca. 10 mL was added to the flask to dissolve the product, then, added to 600 mL stirring anhydrous diethyl ether solution to induce precipitation. The bright orange color product (1.2 g, 1.9 mmol, 68% yield) was collected by vacuum filtration. ESI-MS: $[M-PF_6]^+$, m/z = 841.00. UV/vis (CH_3CN): λ^{abs}_{max} = 465 nm ($\varepsilon = 1.4 \times 10^4\ M^{-1}cm^{-1}$) and λ^{em}_{max} = 668 nm.

2.2.1.4. Synthesis of $[(Me_2phen)_2Ru(dpp)](PF_6)_2$

The synthesis of the starting material $[(Me_2phen)_2RuCl_2]$ is modified from the preparation of $(phen)_2RuCl_2$. 1.0 g (3.8 mmol) of $RuCl_3 \cdot xH_2O$ and 2.0 g (47.1 mmol) of LiCl were added to 50 mL DMF in a 100 mL round bottom flask. The mixture was heated to dissolve the salts. 1.3 g (6.25 mmol) of Me_2phen was added to the warm mixture solution. The reaction was heated to reflux for 5 hours. After being cooled, the mixture was split into two 500 mL separatory funnels with 150 mL of water and 200 mL of methylene chloride. The crude product was extracted 6 times from water by using methylene chloride. Methylene chloride solvent was removed by rotary evaporation. A minimal amount of methylene chloride (ca. 10 mL) was added to the flask to dissolve the residue, then, added to 600 mL of anhydrous diethyl ether solution, stirring to induce precipitation. The dark purple color product (1.5 g, 2.5 mmol, 67% yield) was collected by vacuum filtration.

The synthesis of $[(Me_2phen)_2Ru(dpp)](PF_6)_2$ monometallic complex was modified from the synthesis of $[(phen)_2Ru(dpp)](PF_6)_2$. 0.47 g (2.00 mmol) of dpp was dissolved in 50 mL ethanol in a 100 mL round bottom flask and heated to warm. Then, 0.60 g (1.02 mmol) of $[(Me_2phen)_2RuCl_2]$ was added to the mixture. The mixture solution continued to heat at reflux for 4 hours. After being cooled, 20 mL of saturated KPF_6 (Aq.) was added to the room

temperature product solution to induce precipitation and stirred for 30 min. The crude product was collected via vacuum filtration and purified by column chromatography on 15 cm methanol deactivated adsorption alumina column (2.5 cm diameter) with 1:1 v/v toluene/acetone eluent. The leading orange band was collected, using rotary evaporation to remove the solvent. A minimal amount of acetonitrile (ca. 10 mL) was added to the flask to dissolve the product, then, added to 600 ml of anhydrous diethyl ether solution, stirring to induce precipitation. The bright orange color product (0.54 g, 0.53 mmol, 52% yield) was collected by vacuum filtration. The final product was checked by the electrochemistry. If any impurity was found, the product would be purified by the second time column chromatography. ESI-MS: $[M-PF_6]^+$, m/z = 897.16.

2.2.1.5. Synthesis of $[(Ph_2phen)_2Ru(dpp)](PF_6)_2$

The synthesis of $[(Ph_2phen)_2Ru(dpp)](PF_6)_2$ monometallic complex through a modified previously reported method.[82,114] 0.90 g (3.4 mmol) of $RuCl_3 \bullet xH_2O$, 2.0 g (6.0 mmol) of Ph_2phen and 2.12 g (0.05 mol) of LiCl were combined in 100 mL DMF in a 250 ml round bottom flask. The mixture was heated at reflux with stirring for 8 hours. After being cooled, the mixture was poured into a large beaker containing ca. 100 mL acetone and placed in the freezer overnight. The mixture was added to 600 mL LiCl saturated aqueous solution stirring for 3 hours. The product was collected via vacuum filtration and was rinsed with 400 mL of water followed by 100 mL of anhydrous diethyl ether. The crude product $[(Ph_2phen)_2RuCl_2]$ was purified by column chromatography using a 15 cm methanol deactivated adsorption alumina column (4 cm diameter) with 4:1 v/v methylene chloride/acetone eluent. The leading purple band was collected, using rotary evaporation to remove the solvent. A minimal amount of methylene chloride (ca. 10 mL) was added to the flask to dissolve the residue, then, added to 600 mL

anhydrous diethyl ether solution, stirring to induce precipitation. The dark purple colored $[(Ph_2phen)_2RuCl_2]$ product (1.6 g, 1.9 mmol, 57% yield) was collected by vacuum filtration.

The synthesis of $[(Ph_2phen)_2Ru(dpp)](PF_6)_2$ monometallic complex was similar to the synthesis of $[(phen)_2Ru(dpp)](PF_6)_2$. 1.5 g (1.8 mmol) of $(Ph_2phen)_2RuCl_2$ and 0.86 g (3.6 mmol) of dpp were combined with 60 mL 2:1 v/v ethanol/water in a 100 mL round bottom flask and heated at reflux for 3 hours. After being cooled, the product was flash precipitated by the addition of the reaction mixture to 20 mL of saturated KPF_6 (Aq.). The crude product was isolated by vacuum filtration and dried in a vacuum desiccator. The crude product was purified by column chromatography using a 30 cm methanol deactivated adsorption alumina column (2.5 cm diameter) with 3:2 v/v toluene/acetonitrile eluent. The first purple band was discarded and the red band was collected. Column chromatography was repeated twice to ensure purity. The rotary evaporation was used to remove the solvent. A minimal amount of acetonitrile was added to the flask to dissolve the residue, then, added to 600 mL anhydrous diethyl ether solution, stirring to induce precipitation. The bright orange color product (1.3 g, 1.0 mmol, 56 % yield) was collected by vacuum filtration. ESI-MS: $[M-2PF_6]^{2+}$, m/z = 500.00. UV/visible (CH_3CN): λ^{abs}_{max} = 474 nm ($\varepsilon = 1.5 \times 10^4\ M^{-1}cm^{-1}$) and λ^{em}_{max} = 664 nm.

2.2.1.6. Synthesis of $[(bpy)_2Os(dpp)](PF_6)_2$

The synthesis of $[(bpy)_2Os(dpp)](PF_6)_2$ monometallic synthon was a modified synthesis from the previous previously reported methods.[85,86] 1.0 g (2.2 mmol) of $(NH_3)_2OsCl_6$ and 0.72 g (4.4 mmol) of bpy were added to 50 mL deoxygenated ethylene glycol in a 100 mL round bottom flask under argon and heated at reflux for 45 min. After being cooled, 50 mL of saturated $Na_2S_2O_4$ aqueous solution was added to the room temperature product solution and kept stirring

for 30 min under argon. The purple-black color [$(bpy)_2OsCl_2$] was collected via vacuum filtration and washed by large amount of water ca. 600 mL to remove $[(bpy)_3Os]^{2+}$ followed by 200 mL anhydrous diethyl ether. The starting material [$(bpy)_2OsCl_2$] (0.8 g, 1.4 mmol, 63% yield) was synthesized.

0.62 g (2.65 mmol) of dpp was dissolved in 30 mL ethylene glycol in a 100 mL round bottom flask and heated to warm. Then 0.60 g (1.05 mmol) of [$(bpy)_2OsCl_2$] was added to the warm mixture. The mixture solution continued to heat at reflux for 1 hour. After being cooled, 20 mL of saturated KPF_6 (Aq.) was added to the room temperature product solution and kept stirring for 30 min to induce precipitation. The crude product was collected via vacuum filtration and purified by column chromatography using a 15 cm methanol deactivated adsorption alumina column (2.5 cm diameter) with 3:2 v/v toluene/acetonitrile eluent. The leading brown band was collected, using rotary evaporation to remove the solvent. Column chromatography was repeated twice to ensure purity. A minimal amount of acetonitrile was added to the flask to dissolve the product, then added to 600 mL anhydrous diethyl ether solution, stirring to induce precipitation. The dark green colored product [$(bpy)_2Os(dpp)](PF_6)_2$ (0.72 g, 0.70 mmol, 67% yield) was collected by vacuum filtration. ESI-MS: $[M-PF_6]^+$, m/z = 883.16. UV/vis (CH_3CN): λ^{abs}_{max} = 486 nm ($\varepsilon = 1.3 \times 10^4\ M^{-1}cm^{-1}$) and λ^{em}_{max} = 640 nm.

2.2.1.7. Synthesis of K[Rh(phen)Cl_4]

The synthetic procedure of K[Rh(phen)Cl_4] •$3H_2O$ was through a modified procedure reported by McKenzie and Plowman.[115] 0.67 g (3.2 mmol) of $RhCl_3$·• xH_2O was dissolved in 30 mL of 2 M HCl. After heating ca. 2 hours at 95 °C, 1.8 g (10 mmol) of phen in 10 mL of 2 M HCl was added dropwise to the stirring salt solution. The mixture was kept stirring for 2 hours

and cooled to room temperature. The resulted orange precipitate was collected via vacuum filtration and was dissolved in 20 mL 10 M HCl at 95 °C with stirring for 0.5 hour. Then, the insoluble material was removed by hot vacuum filtration. The orange filtrate was cooled to room temperature, and further with an ice bath to form crystals. The obtained orange crystals were collected by vacuum filtration and were dissolved in a minimal amount of hot 5 M HCl (ca. 5 mL) and added dropwise to 20 ml of saturated KCl in 5 M HCl solution to induce precipitation. The orange crystalline product $K[Rh(phen)Cl_4] \cdot 3H_2O$ (0.80 g 1.54 mmol, 48% yield) was collected by vacuum filtration followed by 10 mL acetone and 30 mL diethyl ether rinse.[15] Rh analysis: Calculated Rh 19.9%, Determined 19.9%.

2.2.1.8. Synthesis of $K[Rh(bpy)Cl_4]$

The preparation of $[Rh^{III}(NN)L_4]^-$ systems in complicated by the tendency of halide starting materials to form $[Rh^{III}(NN)_2L_2]^+$ systems.[115] Complicated procedures using high concentrated halide in acidic conditions are employed. The synthetic procedure of $K[Rh(bpy)Cl_4] \cdot H_2O$ was the similar procedure for preparing $K[Rh(phen)Cl_4] \cdot 3H_2O$.[15] 0.67 g (3.2 mmol) of $RhCl_3 \cdot xH_2O$ was dissolved in 30 mL of 2 M HCl. After heating ca. 2 hours at 95 °C, 1.56 g (10 mmol) of bpy in 10 mL of 2 M HCl was added to the stirring salt solution. The mixture was kept stirring for 0.5 hours and cooled to room temperature. The resulted orange precipitate was collected via vacuum filtration and was dissolved in 10 mL 10 M HCl at 95 °C with stirring for 0.5 hour. Then, the insoluble material was removed by hot vacuum filtration. The orange filtrate was cooled to room temperature, and further with an ice bath to form crystals. The resulted orange crystals were collected by vacuum filtration and were dissolved in a minimal amount of hot 5 M HCl (ca. 5 mL) and added dropwise to 20 mL of saturated KCl in 5 M HCl solution to induce

precipitation. The orange crystaline product $K[Rh(bpy)Cl_4]$ $\cdot H_2O$ (0.87 g 1.9 mmol, 59% yield) was collected by vacuum filtration followed by 10 mL acetone and 30 mL diethyl ether rinse. ESI-MS: $[M+Na]^+$, m/z = 478.80. Rh analysis: Calculated Rh 22.6%, Determined 22.6%.

2.2.1.9. Synthesis of $[(bpy)RhCl_3(CH_3OH)] \cdot CH_3OH$

The synthesis of $[(bpy)RhCl_3(CH_3OH)] \cdot CH_3OH$ complex was modified from the method reported by Sheldrick et al.[116] 200 mg (0.76 mmol) of $RhCl_3 \cdot xH_2O$ was added to 30 mL methanol in a 100 mL round bottom flask. The red color solution was heated to reflux. 118.6 mg (0.76 mmol) of bpy in 10 mL methanol was added dropwise to the refluxing solution. The reaction was heated at reflux for an additional 3 hours. After being cooled to room temperature, the small amount of orange precipitate that formed was removed by vacuum filtration. The bright orange color filtrate was left to stand at RT for 12 hours to form crystals. The crystals were collected by vacuum filtration and are reported to be able to manually separate to *fac*-$[(bpy)RhCl_3(CH_3OH)] \cdot CH_3OH$ and *mer*-$[(bpy)RhCl_3(CH_3OH)] \cdot CH_3OH$ isomers, but that process was not used herein. The total 77% yield of $[(bpy)RhCl_3(CH_3OH)] \cdot CH_3OH$ including *fac* and *mer* isomers (253 mg, 0.59 mmol) was synthesized. ^{1}H-NMR (DMSO-d_6, 400 MHz, 293 K): δ = 3.53 (s, 3H, $MeOH_{Rh}$), 7.80 (t, 1H, bpy-H8), 7.91 (t, 1H, bpy-H3), 8.30 (m, 2H, bpy-H4/H7), 8.66 (m, 2H, bpy-H5/H6), 8.90 (d, 1H, bpy-H2), 9.59 (d, 1H, bpy-H9) shown in Apendix, Figure A-1. ESI-MS: $[M-CH_3OH+NH_4]^+$, m/z = 413.94.

2.2.1.10. Synthesis of $[(Me_2bpy)RhCl_3(CH_3OH)] \cdot CH_3OH$

The synthesis of $[(Me_2bpy)RhCl_3(CH_3OH)] \cdot CH_3OH$ complex was the similar method for preparing $[(bpy)RhCl_3(CH_3OH)] \cdot CH_3OH$.[116,117] 100 mg (0.38 mmol) of $RhCl_3 \cdot xH_2O$ was

added to 30 mL v/v methanol/ methylene chloride in a 100 mL round bottom flask. The red color solution was heated to warm. Then, 70 mg (0.38 mmol) of Me_2bpy in 10 mL v/v methanol/ methylene chloride was added dropwise to the warm solution. The reaction was heated at reflux for 3 hours. The orange color product solution was cooled to room temperature. The small amount of orange precipitate was removed by vacuum filtration. The bright orange color filtrate was left to stand at RT for 12 hours to form crystals. The crystals (113 mg, 0.25 mmol, 66% yield) were collected by vacuum filtration. The crystals of $[(Me_2bpy)RhCl_3(CH_3OH)] \cdot CH_3OH$ including *fac* and *mer* isomers can be used to make bimetallic complex. ^{1}H-NMR (DMSO-d_6, 400 MHz, 293 K): δ = 2.49 (s, 6H, 2Me), 3.50 (s, 3H, $MeOH_{Rh}$), 7.64 (d, 1H, Me_2bpy-H8), 7.74 (d, 1H, Me_2bpy-H3), 8.50 (s, 1H, Me_2bpy-H6), 8.55 (s, 1H, Me_2bpy-H5), 8.71 (d, 1H, Me_2bpy-H2), 9.37 (d, 1H, bpy-H9), shown in Apendix, Figure A-2. ESI-MS: $[M+NH_4]^+$, m/z = 441.97.

2.2.2. Bimetallic Complexes

2.2.2.1. Synthesis of $[(phen)_2Ru(dpp)RhCl_2(bpy)](PF_6)_3$

Cis-$Rh^{III}Cl_2$ subunit containing complexes are not typically amenable to typical chromatography. So synthesis is designed carefully to allow purification by recrystallization or washing. The bimetallic complex $[(phen)_2Ru(dpp)RhCl_2(bpy)](PF_6)_3$ was synthesized using a method previously developed in our laboratory.[15] The Rh based starting material $K[(bpy)RhCl_4] \cdot H_2O$ (0.055 g, 0.12 mmol),[115] was dissolved in an enthanol:water (10 mL:5 mL) mixture. The monometallic complex $[(phen)_2Ru(dpp)](PF_6)_2$,[80] (0.100 g, 0.101 mmol) was added to the bright yellow color solution. The resulting dark brown color mixture was heated at reflux for 45 minutes and converted to purple color. The mixture was cooled to room temperature and precipitated in a 20 mL NH_4PF_6 (Aq.) (1 g, excess). The purple precipitation was isolated using

vacuum filtration. The crude product was dissolved in ca. 5 mL of acetone, syringe filtered and reprecipitated in ca. 400 mL of diethyl ether with the product collected by vacuum filtration. Further purification of $[(phen)_2Ru(dpp)RhCl_2(bpy)](PF_6)_3$ to remove small amounts of ruthenium monometallic synthron for the emission spectroscopy was achieved upon recrystallization from ca. 100 mL of hot ethanol. After being cooled to room temperature, the precipitate was collected by vacuum filtration, dissolved in ca. 5 mL of acetone and flash precipitated in ca. 400 mL of diethyl ether and dried under vacuum, Yield = 0.10 g, 0.068 mmol (67%), ESI-MS: $[M\text{-}PF_6]^+$, m/z = 1314.97. UV/vis (CH_3CN): λ^{abs}_{max} = 505 nm ($\varepsilon = 1.4 \times 10^4\ M^{-1}cm^{-1}$).[118]

2.2.2.2. Synthesis of $[(phen)_2Ru(dpp)RhCl_2(phen)](PF_6)_3$

The synthesis of the bimetallic complex $[(phen)_2Ru(dpp)RhCl_2(phen)](PF_6)_3$ was a similar method for preparing $[(phen)_2Ru(dpp)RhCl_2(bpy)](PF_6)_3$.[15,118] $K[(phen)RhCl_4] \cdot 3H_2O$ (0.1 g, 0.19 mmol) and the monometallic complex $[(phen)_2Ru(dpp)](PF_6)_2$,[80] (0.106 g, 0.11 mmol) was dissolved in an enthanol:water (20 mL:10 mL) mixture. The mixture solution was slowly heated to reflux to make sure all starting materials dissolved before reaching reaction temperature. The solution was heated at reflux for 45 minutes. The purple color product solution was cooled to room temperature and precipitated in a 20 mL NH_4PF_6 (Aq.) (1 g, excess). The purple precipitate was isolated using vacuum filtration. The crude product was dissolved in ca. 5 mL of acetone, syringe filtered and reprecipitated in ca. 400 mL of diethyl ether with the product collected by vacuum filtration. The crude $[(phen)_2Ru(dpp)RhCl_2(phen)](PF_6)_3$ was dissolved in ca. 100 mL of boiling absolute ethanol for 15 min. After being cooled to room temperature, the precipitate was collected by vacuum filtration, dissolved in ca. 5 mL of acetone and flash precipitated in ca. 400 mL of diethyl ether. The final product was filtrated and dried under vacuum. Yield = 0.14 g, 0.10

mmol (77%), ESI-MS: $[M\text{-}PF_6]^+$, m/z = 1339.97. UV/vis (CH_3CN): λ^{abs}_{max} = 508 nm ($\varepsilon = 1.9 \times 10^4\ M^{-1}cm^{-1}$).

2.2.2.3. Synthesis of $[(Me_2phen)_2Ru(dpp)RhCl_2(phen)](PF_6)_3$

The synthesis of the bimetallic complex $[(Me_2phen)_2Ru(dpp)RhCl_2(phen)](PF_6)_3$ was a similar method for preparing $[(phen)_2Ru(dpp)RhCl_2(phen)](PF_6)_3$.[15,118] $K[(phen)RhCl_4] \cdot 3H_2O$ (0.1 g, 0.19 mmol) was heated to warm in an enthanol:water (20 mL:10 mL) mixture. The monometallic complex $[(Me_2phen)_2Ru(dpp)](PF_6)_2$, (0.166 g, 0.16 mmol) was added to the bright yellow solution and the mixture was heated at reflux for 45 minutes. The purple color product solution was cooled to room temperature and precipitated in 20 mL NH_4PF_6 (Aq.) (1 g, excess). The purple precipitate was isolated using vacuum filtration. The purification procedure was the same as the $[(phen)_2Ru(dpp)RhCl_2(phen)](PF_6)_3$. The crude product was dissolved in ca. 5 mL of acetone, syringe filtered and reprecipitated in ca. 400 mL of diethyl ether with the product collected by vacuum filtration. The crude $[(Me_2phen)_2Ru(dpp)RhCl_2(phen)](PF_6)_3$ was dissolved in ca. 100 mL of boiling absolute ethanol for 15 min. After being cooled to room temperature, the precipitate was collected by vacuum filtration, dissolved in ca. 5 mL of acetone and flash precipitated in ca. 400 mL of diethyl ether. The final product was filtrated and dried under vacuum. Yield = 0.16 g, 0.15 mmol (65%), ESI-MS: $[M\text{-}PF_6]^+$, m/z = 1395.03. UV/vis (CH_3CN): λ^{abs}_{max} = 516 nm ($\varepsilon = 1.6 \times 10^4\ M^{-1}cm^{-1}$).

2.2.2.4. Synthesis of $[(Ph_2phen)_2Ru(dpp)RhCl_2(phen)](PF_6)_3$

The synthesis of the bimetallic complex $[(Ph_2phen)_2Ru(dpp)RhCl_2(phen)](PF_6)_3$ was a similar method for preparing $[(phen)_2Ru(dpp)RhCl_2(phen)](PF_6)_3$.[15,118] $K[(phen)RhCl_4] \cdot 3H_2O$ (0.1 g,

0.19 mmol) and the monometallic complex $[(Ph_2phen)_2Ru(dpp)](PF_6)_2$, (0.206 g, 0.16 mmol) was dissolved in an enthanol:water (20 mL:10 mL) mixture. The dark brown mixture was heated at reflux for 45 minutes. The reddish product solution was cooled to room temperature and precipitated in 20 mL NH_4PF_6 (Aq.). The red precipitate was isolated using vacuum filtration. The purification procedure was the same as the $[(phen)_2Ru(dpp)RhCl_2(phen)](PF_6)_3$. The crude product was dissolved in ca. 5 mL of acetone, syringe filtered and reprecipitated in ca. 400 mL of diethyl ether with the product collected by vacuum filtration. Further purification of $[(Ph_2phen)_2Ru(dpp)RhCl_2(phen)](PF_6)_3$ to remove small amounts of ruthenium monometallic synthron for the emission spectroscopy was achieved upon recrystallization from ca. 100 mL of hot ethanol. After being cooled to room temperature, the precipitate was collected by vacuum filtration, dissolved in ca. 5 mL of acetone and flash precipitated in ca. 400 mL of diethyl ether, filtered and the red violet product was dried under vacuum, Yield = 0.19 g, 0.11 mmol (66%), ESI-MS: $[M\text{-}PF_6]^+$, m/z = 1644.09. UV/vis (CH_3CN): λ^{abs}_{max} = 515 nm ($\varepsilon = 1.7 \times 10^4\ M^{-1}cm^{-1}$).

2.2.2.5. Synthesis of $[(bpy)_2Ru(dpp)RhCl_2(bpy)](PF_6)_3$

The synthesis of the bimetallic complex $[(bpy)_2Ru(dpp)RhCl_2(bpy)](PF_6)_3$ was a similar method for preparing $[(phen)_2Ru(dpp)RhCl_2(bpy)](PF_6)_3$.[15,118] $K[(bpy)RhCl_4] \cdot H_2O$ (0.1 g, 0.22 mmol) was dissolved in an enthanol:water (20 mL:10 mL) mixture. The monometallic complex $[(bpy)_2Ru(dpp)](PF_6)_2$, (0.168 g, 0.18 mmol) was added to the bright yellow color mixture and the reaction solution was slowly heated to reflux to make sure all starting materials dissolved before reaching reaction temperature. The reaction solution was heated at reflux for 45 minutes. The purple color product solution was cooled to room temperature and precipitated in a 20 mL NH_4PF_6 (Aq.) (1 g, excess). The purple precipitate was isolated using vacuum filtration.

The purification procedure was the same as the $[(phen)_2Ru(dpp)RhCl_2(bpy)](PF_6)_3$. Yield = 0.18 g, 0.13 mmol (71%), ESI-MS: $[M\text{-}PF_6]^+$, m/z = 1266.97. UV/vis (CH_3CN): λ^{abs}_{max} = 510 nm ($\varepsilon = 1.3 \times 10^4\ M^{-1}cm^{-1}$).

2.2.2.6. Synthesis of $[(bpy)_2Ru(dpp)RhCl_2(Me_2bpy)](PF_6)_3$

The synthesis of the bimetallic complex $[(bpy)_2Ru(dpp)RhCl_2(Me_2bpy)](PF_6)_3$ was a close method for preparing $[(phen)_2Ru(dpp)RhCl_2(bpy)](PF_6)_3$.[15,118] $[(Me_2bpy)RhCl_3(CH_3OH)] \cdot CH_3OH$ (60 mg, 0.13 mmol) prepared by the previously reported method,[116] was heated to warm in an enthanol:water (20 mL:10 mL) mixture. The monometallic complex $[(bpy)_2Ru(dpp)](PF_6)_2$, (100 mg, 0.11 mmol) was added to the bright yellow color mixture. The reaction solution was slowly heated to reflux to make sure all starting materials dissolved before reaching reaction temperature. The reaction solution was heated at reflux for 45 minutes. The mixture was cooled to room temperature and precipitated in a 20 mL NH_4PF_6 (Aq.) (1 g, excess). The purple precipitate was isolated using vacuum filtration. The purification procedure was the same as the $[(phen)_2Ru(dpp)RhCl_2(bpy)](PF_6)_3$. Yield = 0.12 g, 0.083 mmol (75%), ESI-MS: $[M\text{-}PF_6]^+$, m/z = 1294.99. UV/vis (CH_3CN): λ^{abs}_{max} = 506 nm ($\varepsilon = 1.5 \times 10^4\ M^{-1}cm^{-1}$).

2.2.2.7. Synthesis of $[(bpy)_2Os(dpp)RhCl_2(phen)](PF_6)_3$

The Os,Rh bimetallic complex $[(bpy)_2Os(dpp)RhCl_2(phen)](PF_6)_3$ was synthesized using a method recently developed in our laboratory.[119] 0.10 g (0.10 mmol) of $[(bpy)_2Os(dpp)](PF_6)_2$[85,86] and 0.060 g (0.12 mmol) of $K[Rh(phen)Cl_4]$[15] were heated to reflux under Ar in a 30 mL ethanol:water v/v(2:1) solution for 75 min. After being cooled to the room temperature, the dark purple mixture solution was added dropwise into a saturated aqueous solution of NH_4PF_6 (20 mL) to induce precipitation. The precipitate was collected by vacuum filtration and was

dissolved in ca. 10 mL acetone, syringe filtered, reprecipitated in ca. 600 mL diethyl ether and collected by vacuum filtration. The crude $[(bpy)_2Os(dpp)RhCl_2(phen)](PF_6)_3$ was dissolved in ca. 100 mL of boiling absolute ethanol for 15 min. After being cooled to room temperature, the recrystallized product was collected by vacuum filtration, dissolved in ca. 10 mL acetone, precipitated in ca. 500 mL diethyl ether, collected by vacuum filtration and dried under vacuum. Yield = 0.11 g, 0.075 mmol (75 %), ESI-MS: $[M\text{-}PF_6]^+$, m/z = 1381.03. UV/vis (CH_3CN): λ^{abs}_{max} = 521 nm ($\varepsilon = 1.8 \times 10^4\ M^{-1}cm^{-1}$).[119]

2.2.3. Trimetallic Complexes

2.2.3.1. Synthesis of $[\{(bpy)_2Ru(dpp)\}_2RhCl_2](PF_6)_5$

The synthesis of the trimetallic complex $[\{(bpy)_2Ru(dpp)\}_2RhCl_2](PF_6)_5$ used a method previously developed in our laboratory.[70] $[(bpy)_2Ru(dpp)](PF_6)_2$ (0.20 g, 0.22 mmol) and $RhCl_3 \bullet xH_2O$ (0.03 g, 0.11 mmol) were dissolved in 30 mL 2:1 v/v ethanol/water in a 100 mL round bottom flask and heated at reflux for 1 hour. After being cooled, the product was flash precipitated by the addition of the reaction mixture to 20 mL of saturated NH_4PF_6 (Aq.). The precipitate was collected by vacuum filtration and was dissolved in ca. 10 mL acetone, syringe filtered, reprecipitated in ca. 600 mL diethyl ether and collected by vacuum filtration. The crude product was further purified by the recrystallization in ca. 100 mL hot ethanol. The recrystallized product was collected by vacuum filtration, dissolved in ca. 10 mL acetone, precipitated in ca. 500 mL diethyl ether collected by vacuum filtration and dried under vacuum. Yield = 0.17 g, 0.077 mmol (70 %). ESI-MS: $[M\text{-}PF_6]^+$, m/z = 2048.96. UV/vis (CH_3CN): λ^{abs}_{max} = 518 nm ($\varepsilon = 2.6 \times 10^4\ M^{-1}cm^{-1}$).

2.2.3.2. Synthesis of $[\{(phen)_2Ru(dpp)\}_2RhCl_2](PF_6)_5$

The trimetallic complex of $[\{(phen)_2Ru(dpp)\}_2RhCl_2](PF_6)_5$ was synthesized using a method reported from our laboratory.[120] 0.30 g (0.30 mmol) of $[(phen)_2Ru(dpp)](PF_6)_2$[80] and 0.045 g (0.22 mmol) of $RhCl_3 \bullet xH_2O$ were heated at reflux in a 30 mL ethanol:water v/v (2:1) solution for 1 hour. After being cooled to room temperature, the mixture solution was added dropwise into a 20 mL saturated NH_4PF_6 (Aq.) to induce the precipitate. The purification procedure was the same as $[\{(bpy)_2Ru(dpp)\}_2RhCl_2](PF_6)_5$. The precipitate was collected by vacuum filtration and was dissolved in ca. 10 mL acetone, syringe filtered, reprecipitated in ca. 600 mL diethyl ether and collected by vacuum filtration. The crude product was further purified by the recrystallization in ca. 100 mL hot ethanol. The recrystallized product was collected by vacuum filtration, dissolved in ca. 10 mL acetone, precipitated in ca. 500 mL diethyl ether collected by vacuum filtration and dried under vacuum. Yield = 0.26 g, 0.11 mmol (75%), ESI-MS: $[M-PF_6]^+$, m/z = 2145.00. UV/vis (CH_3CN): λ^{abs}_{max} = 520 nm ($\varepsilon = 2.6 \times 10^4\ M^{-1}cm^{-1}$).

2.2.3.3. Synthesis of $[\{(bpy)_2Os(dpp)\}_2RhCl_2](PF_6)_5$

The synthesis of $[\{(bpy)_2Os(dpp)\}_2RhCl_2](PF_6)_5$ used a modified method previously reported from our laboratory.[68] 0.40 g (0.39 mmol) of $[(bpy)_2Os(dpp)](PF_6)_2$[85,86] and 0.054 g (0.26 mmol) of $RhCl_3 \bullet xH_2O$ were heated at reflux under argon in a 40 mL ethanol:water v/v (2:1) solution for 75 min. After being cooled to the room temperature, the mixture solution was added dropwise to a 20 mL saturated NH_4PF_6 (Aq.) to induce precipitation. The purification procedure was the same as $[\{(bpy)_2Ru(dpp)\}_2RhCl_2](PF_6)_5$. Yield = 0.24 g, 0.10 mmol (77%) ESI-MS: $[M-PF_6]^+$, m/z = 2227.00. UV/vis (CH_3CN): λ^{abs}_{max} = 534 nm ($\varepsilon = 3.6 - 10^4\ M^{-1}cm^{-1}$).

2.3. Characterization Methods

2.3.1. ESI-mass Spectrometry

Electrospray ionization (ESI) mass spectrometry was performed in the Virginia Tech Chemistry Department Analytical Service Lab using an Agilent Technologies 6220 Accurate-Mass TOF LC-MS. The samples were dissolved in acetonitrile solvent and either directly injected into the instrument or further diluted by using acetonitrile or methanol as solvents. The mixed metal polyazine samples show isotopic patterns with loss of PF_6^- group and intact ligands. The sample isotopic patterns are consistent with the proposed complex structures and are included in the Appendix.

2.3.2. Electrochemistry

The electrochemistry experiments were performed using a Bioanalytical Systems (BAS) Epsilon potentiostat with a three-electrode system. Cyclic voltammetry (CV) was conducted with three electrodes system shown in Figure 2.1, including a platinum disk or glassy carbon working electrode, a platinum wire auxiliary electrode and a Ag/AgCl reference electrode or a Ag wire pseudo reference electrode. The reference electrodes were calibrated against the $FeCp_2/FeCp_2^+$ redox couple ($E_{1/2}$ of $FeCp_2^{0/+}$ = 0.46 vs. Ag/AgCl with 3 M NaCl solution)[121,122] in 0.1 M Bu_4NPF_6 spectrophotometric grade acetonitrile solution. A typical potential scan rate of CV is 100 mV/s. The scan rate can also be changed according to the redox behavior of the sample. The sample was analyzed after the electrolyte solution was deoxygenated by argon and the background scan was performed. Typically $E_{1/2}$ is determined ± 10 mV.

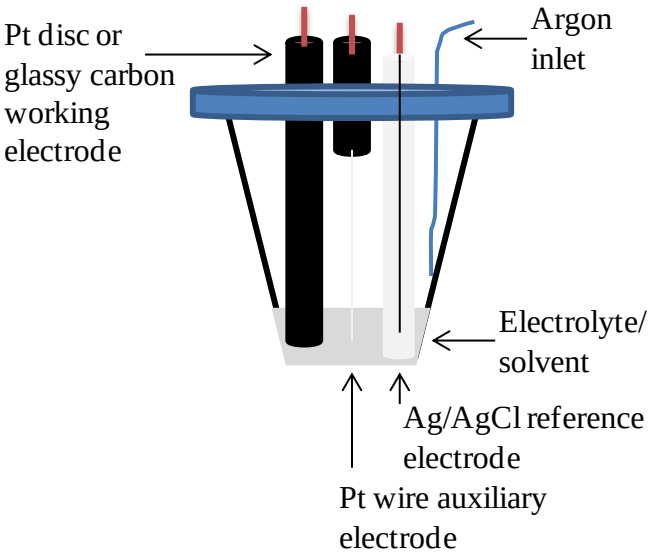

Figure 2.1. The electrochemistry setup for cyclic voltammetry using a Pt disc or glassy carbon working electrode, a Pt wire auxiliary electrode and a Ag/AgCl reference electrode in an electrolyte solution. Samples were deoxygenated using Ar.

The setup of bulk electrolysis is different from that of CV. It also has a three-electrode system including a carbon cloth working electrode, a platinum auxiliary electrode, which is separated from the bulk solution by a fine porous glass frit, and a Ag/AgCl reference electrode (Figure 2.2). During the bulk electrolytic process, the sample bulk solution was deoxygenated and stirred by argon bubbling. A selected steady potential was applied to the working electrode. The current decreases exponentially, and the experiment is considered completed when the current drops to a background non-Faradic current. Charge is obtained by integration of the current passed over time.

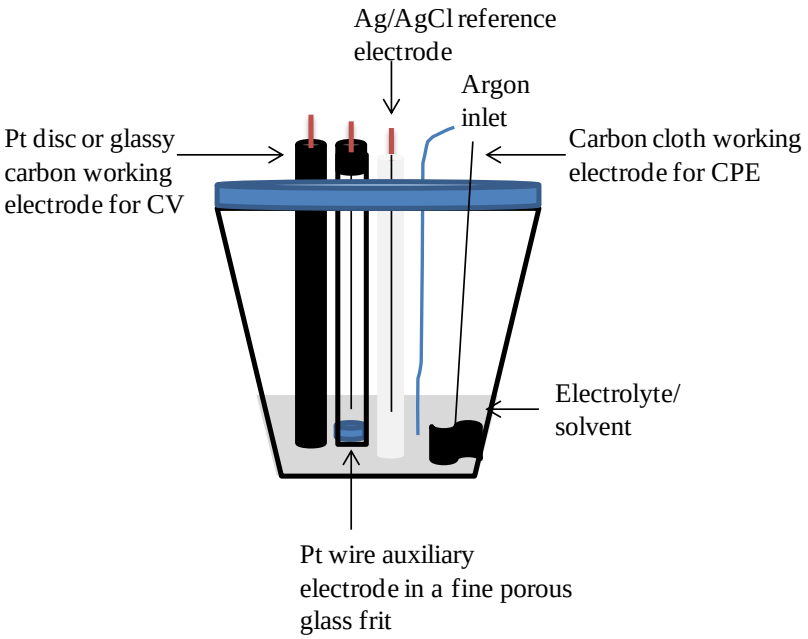

Figure 2.2. The electrochemistry setup for controlled potential bulk electrolysis using a carbon cloth working electrode, a Pt disc or glassy carbon working electrode, a Pt wire auxiliary electrode with a fine porous glass frit and a Ag/AgCl reference electrode in an electrolyte solution. Samples were deoxygenated using Ar.

2.3.3. Electronic Absorption Spectroscopy

Electronic absorption spectra were collected at room temperature using a Hewlett-Packard 8453A diode array spectrophotometer (1 nm resolution) with a 1 cm quartz cuvette. The complex solutions were prepared using spectrophotometric grade acetonitrile (Burdick and Jackson) for hexafluorophosphate salts, or double de-ionized water for chloride salts. The solvent in the same cuvette was used to blank the instrument. Extinction coefficient measurements were repeated three times on independently prepared gravimetric solutions giving typical determination of $\varepsilon \pm 100\ M^{-1}cm^{-1}$.

2.3.4. Luminescence Spectroscopy

Steady state luminescence spectra were collected with a modified QuantaMaster Model QM-200-45E emission spectrophotometer from Photon Technology, Inc. (PTI) modified for low intensity red shifted emissions, Figure 2.3. The excitation light source was a water-cooled 150 W xenon arc lamp. The detector was a thermoelectrically cooled Hamamatsu 1527 photomultiplier tube (PMT) in photon counting mode with 0.25 nm resolution at the right angle of the excitation source. The instrument had two emission gratings which were a 400 and 750 nm blaze. According to the absorption spectroscopy of the analyte, the 750 nm blaze was selected. The slits width for the excitation and emission monochromator can be adjusted manually according to the sample absorption and emission properties. The room temperature samples were prepared in spectrophotometric grade acetonitrile and deoxygenated by argon, while the low temperature samples were made in 4:1 v/v ethanol/methanol solution in a NMR tube, which was immersed in a qartz finger dewar filled with liquid nitrogen. The emission spectra were corrected for PMT response. The correction file applied was provided in Figure 2.4. The emission quantum yields (Φ^{em}) were determined on $[Os(bpy)_3](PF_6)_2$ ($\Phi^{em} = 4.6 \times 10^{-3}$) standard by applying the equation 2.1.[123]

$$\Phi_{\text{sample}} = \Phi_{\text{standard}} \times \frac{Area_{\text{sample}}}{Area_{\text{standard}}} \times \frac{A_{\text{standard}}}{A_{\text{sample}}} \qquad (2.1)$$

Where Φ_{sample} was the quantum yield of the sample, Φ_{standard} was the quantum yield of the standard, $\Phi^{em} = 4.6 \times 10^{-3}$. $Area_{\text{sample}}$ was the area under the sample emission profile, $Area_{\text{standard}}$ was the area under the standard emission profile. A_{standard} was the absorbance of the standard and A_{sample} was the absorbance of the sample.

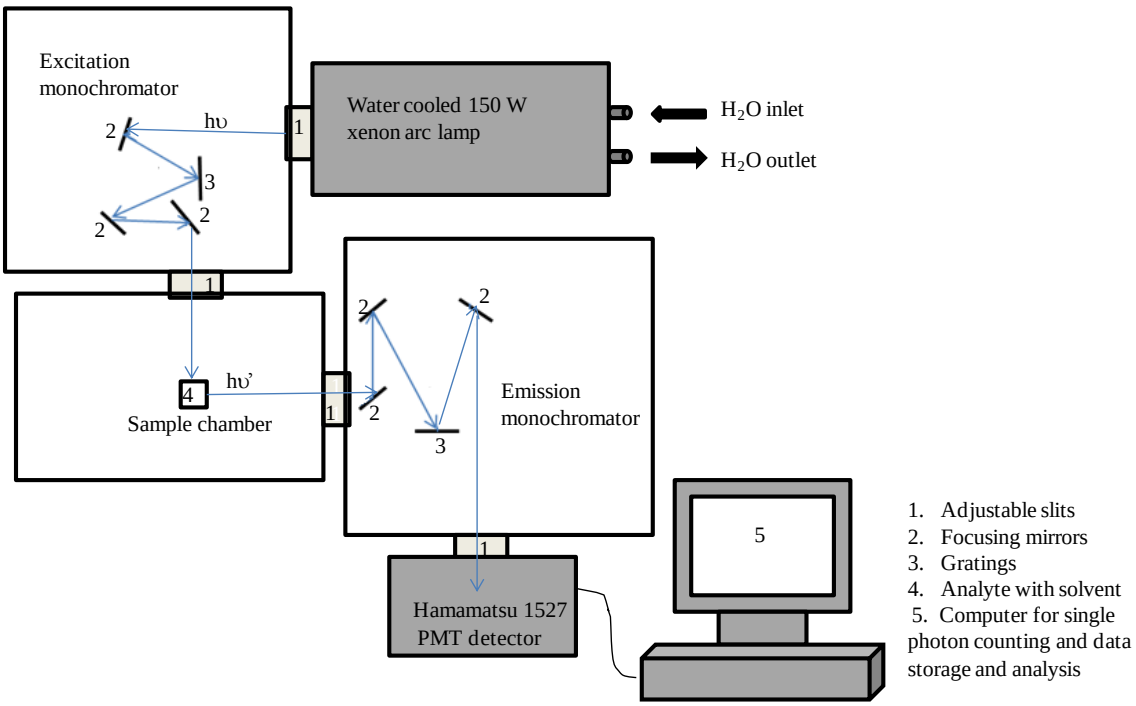

Figure 2.3. Schematic of the steady state emission spectrophotometer, QuantaMaster Model QM-200-45E modified for low intensity red shifted emissions from Photon Technology, Inc. (PTI).

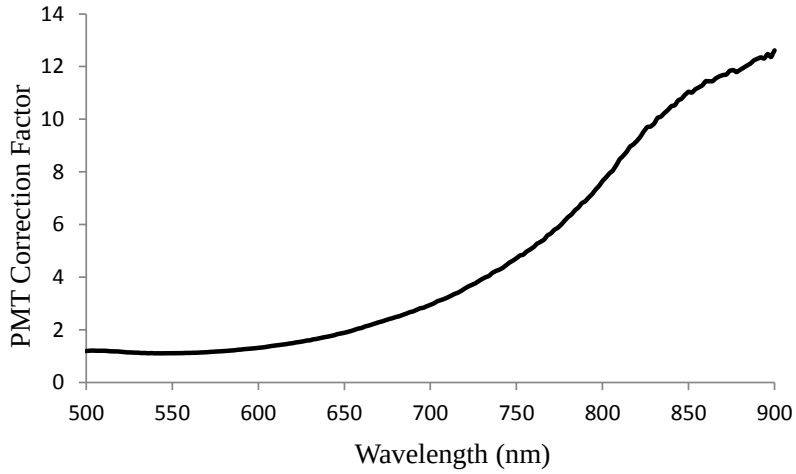

Figure 2.4. The PMT response correction file generated on site following installation of the modified QuantaMaster Model QM-200-45E emission spectrophotometer from PTI with a 750 nm blaze.

2.3.5. Time Resolved Emission

The excited state lifetime measurements were conducted using a PL 2300 nitrogen laser from Photon Technology, Inc. (PTI), coupled to a PL 201 dye laser with a Coumarin 500 laser dye (Figure 2.5). The detector is a single photon counting direct output wired Hamamatsu R928 photomultiplier tube. A LeCroy 9361 Dual 300 MHZ oscilloscope was used to record the voltage from the PMT grounded to resistor and typical lifetime determinations were an average of 300 pulses recorded on three different samples. The laser oscilloscope combination allowed the determination of emission decays with lifetimes greater than 5 ns. The room temperature analytes were dissolved in spectrophotometric grade acetonitrile and deoxygenated by argon, while the low temperature analytes were dissolved in 4:1 v/v ethanol/methanol solution in a NMR tube, which was immersed in a quartz finger dewar filled with liquid nitrogen. The samples were excited in the visible region populating MLCT excited states and detected at the emission maximum.

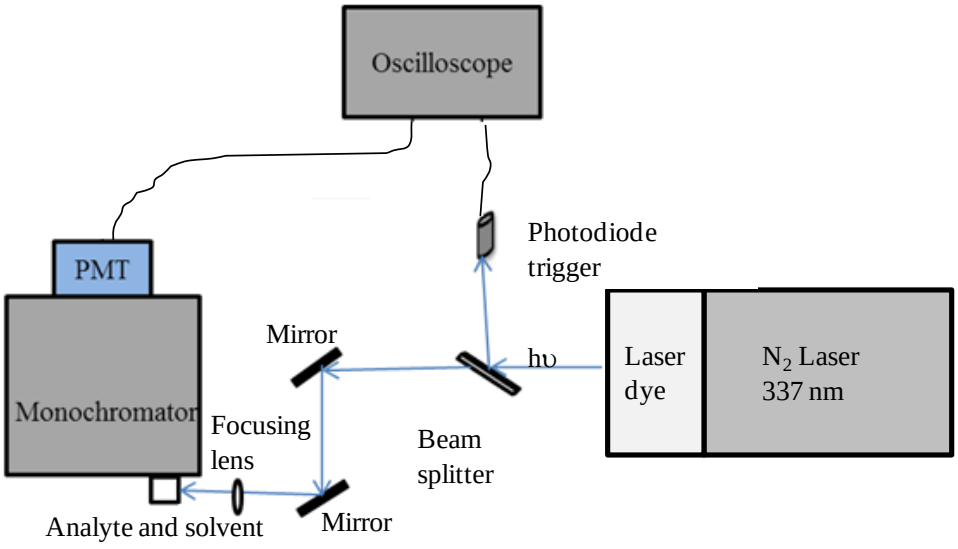

Figure 2.5. Schematic of the time resolved emission spectroscopy with PL-2300 nitrogen gas laser and a tunable PTI PL-201 dye head, monochromator selected emission detector (PMT = Hamamatsu R928 photomultiplier tube, oscilloscope = LeCroy 9361 oscilloscope.

2.4. DNA Photochemical Experiment

2.4.1. Photochemical Protocols for DNA Photocleavage or Photobinding by Metal Complexes

2.4.1.1. Metal Complex Photolysis Using a Xenon Arc Lamp for DNA Photocleavage or Photobinding

The DNA metal complex sample was photolyzed using a 1000 W xenon arc lamp purchased from Oriel Light Source and Spectroscopy Instruments using the experiment apparatus shown in Figure 2.6. A 1 cm optical cuvette containing the appropriate metal complex DNA mixture in buffer on a control was thermostated in a water cooled aluminum sample holder. The light from the 1000 W xenon arc lamp was passed through a water filter which absorbs IR light between 1000-3000 nm, a 455 nm cuton filter from Newport Optics to remove the light $\lambda < 455$ nm and a $\lambda \geq 590$ or $\lambda \geq 645$ nm cuton filter for red light irradiation of the sample. The spectral output of xenon arc lamp and the measured spectra of each filter were shown in Figure 2.7. Sample aliquots were taken over regular time intervals according to the experiment design and stored in dark for future analysis.

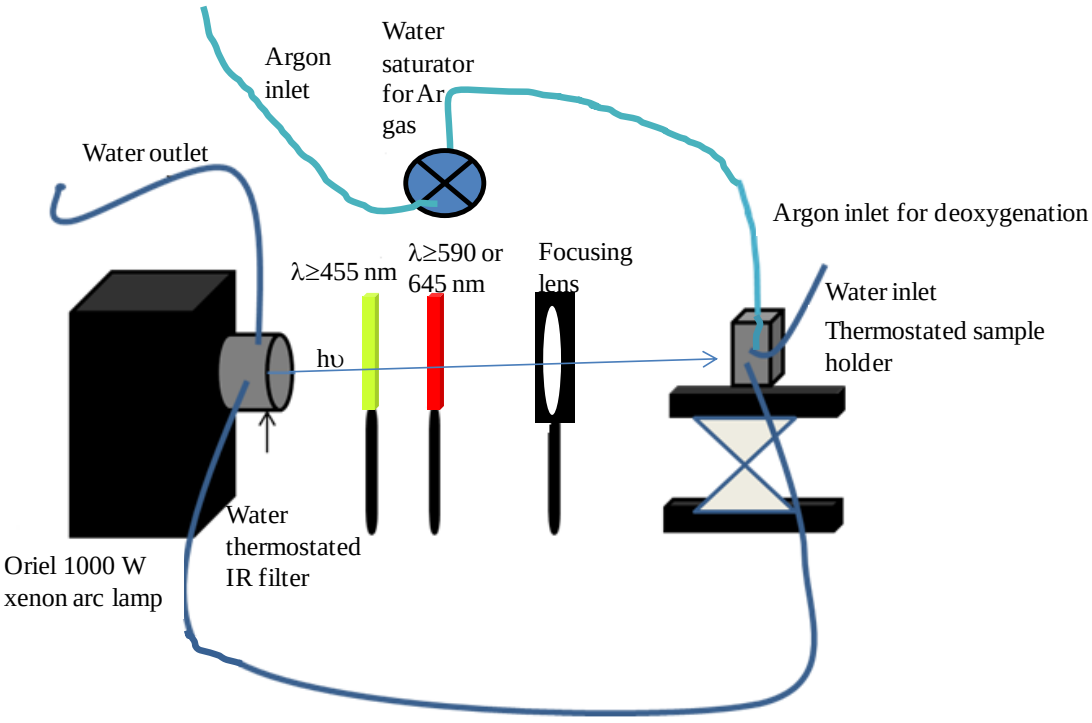

Figure 2.6. Schematic of experimental design for metal complex photolysis for DNA photocleavage or photobinding studies using an Oriel 1000 W xenon arc lamp including a H_2O IR filter (Oriel 17920), and Newport 455, 590, 645 nm cuton filters and a focusing lens (Oriel 6222) with a thermostated sample holder.

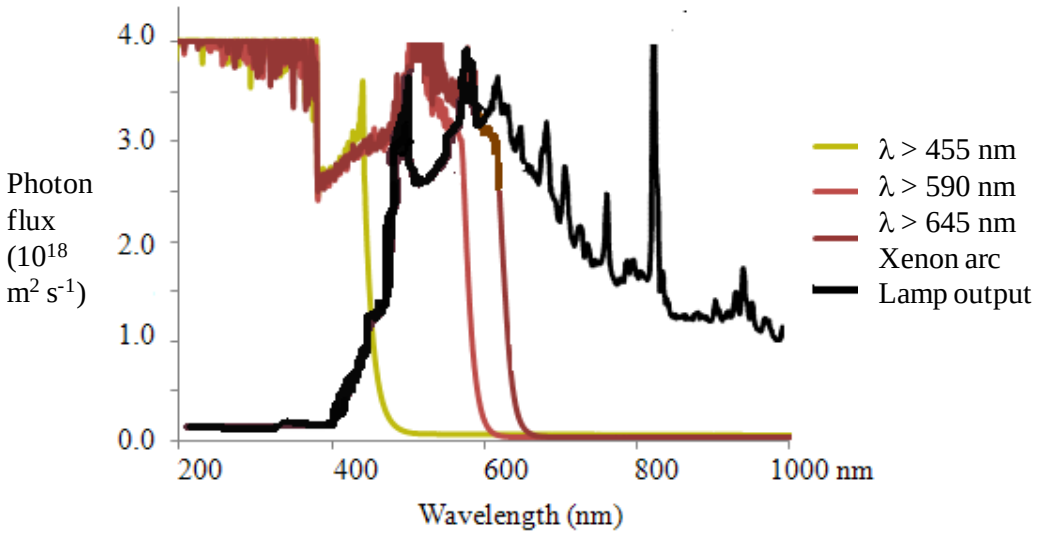

Figure 2.7. The output of Oriel 1000 W xenon arc lamp and the measured spectrum of each cuton filter.

2.4.1.2. DNA Photolysis Using a LED Array

The LED array was constructed by the Brewer group using Luxeon royal blue star light emitting diodes (5 W LED) as a light source.[124] The LED array was designed to photolyze simultaneously eight samples, using visible light (λ = 455 nm, average flux = $2.0 \pm 0.1 \times 10^{19}$ photons/min) from a 5 W LED with eight argon tubing accesses and eight water flowing thermostated cell holders (Figure 2.8 A).[124] Each LED was lined up with one photolysis sample and constructed in an individual circuit which is composed of three resistors, one rheostat, one switch and one LED (Figure 2.8 B). Eight individual circuits were connected parallel to a power supply. The photolysis samples were prepared with the metal complex, DNA, de-ionized water and phosphate buffer at a certain MC (metal complex):BP (base pairs) ratio in an optical cuvette. The protocol of samples photolyzed by a LED array was similar to that by a xenon arc lamp. The sample in an optical cell was set in a water flowing aluminum cell holder and irradiated by visible light (λ = 455 nm, average flux = $2.0 \pm 0.1 \times 10^{19}$ photons/min) from a 5 W LED under argon flow. The sample aliquots were taken over a regular time interval according to the experiment design and stored in the dark for future assay.

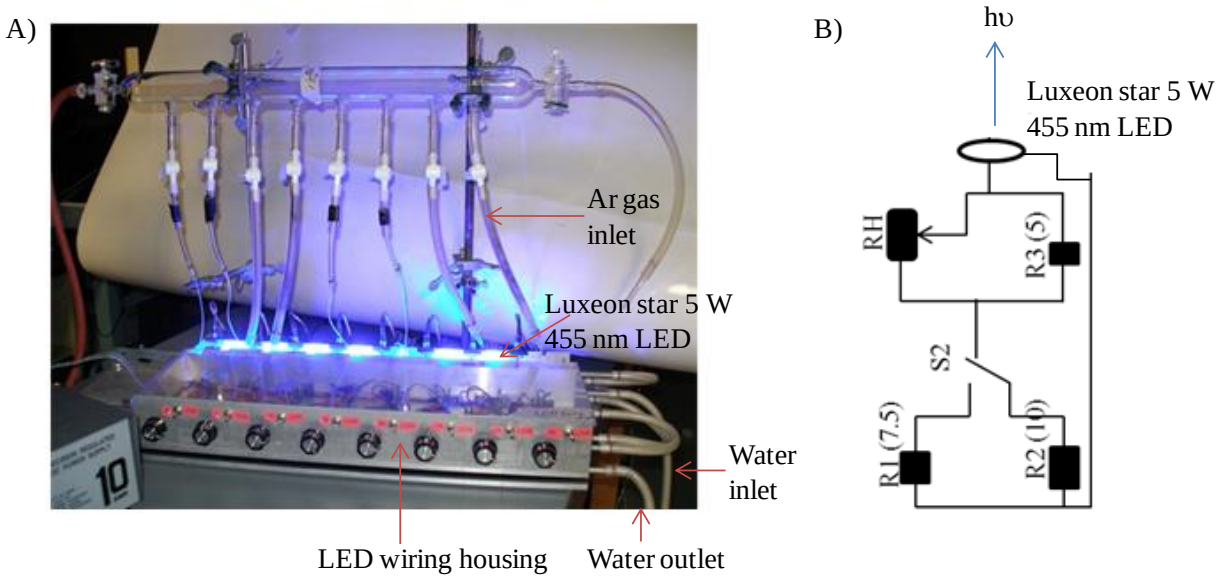

Figure 2.8. The schematic of experimental design for DNA photolysis using a 5 W LED array (λ = 455 nm, average flux = 2.0 ± 0.1 × 10^{19} photons/min) (A), and an individual LED circuit (B).[124]

2.4.2. Agarose Gel Shift Assay

Gel shift assays were performed employing our previously reported methods as shown in Figure 2.9.[68] The agarose gel was prepared according to the protocol. 0.24 g agarose was dissolved with 30 mL deionized water in 250 mL Erlenmeyer flask. The mixture was microwaved for 90 s, and more deionized water was added to the agarose solution to make the total weight equal to 24.0 g. Then, 6 mL 5 × TB buffer (90 mM tris base, 90 mM boric acid) was added into the agarose solution. The agarose solution was poured to a model BIA stage (Owl separation systems) and kept in the stage for 1 hour to form the gel. The DNA photolysis samples were loaded into the wells of a 35 mL 0.8% w/w agarose gel in a model BIA stage with 300 mL 5 × TB buffer. The gel was applied a potential of 104 V for 1.5 hours (or 1 hour for PCR sample). After electrophoresis, gels were stained in 0.5 μg/mL ethidium bromide solution for 30

minutes and destained in double deionized water for 15 minutes. The gels were visualized on a Fisher Biotech UV-trans illuminator. The photographs were taken using an Olympus SP-320 camera equipped with an ethidium bromide filter. Gels were reproduced to ensure these results are reflective of the metal complexes reactivity.

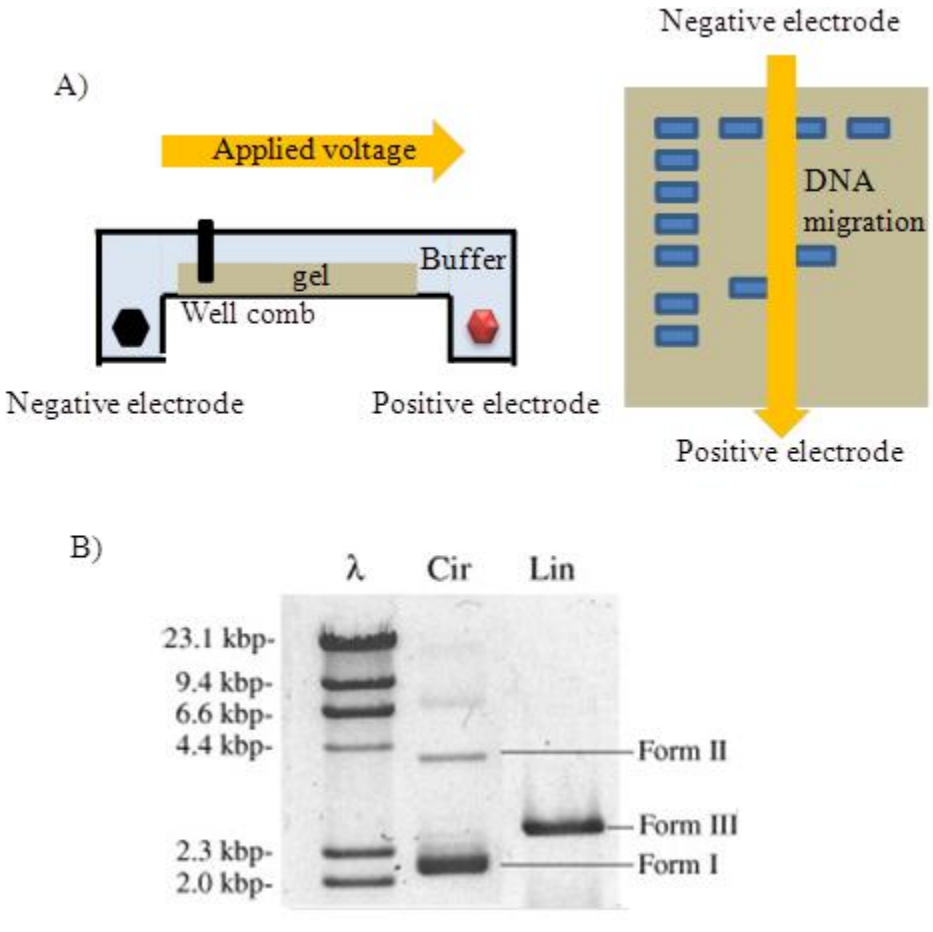

Figure 2.9. The schematics of gel shift assay process (A) and an imaged gel of supercoiled (Form I), open circular (Form II) and linear (Form III) DNA (B). The image (B) was reprinted from Prussin, A. J.; Zigler, D. F.; Jain, A.; Brown, J. R.; Winkel, B. S. J.; Brewer, K. J. *Journal of Inorganic Biochemistry* **2008**, *102*, 731-739, copyright 2008 with permission from Elsevier.[124]

2.4.3. DNA Selective Precipitation Experiment

DNA photobinding was assayed with calf thymus DNA using previously established methods that take advantage of the high molar absorption for the metal complexes.[125] The

sample solutions were prepared with 0.1 mM metal complex and 0.5 mM DNA at a 1:5 MC (metal complex):BP (base pairs) ratio with 10 mM phosphate buffer. The solutions were photolyzed under visible light (λ = 455 nm) from a 5 W LED which has average flux $2.0 \pm 0.1 \times 10^{19}$ photons/min,[124] or in dark under argon flow. 250 μL DNA photolysis sample or dark control was taken at 5, 10, 20, 30, 40 and 50 min. Then, 10 μL 5 M NaCl solution and 1000 μl 95% ethanol were added to the aliquots of the solutions. Calf thymus DNA was precipitated followed by vortex stirring and centrifugation. The absorbance of the resulting supernatant was measured at the MLCT transition of bimetallic complexes plotting A/A_0 vs. time. Experiments were conducted in triplicate.

2.4.4. Polymerase Chain Reaction Experiment

The polymerase chain reaction (PCR) was used to investigate the effect of DNA amplification after metal complex photomodification of supercoiled pUC18 plasmid DNA. Since PCR is prone to contamination, the work area was sterilized using 75% ethanol and reaction tubes and pipette tips were sterilized by autoclaving prior to use. Each 10 μL PCR sample was prepared with 1.0 μL template containing 1 ng supercoiled pUC18 plasmid DNA (alone or mixed with metal complex and either incubated in darkness or subjected to photolysis) or 1 μL deionized H_2O, 0.5 μL 20 μM of each primer (5′-CCCAACGATCAAGGCGAG-3′ and 5′-CGAAAGGGCCTCGTGATACG-3′) as shown in Figure 2.10, 5.0 μL Biomix™ 2X reaction mix (BioLine, Taunton, MA) and 3.0 μL deionized H_2O in a 0.5 mL PCR tube. The PCR samples were set to run 35 thermal cycles using a PTC-100^{TM} Programmable Thermal Controller. Each cycle was heated to 94 °C for 30 s, 58 °C for 30 s, then, 72 °C for 2 min. Heating the PCR samples to 94 °C for 30 s was to denature the DNA template making double

strands DNA to single strand. Keeping the PCR samples to 58 °C for 30 s was to let forward and reverse primers to bind to the single strand DNA. Heating the PCR samples to 72 °C for 2 min was to activate *Thermus aquaticus* (Taq) polymerase to amplificate DNA. The samples which completed the thermal cycles were ready for the agarose gel shift assay to study.

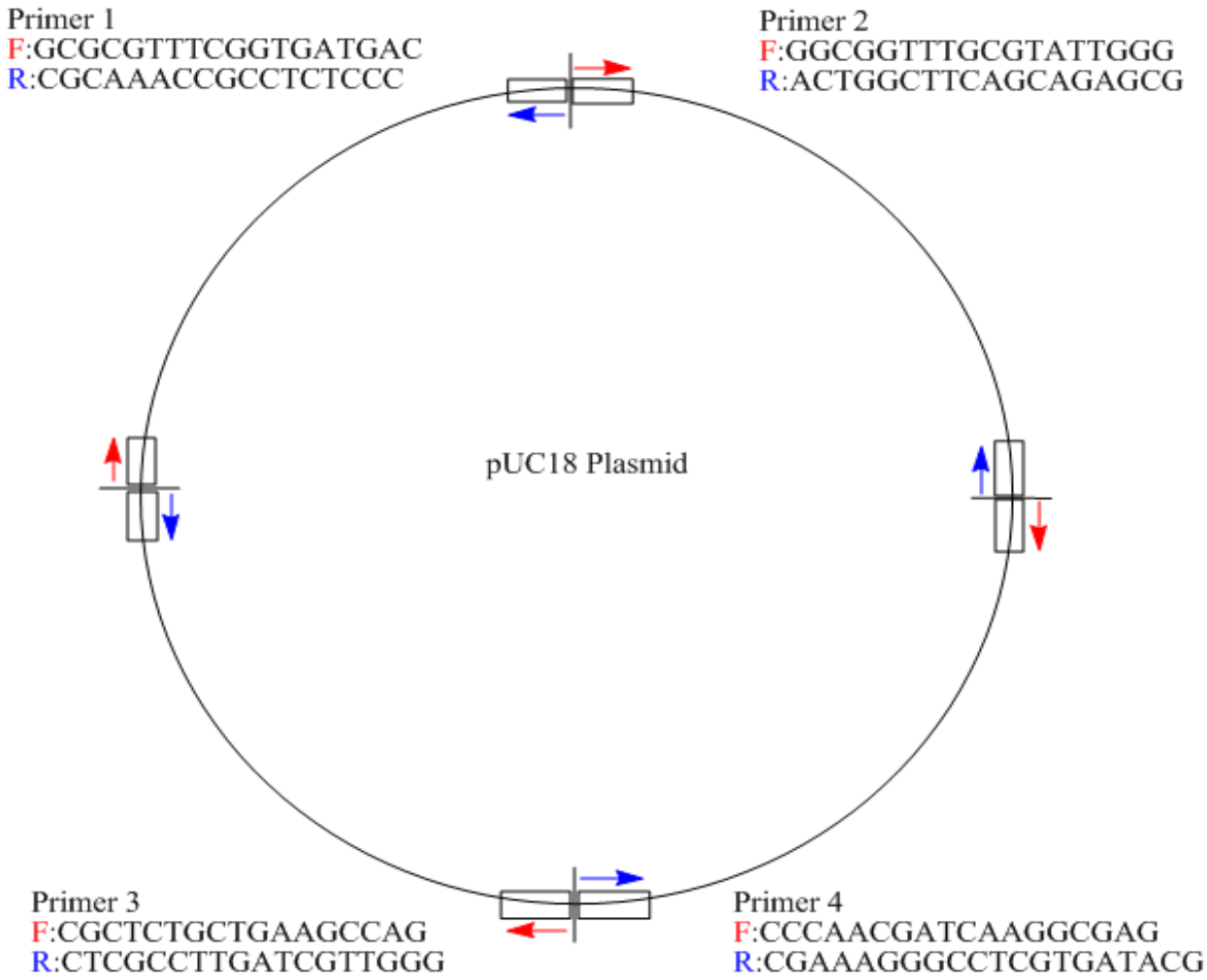

Figure 2.10. The picture of pUC 18 DNA and the location and sequence of the PCR primers.

Chapter 3. Results and Discussion

Since the goal of this research is to design, synthesize and characterize Ru,Rh and Os,Rh bimetallic complexes and understand the effect of component modification on the electrochemical, spectroscopic, photophysical properties and DNA interactions of the bimetallic complexes with comparison to known trimetallic Ru,Rh,Ru and Os,Rh,Os systems, the mixed-metal bimetallic complexes coupling one ruthenium or osmium polyazine light absorber to a *cis*-$Rh^{III}Cl_2$ center through a dpp bridging ligand are the focus of this work. These systems are challenging to prepare due to the tendency of Rh halide starting materials to produce *cis*-$[Rh(NN)_2Cl_2]^+$ motifs with diimine ligands.[115] This bimetallic structural motif provides a sterically accessible Rh reactive site and is more accessible than the Rh sites in known $[(TL)_2Ru(BL)\}_2RhCl_2]^{5+}$ trimetallics (in Figure 3.1).

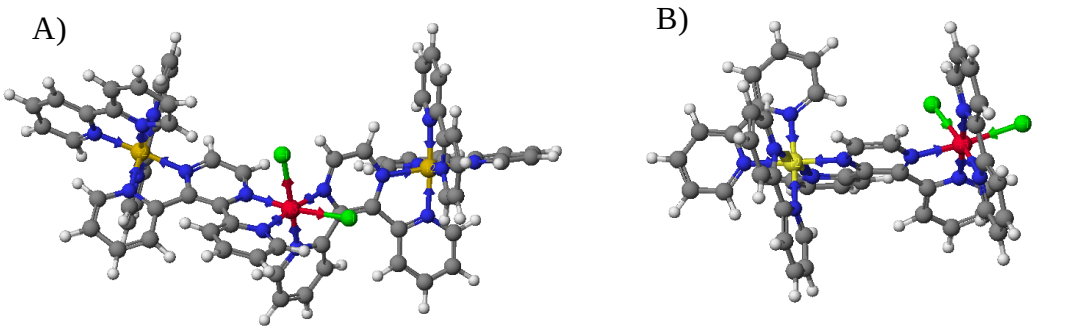

$[\{(bpy)_2Ru(dpp)\}_2RhCl_2]^{5+}$ $[(bpy)_2Ru(dpp)RhCl_2(bpy)]^{3+}$

Figure 3.1. The Scigress structure of trimetallic complex $[\{(bpy)_2Ru(dpp)\}_2RhCl_2]^{5+}$ (A) and bimetallic complex $[(bpy)_2Ru(dpp)RhCl_2(bpy)]^{3+}$ (B), bpy = 2,2′-bipyridine, dpp = 2,3-bis(2-pyridyl)pyrazine.

These bimetallics are efficient visible light absorbers and possess many advantages for biological applications compared to the trimetallics, including lower cationic charges, reduced stereoisomerization, and independent variation of terminal ligands at each metal center to

module properties. Herein a series of bimetallic complexes, $[(TL)_2M(dpp)RhCl_2(TL')]^{3+}$ (M = Ru and Os, TL = phen, Ph_2phen, Me_2phen and bpy, TL′ = phen, bpy and Me_2bpy), were synthesized using a building block method with a variety of terminal ligands in the light absorbers (Figure 3.2 A, B). The light absorber metal center and terminal ligands attached to rhodium center are also varied. The title bimetallics display interesting electrochemical, spectroscopic, photophysical and photochemical properties with all systems providing light induced reactivity with DNA.

3.1. The Synthetic Strategy to Make Bimetallic Complexes

A series of bimetallic complexes $[(TL)_2M(dpp)RhCl_2(TL')](PF_6)_3$ (M = Ru or Os) were synthesized by using a building block method, which is convenient for construction and purification. The mixed-metal bimetallics were made from monometallic M = Ru or Os light absorber synthons $[(TL)_2M(dpp)](PF_6)_2$ and rhodium complexes including $K[(TL')RhCl_4]$ and $[(TL')RhCl_3(CH_3OH)]$ •CH_3OH (Figure 3.2 A and B). The monometallic complexes $[(TL)_2M(dpp)](PF_6)_2$ were synthesized from the starting materials $[(TL)_2MCl_2]$ and bridging ligand (BL) dpp. The $[(TL)_2MCl_2]$ are prepared via a reaction of $MCl_3 \cdot xH_2O$ ($M = Os^{III}$ or Ru^{III}) with terminal ligands. Much care is needed to remove the highly emissive $[M(TL)_3]^{2+}$. The rhodium complexes were synthesized from the starting material $RhCl_3 \cdot xH_2O$ and terminal ligands using large excess of chloride to prevent $[Rh(TL)_2Cl_2]^+$ species.[115] All products from each synthetic step were purified and analyzed prior to the next step of synthesis. Monometallic complexes were commonly purified by using column chromatography on methanol deactivated adsorption alumina with a toluene/acetonitrile as the eluent. The toluene/acetonitrile ratio at 3:2 was used to best separate the desire product $[(TL)_2M(dpp)]^{2+}$ from excess ligands, unreacted

starting materials, and $[(TL)_2M(dpp)M(TL)_2]^{4+}$ byproduct.[95] Bimetallic complexes were commonly purified by precipitation in diethylether and recrystallization in hot ethanol to remove the monometallic synthrons. Typical yields are provided in Figure 3.2 A and B. The bimetallic complexes were synthesized and characterized as PF_6^- salts and metathesized to Cl^- salts for photochemical reactions with DNA.

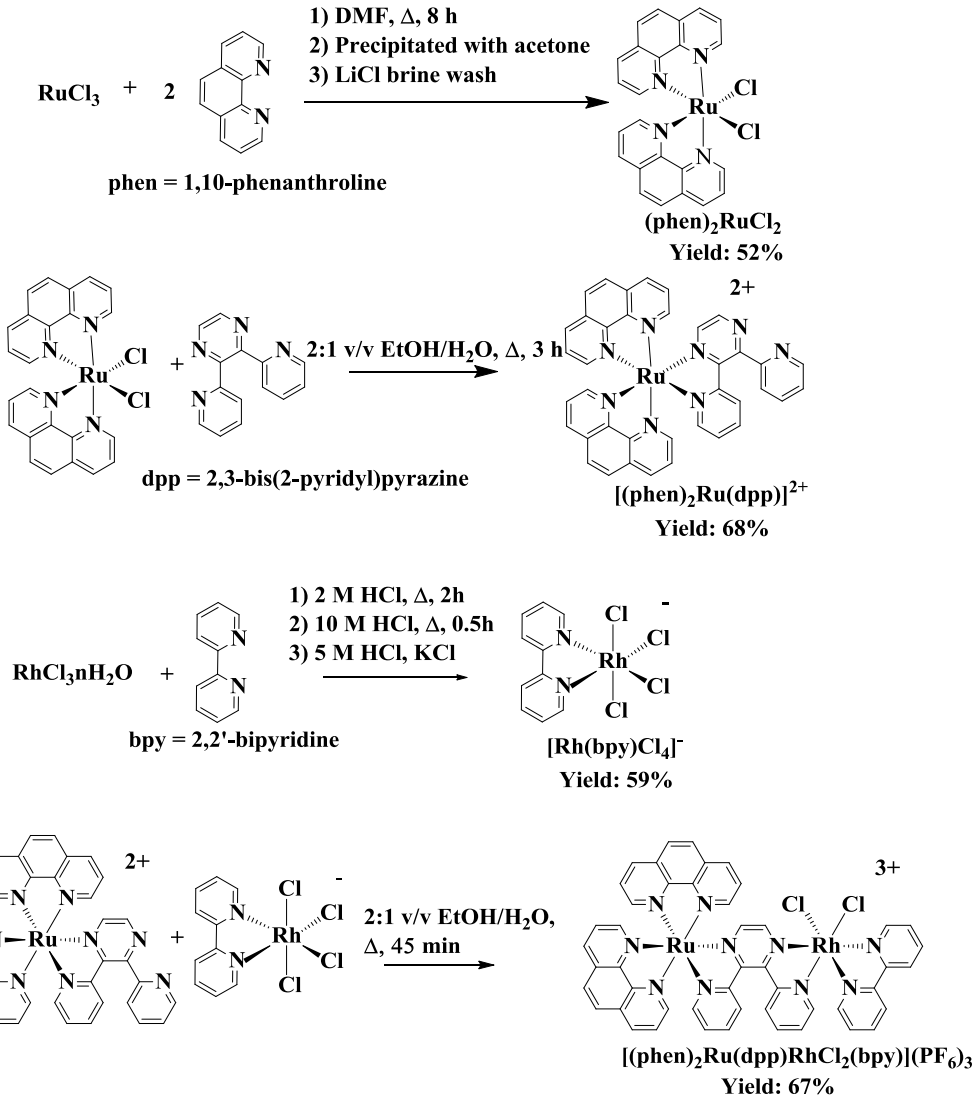

Figure 3.2 A. Building block method used in the synthesis of $[(phen)_2Ru(dpp)RhCl_2(bpy)](PF_6)_3$, phen = 1,10-phenanthroline, bpy = 2,2′-bipyridine and dpp = 2,3-bis(2-pyridyl)pyrazine.

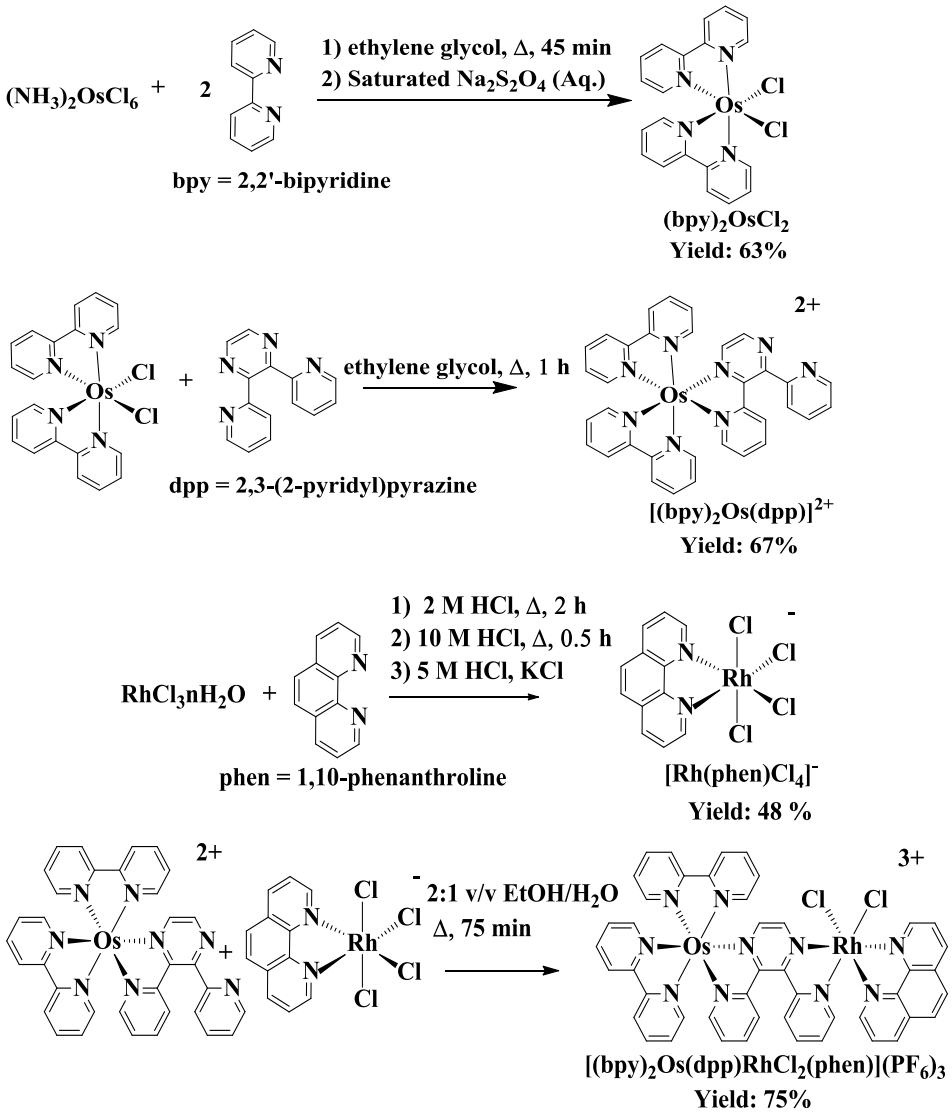

Figure 3.2 B. Building block method used in the synthesis of $[(bpy)_2Os(dpp)RhCl_2(phen)](PF_6)_3$, bpy = 2,2′-bipyridine, phen = 1,10-phenanthroline, and dpp = 2,3-bis(2-pyridyl)pyrazine.

3.1.1. The Improved Method of Making Rh Complexes

Both $K[(TL')RhCl_4]$ and $[(TL')RhCl_3(CH_3OH)] \cdot CH_3OH$ rhodium complexes were used to react with monometallic synthons $[(TL)_2M(dpp)](PF_6)_2$ to make bimetallic complexes. The rhodium complexes $K[(TL')RhCl_4]$ (TL′ = phen and bpy) synthesized by the modified method from Mckenzie and Plowman[115] were initially used to make bimetallics.[15,118] Since the starting

material $RhCl_3 \cdot xH_2O$ tends to react with diimine ligands to produce *cis*-$[Rh^{III}(NN)_2X_2]^+$ motifs (NN = phen and bpy), the procedure of making $K[(TL')RhCl_4]$ is complicated. The method began with adding terminal ligand (TL′) to a hot $RhCl_3$ and 2 M HCl aqueous solution mixture to produce $H[(TL')RhCl_4]$, followed by hot vacuum filtration to remove unwanted byproduct $(HTL')_{n-1}[RhCl_{n+2}(H_2O)_{4-n}]$, n = 0-4,[126] then adding saturated KCl aqueous solution to induce product $K[(TL')RhCl_4]$. In order to make the synthetic procedure easier to handle and more applicable to other terminal ligands, a new method reported by Sheldrick was used to make rhodium complex $[(bpy)RhCl_3(CH_3OH)] \cdot CH_3OH$.[116] The reaction of $RhCl_3 \cdot xH_2O$ with an equivalent of bpy in methanol was heated at reflux for 3 hours and cooled to room temperature before the orange precipitate byproduct was removed by vacuum filtration. The product solution was left to stand for 12 hours to form $[(bpy)RhCl_3(CH_3OH)] \cdot CH_3OH$ crystals. This improved method of making rhodium complexes was also used to make $[(Me_2bpy)RhCl_3(CH_3OH)] \cdot CH_3OH$. The complexes $[(bpy)RhCl_3(CH_3OH)] \cdot CH_3OH$ and $[(Me_2bpy)RhCl_3(CH_3OH)] \cdot CH_3OH$ were characterized by using proton and ^1H-^1H COSY NMR and described in detail in senction 2.2.1.9 and 2.2.1.10. This reaction produces mixtures of *fac* and *mer* isomers but since this is an intermediate product tht is used to produce the bimetallics. This mixture of isomers is not an issue.

3.2. Electrochemical Results

The electrochemical properties of mixed-metal polyazine complexes were investigated by cyclic voltammetry (CV) in deoxygenated solution with a three-electrode system. The choice of solvent, electrolyte and electrode material is important to be able to observe the electrochemistry of complexes. Solvents and electrolytes are important to provide a sufficient electrochemical

window to observe the redox behaviors of the metal complexes. The metals and polyazine ligands are all electroactive providing a way to assay the purity of metallic complexes. The mixed-metal polyazine complexes including bimetallic complexes $[(TL)_2M(dpp)RhCl_2(TL')]^{3+}$ and trimetallic complexes $[\{(TL)_2M(dpp)\}_2RhCl_2]^{5+}$ display reversible metal-based oxidation, reversible BL-based reductions that are ordered by the energy of the π^* acceptor orbital of the ligands and reduced prior to terminal ligands, and irreversible Rh-based reductions. The electrochemical properties of the new bimetallic complexes are complex, and unexpected based on the simple electrochemistry of the related trimetallics.[71]

3.2.1. Electrochemical Properties of the Bimetallic Complex $[(phen)_2Ru(dpp)RhCl_2(bpy)]^{3+}$ Compared with the Trimetallic Complex $[\{(phen)_2Ru(dpp)\}_2RhCl_2]^{5+}$

The electrochemistry of the bimetallic complex $[(phen)_2Ru(dpp)RhCl_2(bpy)]^{3+}$ and the trimetallic complex $[\{(phen)_2Ru(dpp)\}_2RhCl_2]^{5+}$ was investigated using a three electrode system with a Ag/AgCl reference electrode, a carbon glassy disk working electrode and a Pt wire counter electrode in 0.1 M Bu_4PF_6 acetonitrile at room temperature. The cyclic voltammograms of both complexes at the potential scan rate of 100 mV/s with scaning anodically first are shown in Figure 3.3. Electrochemical oxidation of $[\{(phen)_2Ru(dpp)\}_2RhCl_2]^{5+}$ occurs at 1.61 V vs. Ag/AgCl with two overlapping, one-electron reversible waves assigned to $Ru^{II/III}$ couples (Figure 3.3 A), which is 0.16 V positive of the $Ru^{II/III}$ couple in the monometallic complex $[(phen)_2Ru(dpp)]^{2+}$.[81,95] Electrochemical reduction of $[\{(phen)_2Ru(dpp)\}_2RhCl_2]^{5+}$ shows two overlapping irreversible one-electron reductions at −0.35 V vs. Ag/AgCl assigned to $Rh^{III/II/I}$ couple, followed by two reversible reductions at −0.76 and −1.00 V vs. Ag/AgCl attributed to two $dpp^{0/-}$ couples at the scan rate

of 100 mV/s. The CV of $[\{(phen)_2Ru(dpp)\}_2RhCl_2]^{5+}$ is similar to the CV of $[Rh(bpy)_2Cl_2]^+$ which was investigated by DeArmond and coworkers.[87] They proposed that the electrochemical mechanism of $[Rh(bpy)_2Cl_2]^+$ is ECECEE mechanism (section 1.4.3). The first and second one-electron reduction of the complex $[Rh(bpy)_2Cl_2]^+$ is followed by a very fast chemical reaction, chloride loss.[87] The two irreversible one-electron waves of $[\{(phen)_2Ru(dpp)\}_2RhCl_2]^{5+}$ and $[Rh(bpy)_2Cl_2]^+$ can not be seperated even at very fast scan rate at 32.2 V/sec. The electrochemical mechanism for reduction of trimetallic complex $[\{(phen)_2Ru(dpp)\}_2RhCl_2]^{5+}$ proposed by Brewer and coworkers is ECECEE mechanism.[120] The first and second one-electron reductions of $[\{(phen)_2Ru(dpp)\}_2RhCl_2]^{5+}$ are also followed by a very fast chloride loss. The third and forth reductions of $[\{(phen)_2Ru(dpp)\}_2RhCl_2]^{5+}$ are reversibe dpp-based one-electron reductions.

The electrochemical properties of $[(phen)_2Ru(dpp)RhCl_2(bpy)]^{3+}$ are different from those of $[\{(phen)_2Rh(dpp)\}_2RhCl_2]^{5+}$. The cyclic voltammogram of $[(phen)_2Ru(dpp)RhCl_2(bpy)]^{3+}$ at the potential scan rate of 100 mV shows a reversible one electron $Ru^{II/III}$ oxidation couple at 1.62 V vs. Ag/AgCl, 0.17 V positive of the $Ru^{II/III}$ couple in the monometallic synthon $[(phen)_2Ru(dpp)]^{2+}$.[81,118] The reductive electrochemistry shows a quasi-reversible $Rh^{III/II}Cl_2$ couple overlapped with a small amount of $Rh^{II/I}Cl$ reduction at –0.44 V vs. Ag/AgCl and an irreversible $Rh^{II/I}Cl_2$ couple at –0.79 V vs. Ag/AgCl and a reversible $dpp^{0/-}$ couple at –1.03 V vs. Ag/AgCl (Figure 3.3 B). The reduction product of the bimetallic complex $[(phen)_2Ru(dpp)RhCl_2(bpy)]^{3+}$ was also studied by electrochemical analysis.[118] The complex $[(phen)_2Ru(dpp)RhCl_2(bpy)]^{3+}$ was analyzed using controlled potential bulk electrolysis (CPE). The compound was electrolyzed at –0.60 V vs. Ag/AgCl to reduce the Rh center, followed by a CV analysis. The electrolysis potential was held at –0.60 V to reduce the

complex by two electrons and avoid the further reduction.

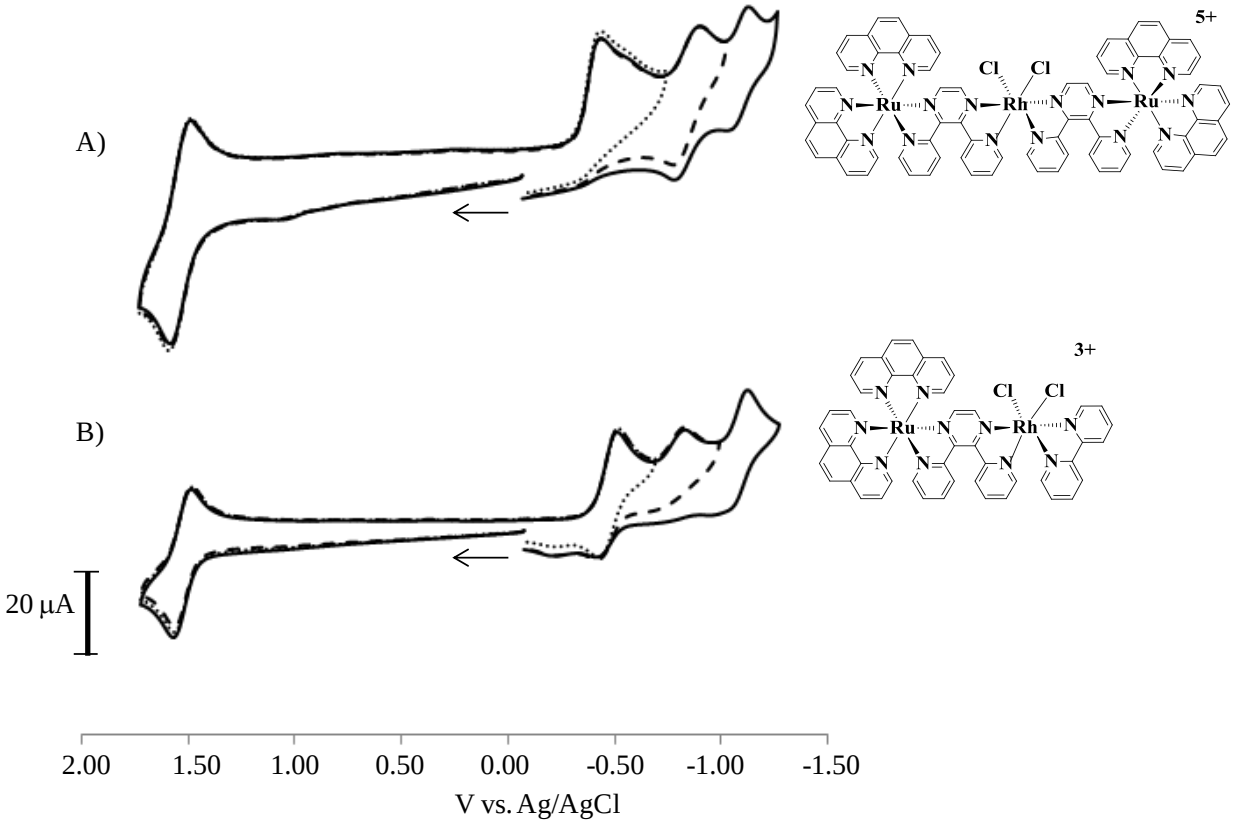

Figure 3.3. Cyclic voltammogram of trimetallic complex $[\{(phen)_2Ru(dpp)\}_2RhCl_2]^{5+}$ (A) bimetallic complex $[(phen)_2Ru(dpp)RhCl_2(bpy)]^{3+}$ (B) and at the scan rate of 100 mV/s in 0.1 M Bu_4NPF_6 acetonitrile at room temperature with bpy = 2,2′-bipyridine, dpp = 2,3-bis(2-pyridyl)pyrazine and phen = 1,10-phenanthroline.

The electrochemistry of the two-electron reduced bimetallic $[(phen)_2Ru(dpp)RhCl_2(bpy)]^{3+}$ is consistent with production of the Rh^I bimetallic $[(phen)_2Ru^{II}(dpp)Rh^I(bpy)]^{3+}$ with the loss of both coordinated chloride.[87,91,120] The reduced bimetallic $[(phen)_2Ru(dpp)RhCl_2(bpy)]^{3+}$ displays a loss of the Rh reduction peaks seen in the CV of the bimetallic complex prior to dpp reduction, the expected shift of a $Ru^{II/III}$ couple to less positive potential, and a new irreversible oxidation representing the oxidation of free chloride in solution (Figure 3.4 B).

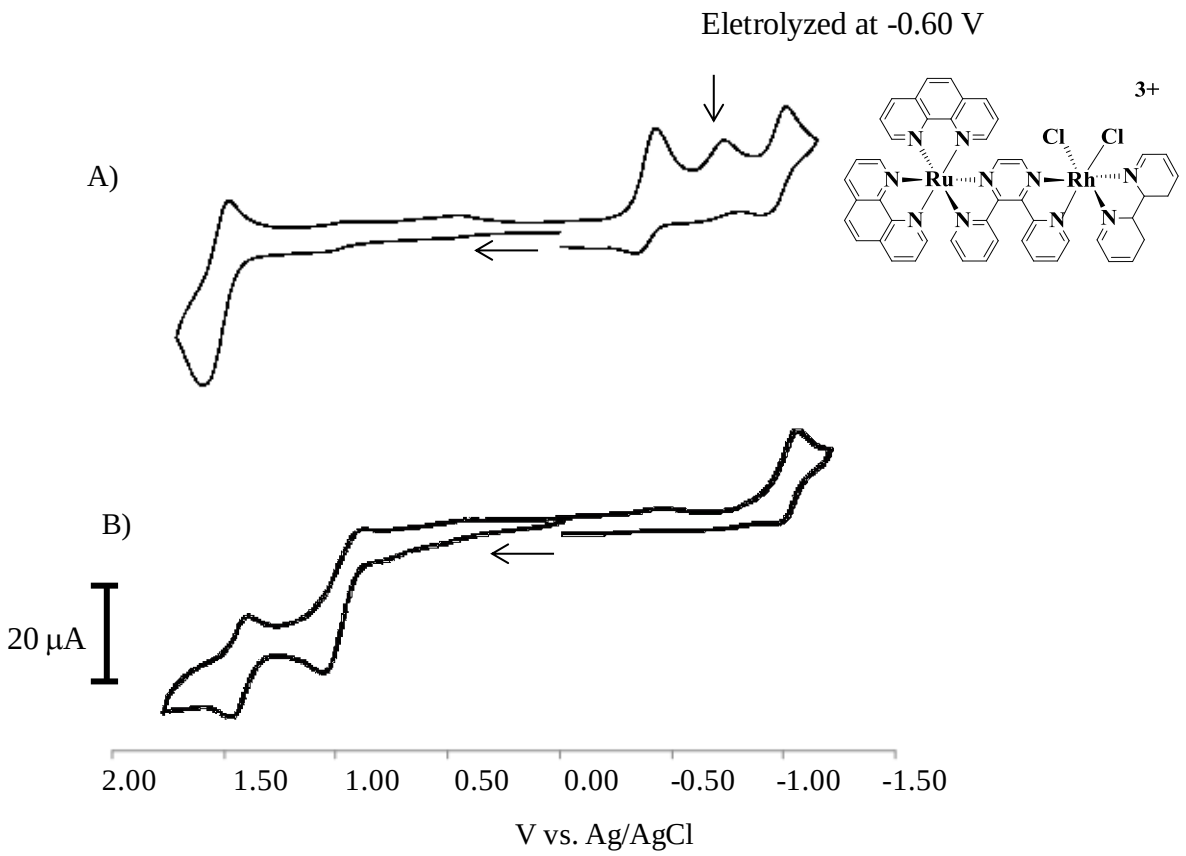

Figure 3.4. Coupled cyclic voltammetry and bulk electrolysis to analyze the product of reduction of $[(phen)_2Ru(dpp)RhCl_2(bpy)]^{3+}$. Cyclic voltammogram of the complex $[(phen)_2Ru(dpp)RhCl_2(bpy)]^{3+}$ at the scan rate of 100 mV/s in 0.1 M Bu_4NPF_6 CH_3CN as synthesized (A) and following electrochemical reduction at –0.60 V vs. Ag/AgCl (B) at the scan rate of 100 mV/s.

These electrochemical signals are consistent with formation of the Rh^I bimetallic, $[(phen)_2Ru^{II}(dpp)Rh^{I}(bpy)]^{3+}$ (Also detected by ESI-mass spectrometry) via Rh reduction and the loss of chloride ($E_{½}oxd$ = 1.48 V $Ru^{II/III}$, E_p^c = 1.06 V Cl^-/Cl_2, $E_{½}red$ = –1.03 V $dpp^{0/-}$, V vs. Ag/AgCl) (Figure 3.4 B). The controlled potential bulk electrolysis with coulometry shows the passage of about 2 electrons when the complex was electrolyzed at –0.60 V vs. Ag/AgCl past the first and second couples. The electrochemistry of the reduced product is indicative of a single metal containing product $[(phen)_2Ru^{II}(dpp)Rh^{I}(bpy)]^{3+}$ and free chloride in solution.

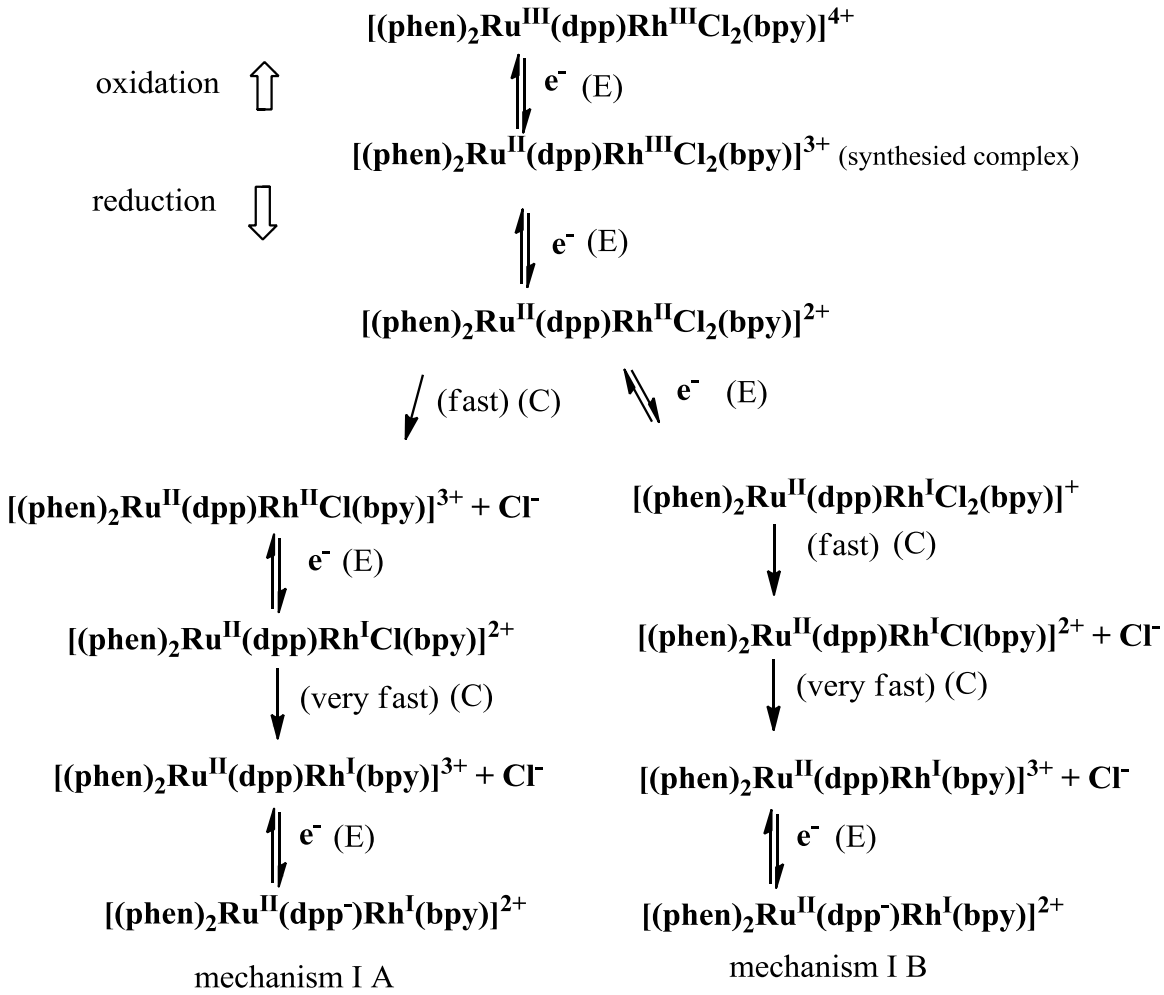

Figure 3.5. The electrochemical mechanisms (I A and I B) of bimetallic complex $[(phen)_2Ru(dpp)RhCl_2(bpy)]^{3+}$, bpy = 2,2′-bipyridine, dpp = 2,3-bis(2-pyridyl)pyrazine and phen = 1,10-phenanthroline.

An ECECE electrochemical mechanism of bimetallic complex $[(phen)_2Ru(dpp)RhCl_2(bpy)]^{3+}$ is proposed here according to the electrochemical data. The first and second reductions of the complex $[(phen)_2Ru(dpp)RhCl_2(bpy)]^{3+}$ are followed by a chemical reaction, chloride loss, supported by free chloride detected electrochemically. The rate of chloride loss after the $Rh^{III/II}$ couple is competitive with further reduction of $Rh^{II/I}$, complicating the observed electrochemistry. As $Rh^{II/I}$ couples occur for both first and second rhodium reductions giving couples unequal current. The CV of bimetallic complex $[(phen)_2Ru(dpp)RhCl_2(bpy)]^{3+}$ is

different from that of trimetallic complex $[\{(phen)_2Rh(dpp)\}_2RhCl_2]^{5+}$ due to the slower halide loss after the first $Rh^{III/II}$ reduction compared to the trimetallic, $[\{(phen)_2Rh(dpp)\}_2RhCl_2]^{5+}$. The CV of the bimetallic $[(phen)_2Ru(dpp)RhCl_2(bpy)]^{3+}$ at 100 mV/s shows a return couple associated with the first reduction but not second reduction. This fact suggests that the rate of chloride loss by Rh^{I} $(k_f)_{II}$ is much larger than that for Rh^{II} $(k_f)_{I}$.[87] These relative rates are confirmed by the result of simulated electrochemistry which shows that the $(k_f)_I$ is about 0.45 s^{-1}, while the $(k_f)_{II}$ is about 10^6 s^{-1} for the complex $[(phen)_2Ru(dpp)RhCl_2(bpy)]^{3+}$. The bimetallic and trimetallic CVs indicate that the $(k_f)_I$ and $(k_f)_{II}$ are close in the previously studied $[\{(phen)_2Rh(dpp)\}_2RhCl_2]^{5+}$ trimetallic system and much different in the $[(phen)_2Ru(dpp)RhCl_2(bpy)]^{3+}$ system. The steric crowding around the Rh in the trimetallic is predicted to give faster chloride loss. The current ratio of the first and second reduction peak $((i_p^c)_I/(i_p^c)_{II})$ of $[(phen)_2Ru(dpp)RhCl_2(bpy)]^{3+}$ being larger than 1 suggests that there is another competitive electrochemical mechanism, an EECCE mechanism. This EECCE mechanism is a result of competitive halide loss and $Rh^{II/I}$ reduction at 100 mV/s scan rate. The proposed electrochemical mechanism of bimetallic complex $[(phen)_2Ru(dpp)RhCl_2(bpy)]^{3+}$ (Figure 3.5) is also supported by the CVs as a fuction of scan rates (25 mV/s to 1000 mV/s). The ratio of the second and first peak current for reduction $(i_p^c)_{II}/(i_p^c)_I$ increases with the increased scan rate (Figure 3.6). In both bimetallic $[(phen)_2Ru(dpp)RhCl_2(bpy)]^{3+}$ and trimetallic $[\{(phen)_2Ru(dpp)\}_2RhCl_2]^{5+}$, the HOMO is Ru ($d\pi$)-based and LUMO is Rh($d\sigma^*$)-based.

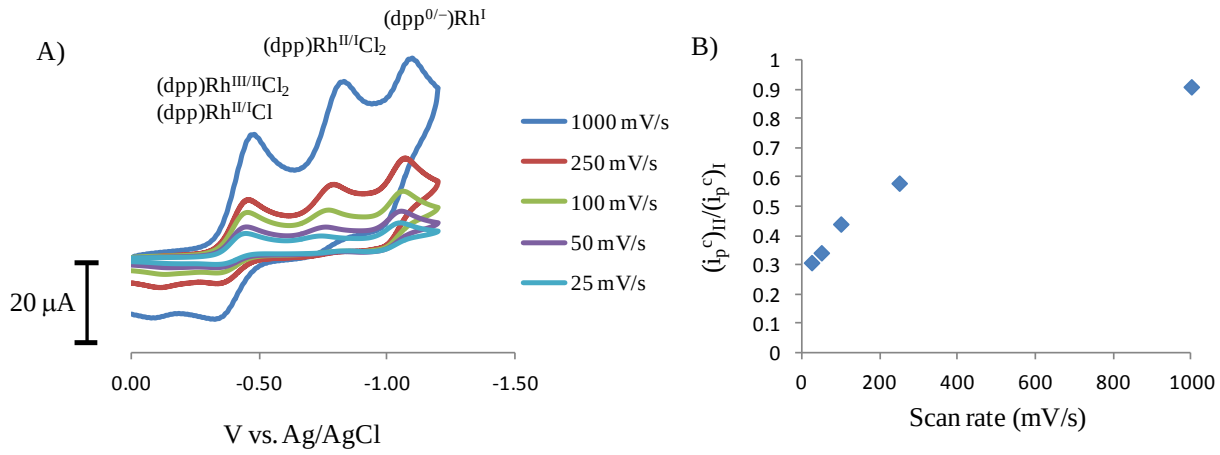

Figure 3.6. Cyclic voltammograms of the complex $[(phen)_2Ru(dpp)RhCl_2(bpy)]^{3+}$ in 0.1 M Bu_4NPF_6 CH_3CN at varied scan rates (25 mV/s to 1000 mV/s) (A) and the plot of the second and first cathodic peak current ratio $(i_p^c)_{II}/(i_p^c)_I$ vs. varied scan rates (25 mV/s to 1000 mV/s) (B).

Table 3.1. Electrochemical properties for Ru monometallic, Ru,Rh bimetallic complex and related Ru,Rh,Ru trimetallic complex in room temperature CH_3CN.

Complex [a]	$E_{1/2}$ (V)	ΔE_p (mV)	i_p^a/i_p^c	Assignments
$[(phen)_2Ru(dpp)]^{2+}$ [81]	+1.45	84	1.05	$Ru^{II/III}$
	–1.02	79	0.93	$dpp^{0/-}$
	–1.42	80	0.89	$phen^{0/-}$
$[(phen)_2Ru(dpp)RhCl_2(bpy)]^{3+}$ [118]	+1.62	82	0.88	$Ru^{II/III}$
	–0.44[b]	99	0.31	$Rh^{III/II}Cl_2$, $Rh^{II/I}Cl$
	–0.79[c]	-	-	$Rh^{II/I}Cl_2$
	–1.03	80	1.05	$dpp^{0/-}$
$[\{(phen)_2Ru(dpp)\}_2RhCl_2]^{5+}$ [120]	+1.61[d]	100	0.95	2 $Ru^{II/III}$
	–0.35[c]	-	-	$Rh^{III/II/I}$
	–0.75	120	0.96	$dpp^{0/-}$
	–1.02	87	0.90	$dpp^{0/-}$

[a]Measured against a Ag/AgCl (3 M NaCl) reference electrode, potential scan rate υ = 100 mV/s with a carbon glassy disk working electrode and a Pt wire counter electrode in 0.1 M Bu_4NPF_6 in acetonitrile at room temperature with bpy = 2,2′-bipyridine, dpp = 2,3-bis(2-pyridyl)pyrazine and phen = 1,10-phenanthroline.
[b] Reported E_p^c of quasi-reversible process.
[c] Reported E_p^c of irreversible process.
[d] Two overlapping, one-electron reversible waves.

3.2.2. Electrochemical Properties of $[(phen)_2Ru(dpp)RhCl_2(phen)]^{3+}$, $[(Ph_2phen)_2Ru(dpp)RhCl_2(phen)]^{3+}$, and $[(Me_2phen)_2Ru(dpp)RhCl_2(phen)]^{3+}$

$[(phen)_2Ru(dpp)RhCl_2(phen)]^{3+}$, $[(Ph_2phen)_2Ru(dpp)RhCl_2(phen)]^{3+}$ and $[(Me_2phen)_2Ru(dpp)RhCl_2(phen)]^{3+}$ have similar electrochemical properties with key differences due to the different TLs on the light absorbers attached to the *cis*-$Rh^{III}Cl_2$ center. The bimetallic complex displays a reversible one-electron $Ru^{II/III}$ oxidation at 1.62, 1.58 and 1.53 V vs. Ag/AgCl for TL = phen, Ph_2phen, Me_2phen, respectively (Figure 3.7) at the potential scan rate of 100 mV/s. All the reductive electrochemistry of $[(TL)_2Ru(dpp)RhCl_2(phen)]^{3+}$ complexes show a quasi-reversible $Rh^{III/II}Cl_2$ couple overlapped with a small amount of $Rh^{II/I}Cl$ reduction and an irreversible $Rh^{II/I}Cl_2$ couple, followed by a reversible $dpp^{0/-}$ couple (Figure 3.7) at the potential scan rate of 100 mV/s. The complex $[(phen)_2Ru(dpp)RhCl_2(phen)]^{3+}$ exhibits a quasi-reversible $Rh^{III/II}Cl_2$ couple overlapped with a small amout of $Rh^{II/I}Cl$ reduction at –0.44 V vs. Ag/AgCl, an irreversible $Rh^{II/I}Cl_2$ reduction at –0.81 V vs. Ag/AgCl and a reversible $dpp^{0/-}$ reduction at –1.03 V vs. Ag/AgCl (Figure 3.7 A). The complex $[(Ph_2phen)_2Ru(dpp)RhCl_2(phen)]^{3+}$ displays a quasi-reversible $Rh^{III/II}Cl_2$ couple overlapped with a small amout of $Rh^{II/I}Cl$ reduction at –0.42 V vs. Ag/AgCl and an irreversible $Rh^{II/I}Cl_2$ reduction at –0.79 V vs. Ag/AgCl, followed by a reversible $dpp^{0/-}$couple at –1.02 V vs. Ag/AgCl (Figure 3.7 B). The complex $[(Me_2phen)_2Ru(dpp)RhCl_2(phen)]^{3+}$ shows two similar Rh-based reductions at –0.44 and –0.79 V vs. Ag/AgCl, and a reversible $dpp^{0/-}$ reduction at –1.02 V vs. Ag/AgCl (Figure 3.7 C). The $Ru^{II/III}$ oxidation couple of $[(Me_2phen)_2Ru(dpp)RhCl_2(phen)]^{3+}$ occurs at 1.53 V vs. Ag/AgCl, a less positive potential compared to the other bimetallic complexes $[(phen)_2Ru(dpp)RhCl_2(phen)]^{3+}$ and $[(Ph_2phen)_2Ru(dpp)RhCl_2(phen)]^{3+}$. This negative shift in the oxidation potential of $[(Me_2phen)_2Ru(dpp)RhCl_2(phen)]^{3+}$ is due to the electron donating

character of the methyl groups on the phen ligand, making the Ru center more electron-rich and easier to oxidize.

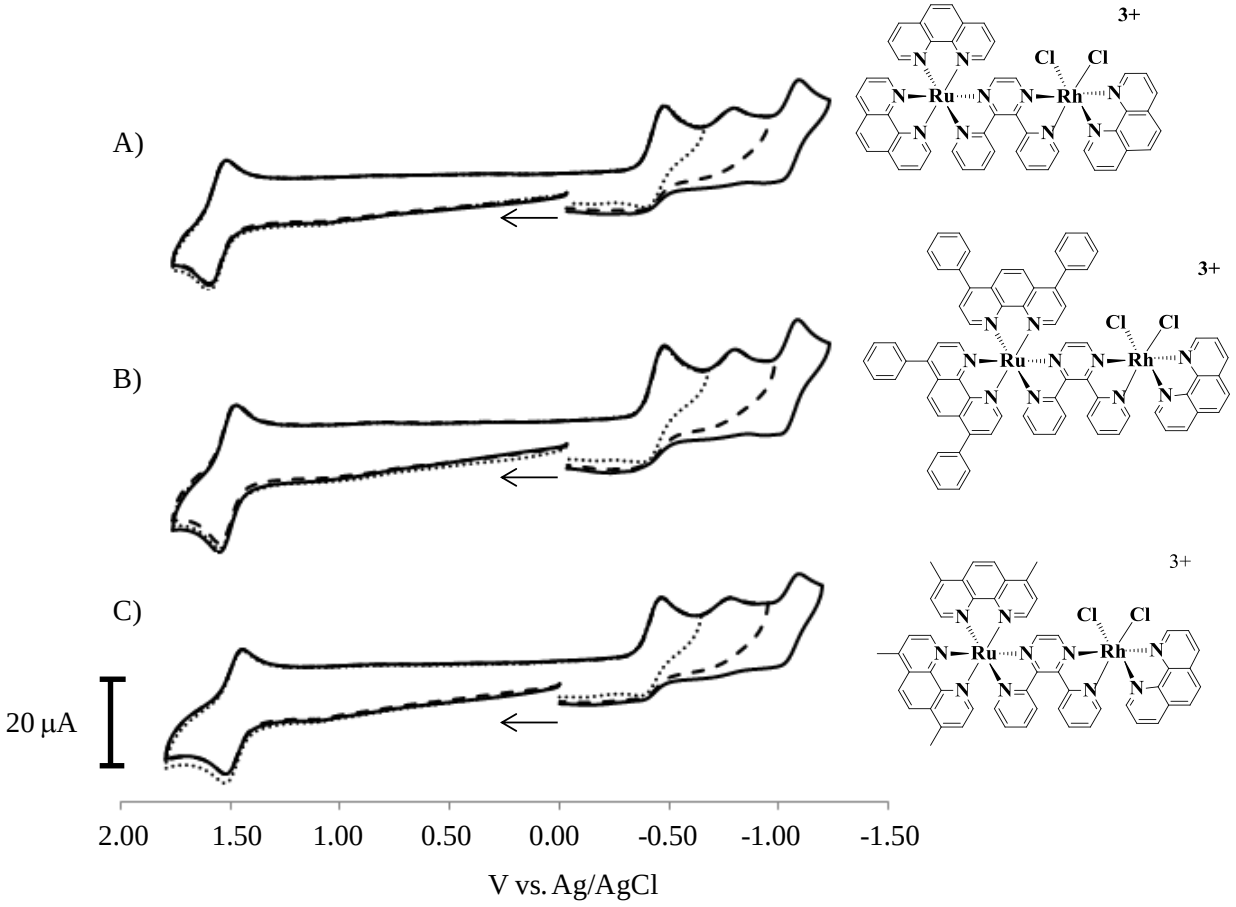

Figure 3.7. Cyclic voltammograms of the bimetallic complexes $[(phen)_2Ru(dpp)RhCl_2(phen)]^{3+}$ (A), $[(Ph_2phen)_2Ru(dpp)RhCl_2(phen)]^{3+}$ (B) and $[(Me_2phen)_2Ru(dpp)RhCl_2(phen)]^{3+}$ (C) at the potential scan rate of 100 mV/s in 0.1 M Bu_4NPF_6 acetonitrile at room temperature with dpp = 2,3-bis(2-pyridyl)pyrazine, phen = 1,10-phenanthroline, Ph_2phen = 4,7-diphenyl-1,10-phenanthroline and Me_2phen = 4,7-dimethyl-1,10-phenanthroline.

The reductive electrochemistry of $[(phen)_2Ru(dpp)RhCl_2(phen)]^{3+}$, $[(Ph_2phen)_2Ru(dpp)RhCl_2(phen)]^{3+}$ and $[(Me_2phen)_2Ru(dpp)RhCl_2(phen)]^{3+}$ was investigated as a function of scan rate 25 mV/s to 1000 mV/s. The CVs of these complexes show the behavior similar to $[(phen)_2Ru(dpp)RhCl_2(bpy)]^{3+}$. All of these bimetallic complexes have

the same proposed electrochemical mechanism (mechanism I A and I B in Figure 3.5). The cathodic peak currents of all three reductions increase with the increased scan rate. The ratio of the second and first cathodic peak currents $(i_p^c)_{II}/(i_p^c)_I$ increases with increased scan rate (Figure 3.8).

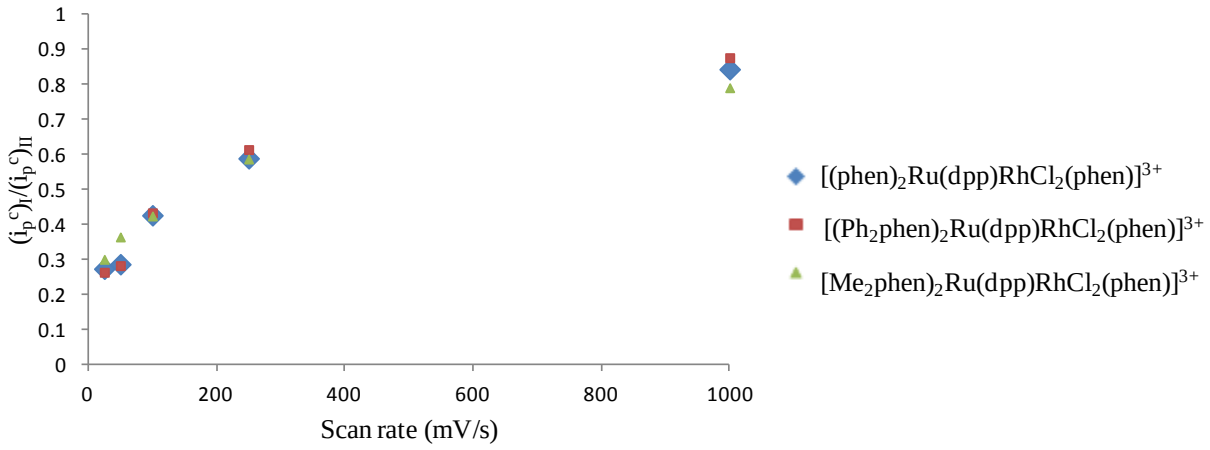

Figure 3.8. The plots of the second and first cathodic peak current ratio $(i_p^c)_{II}/(i_p^c)_I$ in CVs of complex $[(phen)_2Ru(dpp)RhCl_2(phen)]^{3+}$, $[(Ph_2phen)_2Ru(dpp)RhCl_2(phen)]^{3+}$, and $[(Me_2phen)_2Ru(dpp)RhCl_2(phen)]^{3+}$ vs. varied scan rates (25 mV/s to 1000 mV/s) in 0.1 M Bu_4NPF_6 CH_3CN, where dpp = 2,3-bis(2-pyridyl)pyrazine, phen = 1,10-phenanthroline, Ph_2phen = 4,7-diphenyl-1,10-phenanthroline and Me_2phen = 4,7-dimethyl-1,10-phenanthrolin.

The electrochemical properties of the bimetallic complexes $[(TL)_2Ru(dpp)RhCl_2(phen)]^{3+}$ (TL = phen, Ph_2phen, Me_2phen) suggest that all systems have Ru(dπ)-based HOMO and Rh(dσ*)-based LUMO. The fact that the rhodium center is reduced prior to the bridging ligand dpp indicates the presence of a low-lying Ru→Rh ^{3}MMCT excited state, which is important to bioreactivity of these complexes. ^{3}MMCT states have been implicated as the reactive state that leads to O_2 independent DNA photocleavage for related trimetallic systems.[68]

Table 3.2. Electrochemical properties for bimetallic complexes $[(TL)_2Ru(dpp)RhCl_2(phen)]^{3+}$, TL = phen, Ph_2phen, Me_2phen in room temperature CH_3CN.

Complex [a]	$E_{1/2}$ (V)	ΔE_p (mV)	i_p^a/i_p^c	Assignments
$[(phen)_2Ru(dpp)RhCl_2(phen)]^{3+}$	+1.62	80	1.05	$Ru^{II/III}$
	–0.44[b]	95	0.40	$Rh^{III/II}Cl_2$, $Rh^{II/I}Cl$
	–0.81[c]	-	-	$Rh^{II/I}Cl_2$
	–1.03	78	0.92	$dpp^{0/-}$
$[(Ph_2phen)_2Ru(dpp)RhCl_2(phen)]^{3+}$	+1.58	80	1.00	$Ru^{II/III}$
	–0.42[b]	90	0.35	$Rh^{III/II}Cl_2$, $Rh^{II/I}Cl$
	–0.79[c]	-	-	$Rh^{II/I}Cl_2$
	–1.02	82	1.00	$dpp^{0/-}$
$[(Me_2phen)_2Ru(dpp)RhCl_2(phen)]^{3+}$	+1.53	80	0.94	$Ru^{II/III}$
	–0.44[b]	91	0.29	$Rh^{III/II}Cl_2$, $Rh^{II/I}Cl$
	–0.79[c]	-	-	$Rh^{II/I}Cl_2$
	–1.02		0.87	$dpp^{0/-}$

[a]Measured against a Ag/AgCl (3 M NaCl) reference electrode, the potential scan rate υ = 100 mV/s with a carbon glassy disk working electrode and a Pt wire counter electrode in 0.1 M Bu_4NPF_6 in acetonitrile at room temperature with dpp = 2,3-bis(2-pyridyl)pyrazine, phen = 1,10-phenanthroline, Ph_2phen = 4,7-diphenyl-1,10-phenanthroline and Me_2phen = 4,7-dimethyl-1,10-phenanthroline.
[b]Reported E_p^c of quasi-reversible process.
[c] Reported E_p^c of irreversible process.

3.2.3. Electrochemical Properties of the Bimetallic Complexes $[(bpy)_2Ru(dpp)RhCl_2(bpy)]^{3+}$, $[(bpy)_2Ru(dpp)RhCl_2(Me_2bpy)]^{3+}$ Compared with the Trimetallic Complex $[\{(bpy)_2Ru(dpp)\}_2RhCl_2]^{5+}$

The electrochemistry of the trimetallic $[\{(bpy)_2Ru(dpp)\}_2RhCl_2]^{5+}$ has been reported, provided herein for comparison.[72] The electrochemical oxidation of $[\{(bpy)_2Ru(dpp)\}_2RhCl_2]^{5+}$ occurs at 1.60 V vs. Ag/AgCl with two overlapping, one-electron reversible waves assigned to $Ru^{II/III}$ couples (Figure 3.9 A), which is 0.23 V positive of the $Ru^{II/III}$ couple in the monometallic complex.[80] The electrochemical reduction of $[\{(bpy)_2Ru(dpp)\}_2RhCl_2]^{5+}$, which is similar to that of $[\{(phen)_2Ru(dpp)\}_2RhCl_2]^{5+}$ displays two overlapping irreversible one-electron reductions at –0.39 V vs. Ag/AgCl assigned to $Rh^{III/II/I}$ couple, followed by two reversible reductions at –0.79 and –1.02 V vs. Ag/AgCl attributed to two $dpp^{0/-}$ couples.

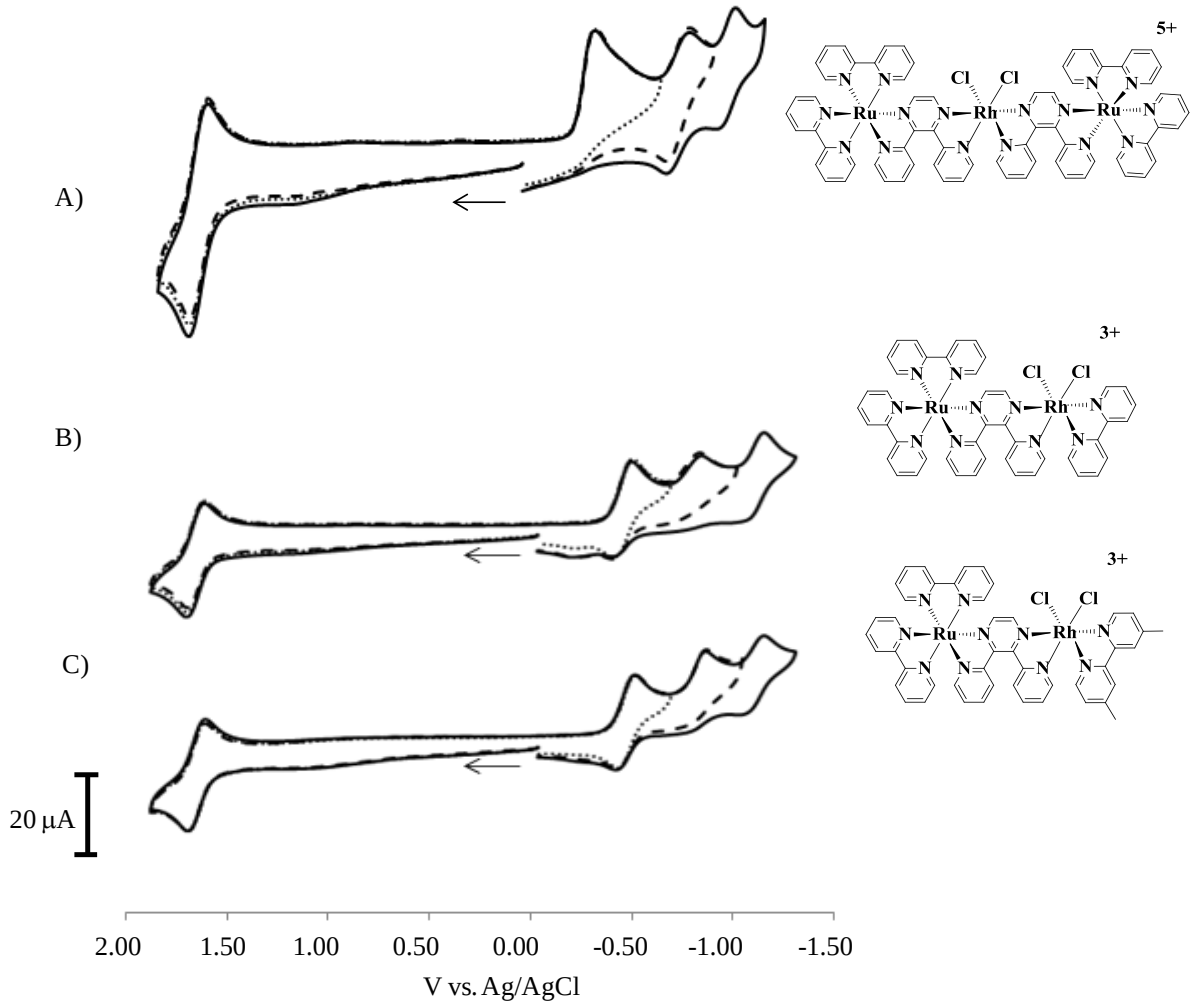

Figure 3.9. Cyclic voltammogram of trimetallic complex $[\{(bpy)_2Ru(dpp)\}_2RhCl_2]^{5+}$ (A) bimetallic complex $[(bpy)_2Ru(dpp)RhCl_2(bpy)]^{3+}$ (B) and $[(bpy)_2Ru(dpp)RhCl_2(Me_2bpy)]^{3+}$ (C) and at the potential scan rate of 100 mV/s in 0.1 M Bu_4NPF_6 acetonitrile room temperature dpp = 2,3-bis(2-pyridyl)pyrazine, bpy = 2,2′-bipyridine and Me_2bpy =4,4′-dimethyl-2,2′-bipyridine.

The electrochemical properties of the bimetallic complexes $[(bpy)_2Ru(dpp)RhCl_2(TL')]^{3+}$ (TL = bpy and Me_2bpy) are different from that of the trimetallic complex $[\{(bpy)_2Ru(dpp)\}_2RhCl_2]^{5+}$ (Figure 3.9). The CV of bimetallic complex $[(bpy)_2Ru(dpp)RhCl_2(bpy)]^{3+}$ at the potential scan rate of 100 mV/s displays a reversible one-electron $Ru^{II/III}$ oxidation at 1.57 V vs. Ag/AgCl. The complex $[(bpy)_2Ru(dpp)RhCl_2(bpy)]^{3+}$ exhibits a quasi-reversible $Rh^{III/II}Cl_2$ couple overlapped with a small amout of $Rh^{II/I}Cl$ reduction at –0.45 V vs. Ag/AgCl and an irreversible $Rh^{II/I}Cl_2$

reduction at −0.74 V vs. Ag/AgCl, and a reversible $dpp^{0/-}$ couple at −1.02 V vs. Ag/AgCl at the potential scan rate of 100 mV/s (Figure 3.9 B). The complex $[(bpy)_2Ru(dpp)RhCl_2(Me_2bpy)]^{3+}$ displays a reversible one-electron $Ru^{II/III}$ oxidation at 1.59 V vs. Ag/AgCl, a more reversible reduction at −0.46 V vs. Ag/AgCl and an irreversible reduction at −0.74 V vs. Ag/AgCl, followed by a reversible $dpp^{0/-}$ reduction at −1.01 V vs. Ag/AgCl at the potential scan rate of 100 mV/s (Figure 3.9 C). When the terminal ligand bpy on the rhodium center is substituted by Me_2bpy, the first reduction of $[(bpy)_2Ru(dpp)RhCl_2(Me_2bpy)]^{3+}$ appears more reversible than the same reductive wave of $[(bpy)_2Ru(dpp)RhCl_2(bpy)]^{3+}$, indicating that the Rh($d\sigma^*$) orbital is modulated by the terminal ligand attached to the rhodium center which may cause orbital inversion of the dpp ($d\pi$) and Rh ($d\sigma^*$) orbitals.[91]

The electrochemical properties of $[(bpy)_2Ru(dpp)RhCl_2(bpy)]^{3+}$ and $[(bpy)_2Ru(dpp)RhCl_2(Me_2bpy)]^{3+}$ were also investigated by CV with varied potential scan rates between 25 mV/s to 1000 mV/s. The cathodic peak currents of all three reductions of both bimetallic complexes increase with the increased potential scan rate as expected. The second and first cathodic peak current ratio $(i_p^c)_{II}/(i_p^c)_I$ of $[(bpy)_2Ru(dpp)RhCl_2(bpy)]^{3+}$ increases with increased potential scan rate (Figure 3.10). However, the same current ratio $(i_p^c)_{II}/(i_p^c)_I$ of $[(bpy)_2Ru(dpp)RhCl_2(Me_2bpy)]^{3+}$ does not increase when the scan rate is increased (Figure 3.10). According to the CVs at the scan rates between 25 mV/s to 1000 mV/s, the electrochemical properties of $[(bpy)_2Ru(dpp)RhCl_2(bpy)]^{3+}$ and $[(bpy)_2Ru(dpp)RhCl_2(Me_2bpy)]^{3+}$ are different from each other, which suggests different electrochemical mechanisms. The electrochemical properties of $[(bpy)_2Ru(dpp)RhCl_2(bpy)]^{3+}$ are similar to those of $[(phen)_2Ru(dpp)RhCl_2(bpy)]^{3+}$ shown as mechanism I A and I B in Figure 3.5, which has a slow chloride loss following the $Rh^{III/II}$couple (the first reduction) and a fast

chloride loss following the second reduction $Rh^{II/I}$, followed by reversible one-electron dpp^{-} based reduction.

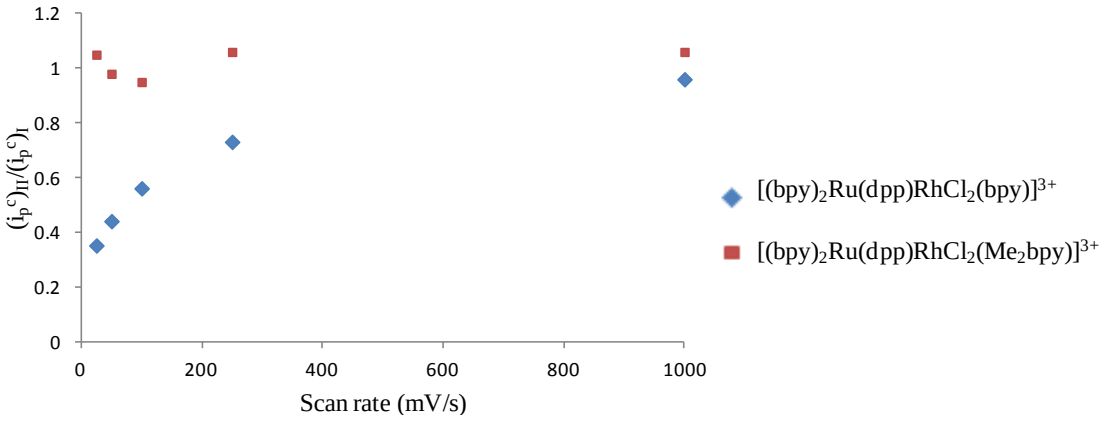

Figure 3.10. The plots of the second and first cathodic peak current ratio $(i_p^c)_{II}/(i_p^c)_I$ in CVs of complex $[(bpy)_2Ru(dpp)RhCl_2(bpy)]^{3+}$, $[(bpy)_2Ru(dpp)RhCl_2(Me_2bpy)]^{3+}$ vs. varied scan rates (25 mV/s to 1000 mV/s) in 0.1 M Bu_4NPF_6 CH_3CN, where dpp = 2,3-bis(2-pyridyl)pyrazine, bpy = 2,2′-bipyridine and Me_2bpy = 4,4′-dimethyl-2,2′-bipyridine.

The electrochemical mechanism of $[(bpy)_2Ru(dpp)RhCl_2(Me_2bpy)]^{3+}$ is proposed here according to its electrochemical data, presented in Figure 3.11 (mechanism II A and II B). The bridging ligand dpp is reduced first based on the reversible one-electron reduction. The highly electron rich dpp^{-} attached to *cis*-$Rh^{III}Cl_2$ facilitates chloride loss from the rhodium center. Then, the Rh^{III} is reduced to Rh^{II} through an intramolecular electron transfer from dpp^{-}. This is analogous to the proposed electrochemistry of the complex $[Re^{I}(^{t}Bu_2bpy)(CO)_3Cl]$ (^{t}Bubpy = 4,4′-ditert-butyl-2,2′-bipyridine), where the ligand $^{t}Bu_2bpy$ reduction leads to halide loss and an intramolecular electron transfers to Re center and produces $Re(^{t}Bu_2bpy)(CO)_3$.[127] For the $[(bpy)_2Ru(dpp)RhCl_2(Me_2bpy)]^{3+}$, the $Rh^{II/I}$ reduction is followed by the second chloride loss. The third reduction is assigned to $dpp^{0/-}$ reduction. At a fast potential scan rate, the bridging ligand dpp is also reduced first followed by $Rh^{III/II}$ reduction before chloride loss. Then, the

highly electron rich dpp^{-} attached to reduced Rh^{II} in *cis*-$Rh^{II}Cl_2$ promotes chloride loss from the rhodium center to produce $(dpp^{-})Rh^{II}Cl$ center. The Rh^{II} becomes Rh^{I} through an intramolecular electron transfer from dpp^{-} followed by the second chloride loss. The third reduction is assigned to $dpp^{0/-}$ reduction. The electrochemical properties of the bimetallic complex $[(bpy)_2Ru(dpp)RhCl_2(Me_2bpy)]^{3+}$ suggest that the system has Ru(dπ)-based HOMO and dpp(π*)-based LUMO.

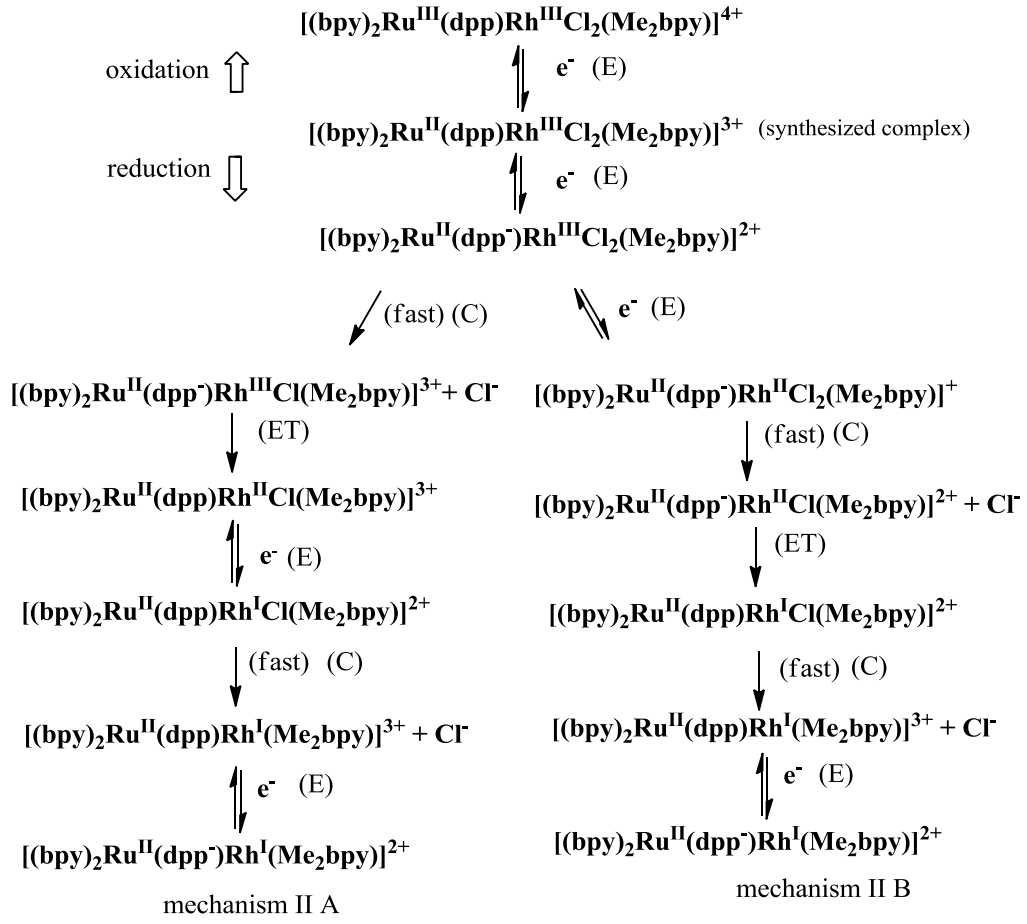

Figure 3.11. The electrochemical mechanisms (II A and II B) of bimetallic complex $[(bpy)_2Ru(dpp)RhCl_2(Me_2bpy)]^{3+}$, bpy = 2,2′-bipyridine, dpp = 2,3-bis(2-pyridyl)pyrazine and Me_2bpy = 4,4′-dimethyl-2,2′-bipyridine.

Table 3.3. Electrochemical properties for Ru monometallic complex and Ru,Rh bimetallic complexes and related Ru,Rh,Ru trimetallic complex in room temperature CH_3CN.

Complex [a]	$E_{1/2}$ (V)	ΔE_p (mV)	i_p^a/i_p^c	Assignments
$[(bpy)_2Ru(dpp)]^{2+}$ [80]	+1.43	82	0.99	$Ru^{II/III}$
	−1.03	87	1.00	$dpp^{0/-}$
	−1.45	102	0.86	$bpy^{0/-}$
$[(bpy)_2Ru(dpp)RhCl_2(bpy)]^{3+}$	+1.57	80	0.98	$Ru^{II/III}$
	−0.45[b]	98	0.33	$Rh^{III/II}Cl_2$, $Rh^{II/I}Cl$
	−0.74[c]	-	-	$Rh^{II/I}Cl_2$
	−1.02	96	0.88	$dpp^{0/-}$
$[(bpy)_2Ru(dpp)RhCl_2(Me_2bpy)]^{3+}$	+1.59	96	1.06	$Ru^{II/III}$
	−0.46[b]	85	0.72	$dpp^{0/-}$, $Rh^{III/II}Cl_2$, $Rh^{II/I}Cl$
	−0.74[c]	-	-	$Rh^{II/I}Cl_2$
	−1.01	98	1.05	$dpp^{0/-}$
$[\{(bpy)_2Ru(dpp)\}_2RhCl_2]^{5+}$ [68]	+1.60[d]	86	1.04	2 $Ru^{II/III}$
	−0.39[c]	-	-	$Rh^{III/II/I}$
	−0.79	112	1.00	$dpp^{0/-}$
	−1.02	97	1.00	$dpp^{0/-}$

[a]Measured against a Ag/AgCl (3 M NaCl) reference electrode, the potential scan rate υ = 100 mV/s with a glassy carbon working electrode and a Pt wire counter electrode in 0.1 M Bu_4NPF_6 acetonitrile at room temperature with dpp = 2,3-bis(2-pyridyl)pyrazine, bpy = 2,2′-bipyridine and Me_2bpy = 4,4′-dimethyl-2,2′-bipyridine.
[b]Reported E_p^c of quasi-reversible process.
[c]Reported E_p^c of irreversible process.
[d]Two overlapping, one-electron reversible waves.

3.2.4. Electrochemical Properties of the Bimetallic Complex $[(bpy)_2Os(dpp)RhCl_2(phen)]^{3+}$ Compared with the Trimetallic Complex $[\{(bpy)_2Os(dpp)\}_2RhCl_2]^{5+}$

The electrochemistry of the bimetallic complex $[(bpy)_2Os(dpp)RhCl_2(phen)]^{3+}$ and the trimetallic complex $[\{(bpy)_2Os(dpp)\}_2RhCl_2]^{5+}$ was investigated using a three electrode system with a Ag/AgCl reference electrode, a carbon glassy disk working electrode and a Pt wire counter electrode in 0.1 M Bu_4PF_6 acetonitrile at room temperature. The cyclic voltammograms (CVs) of both complexes at the potential scan rate of 100 mV/s are shown in Figure 3.12 and electrochemical data are presented in Table 3.4. The electrochemistry of the

trimetallic $[\{(bpy)_2Os(dpp)\}_2RhCl_2]^{5+}$ correlates well with that reported previously.[68] The oxidative electrochemistry of $[\{(bpy)_2Os(dpp)\}_2RhCl_2]^{5+}$ shows two reversible one-electron overlapping $Os^{II/III}$ couples at 1.21 V vs. Ag/AgCl due to the nearly simultaneous oxidation of the two equivalent Os centers. Two overlapping one-electron irreversible reductions occur at –0.39 V vs. Ag/AgCl assigned to the $Rh^{III/II/I}$ couple, followed by two reversible reductions at –0.76 and –1.00 V vs. Ag/AgCl corresponding to two $dpp^{0/-}$ couples.[68] The CV of $[\{(bpy)_2Os(dpp)\}_2RhCl_2]^{5+}$ looks similar to the CV of $[\{(bpy)_2Ru(dpp)\}_2RhCl_2]^{5+}$ at the potential scan rate of 100 mV/s. The Os complex is easier to oxidize consisted with the relative 3d vs. 4d orbitals. The electrochemical mechanism of trimetallic complex $[\{(bpy)_2Os(dpp)\}_2RhCl_2]^{5+}$ proposed by Brewer and coworkers for the reductive region is ECECEE mechanism which is the same as the Ru trimetallics. The first and second one-electron reductions of $[\{(bpy)_2Os(dpp)\}_2RhCl_2]^{5+}$ are also followed by a very fast chemical reaction, chloride loss. The third and forth reductions of $[\{(bpy)_2Os(dpp)\}_2RhCl_2]^{5+}$ are reversibe dpp-based one-electron reductions.

The electrochemical properties of $[(bpy)_2Os(dpp)RhCl_2(phen)]^{3+}$ are different from those of $[\{(bpy)_2Os(dpp)\}_2RhCl_2]^{5+}$. The oxidative electrochemistry of $[(bpy)_2Os(dpp)RhCl_2(phen)](PF_6)_3$ at the scan rate of 100 mV/s shows a reversible one-electron $Os^{II/III}$ couple at 1.20 V vs. Ag/AgCl, 0.26 V positive of the $Os^{II/III}$ couple in the monometallic synthon $[(bpy)_2Os(dpp)](PF_6)_2$.[85] The reductive electrochemistry at the potential scan rate of 100 mV/s shows a quasi-reversible $Rh^{III/II}Cl_2$ couple overlapped with a small amout of $Rh^{II/I}Cl$ reduction at –0.46 vs. Ag/AgCl, an irreversible $Rh^{II/I}Cl_2$ reduction at –0.75 V and a reversible $dpp^{0/-}$ couple at –0.98 V vs. Ag/AgCl (Figure 3.12 B).[119]

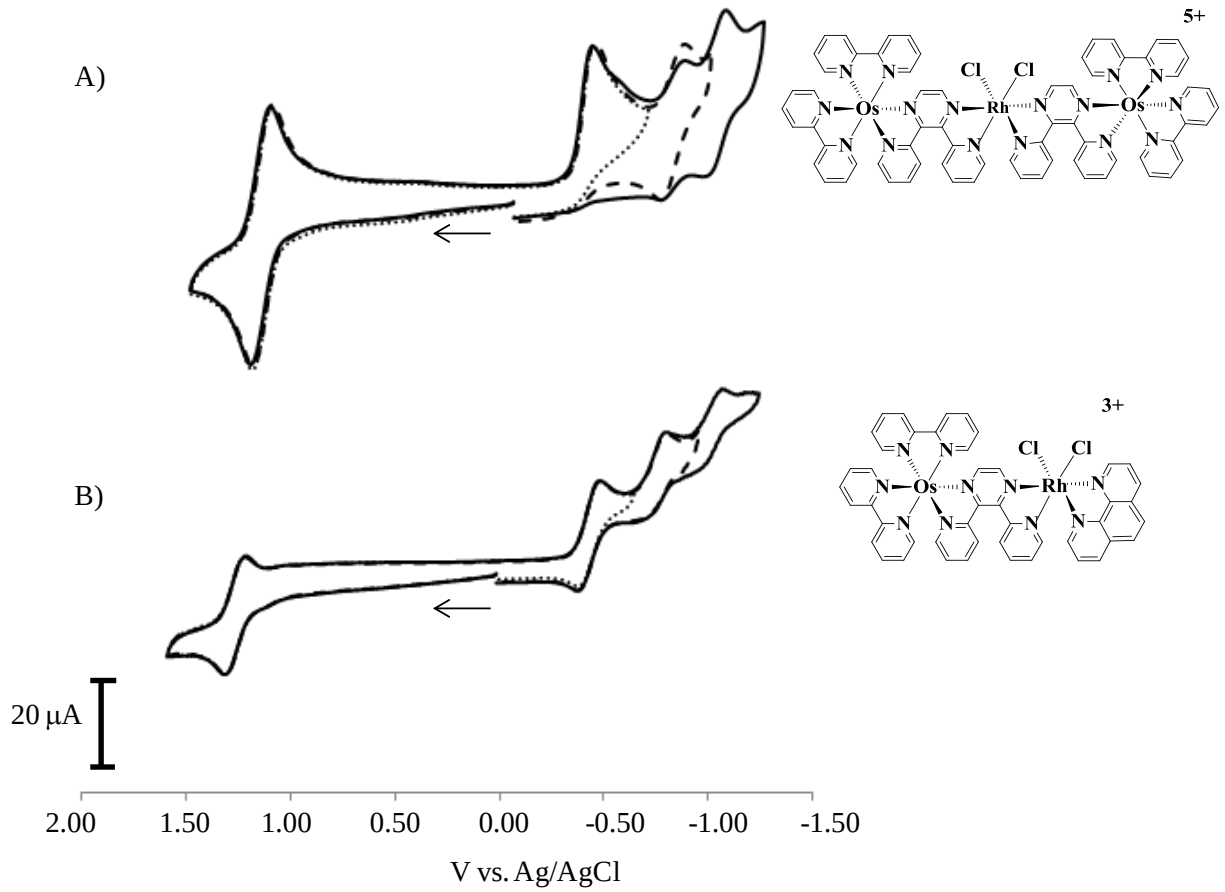

Figure 3.12. Cyclic voltammograms of the trimetallic complex $[\{(bpy)_2Os(dpp)_2RhCl_2](PF_6)_5$ (A) the bimetallic complex $[(bpy)_2Os(dpp)RhCl_2(phen)](PF_6)_3$ (B) and at the potential scan rate of 100 mV/s in 0.1 M Bu_4NPF_6 in acetonitrile at room temperature with bpy = 2,2′-bipyridine, dpp = 2,3-bis(2-pyridyl)pyrazine and phen = 1,10-phenanthroline.

The CVs of bimetallic complex $[(bpy)_2Os(dpp)RhCl_2(phen)]^{3+}$ at the varied potential scan rates from 25 mV/s to 1000 mV/s were shown in Figure 3.13. The complex $[(bpy)_2Os(dpp)RhCl_2(phen)]^{3+}$ shows similar behavior as the complex $[(phen)_2Ru(dpp)RhCl_2(bpy)]^{3+}$ which suggests similar electrochemical mechanisms in Figure 3.5 (mechanism I A and I B). The electrochemical data shows that dpp (π^*) and Rh($d\sigma^*$) orbitals are close in energy, and both the bimetallic and trimetallic complexes display an Os($d\pi$)-based HOMO and a Rh($d\sigma^*$)-based LUMO, indicating the Os,Rh complexes with dpp bridging ligand possess a low-lying Os→Rh metal-to-metal charge transfer (MMCT)

excited state.[68,119]

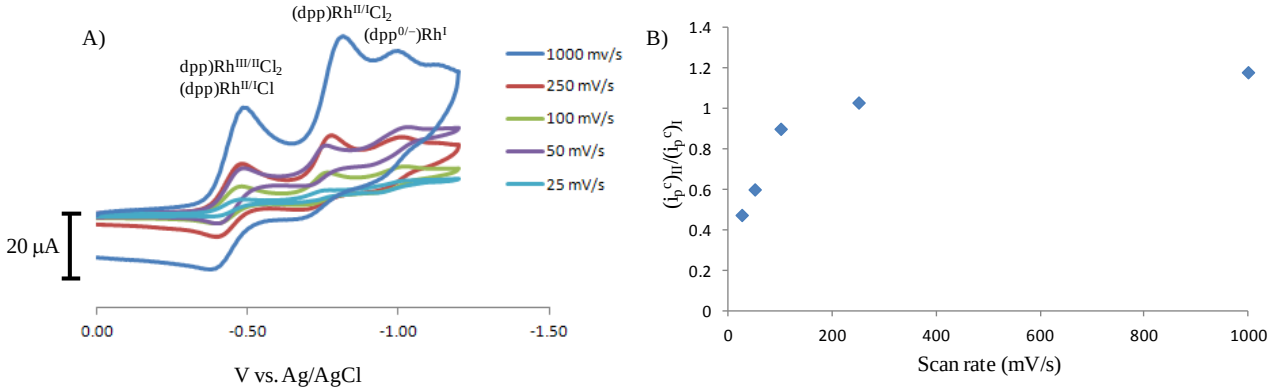

Figure 3.13. Cyclic voltammograms of the complex $[(bpy)_2Os(dpp)RhCl_2(phen)]^{3+}$ in 0.1 M Bu_4NPF_6 CH_3CN at varied potential scan rates (25 mV/s to 1000 mV/s) (A) and the plot of the second and first cathodic peak current ratio $(i_p^c)_{II}/(i_p^c)_I$ vs. varied scan rates (25 mV/s to 1000 mV/s) (B), bpy = 2,2′-bipyridine, dpp = 2,3-bis(2-pyridyl)pyrazine and phen = 1,10-phenanthroline.

Table 3.4. Electrochemical properties for Os monometallic complex and Os,Rh bimetallic complex and related Os,Rh,Os trimetallic complex in room temperature CH_3CN.

Complex [a]	$E_{1/2}$ (V)	ΔE_p	i_p^a/i_p^c	Assignments
$[(bpy)_2Os(dpp)]^{2+}$ [85]	+0.94	94	0.93	$Os^{II/III}$
	−1.02	89	0.95	$dpp^{0/-}$
	−1.38	106	0.98	$bpy^{0/-}$
	−1.58	99	0.88	$bpy^{0/-}$
$[(bpy)_2Os(dpp)RhCl_2(phen)]^{3+}$	+1.20	91	0.92	$Os^{II/III}$
	−0.46[b]	104	0.47	$Rh^{III/II}Cl_2$, $Rh^{II/I}Cl$
	−0.75[c]	-	-	$Rh^{II/I}Cl_2$
	−0.98	96	1.00	$dpp^{0/-}$
$[\{(bpy)_2Os(dpp)\}_2RhCl_2]^{5+}$ [68]	+1.21[d]	96	1.06	$Os^{II/III}$
	−0.39[c]	-	-	$Rh^{III/II/I}$
	−0.76	116	0.86	$dpp^{0/-}$
	−1.00	99	0.92	$dpp^{-/2-}$

[a]Measured against a Ag/AgCl (3 M NaCl) reference electrode, υ = 100 mV/s with a Pt disk working electrode and a Pt wire counter electrode in 0.1 M Bu_4NPF_6 in acetonitrile at room temperature with bpy = 2,2′-bipyridine, dpp = 2,3-bis(2-pyridyl)pyrazine and phen = 1,10-phenanthroline.
[b]Reported E_p^c of quasi-reversible process.
[c]Reported E_p^c of irreversible process.
[d]Two overlapping, one-electron reversible waves.

3.2.5. Summary Comments about Electrochemical Properties of Mixed-Metal Polyazine Complexes.

The electrochemical properties of mixed-metal complexes with coordinated electrochemically active polyazine ligands are complex. The mixed-metal complexes with polyazine ligands exhibit reversible metal-based oxidations and reversible ligand-based reductions, which are ordered by the energy of the ligand π^* orbital. The electrochemical reductions of Rh containing mixed-metal polyazine complexes involve metal and ligand based processes. The Rh($d\sigma^*$) and bridging ligand dpp (π^*) orbitals are energetically close, especially in the bimetallic motifs. The sterics around the Rh center in the bimetallics as well as modulated electronics allow slower chloride loss following Rh reduction complicating observed electrochemistry.

The mixed-metal polyazine complexes discussed herein consist of coupling one or two light absorbers to *cis*-$Rh^{III}Cl_2$ center through the bridging ligand dpp. The structural difference between bimetallic complexes having one light absorber and trimetallic complexes having two light absorbers causes different electrochemical properties. The oxidative electrochemistry of trimetallic complexes $[\{(TL)_2M(dpp)\}_2RhCl_2]^{5+}$ shows two overlapping, one-electron reversible $M^{II/III}$ couples due to the nearly simultaneous oxidation of the two light absorbers. The oxidation of bimetallic complexes $[(TL)_2M(dpp)RhCl_2(TL')]^{3+}$ displays a reversible one-electron $M^{II/III}$ couple due to having only one light absorber. The reductive electrochemistry of trimetallic complexes shows two overlapping, irreversible one-electron $Rh^{III/II/I}$ reductions, followed by the BL $dpp^{0/-}$ reduction. However, the reductive electrochemistry of bimetallic complexes is different from that of trimetallics due to different electronics and sterics in the bimetallic system. The electrochemical mechanisms for bimetallic complexes $[(TL)_2M(dpp)RhCl_2(TL')]^{3+}$ (M = Ru

and Os, TL = bpy, phen, Ph_2phen and Me_2phen, TL′ = phen, bpy and Me_2bpy) are illustrated in Figure 3.14.[88,118] The electrochemical mechanism I A and I B are proposed for bimetallic complexes $[(phen)_2Ru(dpp)RhCl_2(bpy)]^{3+}$, $[(phen)_2Ru(dpp)RhCl_2(phen)]^{3+}$, $[(Ph_2phen)_2Ru(dpp)RhCl_2(phen)]^{3+}$, $[(Me_2phen)_2Ru(dpp)RhCl_2(phen)]^{3+}$, $[(bpy)_2Ru(dpp)RhCl_2(bpy)]^{3+}$ and $[(bpy)_2Os(dpp)RhCl_2(phen)]^{3+}$. At a slow potential scan (mechanism I A), the first and second one-electron reduction of the complex $[(phen)_2Ru(dpp)RhCl_2(bpy)]^{3+}$ is followed by a chemical reaction of a chloride loss. The chloride loss followed by the $Rh^{II/I}$ reduction is much faster than the chloride loss followed by $Rh^{III/II}$ reduction. The third reduction is bridging ligand $dpp^{0/-}$ reduction. At a fast potential scan (mechanism I B), the *cis*-$Rh^{III}Cl_2$ center reduced by two electrons before chloride loss occurs. Often a mix of mechanism I A and I B are seen giving reductive couples with unequal current. The electrochemical mechanism II A and II B are proposed for bimetallic complex $[(bpy)_2Ru(dpp)RhCl_2(Me_2bpy)]^{3+}$. At slow potential scan (mechanism II A), the bridging ligand dpp of $[(bpy)_2Ru(dpp)RhCl_2(Me_2bpy)]^{3+}$ is reduced first based on the reversibility of the first one-electron reduction. The highly electron rich dpp^- attached to *cis*-$Rh^{III}Cl_2$ facilitates chloride loss from the rhodium center. After chloride loss, the Rh^{III} is reduced to Rh^{II} through an intramolecular electron transfer from dpp^-. The $Rh^{II/I}$ reduction is followed by the second chloride loss. The third reduction is assigned to $dpp^{0/-}$ reduction. At a fast potential scan (mechanism II B), the bridging ligand dpp is also reduced first, followed by a $Rh^{III/II}$ reduction before chloride loss. Then, the high electron rich dpp^- attached to *cis*-$Rh^{II}Cl_2$ promotes chloride loss. The Rh^{II} is reduced to Rh^{I} through an intramolecular electron transfer from dpp^- followed by the second chloride loss. The third reduction is assigned to $dpp^{0/-}$ reduction. Often the two mechanisms (II A and II B) occur simultaneously providing unequal reductive peak currents.

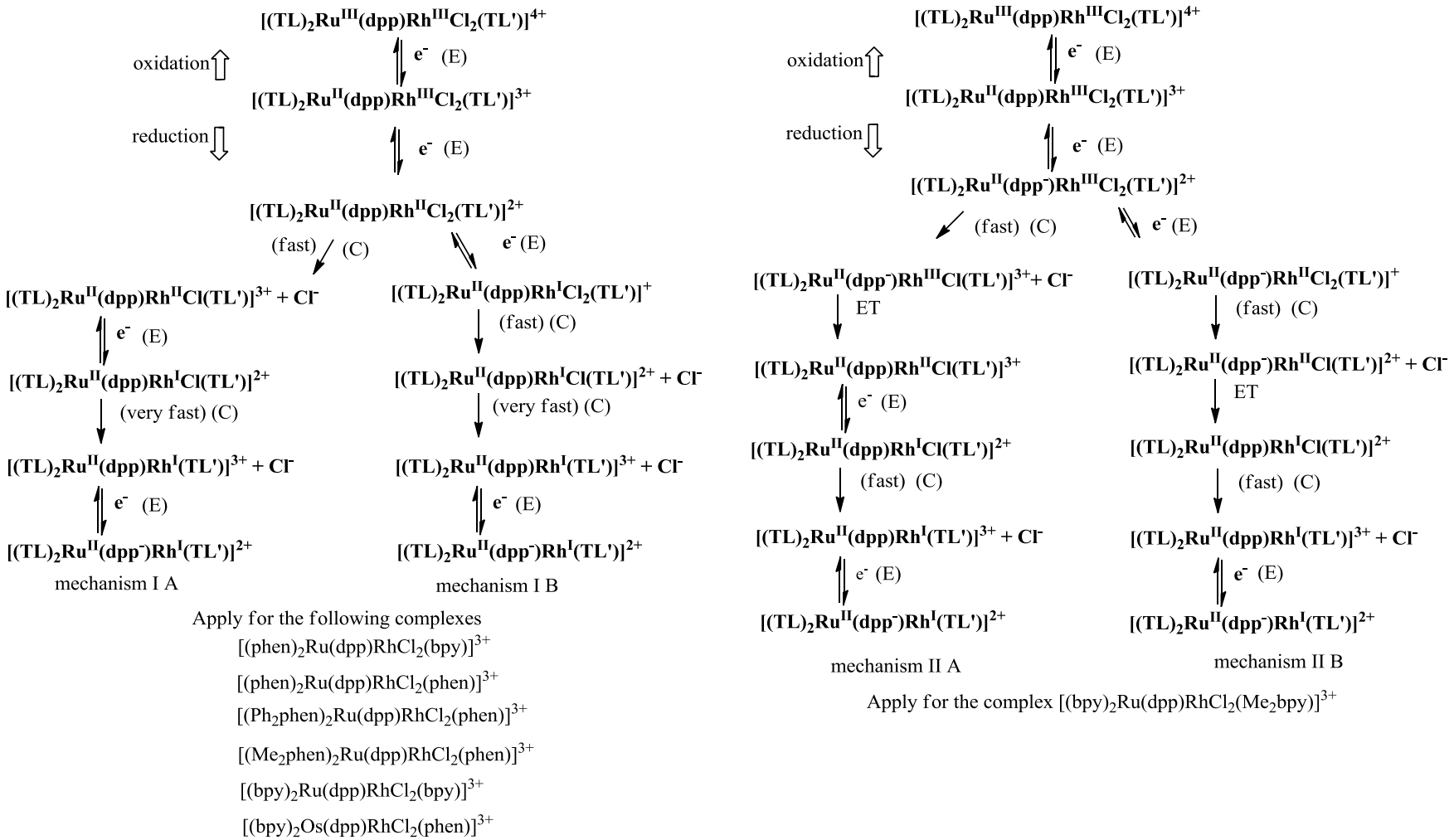

Figure 3.14. The electrochemical mechanisms of bimetallic complexes $[(TL)_2M(dpp)RhCl_2(TL')]^{3+}$ (M = Ru and Os, TL = bpy, phen, Ph_2phen and Me_2phen, TL′ = phen, bpy and Me_2bpy), bpy = 2,2′-bipyridine, dpp = 2,3-bis(2-pyridyl)pyrazine and phen = 1,10-phenanthroline, Ph_2phen = 4,7-diphenyl-1,10-phenanthroline, Me_2phen = 4,7-dimethyl-1,10-phenanthroline and Me_2bpy = 4,4′-dimethyl-2,2′-bipyridine.

The reductive electrochemistry of bimetallic complexes $[(TL)_2Ru(dpp)RhCl_2(TL')]^{3+}$ is more complex than that of trimetallic complexes $[\{(TL)_2Ru(dpp)\}_2RhCl_2]^{5+}$. The trimetallics are sterically crowded and the *cis*-$Rh^{III}Cl_2$ is bound to two withdrawing μ-dpp ligands, which enhances the rate of loss of the first chloride ligand following the first rhodium reduction $Rh^{III/II}$. However, for the bimetallic system, the Rh(dσ*) and BL dpp (π*) orbital energy are modulated by the electronic property of the terminal ligand TL′ attached to the *cis*-$Rh^{III}Cl_2$. Since the *cis*-$Rh^{III}Cl_2$ is bound to a μ-dpp ligand and a terminal ligand, the electronic and steric properties of the bimetallic complexes depend on the terminal ligand attached to the *cis*-$Rh^{III}Cl_2$ center. These factors make the reductive electrochemistry of bimetallic complexes complicated and occur via multiple mechanisms as proposed herein (Figure 3.14).

The electrochemical properties of bimetallic complexes can be modulated by variation of the light absorber's metal center, the terminal ligand on the light absorber and the terminal ligand attached to the rhodium center. The $Os^{II/III}$ oxidation couple of $[(bpy)_2Os(dpp)RhCl_2(phen)]^{3+}$ occurs at 1.20 V vs. Ag/AgCl, ca. 0.40 V less positive than the $Ru^{II/III}$ oxidation of Ru,Rh bimetallic complexes $[(TL)_2Ru(dpp)RhCl_2(TL')]^{3+}$ due to the energy of the Os(dπ) orbital that is higher than that of Ru (dπ) orbital. The $Ru^{II/III}$ oxidation couple of $[(Me_2phen)_2Ru(dpp)RhCl_2(phen)]^{3+}$ occurs at a less positive potential compared to the bimetallic complexes with TL = phen or Ph_2phen in light absorbers attributed to the electronic donating character of Me_2phen. The first Rh reduction of $[(bpy)_2Ru(dpp)RhCl_2(Me_2bpy)]^{3+}$ appears more reversible than the same reductive wave of complex $[(bpy)_2Ru(dpp)RhCl_2(bpy)]^{3+}$ indicating that the Rh(dσ*) orbital is modulated by the terminal ligand attached to the rhodium center and is proposed to have different electrochemical mechanisms from other bimetallic complexes discussed in this dissertation.[91]

3.3. Electronic Absorption Spectroscopic Results

Electronic absorption spectra of the mixed-metal polyazine complexes were collected using a Hewlett-Packard 8453A diode array spectrophotometer in spectrophotometric grade acetonitrile at room temperature. This instrument provides a 1 nm resolution and is adequate for the very broad transitions in these complexes. Determination of ε is conducted using gravimeteric and volumetric methods collected in triplicate with three separated masses of sample dissolved in a known solution volume. The mixed-metal polyazine complexes discussed herein consist of one or two light absorbers coupled to a *cis*-$Rh^{III}Cl_2$ center through the bridging ligand dpp. They are efficient light absorbers and display ligand based $\pi \rightarrow \pi^*$ transitions in the UV region of the spectrum. They also display metal-to-ligand charge transfer (MLCT) transitions in the visible and low energy visible region of the spectrum. The electronic absorption spectroscopic properties of the new bimetallic complexes will be discussed in detail and compared with those of the previously reported trimetallic complexes in CH_3CN solvent.

3.3.1. Electronic Absorption Spectroscopy of the Bimetallic Complex $[(phen)_2Ru(dpp)RhCl_2(bpy)]^{3+}$ Compared with the Trimetallic Complex $[\{(phen)_2Ru(dpp)\}_2RhCl_2]^{5+}$

In contrast to the electrochemical properties, the light absorbing properties of the bimetallic vs. trimetallic systems are quite similar, primarily modulated by intensity of transitions being additive and reflective of the number of each subunit in the complexes. The electronic absorption spectrum of $[\{(phen)_2Ru(dpp)\}_2RhCl_2]^{5+}$ displays the characteristic absorptions from the ruthenium polyazine light absorbers in the UV and visible region of the spectrum which is presented in Figure 3.15 and summarized in Table 3.5. The trimetallic complex

$[\{(phen)_2Ru(dpp)\}_2RhCl_2]^{5+}$, as previously reported, strongly absorbs at 262 nm ($\varepsilon = 15.6 \times 10^4$ $M^{-1}cm^{-1}$) in the UV region due to phen $\pi \rightarrow \pi^*$ IL transition,[95] and displays a shoulder at 346 nm ($\varepsilon = 4.6 \times 10^4$ $M^{-1}cm^{-1}$) attributed to dpp $\pi \rightarrow \pi^*$ IL transition (Figure 3.15)[84,92,95]. The Ru-based MLCT transitions of $[\{(phen)_2Ru(dpp)\}_2RhCl_2]^{5+}$ in the visible region of the spectrum consist of the Ru(dπ)→phen(π^*) CT transition (λ_{max}^{abs} = 414 nm, $\varepsilon = 2.2 \times 10^4$ $M^{-1}cm^{-1}$) at the higher energy region and the Ru(dπ)→dpp(π^*) CT transition (λ_{max}^{abs} = 512 nm, $\varepsilon = 2.7 \times 10^4$ $M^{-1}cm^{-1}$) at the lower energy region.[81]

The bimetallic complex $[(phen)_2Ru(dpp)RhCl_2(bpy)]^{3+}$ with only one ruthenium polyazine light absorber shows similar spectroscopic properties as Ru trimetallic complexes, with approximately half the extinction coefficient values relative to the trimetallics both in the UV and visible regions of the spectrum (Table 3.5).[118] The bimetallic complex $[(phen)_2Ru(dpp)RhCl_2(bpy)]^{3+}$ also strongly absorbs at 262 nm ($\varepsilon = 8.6 \times 10^4$ $M^{-1}cm^{-1}$) in the UV region assigned to phen and bpy $\pi \rightarrow \pi^*$ IL transitions. A shoulder appears at 356 nm ($\varepsilon = 2.1 \times 10^4$ $M^{-1}cm^{-1}$) attributed to dpp $\pi \rightarrow \pi^*$ IL transition in the UV region (Figure 3.15). The transitions in the visible region of the spectrum are assigned to the Ru(dπ)→phen(π^*) CT transition at 413 nm ($\varepsilon = 1.1 \times 10^4$ $M^{-1}cm^{-1}$) and the Ru(dπ)→dpp(π^*) CT transition at 505 nm ($\varepsilon = 1.4 \times 10^4$ $M^{-1}cm^{-1}$).[118]

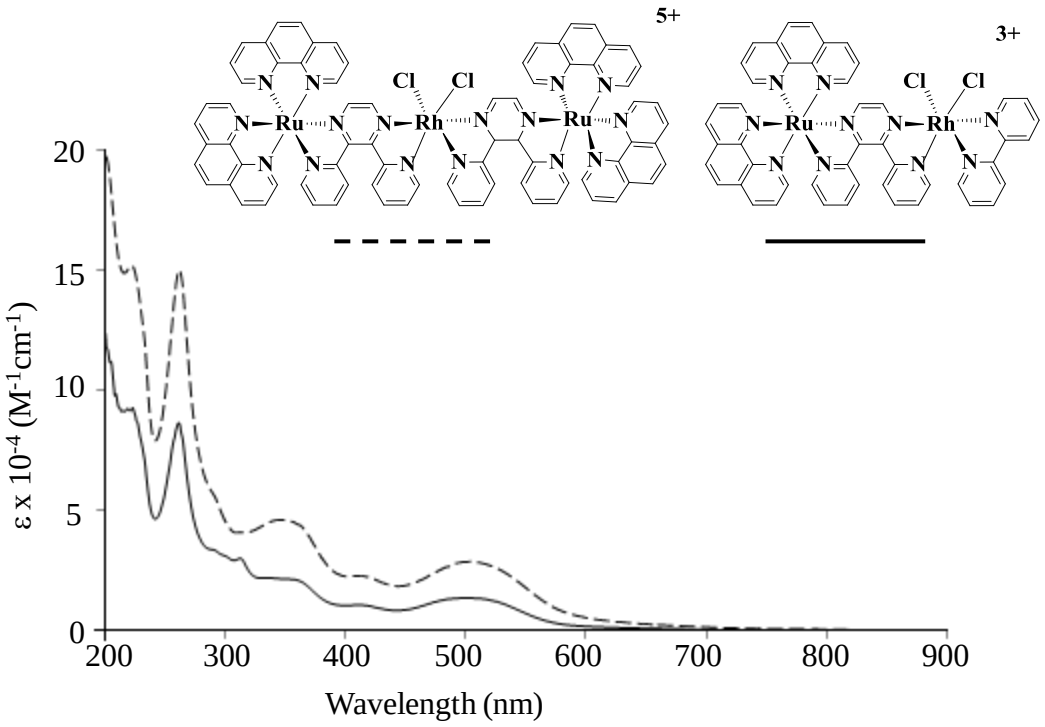

Figure 3.15. Electronic absorption spectra of $[(phen)_2Ru(dpp)RhCl_2(bpy)]^{3+}$ (solid line) and $[\{(phen)_2Ru(dpp)\}_2RhCl_2]^{5+}$ (dashed line) in CH_3CN at room temperature with bpy = 2,2′-bipyridine, dpp = 2,3-bis(2-pyridyl)pyrazine and phen = 1,10-phenanthroline.

Table 3.5. Light absorbing properties of Ru,Rh bimetallic and related Ru,Rh,Ru trimetallic in room temperature CH_3CN.

Complex [a]	λ^{abs} (nm)	$\varepsilon \times 10^{-4}$ ($M^{-1}cm^{-1}$)	Assignment
$[(phen)_2Ru(dpp)RhCl_2(bpy)]^{3+}$	262	8.6	phen, bpy π→π*
	356	2.1	dpp π→π*
	413	1.1	Ru(dπ)→phen(π*) CT
	505	1.4	Ru(dπ)→dpp(π*) CT
$[\{(phen)_2Ru(dpp)\}_2RhCl_2]^{5+}$	262	15.6	phen π→π*
	346	4.6	dpp π→π*
	414	2.2	Ru(dπ)→phen(π*) CT
	512	2.7	Ru(dπ)→dpp(π*) CT

[a] Measured in CH_3CN at room temperature, bpy = 2,2′-bipyridine, dpp = 2,3-bis(2-pyridyl)pyrazine and phen = 1,10-phenanthroline.

3.3.2. Electronic Absorption Spectroscopy Properties of $[(phen)_2Ru(dpp)RhCl_2(phen)]^{3+}$, $[(Me_2phen)_2Ru(dpp)RhCl_2(phen)]^{3+}$ and $[(Ph_2phen)_2Ru(dpp)RhCl_2(phen)]^{3+}$

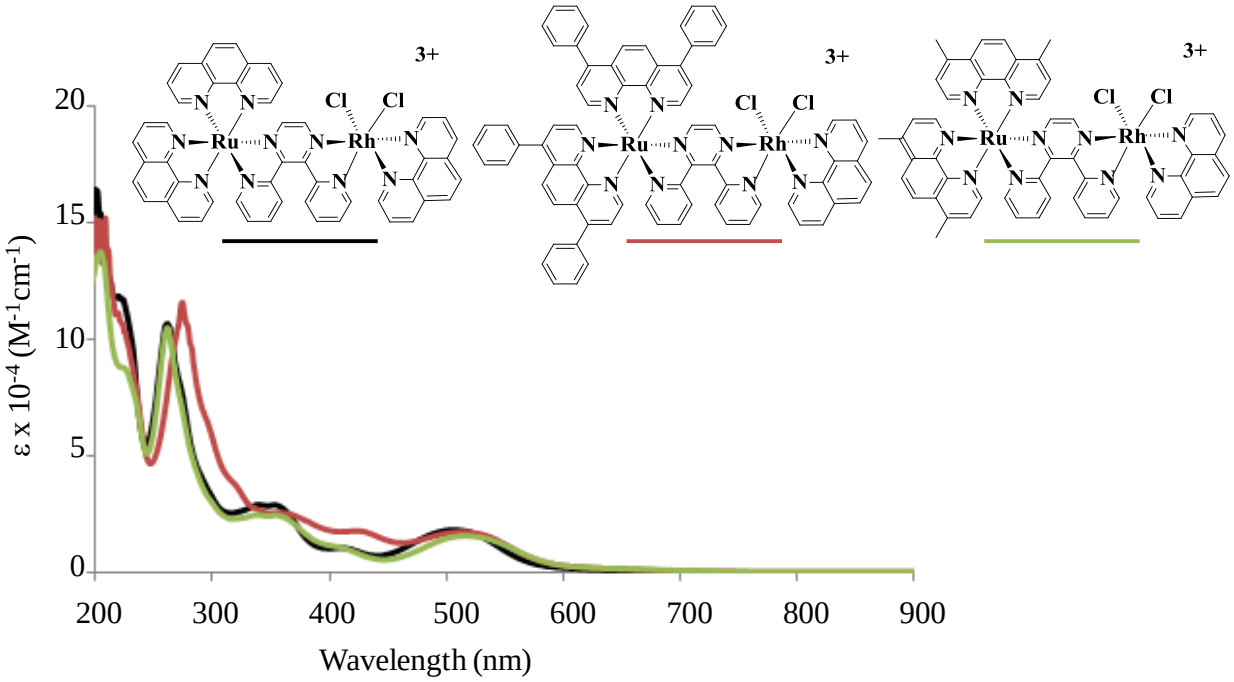

Figure 3.16. Electronic absorption spectra of $[(phen)_2Ru(dpp)RhCl_2(phen)]^{3+}$ (black line), $[(Ph_2phen)_2Ru(dpp)RhCl_2(phen)]^{3+}$ (red line) and $[(Me_2phen)_2Ru(dpp)RhCl_2(phen)]^{3+}$ (green line) in CH_3CN at room temperature, dpp = 2,3-bis(2-pyridyl)pyrazine, phen = 1,10-phenanthroline, Ph_2phen = 4,7-diphenyl-1,10-phenanthroline and Me_2phen = 4,7-dimethyl-1,10-phenanthroline.

The electronic absorption spectra of bimetallic complexes $[(TL)_2Ru(dpp)RhCl_2(phen)]^{3+}$ (TL = phen, Ph_2phen and Me_2phen) display ligand-based $\pi\rightarrow\pi^*$ transitions in the UV region of the spectrum and metal-to-ligand charge transfer (MLCT) transitions in the visible region of the spectrum (Figure 3.16 and Table 3.6). The electronic absorption spectrum of complex $[(phen)_2Ru(dpp)RhCl_2(phen)]^{3+}$ displays phen-based $\pi\rightarrow\pi^*$ transition at 262 nm ($\varepsilon = 10.7 \times 10^4$ $M^{-1}cm^{-1}$), the same wavelength as phen-based transition of trimetallic complex $[\{(phen)_2Ru(dpp)\}_2RhCl_2]^{5+}$, indicating that the energy of ligand-based $\pi\rightarrow\pi^*$ transition is not impacted by the number of coordinated metal centers. A shoulder of the complex absorption

spectrum appears at 346 nm ($\varepsilon = 2.9 \times 10^4\ M^{-1}cm^{-1}$) attributed to dpp-based $\pi\rightarrow\pi^*$ transition, which is similar to the spectrum of trimetallic complex $[\{(phen)_2Ru(dpp)\}_2RhCl_2]^{5+}$.[128] The complex $[(phen)_2Ru(dpp)RhCl_2(phen)]^{3+}$ displays a $Ru(d\pi)\rightarrow phen(\pi^*)$ CT transition at 411 nm ($\varepsilon = 1.1 \times 10^4\ M^{-1}cm^{-1}$), followed by an intense $Ru(d\pi)\rightarrow dpp(\pi^*)$ CT transition at 508 nm ($\varepsilon = 1.9\times10^4\ M^{-1}cm^{-1}$). The electronic absorption spectrum of complex $[(Me_2phen)_2Ru(dpp)RhCl_2(phen)]^{3+}$ is close to that of complex $[(phen)_2Ru(dpp)RhCl_2(phen)]^{3+}$ except that several transitions red shift to the longer wavelength. The bimetallic complex $[(Me_2phen)_2Ru(dpp)RhCl_2(phen)]^{3+}$ strongly absorbs at 262 nm ($\varepsilon = 10.5 \times 10^4\ M^{-1}cm^{-1}$, Me_2phen and phen $\pi\rightarrow\pi^*$ transitions) with a shoulder at 354 nm($\varepsilon = 2.4 \times 10^4\ M^{-1}cm^{-1}$, dpp $\pi\rightarrow\pi^*$ transition) in the UV region. The $Ru(d\pi)\rightarrow Me_2phen(\pi^*)$ CT transition red shifts to 414 nm ($\varepsilon = 1.0 \times 10^4\ M^{-1}cm^{-1}$), and the $Ru(d\pi)\rightarrow dpp(\pi^*)$ CT transition red shifts to 516 nm ($\varepsilon = 1.6 \times 10^4\ M^{-1}cm^{-1}$), compared with the MLCT transitions of $[(phen)_2Ru(dpp)RhCl_2(phen)]^{3+}$.

The electronic absorption spectrum of $[(Ph_2phen)_2Ru(dpp)RhCl_2(phen)]^{3+}$ displays enhanced spectral coverage in the UV and visible regions without the absorption dropping between 350 nm and 450 nm which is typical for the bpy and phen systems.[129,130] The electronic spectrum of $[(Ph_2phen)_2Ru(dpp)RhCl_2(phen)]^{3+}$ shows an intense Ph_2phen-based $\pi\rightarrow\pi^*$ transition at 274 nm ($\varepsilon = 11.6 \times 10^4\ M^{-1}cm^{-1}$) in the UV region,[99] with a shoulder at 362 nm ($\varepsilon = 2.6 \times 10^4\ M^{-1}cm^{-1}$) corresponding to dpp-based $\pi\rightarrow\pi^*$ transition. The $Ru(d\pi)\rightarrow Ph_2phen(\pi^*)$ CT transition occurs at 425 nm ($\varepsilon = 1.8 \times 10^4\ M^{-1}cm^{-1}$), and the $Ru(d\pi)\rightarrow dpp(\pi^*)$ CT transition is centered at 515 nm ($\varepsilon = 1.7 \times 10^4\ M^{-1}cm^{-1}$).

Table 3.6. Light absorbing properties of Ru,Rh bimetallic $[(TL)_2Ru(dpp)RhCl_2(phen)]^{3+}$ in room temperature CH_3CN.

Complex [a]	λ^{abs} (nm)	$\varepsilon \times 10^{-4}$ ($M^{-1}cm^{-1}$)	Assignment
$[(phen)_2Ru(dpp)RhCl_2(phen)]^{3+}$	262	10.7	phen $\pi\rightarrow\pi^*$
	346	2.9	dpp $\pi\rightarrow\pi^*$
	411	1.1	$Ru(d\pi)\rightarrow phen(\pi^*)$ CT
	508	1.9	$Ru(d\pi)\rightarrow dpp(\pi^*)$ CT
$[(Ph_2phen)_2Ru(dpp)RhCl_2(phen)]^{3+}$	274	11.6	Ph_2phen, phen $\pi\rightarrow\pi^*$
	362	2.6	dpp $\pi\rightarrow\pi^*$
	425	1.8	$Ru(d\pi)\rightarrow Ph_2phen(\pi^*)$ CT
	515	1.7	$Ru(d\pi)\rightarrow dpp(\pi^*)$ CT
$[(Me_2phen)_2Ru(dpp)RhCl_2(phen)]^{3+}$	262	10.5	Me_2phen, phen $\pi\rightarrow\pi^*$
	354	2.4	dpp $\pi\rightarrow\pi^*$
	414	1.0	$Ru(d\pi)\rightarrow Me_2phen(\pi^*)$ CT
	516	1.6	$Ru(d\pi)\rightarrow dpp(\pi^*)$ CT

[a]Measured in CH_3CN at room temperature, dpp = 2,3-bis(2-pyridyl)pyrazine, phen = 1,10-phenanthroline, Ph_2phen = 4,7-diphenyl-1,10-phenanthroline and Me_2phen = 4,7-dimethyl-1,10-phenanthroline.

3.3.3. Electronic Absorption Spectroscopy of the Bimetallic Complexes $[(bpy)_2Ru(dpp)RhCl_2(bpy)]^{3+}$ and $[(bpy)_2Ru(dpp)RhCl_2(Me_2bpy)]^{3+}$ Compared with the Trimetallic Complex $[\{(bpy)_2Ru(dpp)\}_2RhCl_2]^{5+}$

The electronic absorption spectra of the bimetallic complexes $[(bpy)_2Ru(dpp)RhCl_2(TL')]^{3+}$ (TL′ = bpy and Me_2bpy) and the trimetallic complex $[\{(bpy)_2Ru(dpp)\}_2RhCl_2]^{5+}$ display the characteristic absorptions from the ruthenium polyazine light absorbers in the UV and visible region of the spectrum which are presented in Figure 3.17 and summarized in Table 3.7. The electronic absorption spectrum of trimetallic complex $[\{(bpy)_2Ru(dpp)\}_2RhCl_2]^{5+}$ reported previously, displays bpy-based $\pi\rightarrow\pi^*$ transition at 284 nm ($\varepsilon = 9.8 \times 10^4$ $M^{-1}cm^{-1}$) in the UV region of the spectrum.[95] A shoulder of the complex absorption spectrum occurs at 338 nm ($\varepsilon = 4.1 \times 10^4$ $M^{-1}cm^{-1}$) attributed to dpp-based $\pi\rightarrow\pi^*$ transition. The $Ru(d\pi)\rightarrow bpy(\pi^*)$ CT transition

(λ_{max}^{abs} = 414 nm, ε = 1.6 × 10^4 $M^{-1}cm^{-1}$) occurs at a higher energy than the Ru(dπ)→dpp(π*) CT transition (λ_{max}^{abs} = 518 nm, ε = 2.6 × 10^4 $M^{-1}cm^{-1}$).[68,120]

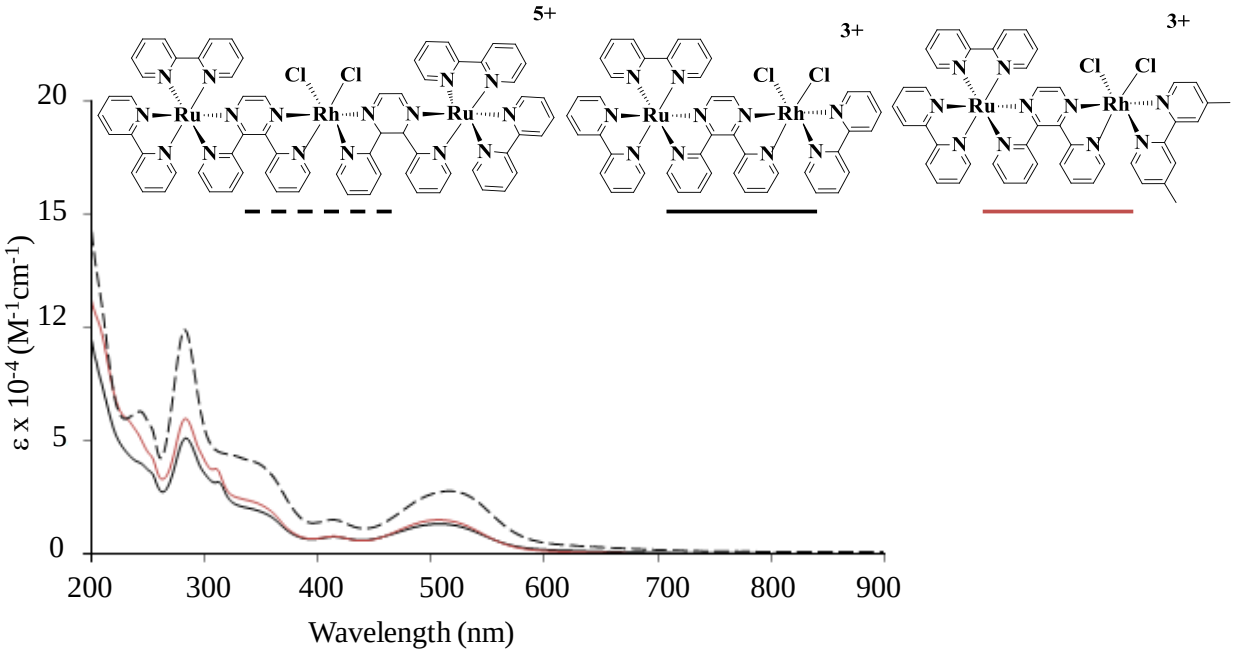

Figure 3.17. Electronic absorption spectra of $[(bpy)_2Ru(dpp)RhCl_2(bpy)]^{3+}$ (black line), $[(bpy)_2Ru(dpp)RhCl_2(Me_2bpy)]^{3+}$ (red line) and $[\{(bpy)_2Ru(dpp)\}_2RhCl_2]^{5+}$ (dash line) in CH_3CN at room temperature with dpp = 2,3-bis(2-pyridyl)pyrazine, bpy = 2,2′-bipyridine and Me_2bpy = 4,4′-dimethyl-2,2′-bipyridine.

The electronic absorption spectrum of the bimetallic complex $[(bpy)_2Ru(dpp)RhCl_2(bpy)]^{3+}$ is similar to that of the trimetallic complex $[\{(bpy)_2Ru(dpp)\}_2RhCl_2]^{5+}$ with extinction coefficients consistent with the number of light absorbers. An intense transition band at 284 nm (ε = 5.1 × 10^4 $M^{-1}cm^{-1}$) in the UV region is assigned to bpy π→π* IL transition[95], which is at the same wavelength as bpy-based transition of trimetallic complex $[\{(bpy)_2Ru(dpp)\}_2RhCl_2]^{5+}$.[120] A shoulder at 338 nm (ε = 2.0 × 10^4 $M^{-1}cm^{-1}$) is attributed to dpp π→π* IL transition. The Ru(dπ)→bpy(π*) CT transition is observed at 414 nm (ε = 0.7 × 10^4 $M^{-1}cm^{-1}$), and the

Ru(dπ)→dpp(π*) CT transition is shown at 510 nm (ε = 1.3 × 10^4 $M^{-1}cm^{-1}$). The electronic absorption spectrum of $[(bpy)_2Ru(dpp)RhCl_2(Me_2bpy)]^{3+}$ is close to that of $[(bpy)_2Ru(dpp)RhCl_2(bpy)]^{3+}$. An intense transition band of the complex $[(bpy)_2Ru(dpp)RhCl_2(Me_2bpy)]^{3+}$ at 284 nm (ε = 6.0 × 10^4 $M^{-1}cm^{-1}$) in the UV region is assigned to bpy and Me_2bpy π→π* IL transitions. The extinction coefficient of this ligand-based transition band at 284 nm is 6.0 x 10^4 $M^{-1}cm^{-1}$ higher than the extinction coefficient (2.4 x 10^4 $M^{-1}cm^{-1}$) of the similar transition band of $[(bpy)_2Ru(dpp)RhCl_2(bpy)]^{3+}$, which suggests the contribution of the terminal ligand Me_2bpy π→π* IL transition. A shoulder of $[(bpy)_2Ru(dpp)RhCl_2(Me_2bpy)]^{3+}$ absorption spectrum occurs at 338 nm (ε = 0.8 × 10^4 $M^{-1}cm^{-1}$) attributed to dpp-based π→π* transition. The Ru(dπ)→bpy(π*) CT transition occurs at 425 nm, and the Ru(dπ)→dpp(π*) CT transition exhibits at 515 nm (ε = 1.5 × 10^4 $M^{-1}cm^{-1}$).

Table 3.7. Light absorbing properties of Ru,Rh bimetallic complexes and related Ru,Rh,Ru trimetallic Complex in room temperature CH_3CN.

Complex [a]	λ^{abs} (nm)	ε × 10^{-4} ($M^{-1}cm^{-1}$)	Assignment
$[(bpy)_2Ru(dpp)RhCl_2(bpy)]^{3+}$	284	5.1	bpy π→π*
	338	2.0	dpp π→π*
	414	0.7	Ru(dπ)→bpy(π*) CT
	510	1.3	Ru(dπ)→dpp(π*) CT
$[(bpy)_2Ru(dpp)RhCl_2(Me_2bpy)]^{3+}$	284	6.0	bpy, Me_2bpy π→π*
	338	2.4	dpp π→π*
	414	0.8	Ru(dπ)→bpy(π*) CT
	506	1.5	Ru(dπ)→dpp(π*) CT
$[\{(bpy)_2Ru(dpp\}_2RhCl_2]^{5+}$	284	9.8	bpy π→π*
	338	4.1	dpp π→π*
	414	1.6	Ru(dπ)→bpy(π*) CT
	518	2.6	Ru(dπ)→dpp(π*) CT

[a]Measured in CH_3CN at room temperature at room temperature with dpp = 2,3-bis(2-pyridyl)pyrazine, bpy = 2,2′-bipyridine and Me_2bpy = 4,4′-dimethyl-2,2′-bipyridine.

3.3.4. Electronic Absorption Spectroscopy of the Bimetallic Complex $[(bpy)_2Os(dpp)RhCl_2(phen)]^{3+}$ Compared with the Trimetallic Complex $[\{(bpy)_2Os(dpp)\}_2RhCl_2]^{5+}$

The electronic absorption spectrum of $[\{(bpy)_2Os(dpp)\}_2RhCl_2]^{5+}$, which is reported previously, displaying the characteristic absorptions from the osmium polyazine light absorbers in the UV and visible region of the spectrum is presented in Figure 3.18 and summarized in Table 3.8. The spectroscopy of $[\{(bpy)_2Os(dpp)\}_2RhCl_2]^{5+}$ in the UV region is dominated by one major transition at 284 nm ($\varepsilon = 12.0 \times 10^4\ M^{-1}cm^{-1}$) assigned to bpy-based $\pi\rightarrow\pi^*$ intraligand (IL) transition, and the shoulder at 336 nm ($\varepsilon = 5.1 \times 10^4\ M^{-1}cm^{-1}$) attributed to dpp-based $\pi\rightarrow\pi^*$ IL transition (Figure 3.18). One of two MLCT bands in the visible region at 412 nm ($\varepsilon = 2.2 \times 10^4\ M^{-1}cm^{-1}$) corresponds to the Os(dπ)→bpy(π*) CT transition, and the other lowest energy band at 534 nm ($\varepsilon = 3.6 \times 10^4\ M^{-1}cm^{-1}$) is assigned to Os(dπ)→dpp(π*) CT transition consistent with the stabilized dpp (π*) acceptor orbitals relative to the bpy(π*) orbitals.[68] The $[\{(bpy)_2Os(dpp)\}_2RhCl_2]^{5+}$ also displays a low energy transition at 798 nm ($\varepsilon = 6.1 \times 10^3\ M^{-1}cm^{-1}$) assigned as a $^1GS\rightarrow{}^3MLCT$ (Os(dπ)→dpp(π*) CT) transition. Such transition is due to the high degree of spin orbital coupling in osmium complexes which provides the mixing of the spin and orbital angular momentum quantum numbers, making poorly defined spin termed as a "bad" or mixed quantum number.[68] The bimetallic complex $[(bpy)_2Os(dpp)RhCl_2(phen)]^{3+}$ with only one osmium polyazine LA shows similar spectroscopic properties as the Os trimetallic complex with roughly half the extinction coefficient values relative to the trimetallics both in the UV and visible regions of the spectrum (Table 3.8).[119] An intense transition band at 284 nm ($\varepsilon = 7.0 \times 10^4\ M^{-1}cm^{-1}$) in the UV region is assigned to bpy and phen $\pi\rightarrow\pi^*$ IL transition with a shoulder at 340 nm ($\varepsilon = 2.6 \times 10^4\ M^{-1}cm^{-1}$) attributed to dpp $\pi\rightarrow\pi^*$ IL transition (Figure 3.18).

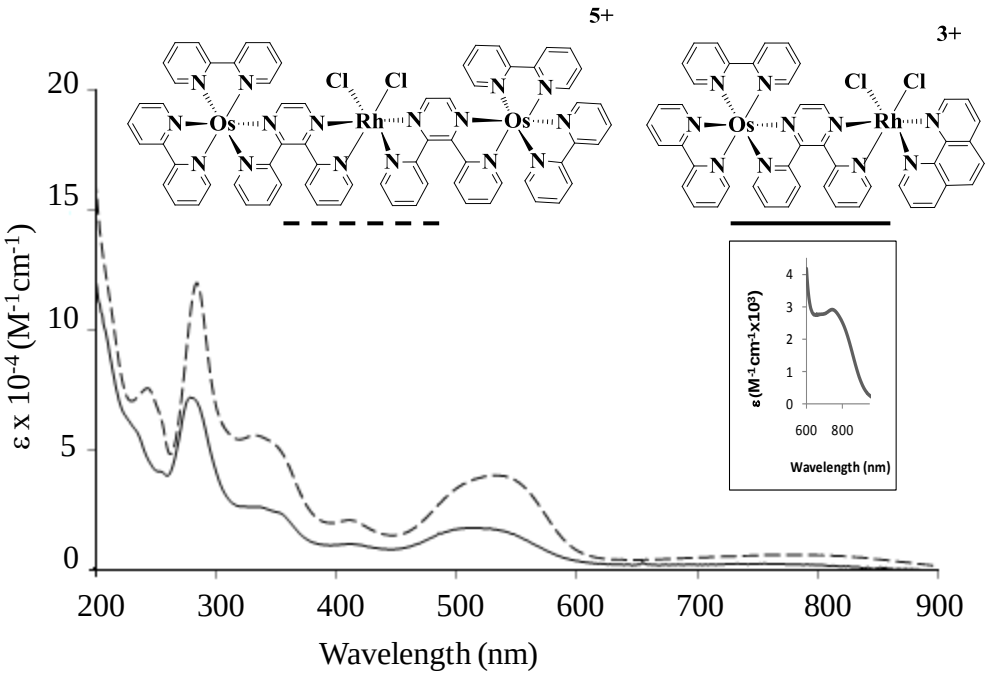

Figure 3.18. Electronic absorption spectra of $[(bpy)_2Os(dpp)RhCl_2(phen)]^{3+}$ (solid line) with a low energy $^1GS \rightarrow {}^3MLCT$ absorption band inset and $[\{(bpy)_2Os(dpp)\}_2RhCl_2]^{5+}$ (dashed line) in CH_3CN at room temperature with bpy = 2,2′-bipyridine, dpp = 2,3-bis(2-pyridyl)pyrazine and phen = 1,10-phenanthroline.

The Os(dπ)→bpy(π*) CT transition is observed at 413 nm ($\varepsilon = 1.0 \times 10^4\ M^{-1}cm^{-1}$) and the Os(dπ)→dpp(π*) CT transition appears at 521 nm ($\varepsilon = 1.8 \times 10^4\ M^{-1}cm^{-1}$). The bimetallic complex $[(bpy)_2Os(dpp)RhCl_2(phen)]^{3+}$ also displays a low energy absorption band at ca. 750 nm ($\varepsilon = 2.9 \times 10^3\ M^{-1}cm^{-1}$) corresponding to $^1GS \rightarrow {}^3MLCT$ transition because of spin orbital coupling.[119] This transition can be utilized for therapeutic window (600-900 nm) excitation of these complexes in biological applications avoiding direct excitation of biomolecules such as DNA.[119]

Table 3.8. Light absorbing properties of Os monometallic complex and Os,Rh bimetallic complex and related Os,Rh,Os trimetallic complex in room temperature CH_3CN.

Complex [a]	λ^{abs} (nm)	$\varepsilon \times 10^{-4}$ ($M^{-1}cm^{-1}$)	Assignment
$[(bpy)_2Os(dpp)]^{2+}$ [85]	290	6.7	bpy $\pi\rightarrow\pi^*$
	432	1.1	$Os(d\pi)\rightarrow bpy(\pi^*)$ ^1CT
	486	1.3	$Os(d\pi)\rightarrow dpp(\pi^*)$ ^1CT
$[(bpy)_2Os(dpp)RhCl_2(phen)]^{3+}$	284	7.0	bpy, phen $\pi\rightarrow\pi^*$
	340	2.6	dpp $\pi\rightarrow\pi^*$
	413	1.0	$Os(d\pi)\rightarrow bpy(\pi^*)$ ^1CT
	521	1.8	$Os(d\pi)\rightarrow dpp(\pi^*)$ ^1CT
	750	0.29	$Os(d\pi)\rightarrow dpp(\pi^*)$ ^3CT
$[\{(bpy)_2Os(dpp\}_2RhCl_2]^{5+}$	284	12.0	bpy $\pi\rightarrow\pi^*$
	336	5.1	dpp $\pi\rightarrow\pi^*$
	412	2.2	$Os(d\pi)\rightarrow bpy(\pi^*)$ ^1CT
	534	3.6	$Os(d\pi)\rightarrow dpp(\pi^*)$ ^1CT
	798	0.61	$Os(d\pi)\rightarrow dpp(\pi^*)$ ^3CT

[a] Measured in CH_3CN at room temperature, bpy = 2,2′-bipyridine, dpp = 2,3-bis(2-pyridyl)pyrazine and phen = 1,10-phenanthroline.

3.3.5. Summary Comments about Electronic Absorption Spectroscopy of Mixed-Metal Polyazine Complexes

The electronic absorption spectroscopic properties of mixed-metal polyazine complexes are important for their photochemical applications. The bimetallic complexes discussed in this dissertation consist of coupling one light absorber to *cis*-$Rh^{III}Cl_2$ center through the bridging ligand dpp. Although bimetallic complexes only have one light absorber, they display similar electronic absorption spectroscopic properties as the trimetallics, with approximately half the extinction coefficient values relative to the trimetallics both in the UV and visible regions of the spectrum. They are efficient light absorbers and display ligand-based $\pi\rightarrow\pi^*$ transitions in the UV region of the spectrum and metal-to-ligand charge transfer (MLCT) transitions in the visible region of the spectrum.

The mixed-metal complexes with osmium polyazine light absorbers display ligand-based $\pi \rightarrow \pi^*$ transitions in the UV region of the spectrum and MLCT transitions in the visible region of the spectrum as complexes with ruthenium light absorbers do. They also display a more intense low energy absorption band in the near-infrared region relative to Ru complexes due to spin orbital coupling. Energy of the $^1GS \rightarrow {}^3MLCT$ transition makes these complexes promising as PDT agents allowing excitation in the photodynamic window where biomolecules do not significantly absorb.[119] The complexes with TL = Ph_2phen in light absorbers display enhanced absorption in the UV and visible regions without the absorption dropping between 350 nm and 450 nm which is typical for the bpy and phen systems.[129,130] This enhanced electronic absorption properties allow $[(Ph_2phen)_2Ru(dpp)RhCl_2(phen)]^{3+}$ to absorb visible light more efficiently than the other complexes, and make the title complex more useful for PDT applications. The electronic absorption spectra of bimetallic complexes illustrate that the terminal ligand attached to rhodium center also contributes to ligand-based $\pi \rightarrow \pi^*$ transitions in the UV region.

3.4. Photophysical Properties of Mixed-Metal Polyazine Complexes

The photophysical properties of mixed-metal polyazine complexes are investigated by using steady-state and time-resolved emission spectroscopy.[131,132] The Ru,Rh bimetallic and trimetallic complexes are efficient light absorbers in the UV and visible regions of the spectrum and display emissions from their lowest lying $Ru(d\pi) \rightarrow dpp(\pi^*)$ ^3MLCT excited states. The Os,Rh bimetallic and trimetallic complexes are also good light absorbers in the UV and visible regions of the spectrum, but no emission could be detected by our instruments due to the low sensitivity of the PMT below 900 nm. In the following sections, the photophysical properties of the new bimetallic complexes will be discussed in detail and compared with the known trimetallic complexes and

the appropriate Ru,Ru bimetallic model complexes with photophysical data summarized in Table 3.9.

3.4.1. Photophysical Properties of $[(phen)_2Ru(dpp)RhCl_2(bpy)]^{3+}$ Compared with Trimetallic Complex $[\{(phen)_2Ru(dpp)\}_2RhCl_2]^{5+}$

The room temperature emission spectrum of the bimetallic complex $[(phen)_2Ru(dpp)RhCl_2(bpy)]^{3+}$ is measured in deoxygenated CH_3CN by absorbance matching at the wavelength of excitation (520 nm) to the emission standard complex $[Os(bpy)_3]^{2+}$ in deoxygenated CH_3CN ($\Phi^{em} = 4.6 \times 10^{-3}$).[123] The low temperature emission spectrum of $[(phen)_2Ru(dpp)RhCl_2(bpy)]^{3+}$, measured in 4:1 ethanol/methanol glass at 77 K, is blue-shifted compared to the room temperature measurement (shown in Figure 3.19). A weak and short-lived room temperature emission of $[(phen)_2Ru(dpp)RhCl_2(bpy)]^{3+}$ at 766 nm with $\Phi^{em} = 1.5 \times 10^{-4}$ (τ = 42 ns) is from the $Ru(d\pi)\rightarrow dpp(\pi^*)$ ^{3}MLCT excited state. At 77 K, the low temperature emission from the same ^{3}MLCT state of $[(phen)_2Ru(dpp)RhCl_2(bpy)]^{3+}$ blue-shifts to 706 nm with the emission lifetime of 1.8 μs.[118] The photophysical properties of $[(phen)_2Ru(dpp)RhCl_2(bpy)]^{3+}$ are similar to those of the analogous trimetallic complex $[\{(phen)_2Ru(dpp)\}_2RhCl_2]^{5+}$. At room temperature, $[\{(phen)_2Ru(dpp)\}_2RhCl_2]^{5+}$ emits at 760 nm ($\Phi^{em} = 2.2 \times 10^{-4}$, τ = 35 ns), and the trimetallic emits at 706 nm (τ = 1.8 μs) at 77 K.[81,118]

Compared to the Ru homobimetallic complex at room temperature, $[\{(phen)_2Ru\}_2(dpp)]^{4+}$ (λ_{RT}^{em} = 750 nm, $\Phi^{em} = 1.6 \times 10^{-3}$, and τ = 170 ns), the bimetallic complex $[(phen)_2Ru(dpp)RhCl_2(bpy)]^{3+}$ and trimetallic complex $[\{(phen)_2Ru(dpp)\}_2RhCl_2]^{5+}$ show a lower emission quantum yield ($\Phi^{em} = 1.5 \times 10^{-4}$ and $\Phi^{em} = 2.2 \times 10^{-4}$). The reduced quantum yield of the emission from the ^{3}MLCT state in the bimetallic and trimetallic complexes is due to

the population of the lower lying Ru(dπ)→Rh(dσ*) ^{3}MMCT excited state through intramolecular electron transfer at room temperature, and the percentage of population of the non-emissive ^{3}MMCT excited state is 75% for the bimetallic complex $[(phen)_2Ru(dpp)RhCl_2(bpy)]^{3+}$ and 79% for the trimetallic complex $[\{(phen)_2Ru(dpp)\}_2RhCl_2]^{5+}$ at the ^{3}MLCT excited state.[133] However, the low temperature lifetimes detected by the time-resolved emission from a rigid matrix at 77 K of the bimetallic and trimetallic complexes and the Ru homobimetallic system are the same. This suggests that the intramolecular electron transfer which populates the non-emissive ^{3}MMCT excited state from the ^{3}MLCT excited state at room temperature is impeded at 77 K.[112] Since Ru,Ru homobimetallic complex $[\{(phen)_2Ru\}_2(dpp)]^{4+}$, which has the same ruthenium light absorbers without an intervening Rh center, has similar nature and energy of the emissive Ru(dπ)→μ-dpp(π*) ^{3}MLCT excited states as those of Ru,Rh bimetallic and trimetallic systems and nearly identical 77 K emission energy and lifetime. The bimetallic models are chosen with great care to have the same Ru(dπ) donor with the same terminal ligands, as they may contribute to mainly Ru(dπ) donor orbital. Ru,Ru homobimetallic complexes are suitable to be used as selective model to study the photophysical properties of mixed-metal complexes.

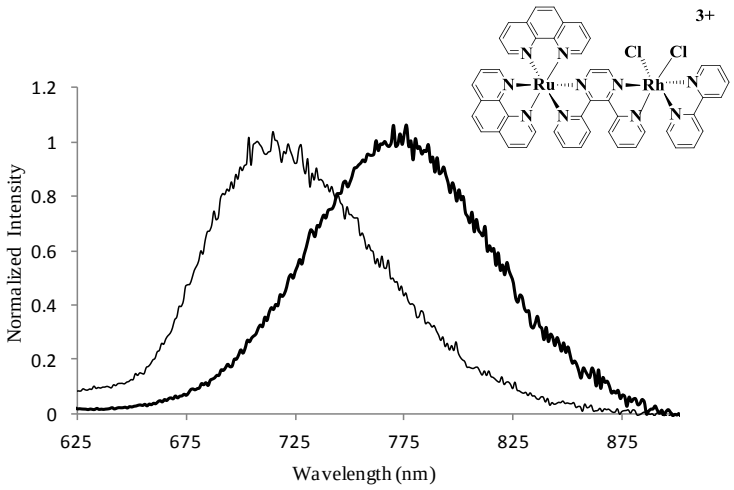

Figure 3.19. The normalized emission spectra of $[(phen)_2Ru(dpp)RhCl_2(bpy)]^{3+}$ in deoxygenated room temperatue CH_3CN (thick line) and 4:1 EtOH/MeOH glass at 77 K (thin line) at the excitation wavelength (λ^{ex} = 520 nm), where each spectrum is corrected for PMT response, bpy = 2,2′-bipyridine, dpp = 2,3-bis(2-pyridyl)pyrazine and phen = 1,10-phenanthroline.

With the assumption that the k_r and k_{nr} of the bimetallic complex $[(phen)_2Ru(dpp)RhCl_2(bpy)]^{3+}$and trimetallic complex $[\{(phen)_2Ru(dpp)\}_2RhCl_2]^{5+}$ are the same as the Ru homobimetallic model system $[\{(phen)_2Ru\}_2(dpp)]^{4+}$, the rate of intramolecular electron transfer, k_{et} (listed in Table 3.9), can be calculated by using equations 3.1-3.3.[133,134] τ is the measured lifetimes of bimetallic or trimetallic ^{3}MLCT excited state, and τ_0 is the measured lifetime of selective model system ^{3}MLCT excited state.

$$\tau = \frac{1}{k_r + k_{nr} + k_{et}} \quad (3.1)$$

$$\tau_0 = \frac{1}{k_r + k_{nr}} \quad (3.2)$$

$$k_{et} = \frac{1}{\tau} - \frac{1}{\tau_0} \quad (3.3)$$

3.4.2. Photophysical Properties of $[(phen)_2Ru(dpp)RhCl_2(phen)]^{3+}$, $[(Ph_2phen)_2Ru(dpp)RhCl_2(phen)]^{3+}$ and $[(Me_2phen)_2Ru(dpp)RhCl_2(phen)]^{3+}$

The emission spectra of the bimetallic complexes $[(TL)_2Ru(dpp)RhCl_2(phen)]^{3+}$ (TL = phen, Ph_2phen and Me_2phen) are measured in deoxygenated CH_3CN and in 4:1 ethanol/methanol glass at 77 K at the excitation wavelength (λ^{ex} = 520 nm), compared with the trimetallic complexes $[\{(TL)_2Ru(dpp)\}_2RhCl_2]^{5+}$ and Ru homobimetallic model complexes $[\{(TL)_2Ru\}_2(dpp)]^{4+}$, Table 3.9. The emission ($\Phi^{em} = 2.4 \times 10^{-4}$ and τ = 64 ns) from the Ru(dπ)→dpp(π*) ^{3}MLCT excited state of the bimetallic complex $[(phen)_2Ru(dpp)RhCl_2(phen)]^{3+}$ in room temperature deoxygenated CH_3CN is observed at 770 nm (Figure 3.20). The emission band at room temperature missing the tail is due to low PMT sensitivity between 800-950 nm (seen in Figure 2.4. the PMT response correction file) At 77 K, the emission from the same ^{3}MLCT state blue-shifts to 700 nm with a longer lifetime (τ = 1.7 μs) (Figure 3.20).

The photophysical properties of the trimetallic complex $[\{(phen)_2Ru(dpp)\}_2RhCl_2]^{5+}$ reported previously are similar to those of $[(phen)_2Ru(dpp)RhCl_2(phen)]^{3+}$.[81,120] The room temperature emission ($\Phi^{em} = 2.2 \times 10^{-4}$ and τ = 35 ns) from the Ru(dπ)→dpp(π*) ^{3}MLCT excited state of $[\{(phen)_2Ru(dpp)\}_2RhCl_2]^{5+}$ occurs at 760 nm and the 77 K emission from the same ^{3}MLCT state shifts to 706 nm (τ = 1.8 μs). The room temperature emission from the ^{3}MLCT state of $[(phen)_2Ru(dpp)RhCl_2(phen)]^{3+}$ and $[\{(phen)_2Ru(dpp)\}_2RhCl_2]^{5+}$ quenches 85% and 86%, respectively, relative to the Ru homobimetallic model $[\{(phen)_2Ru\}_2(dpp)]^{4+}$ (λ_{RT}^{em} = 750 nm, $\Phi^{em} = 1.6 \times 10^{-3}$ and τ = 170 ns).[112] The 77 K emission of $[(phen)_2Ru(dpp)RhCl_2(phen)]^{3+}$ (λ_{77k}^{em} = 700 nm, and τ = 1.7 μs) and $[\{(phen)_2Ru(dpp)\}_2RhCl_2]^{5+}$ (λ_{77k}^{em} = 700 nm, and τ = 1.7 μs)

is close to the Ru homobimetallic model $[\{(phen)_2Ru\}_2(dpp)]^{4+}$ ($\lambda_{77\,k}^{em}$ = 695 nm, and τ = 2.0 μs).[112]

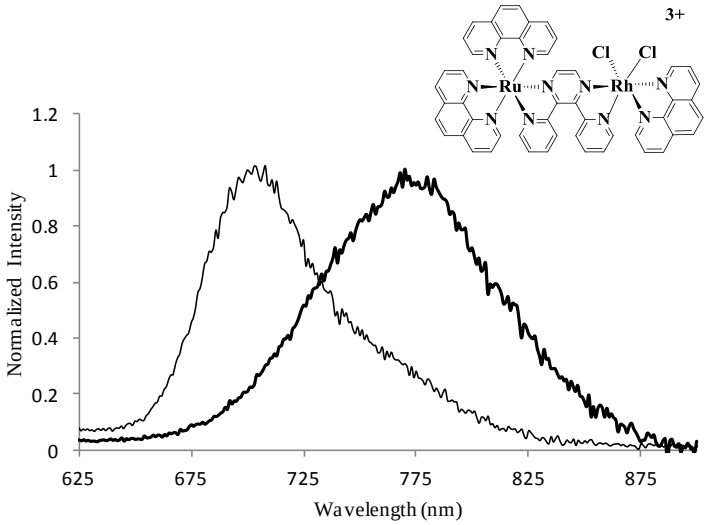

Figure 3.20. The normalized emission spectra of $[(phen)_2Ru(dpp)RhCl_2(phen)]^{3+}$ in deoxygenated room temperature CH_3CN (thick line) and 4:1 EtOH/MeOH glass at 77 K (thin line) at the excitation wavelength (λ^{ex} = 520 nm), where each spectrum is corrected for PMT response, phen = 1,10-phenanthroline and dpp = 2,3-bis(2-pyridyl)pyrazine.

The variation of terminal ligand in $[(TL)_2Ru(dpp)RhCl_2(phen)]^{3+}$ and $[\{(TL)_2Ru(dpp)\}_2RhCl_2]^{5+}$ affects their photophysical properties due to the contributions from the terminal ligands orbitals to the formally Ru ($d\pi$) HOMO which is the donor orbital in the lowest lying and emissive Ru($d\pi$)$\rightarrow\mu$-dpp(π^*) ^{3}MLCT excited state.[112] This is illustrated by the longer room temperature lifetimes of Ph_2phen containing Ru light absorber systems.[112] The room temperature emission ($\Phi^{em} = 1.8 \times 10^{-4}$ and τ = 46 ns) of $[(Ph_2phen)_2Ru(dpp)RhCl_2(phen)]^{3+}$ red-shifts to 786 nm compared to the emission of $[(phen)_2Ru(dpp)RhCl_2(phen)]^{3+}$. The 77 K emission of $[(Ph_2phen)_2Ru(dpp)RhCl_2(phen)]^{3+}$ occurs at 706 nm (Figure 3.21) with the same lifetime (τ = 1.8 μs) as $[(phen)_2Ru(dpp)RhCl_2(phen)]^{3+}$.

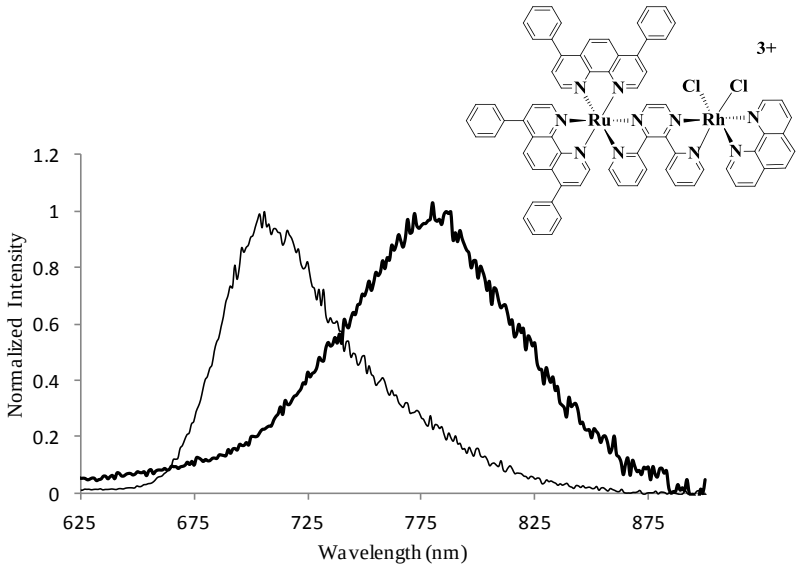

Figure 3.21. The normalized emission spectra of $[(Ph_2phen)_2Ru(dpp)RhCl_2(phen)]^{3+}$ in deoxygenated room temperature CH_3CN (thick line) and 4:1 EtOH/MeOH glass at 77 K (thin line)) at the excitation wavelength (λ^{ex} = 520 nm), where each spectrum is corrected for PMT response, Ph_2phen = 4,7-diphenyl-1,10-phenanthroline, phen = 1,10-phenanthroline and dpp = 2,3-bis(2-pyridyl)pyrazine.

The photophysical properties of the previous studied trimetallic complex $[\{(Ph_2phen)_2Ru(dpp)\}_2RhCl_2]^{5+}$ are similar to those of the bimetallic analogue.[81,120] The room temperature emission ($\Phi^{em} = 2.4 \times 10^{-4}$ and τ = 52 ns) from the Ru(dπ)→dpp(π*) ^{3}MLCT excited state of $[\{(Ph_2phen)_2Ru(dpp)\}_2RhCl_2]^{5+}$ is shown at 770 nm and the 77 K emission from the same ^{3}MLCT state displays at 696 nm (τ = 1.8 μs). The room temperature emission from the ^{3}MLCT state of bimetallic complex $[(Ph_2phen)_2Ru(dpp)RhCl_2(phen)]^{3+}$ and trimetallic complex $[\{(Ph_2phen)_2Ru(dpp)\}_2RhCl_2]^{5+}$ displays respectively 89% and 86% quenching of the emissive Ru(dπ)→dpp(π*) ^{3}MLCT excited state compared to the Ru homobimetallic model $[\{(Ph_2phen)_2Ru\}_2(dpp)]^{4+}$ (λ_{RT}^{em} = 754 nm, $\Phi^{em} = 1.7 \times 10^{-3}$ and τ = 192 ns).[112] The 77 K emission of the Ru homo-bimetallic model $[\{(phen)_2Ru\}_2(dpp)]^{4+}$ is observed at 695 nm with a lifetime of 2.0 μs.[112]

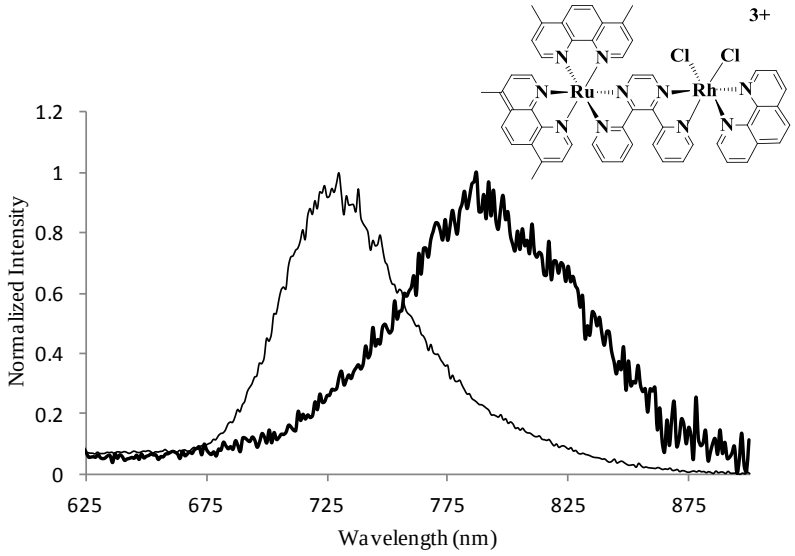

Figure 3.22. The normalized emission spectra of $[(Me_2phen)_2Ru(dpp)RhCl_2(phen)]^{3+}$ in deoxygenated room temperature CH_3CN (thick line) and 4:1 EtOH/MeOH glass at 77 K (thin line)) at the excitation wavelength (λ^{ex} = 520 nm), where each spectrum is corrected for PMT response, Me_2phen = 4,7-dimethyl-1,10-phenanthroline, phen = 1,10-phenanthroline and dpp = 2,3-bis(2-pyridyl)pyrazine

Room temperature and 77 K emissions of the bimetallic complex $[(Me_2phen)_2Ru(dpp)RhCl_2(phen)]^{3+}$ become weaker and shorter-lived, when terminal ligand on the light absorber is substituted by the Me_2phen ligand. The room temperature emission (Φ^{em} = 5.5×10^{-5} and τ = 27 ns) of $[(Me_2phen)_2Ru(dpp)RhCl_2(phen)]^{3+}$ red-shifts to 786 nm compared to the emission ($\Phi^{em} = 2.4 \times 10^{-4}$ and τ = 64 ns) of $[(phen)_2Ru(dpp)RhCl_2(phen)]^{3+}$. The room temperature emission shape of $[(Me_2phen)_2Ru(dpp)RhCl_2(phen)]^{3+}$ (figure 3.22) is different from other bimetallics due to the $[(Me_2phen)_2Ru(dpp)RhCl_2(phen)]^{3+}$ emission is weaker than others and red-shifts to 786 nm, and also due to the low PMT sensitivity between 800-950 nm of the spectrophotometer. The 77 K emission of $[(Me_2phen)_2Ru(dpp)RhCl_2(phen)]^{3+}$ shifts to lower energy at 730 nm with a shorter lifetime (τ = 1.3 μs) compared to the 77 K emission (λ_{77k}^{em} = 700 nm and τ = 1.7 μs) of $[(phen)_2Ru(dpp)RhCl_2(phen)]^{3+}$. The 77 K emission profile of

$[(Me_2phen)_2Ru(dpp)RhCl_2(phen)]^{3+}$ is blue-shifted relative to the room temperature measurement (shown in Figure 3.22). The bimetallic complex $[(Me_2phen)_2Ru(dpp)RhCl_2(phen)]^{3+}$ quenches 93% the room temperature emission from the ^{3}MLCT state, relative to the Ru homo-bimetallic model $[\{(Me_2phen)_2Ru\}_2(dpp)]^{4+}$ (λ_{RT}^{em} = 764 nm, Φ^{em} = 7.4×10^{-4} and τ = 126 ns).[112] The 77 K emission of the Ru homo-bimetallic model $[\{(Me_2phen)_2Ru\}_2(dpp)]^{4+}$ occurs at 710 nm with lifetime 1.7 μs.

Since the goal of this research is to understand the effect of the sub-unit variation on the photophysical and photochemical properties of the new bimetallic complexes, the photophysical information about the series of the complexes $[(TL)_2Ru(dpp)RhCl_2(phen)]^{3+}$ (TL = phen, Ph_2phen and Me_2phen) with the light absorbers variation is important. It will be helpful to answer the question about why the bimetallic complexes in the excited state have different ability to photo-modify DNA supporting hypotheses that the complexes with longer exicted state lifetime and high percentage of population a reactive ^{3}MMCT excited state (62% for $[(phen)_2Ru(dpp)RhCl_2(phen)]^{3+}$, 76% for $[(Ph_2phen)_2Ru(dpp)RhCl_2(phen)]^{3+}$ and 78% for $[(Me_2phen)_2Ru(dpp)RhCl_2(phen)]^{3+}$ at the ^{3}MLCT excited state) will photomodify DNA more effective. The photophysical data such as the emission intensity, excited state lifetime and emission profile will provide useful information to design the new bimetallic complexes for many applications that require light harvesting including PDT.

3.4.3. Photophysical Properties of Bimetallic Complexes $[(bpy)_2Ru(dpp)RhCl_2(bpy)]^{3+}$ and $[(bpy)_2Ru(dpp)RhCl_2(Me_2bpy)]^{3+}$ Compared with Trimetallic Complex $[\{(bpy)_2Ru(dpp)\}_2RhCl_2]^{5+}$

Changing the TL′ from phen to bpy in the bimetallic complexes $[(bpy)_2Ru(dpp)RhCl_2(TL')]^{3+}$ (TL′ = bpy and Me_2bpy) results in different photophysical properties compared to those of the bimetallic complex $[(phen)_2Ru(dpp)RhCl_2(phen)]^{3+}$. A weaker and shorter-lived emission ($\Phi^{em} = 1.5 \times 10^{-4}$ and τ = 42 ns) of $[(bpy)_2Ru(dpp)RhCl_2(bpy)]^{3+}$ is observed at 786 nm from room temperature acetonitrile complex solution assigned to the Ru(dπ)→dpp(π*) ^{3}MLCT emission consistent with ^{3}MMCT population from the ^{3}MLCT state. The 77 K emission of $[(bpy)_2Ru(dpp)RhCl_2(bpy)]^{3+}$ blue-shifts to 715 nm with a longer lifetime (τ = 1.7 μs) (Figure 3.23). The photophysical properties of trimetallic complex $[\{(bpy)_2Ru(dpp)\}_2RhCl_2]^{5+}$ are close to that of the bimetallic analogue, $[(bpy)_2Ru(dpp)RhCl_2(bpy)]^{3+}$.[15] The room temperature emission ($\Phi^{em} = 2.6 \times 10^{-4}$ and τ = 38 ns) from the Ru(dπ)→dpp(π*) ^{3}MLCT excited state of $[\{(bpy)_2Ru(dpp)\}_2RhCl_2]^{5+}$ is shown at 776 nm and the 77 K emission of $[\{(bpy)_2Ru(dpp)\}_2RhCl_2]^{5+}$ is observed at 730 nm (τ = 1.9 μs). The room temperature emission from the ^{3}MLCT state of bimetallic complex $[(bpy)_2Ru(dpp)RhCl_2(bpy)]^{3+}$ and trimetallic complex $[\{(bpy)_2Ru(dpp)\}_2RhCl_2]^{5+}$ shows 85% and 74% emission quenching, respectively, according to the Ru homobimetallic model, $[\{(bpy)_2Ru\}_2(dpp)]^{4+}$ (λ_{RT}^{em} = 758 nm, $\Phi^{em} = 9.8 \times 10^{-4}$ and τ = 126 ns).[81] At 77 K, the low temperature emission of $[\{(bpy)_2Ru\}_2(dpp)]^{4+}$ is blue-shifted at 715 nm with a longer lifetime 2.0 μs.[112] The room temperatue emission lifetimes of $[(bpy)_2Ru(dpp)RhCl_2(bpy)]^{3+}$, $[\{(bpy)_2Ru(dpp)\}_2RhCl_2]^{5+}$ and $[\{(bpy)_2Ru\}_2(dpp)]^{4+}$ are much shorter than their 77 K emission lifetime (42 ns, 38 ns and 126 ns vs. 1.7 μs, 1.9 μs and 2.0 μs), suggesting at room temperature a non-emissive ^{3}MMCT excited state can be populated from the ^{3}MLCT excited state through intramoleculer electron transfer. The percentage of population of the non-emssive ^{3}MMCT excited state is 67% for $[(bpy)_2Ru(dpp)RhCl_2(bpy)]^{3+}$ and 70% for $[\{(bpy)_2Ru(dpp)\}_2RhCl_2]^{5+}$ at

^{3}MLCT excited state. Assuming that the k_r and k_{nr} at room temperature of $[(bpy)_2Ru(dpp)RhCl_2(bpy)]^{3+}$and $[\{(bpy)_2Ru(dpp)\}_2RhCl_2]^{5+}$ are the same as the model system $[\{(bpy)_2Ru\}_2(dpp)]^{4+}$, the rate of intramolecular electron transfer, $k_{et} = 1.7 \times 10^7$ s^{-1} for $[(bpy)_2Ru(dpp)RhCl_2(bpy)]^{3+}$ and 1.9×10^7 s^{-1} for $[\{(bpy)_2Ru(dpp)\}_2RhCl_2]^{5+}$ (listed in Table 3.9), are calculated by using the equations 3.1-3.3**.**

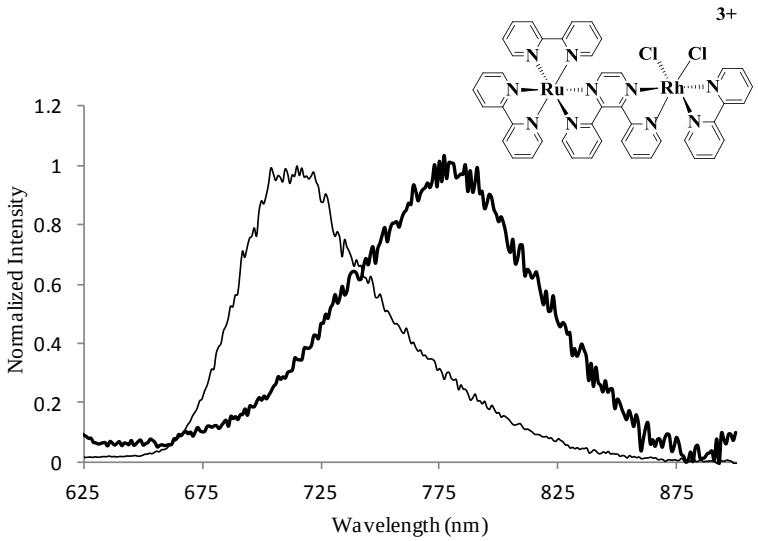

Figure 3.23. The normalized emission spectra of $[(bpy)_2Ru(dpp)RhCl_2(bpy)]^{3+}$ in deoxygenated room temperature CH_3CN (thick line) and 4:1 EtOH/MeOH glass at 77 K (thin line)) at the excitation wavelength (λ^{ex} = 520 nm), where each spectrum is corrected for PMT response, bpy = 2,2′-bipyridine and dpp = 2,3-bis(2-pyridyl)pyrazine.

The variation of TL′ attached to the Rh metal center also impacts bimetallic photophysical properties due to modulating the energy of the Rh (dσ*) orbital. The room temperature emission of $[(bpy)_2Ru(dpp)RhCl_2(Me_2bpy)]^{3+}$ is observed at the same wavelength (λ_{RT}^{em} = 786 nm) as the room temperature emission of $[(bpy)_2Ru(dpp)RhCl_2(bpy)]^{3+}$ with a higher emission quantum yield and a longer room temperature emission lifetime ($\Phi^{em} = 1.7 \times 10^{-4}$ vs. 1.5×10^{-4} , τ = 44 ns vs. 42 ns). The percentage of population of the non-emssive ^{3}MMCT excited state at room temperature is 65% for $[(bpy)_2Ru(dpp)RhCl_2(Me_2bpy)]^{3+}$ at the ^{3}MLCT excited state. The 77 K

emission of $[(bpy)_2Ru(dpp)RhCl_2(Me_2bpy)]^{3+}$ is blue-shifted to 708 nm with a lifetime (τ = 1.7 μs), Figure 3.24.

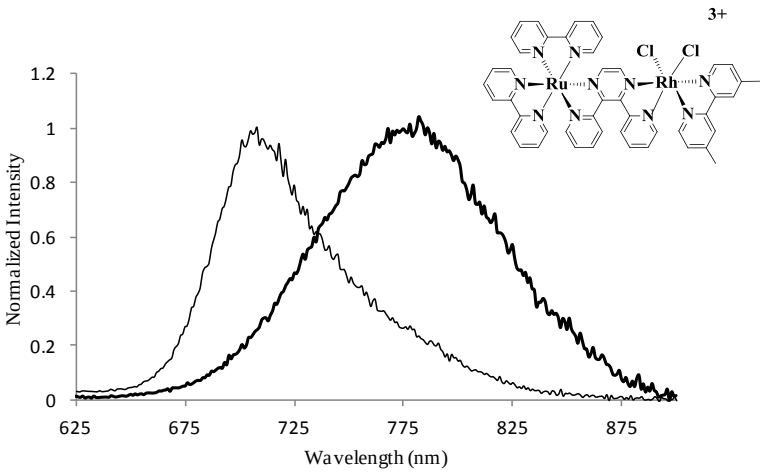

Figure 3.24. The normalized emission spectra of $[(bpy)_2Ru(dpp)RhCl_2(Me_2bpy)]^{3+}$ in deoxygenated room temperature CH_3CN (thick line) and 4:1 EtOH/MeOH glass at 77 K (thin line)at the excitation wavelength (λ^{ex} = 520 nm), where each spectrum is corrected for PMT response, Me_2bpy = 4,4′-dimethyl-2,2′-bipyridine, bpy = 2,2′-bipyridine and dpp = 2,3-bis(2-pyridyl)pyrazine.

The study of tuning photophysical properties of the bimetallic complexes by changing terminal ligands attached to the Rh metal center is also important. This can modulate Rh(dσ*) acceptor orbital. In addition, sterics at the Rh center impact DNA photobinding through the Rh center in the excited states. The photophysical information will help to select suitable terminal ligands to tune excited state dynamics and steric accessibility to unprecedented DNA photobinding via ^{3}MMCT excited state.

3.4.4. Summary Comments about Photophysical Properties of Mixed-Metal Polyazine Complexes.

The photophysical properties of Ru,Rh bimetallic and trimetallic complexes are studied using steady-state and time-resolved emission spectroscopy and summarized in Table 3.9. Both Ru,Rh bimetallic and trimetallic complexes absorb light from the UV and visible regions of the spectrum and are excited to singlet excited states (^{1}IL and ^{1}MLCT), which then populate the lowest lying Ru(dπ)→dpp(π*) ^{3}MLCT excited state through intersystem crossing with near unit efficiency. The Ru,Rh complexes undergo additional dynamics with the ^{3}MLCT excited state undergoing expected a non-radiative decay, a radiative decay or intramolecular electron transfer to generate the photoreactive Ru→Rh ^{3}MMCT state.[68]

At room temperature, the Ru,Rh complexes in the ^{3}MLCT excited state can populate a Ru(dπ)→Rh(dσ*) ^{3}MMCT excited state through the intramolecular electron transfer.[68] However, the Ru homobimetallic models $[\{(TL)_2Ru\}_2(dpp)]^{4+}$ (TL = phen, Ph_2phen, Me_2phen and bpy) without a Rh center cannot populate a ^{3}MMCT excited state at room temperature because the Ru(dπ)→μ-dpp(π*) ^{3}MLCT excited state is the lowest lying state of the Ru homonuclear model systems. An appropriate model systems must have similar nature and energy of the emissive Ru(dπ)→μ-dpp(π*) ^{3}MLCT excited states as those of Ru,Rh bimetallic and trimetallic systems provided by using the same terminals and a μ-dpp. With the assumption that the k_r and k_{nr} of the bimetallic and trimetallic complexes are the same as the Ru homobimetallic model system, k_{et} around 10^7 s^{-1} (listed in Table 3.9), are calculated by using the equations 3.1-3.3. At 77 K, the intramolecular electron transfer of those systems is inhibited in the rigid matrix due to the large reorganizational energy.[133-135]

The variation of terminal ligands on the light absorbers influences the Ru,Rh bimetallic and trimetallic photophysical properties due to the terminal impacting the energy of Ru(dπ) orbital

which is the donor orbital in the ^{3}MLCT excited state. The variation of TL′ attached to the Rh metal center also modulates the Rh (dσ*) orbital modifying photophysical properties. Photophysical properties of series of Ru,Rh complexes are important and provide the insight into excited state properties and the impact of sub-unit variation for photochemical applications.

Table 3.9. The photophysical properties of Ru,Rh bimetallic and trimetallic complexes and relevant model systems, at room temperature and 77 K.

Complex[d]	RT[a]					77 K[b]		Ref.
	λ^{abs} (nm)	λ^{em} (nm)	Φ^{em} ± 5.0%	τ± 5.0% (ns)	k_{et} (s^{-1})[c]	λ^{em} (nm)	τ± 5.0% (μs)	
$[(phen)_2Ru(dpp)RhCl_2(bpy)]^{3+}$	505	766	1.5×10^{-4}	42	1.8×10^{7}	706	1.8	118
$[(phen)_2Ru(dpp)RhCl_2(phen)]^{3+}$	508	770	2.4×10^{-4}	64	1.0×10^{7}	700	1.7	
$[(Ph_2phen)_2Ru(dpp)RhCl_2(phen)]^{3+}$	515	786	1.8×10^{-4}	46	1.7×10^{7}	706	1.7	
$[(Me_2phen)_2Ru(dpp)RhCl_2(phen)]^{3+}$	516	786	5.5×10^{-5}	27	2.9×10^{7}	730	1.3	
$[(bpy)_2Ru(dpp)RhCl_2(bpy)]^{3+}$	510	786	1.5×10^{-4}	42	1.6×10^{7}	715	1.7	
$[(bpy)_2Ru(dpp)RhCl_2(Me_2bpy)]^{3+}$	506	786	1.7×10^{-4}	44	1.5×10^{7}	708	1.7	
$[\{(phen)_2Ru(dpp)\}_2RhCl_2]^{5+}$	512	760	2.2×10^{-4}	35	2.3×10^{7}	706	1.8	118
$[\{(Ph_2phen)_2Ru(dpp)\}_2RhCl_2]^{5+}$	520	770	2.4×10^{-4}	52	1.4×10^{7}	696	1.8	112
$[\{(bpy)_2Ru(dpp)\}_2RhCl_2]^{5+}$	518	776	2.6×10^{-4}	38	1.8×10^{7}	730	1.9	15
$[\{(phen)_2Ru\}_2(dpp)]^{4+}$	524	750	1.6×10^{-3}	170		695	2.0	81
$[\{(Ph_2phen)_2Ru\}_2(dpp)]^{4+}$	540	754	1.7×10^{-3}	192		698	2.0	112
$[\{(Me_2phen)_2Ru\}_2(dpp)]^{4+}$	536	764	7.4×10^{-4}	126		710	1.7	112
$[\{(bpy)_2Ru\}_2(dpp)]^{4+}$	526	758	9.8×10^{-4}	126		715	2.0	112

[a]Measured in CH_3CN at room temperature at the excitation wavelength (λ^{ex} = 520 nm).
[b]Measured in 4:1 EtOH/MeOH glass at 77 k at the excitation wavelength (λ^{ex} = 520 nm).
[c]The rate of intramolecular electron transfer calculated by using equation 3.1-3.3.

[d]bpy = 2,2′-bipyridine, dpp = 2,3-bis(2-pyridyl)pyrazine and phen = 1,10-phenanthroline, Ph_2phen = 4,7-diphenyl-1,10-phenanthroline, Me_2phen = 4,7-dimethyl-1,10-phenanthroline and Me_2bpy = 4,4′-dimethyl-2,2′-bipyridine.

3.5. Summary of Bimetallic Complexes DNA Interations

The Ru,Rh and Os,Rh bimetallic complexes $[(TL)_2M(dpp)RhCl_2(TL')]^{3+}$ (M = Ru and Os, TL = phen, Ph_2phen, Me_2phen and bpy, TL′ = phen, bpy and Me_2bpy) couple only one Ru or Os polyazine light absorber to a *cis*-$Rh^{III}Cl_2$ center through a bridging ligand dpp. These bimetallic complexes are synthetically challenging to prepare in high purity, but present less positive charge and smaller size as well as desirable photoreactivity. These Ru,Rh and Os,Rh bimetallics are efficient light absorbers through the UV and visible regions. In contrast to polymetallic Rh complexes,[108,119,136] bimetallic complexes have complex redox properties as a result of energetically close frontier orbitals,[15,118] and populate an emissive ^{3}MLCT excited state undergo intramolecular electron transfer to populate the ^{3}MMCT state. The title bimetallics are designed to display O_2 independent reactivity with DNA by virtue of the lowest lying MMCT state.[119] The bimetallic complexes have lower cationic charge to enhance cell membrane permeability, a sterically accessible Rh reactive center and independently variable terminal ligand on the light absorbers and Rh center[15,118] compared to the previous reported trimetallic analogues.[68,69,72,120,128] The study of photochemical reactivity of Ru,Rh and Os,Rh bimetallic complexes with DNA is explored in detail showing new unprecedented light induced reactivity, and Os,Rh bimetallic complex moves O_2 independent reactivity, for the first time, into the therapeutic window.

3.5.1. Photobinding and Photocleavage of DNA with Bimetallic Complex $[(phen)_2Ru(dpp)RhCl_2(bpy)]^{3+}$ under Visible Light

The interactions of the Ru,Rh bimetallic complex $[(phen)_2Ru(dpp)RhCl_2(bpy)]^{3+}$ with pUC18 plasmid DNA were investigated using previously described photolysis and agarose gel electrophoresis shift assay (Figure 3.25).[68,72] Excitation occurs at 455 nm with a light flux of 2.0 $\pm$ 0.1 $\times$ 10^{19} photons/min.[124] The number of excited molecules is related to light flux and absorptivity of the complex. The image of the agarose gel (Figure 3.25) shows a molecular weight marker (lane λ), a DNA plasmid control without any metal complex presented (lane C), a complex/DNA solution at 1:5 metal complex: base pairs ratio (1:5 MC:BP ratio) in dark (lane MC) and a complex/DNA solution at 1:5 MC:BP ratio irradiated for 10, 20, 30, 40, 50 and 60 min under argon (lanes 10, 20, 30, 40, 50 and 60). DNA migration through a gel is reduced by decreased anionic charge or increased molecular size. Conversion of supercoiled plasmid DNA (SC) to open circular plasmid DNA (OC) results from a single strand cleavage, greatly changing DNA migration.

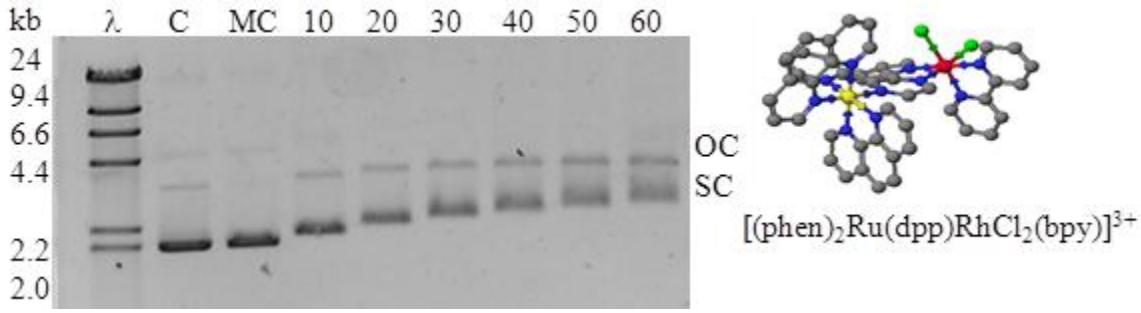

Figure 3.25. The imaged agarose gel showing photochemical interactions of Ru,Rh bimetallic complex, $[(phen)_2Ru(dpp)RhCl_2(bpy)]^{3+}$ with DNA and the Scigress stuctrure of $[(phen)_2Ru(dpp)RhCl_2(bpy)]^{3+}$. λ lane is molecular weight marker, C lane is DNA plasmid control, MC lane is the dark plasmid control incubated at RT in the dark for 2 h in the presence of 1:5 metal complex:base pairs ratio, Lane 10, 20, 30, 40, 50, 60 are the same plasmid DNA solution (1:5 metal complex:base pairs) irradiated for 10, 20, 30, 40, 50, 60 min under visible light (λ = 455 nm) from a 5 W LED with average flux of 2.0 $\pm$ 0.1 $\times$ 10^{19} photons/min under argon flow, bpy = 2,2′-bipyridine, dpp = 2,3-bis(2-pyridyl)pyrazine, and phen = 1,10-phenanthroline.

In the dark control, DNA was incubated at room temperature in the dark for 2 hours with $[(phen)_2Ru(dpp)RhCl_2(bpy)]^{3+}$ (1:5 MC:BP ratio). Incubation of the pUC18 DNA with the metal complex in the dark does not affect DNA migration through the gel, indicating no dark reactivity of the complex with DNA (lane MC). $[(phen)_2Ru(dpp)RhCl_2(bpy)]^{3+}$ was photolyzed in the presence of the DNA, under argon flow, using a 5 W light emitting diode (LED) (λ = 455 nm) with average flux of $2.0 \pm 0.1 \times 10^{19}$ photons/min.[124] The DNA metal complex solutions irradiated with visible light exhibited a slowing of DNA migration (lanes 10, 20, 30, 40, 50 and 60). The retardation of DNA migration is characteristic of metal-bound DNA consistent with photobinding of the complex to DNA.[137] Visible light induced DNA binding is a new light activated reactivity for Ru,Rh bimetallic systems, not observed for the previously reported Ru,Rh,Ru trimetallic systems.[68,72] This also represents unprecedented reactivity from a ^{3}MMCT state. The bimetallic complexes $[(TL)_2M^{II}(dpp)RhCl_2(TL')]^{3+}$ provide a sterically accessible Rh reactive site, more accessible than the Rh sites in known $[(TL)_2M^{II}(BL)\}_2RhCl_2]^{5+}$ trimetallics. As only one large $[(TL)_2M^{II}(dpp)]^{2+}$ sub-unit is bound to the Rh center instead of two large $[(TL)_2M^{II}(dpp)]^{2+}$ sub-units in the trimetallic motif (Figure 2.26), the less sterically crowded structure around Rh of the bimetallic complexes makes photobinding to the plasmid DNA possible. Figure 3.25 shows that $[(phen)_2Ru(dpp)RhCl_2(bpy)]^{3+}$ can photocleave DNA when excited by light (λ = 455 nm) in the absence of O_2 (lanes 10, 20, 30, 40, 50, 60). This is supported by the conversion of supercoiled DNA (SC) to open-circular DNA (OC) (most visible in lanes 50 and 60). [101,113]

A)

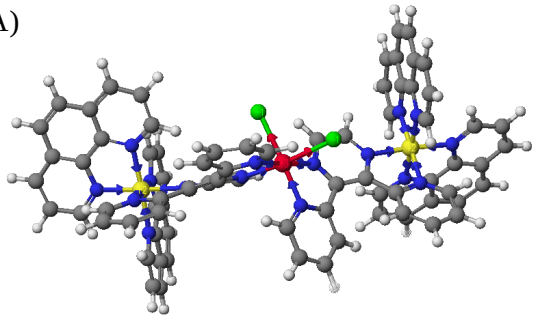

$[\{(phen)_2Ru(dpp)\}_2RhCl_2]^{5+}$

B)

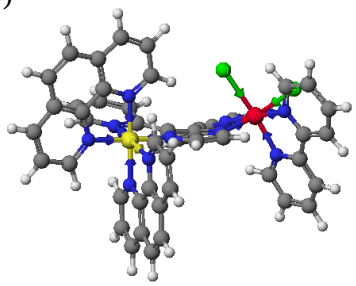

$[(phen)_2Ru(dpp)RhCl_2(bpy)]^{3+}$

Figure 3.26. The Scigress structure of trimetallic complex $[\{(phen)_2Ru(dpp)\}_2RhCl_2]^{5+}$ (A) and bimetallic complex $[(phen)_2Ru(dpp)RhCl_2(bpy)]^{3+}$ (B), bpy = 2,2′-bipyridine, dpp = 2,3-bis(2-pyridyl)pyrazine, and phen = 1,10-phenanthroline.

3.5.2. Photobinding and Photocleavage of DNA with Bimetallic Complex $[(phen)_2Ru(dpp)RhCl_2(phen)]^{3+}$, $[(Ph_2phen)_2Ru(dpp)RhCl_2(phen)]^{3+}$ and $[(Me_2phen)_2Ru(dpp)RhCl_2(phen)]^{3+}$ under Visible Light

The interactions of Ru,Rh bimetallic complexes $[(TL)_2Ru(dpp)RhCl_2(phen)]^{3+}$ (TL = phen, Ph_2phen and Me_2phen) with pUC18 plasmid DNA were also investigated by previously reported photolysis and agarose gel electrophoresis shift assays (Figure 3.27) to show the effect on Ru,Rh bimetallic photochemical properties by the modification of terminal ligand on the Ru light aborbers.[68,72] The photolysis experiment was performed under visible light ($\lambda = 455$ nm) from a 5 W LED with average flux of $2.0 \pm 0.1 \times 10^{19}$ photons/min under argon flow.[124]

The results of the DNA interactions with Ru,Rh bimetallic complexes $[(TL)_2Ru(dpp)RhCl_2(phen)]^{3+}$ (TL = phen, Ph_2phen and Me_2phen) illustrate that the photochemical properties of $[(TL)_2Ru(dpp)RhCl_2(phen)]^{3+}$ are similar. Lanes λ (Figure 1.27) are molecular weight markers. Lanes C are DNA plasmid controls showing most of DNA in the supercoiled form (SC) with a small amount of the open circular form (OC). Lanes MC are

complex/DNA solutions at 1:10 MC:BP ratio in the dark which resemble the controls (lanes C), indicative of no dark reactivity of the complexes with DNA. Lanes 10, 20, 30, 40, 50 and 60 are the complex /DNA solutions at 1:10 MC:BP ratio irradiated by the visible light for 10, 20, 30, 40, 50 and 60 min under argon. These lanes display the retardation of the SC DNA migration, suggesting the bimetallic complexes binding to the DNA. Binding of metal complexes to supercoiled DNA results in uncoiling of the DNA as well as decreased anionic charge and increased molecular size. Lanes 10, 20, 30, 40, 50 and 60 also display the increased intensity of the DNA open circular form consistent with longer irradiation time. The completed DNA photocleavage was observed for $[(TL)_2Ru(dpp)RhCl_2(phen)]^{3+}$ in lanes 40, 50 and 60, which is supported by the conversion of supercoiled form DNA (SC) to open-circular form DNA (OC).[101,113]

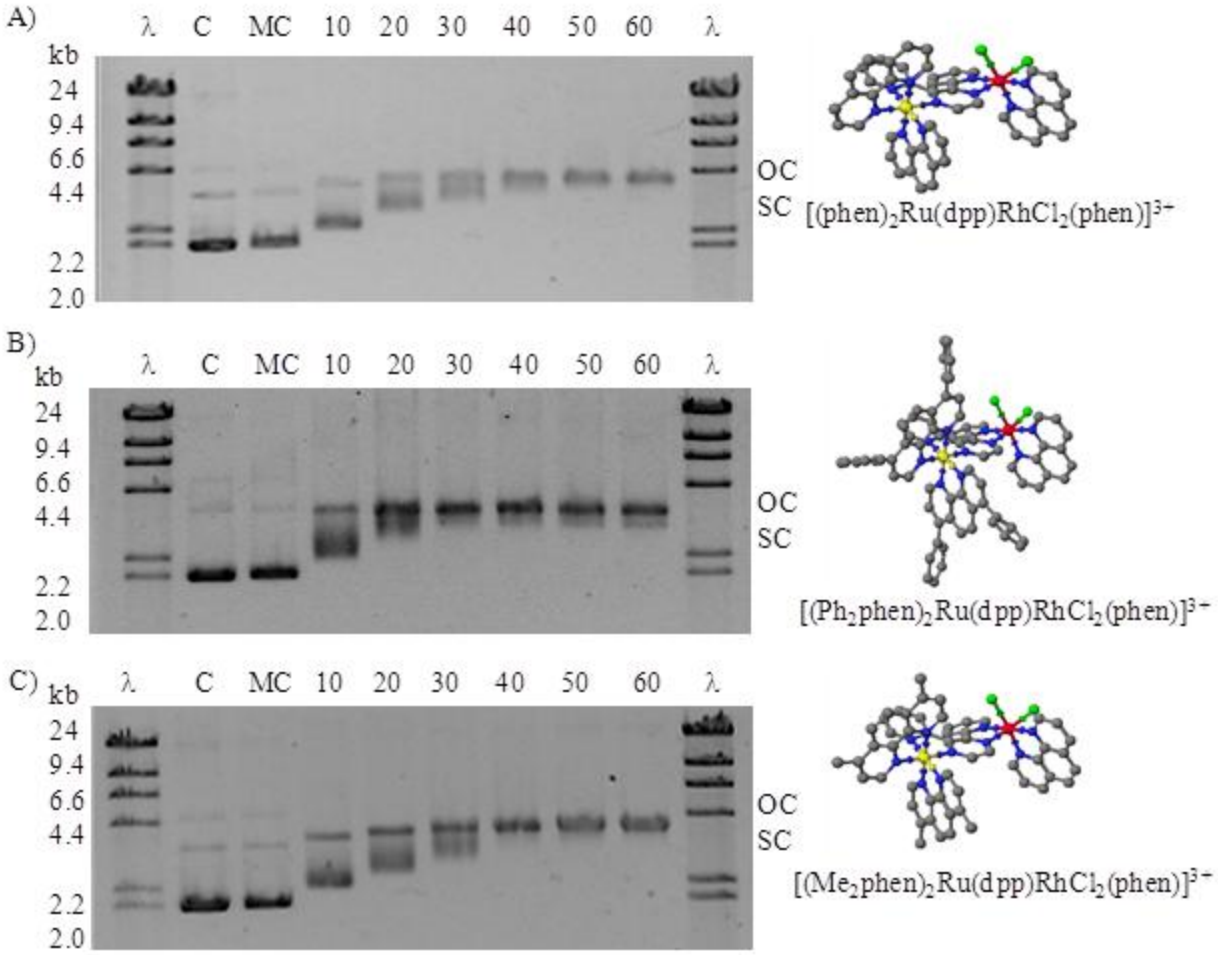

Figure 3.27. The imaged gels showing photochemical interactions of Ru,Rh bimetallic complexes, $[(phen)_2Ru(dpp)RhCl_2(phen)]^{3+}$ (A) $[(Ph_2phen)_2Ru(dpp)RhCl_2(phen)]^{3+}$ (B) $[(Me_2phen)_2Ru(dpp)RhCl_2(phen)]^{3+}$ (C) with DNA and Scigress structures of $[(TL)_2Ru(dpp)RhCl_2(phen)]^{3+}$. λ lanes are molecular weight markers, C lanes are DNA plasmid controls, MC lanes are dark plasmid controls incubated at RT in the dark for 2 h in the presence of 1:10 metal complex:base pairs ratio, Lane 10, 20, 30, 40, 50, 60 are the same plasmid DNA solution (1:10 metal complex:base pairs) irradiated for 10, 20, 30, 40, 50, 60 min under visible light (λ = 455 nm) from a 5 W LED with average flux of $2.0 \pm 0.1 \times 10^{19}$ photons/min under argon flow, Ph_2phen = 4,7-diphenyl-1,10-phenanthroline, Me_2phen = 4,7-dimethyl-1,10-phenanthroline, dpp = 2,3-bis(2-pyridyl)pyrazine, and phen = 1,10-phenanthroline.

Compared to $[(phen)_2Ru(dpp)RhCl_2(bpy)]^{3+}$, the efficiency of DNA photocleavage by $[(TL)_2Ru(dpp)RhCl_2(phen)]^{3+}$ is significantly enhanced by substituting bpy with phen attached to the Rh center. All of $[(TL)_2Ru(dpp)RhCl_2(phen)]^{3+}$/DNA solutions are prepared at 1:10 MC:BP

ratio instead of 1:5 MC:BP ratio for the $[(phen)_2Ru(dpp)RhCl_2(bpy)]^{3+}$/DNA solution. Although the concentrations of complexes $[(TL)_2Ru(dpp)RhCl_2(phen)]^{3+}$ in the DNA solutions decreased, complete conversion of supercoiled form to open circular form by $[(TL)_2Ru(dpp)RhCl_2(phen)]^{3+}$ was observed in lanes 40, 50 and 60 (Figure 3.27) versus partial DNA photocleavage by $[(phen)_2Ru(dpp)RhCl_2(bpy)]^{3+}$ in lane 60 (Figure 3.25). In addition, there is a slight change in the interactions of the Ru,Rh bimetallic complex $[(Ph_2phen)_2Ru(dpp)RhCl_2(phen)]^{3+}$ with DNA relative to the phen and Me_2phen bimetallic analogues. The trend in the DNA photocleavage ability of these $[(TL)_2Ru(dpp)RhCl_2(phen)]^{3+}$ systems suggests that the complex $[(Ph_2phen)_2Ru(dpp)RhCl_2(phen)]^{3+}$ is the most efficient DNA cleavage agent which shows the complete conversion of supercoiled form to open circular form in lane 30 (Figure 3.27 B). Such high efficiency may be due to the complex having enhanced absorption in the visible region without the absorption dropping between 350 nm and 450 nm compared to the phen and Me_2phen systems and enhanced excited lifetime.[129,130,99]

3.5.3. Photobinding and Photocleavage of DNA with Bimetallic Complex $[(bpy)_2Ru(dpp)RhCl_2(bpy)]^{3+}$, $[(bpy)_2Ru(dpp)RhCl_2(Me_2bpy)]^{3+}$ and $[(bpy)_2Ru(dpp)RhCl_2(phen)]^{3+}$ under Visible Light

The interactions of Ru,Rh bimetallic complexes $[(bpy)_2Ru(dpp)RhCl_2(TL')]^{3+}$ (TL′ = bpy, Me_2bpy and phen) with pUC18 plasmid DNA were studied by the photolysis and agarose gel electrophoresis shift assays to show the effect on Ru,Rh bimetallic photochemical properties by the modification of TL′ attached to the Rh center (Figure 3.28).[68,72] The photolysis experiment was performed under visible light (λ = 455 nm) from a 5 W LED with average flux of $2.0 \pm 0.1 \times 10^{19}$ photons/min under argon flow.[124] The results of the DNA interactions with Ru,Rh bimetallic

complexes $[(bpy)_2Ru(dpp)RhCl_2(TL')]^{3+}$ (TL′ = bpy, Me_2bpy and phen) show that the photochemical properties of the bimetallic complexes $[(bpy)_2Ru(dpp)RhCl_2(TL')]^{3+}$ are similar. Lanes λ (Figure 3.28) are molecular weight markers, and lanes C are DNA plasmid controls. Lanes MC are complex/DNA solutions at 1:5 MC:BP ratio in the dark which are similar to the controls (lanes C) indicating $[(bpy)_2Ru(dpp)RhCl_2(TL')]^{3+}$ not modifying DNA in the dark. Lanes 10, 20, 30, 40, 50 and 60 are the complex/DNA solutions at 1:5 MC:BP ratio irradiated for 10, 20, 30, 40, 50 and 60 min under argon, which show a slowing migration of DNA supercoiled form indicative of the bimetallic complexes binding to the DNA. Lanes 10, 20, 30, 40, 50 and 60 also display the increased intensity of the open circular form DNA with longer irradiation time, which is the same as other Ru,Rh bimetallic systems.

Compared to the complex $[(phen)_2Ru(dpp)RhCl_2(bpy)]^{3+}$, the efficiency of complexes $[(bpy)_2Ru(dpp)RhCl_2(TL')]^{3+}$ (TL = bpy, Me_2bpy and phen) DNA photocleavage is similar, by substituting phen with bpy on Ru light absorbers. However, the Ru,Rh bimetallic complex $[(bpy)_2Ru(dpp)RhCl_2(Me_2bpy)]^{3+}$ shows different photo-reactivity with DNA relative to the bpy and phen bimetallic analogues. The trend in the DNA photocleavage ability of these $[(bpy)_2Ru(dpp)RhCl_2(TL')]^{3+}$ systems shows that the complex $[(bpy)_2Ru(dpp)RhCl_2(Me_2bpy)]^{3+}$ is not an efficient DNA cleavage agent (Figure 3.28 B). This fact may be caused by the steric hindrance of Me_2bpy ligand, which prevents the Rh center from binding to DNA.

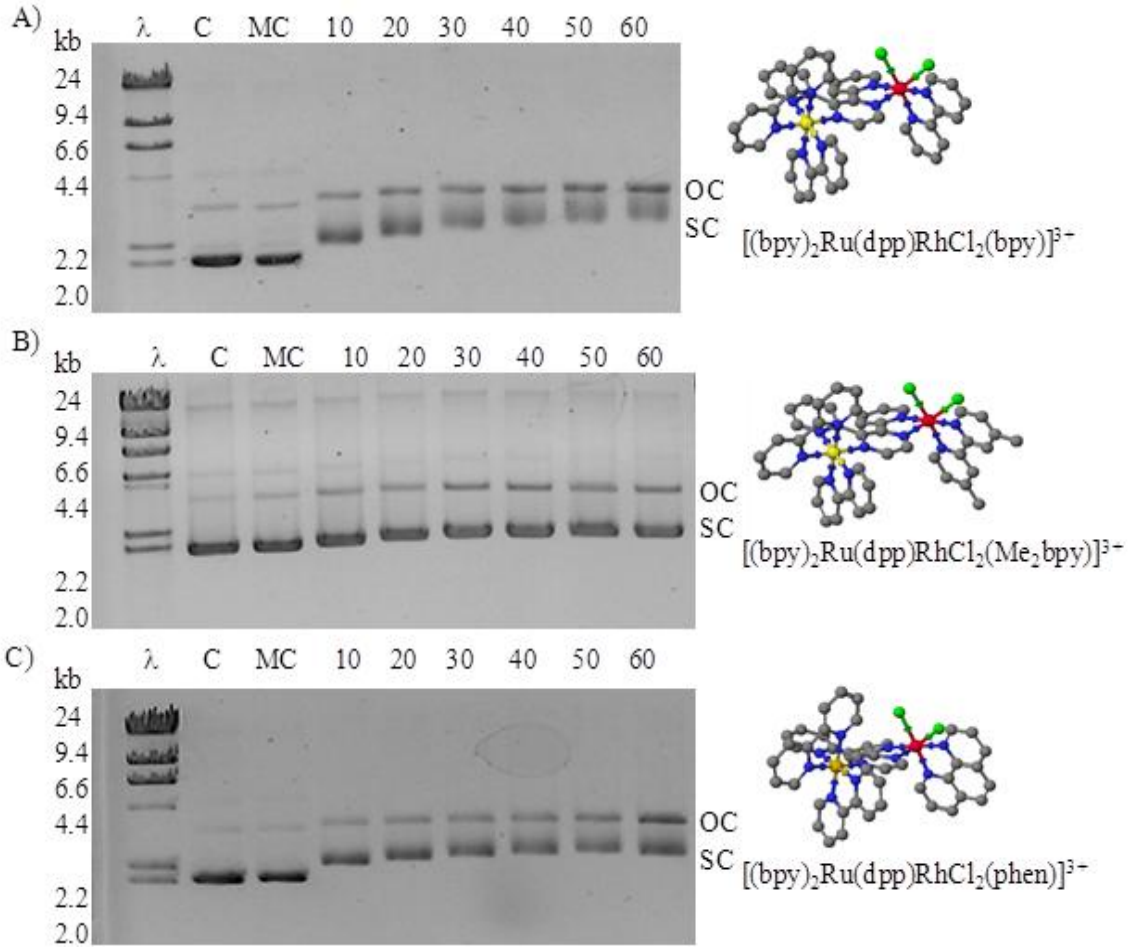

Figure 3.28. The imaged gels showing photochemical interactions of Ru,Rh bimetallic complexes, $[(bpy)_2Ru(dpp)RhCl_2(bpy)]^{3+}$ (A) $[(bpy)_2Ru(dpp)RhCl_2(Me_2bpy)]^{3+}$ (B) $[(bpy)_2Ru(dpp)RhCl_2(phen)]^{3+}$ (C) with DNA and Scigress structures of $[(bpy)_2Ru(dpp)RhCl_2(TL')]^{3+}$. λ lanes are molecular weight markers, C lanes are DNA plasmid controls, MC lanes are dark plasmid controls incubated at RT in the dark for 2 h in the presence of 1:5 metal complex:base pairs ratio, Lane 10, 20, 30, 40, 50, 60 are the same plasmid DNA solution (1:5 MC:BP) irradiated for 10, 20, 30, 40, 50, 60 min under visible light (λ = 455 nm) from a 5 W LED with average flux of $2.0 \pm 0.1 \times 10^{19}$ photons/min under argon flow, bpy = 2,2′-bipyridine, dpp = 2,3-bis(2-pyridyl)pyrazine, Me_2bpy = 4,4′-dimethyl-2,2′-bipyridine and phen = 1,10-phenanthroline.

The visible light induced DNA photobinding of $[(bpy)_2Ru(dpp)RhCl_2(phen)]^{3+}$ was further investigated by the DNA selective precipitation experiment adapted from previously reported methods.[125,138] Metal complex/calf thymus DNA solutions were photolyzed with visible light (λ = 455 nm) from a 5 W LED with average flux of $2.0 \pm 0.1 \times 10^{19}$ photons/min in the presence of

$[(bpy)_2Ru(dpp)RhCl_2(phen)]^{3+}$. DNA was selectively precipitated which removed any photo-bound metal complex with the precipitated DNA from the solution. The analysis of the absorbance of the supernatant before and after the photolysis allows determination of the amount of metal complex with remained bound to DNA in solution (Figure 3.29).

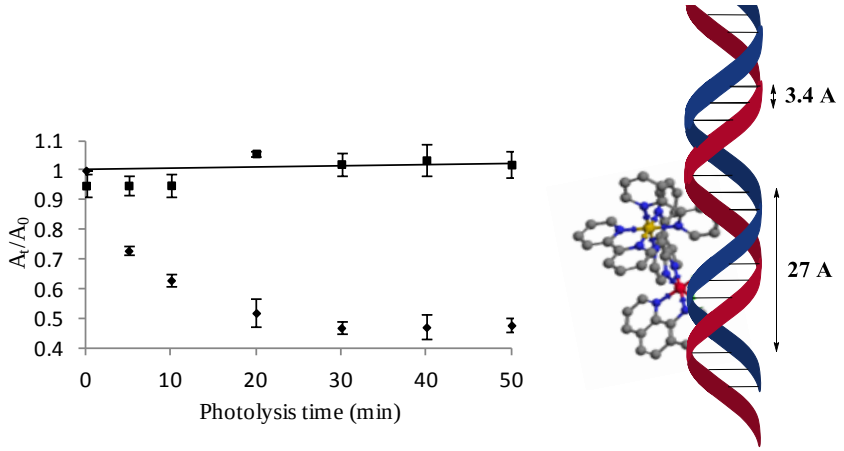

Figure 3.29. The plots of the absorbance of $[(bpy)_2Ru(dpp)RhCl_2(phen)]^{3+}$ at 515 nm remaining in the ethanolic supernatant versus time (0, 5, 10, 20, 30, 40, 50 min) following photolysis and selective precipitation of calf thymus DNA (1:5 metal complex:base pairs). The solutions were photolyzed with light (λ = 455 nm) from a 5 W LED with average flux of $2.0 \pm 0.1 \times 10^{19}$ photons/min under argon flow, sample points (◆) and dark control (■).

Upon the photolysis of $[(bpy)_2Ru(dpp)RhCl_2(phen)]^{3+}$ with DNA, a dramatic change in supernatant absorbance is observed, indicating bimetallic complex photobinding to DNA. No such change is observed for metal complex $[(bpy)_2Ru(dpp)RhCl_2(phen)]^{3+}$ incubated with the DNA for 50 min in the dark (Figure 3.29), suggesting that the Ru,Rh bimetallic complex does not covalently bind to DNA in the dark at room temperature. Metal complex photobinding is saturated at ca. 40 min of the photolysis. The results are consistent with the changes of pUC18 DNA migration in the gels in Figure 3.28 C. The saturation of the 1:5 MC:BP ratio solution photobinding occurs at ca. 60% metal complex bound. The result shows the actual bimetallic complexes bound to DNA at 0.6:5 MC:BP ratio which equals 1:8.3, suggesting that the bound

metal complex occupies ca. 8 DNA base pairs (3.4 A for the normal base pair to base pair distance) upon binding, which is consistent with the size (ca. 20 A) of the bimetallic complex $[(bpy)_2Ru(dpp)RhCl_2(phen)]^{3+}$.[139]

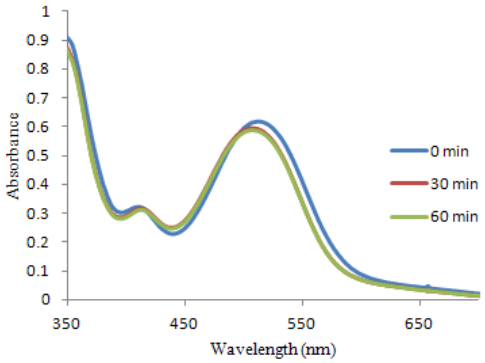

Figure 3.30. Electronic absorption spectra of 0.1 mM $[(bpy)_2Ru(dpp)RhCl_2(phen)]^{3+}$ in 10 mM NaH_2PO_4 buffer solution under visible light (λ = 455 nm) irradiation from a 5 W LED with average flux of $2.0 \pm 0.1 \times 10^{19}$ photons/min under argon flow for 0, 30, 60 min.

In order to further understand the Ru,Rh bimetallic complex DNA interaction, 0.1 mM $[(bpy)_2Ru(dpp)RhCl_2(phen)]^{3+}$ in 10 mM NaH_2PO_4 buffer solution was photolyzed under visible light (λ = 455 nm) irradiation from a 5 W LED with average flux of $2.0 \pm 0.1 \times 10^{19}$ photons/min under argon flow for 0, 30, 60 min. The changes of the electronic absorption spectra were observed in Figure 3.30. The Ru(dπ)→dpp(π*) MLCT transition (λ_{max} = 515 nm) blue-shifted 15 nm after 30 min visible light irradiation. No clear spectrum change was observed for an additional 30 min under visible light irradiation. The result is consistent with the DNA gel shift assay and the selective DNA precipitation result, which shows metal complexes photobinding saturated at ca. 40 min. Several molecules in the photolysis solution after 60 min visible light irradiation in the presence of the DNA buffer but absence of DNA include $[(bpy)_2Ru(dpp)Rh(HPO_4)(phen)]^{3+}$ (m/z = 342.35), $[(bpy)_2Ru(dpp)Rh(OH)(HPO_4)(phen)]^{2+}$ (m/z

= 522.03) and $[(bpy)_2Ru(dpp)Rh(H_2O)(HPO_4)(phen)]^{3+}$ (m/z = 348.36) found by ESI-mass spectrometry (Figure 3.31).

A) $[(bpy)_2Ru(dpp)Rh(HPO_4)(phen)]^{3+}$

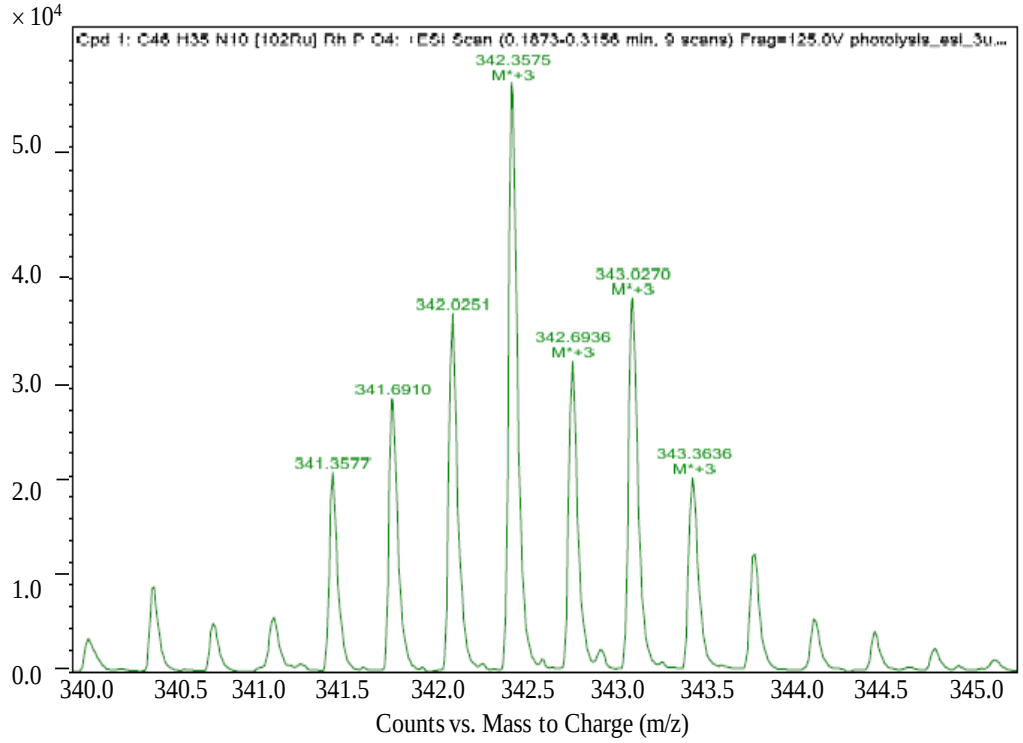

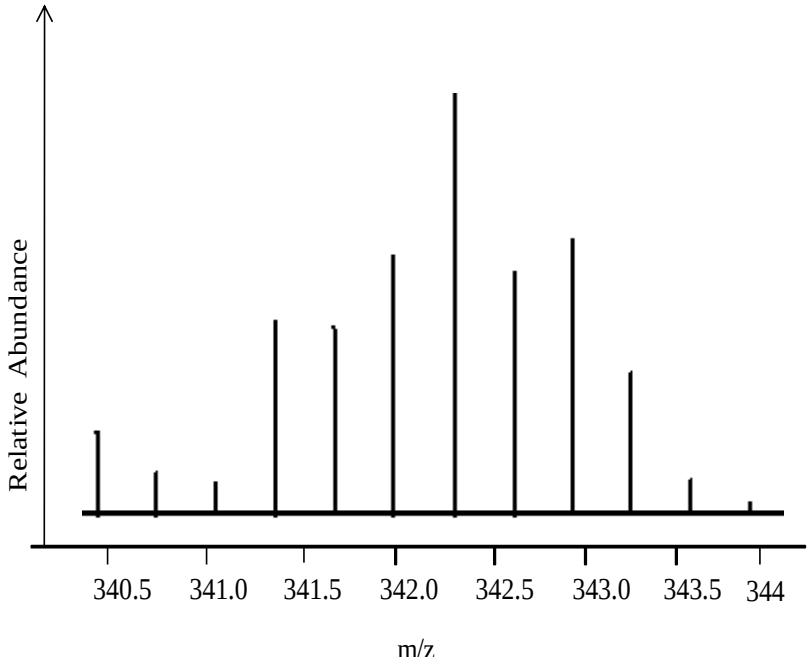

B) $[(bpy)_2Ru(dpp)Rh(OH)(HPO_4)(phen)]^{2+}$

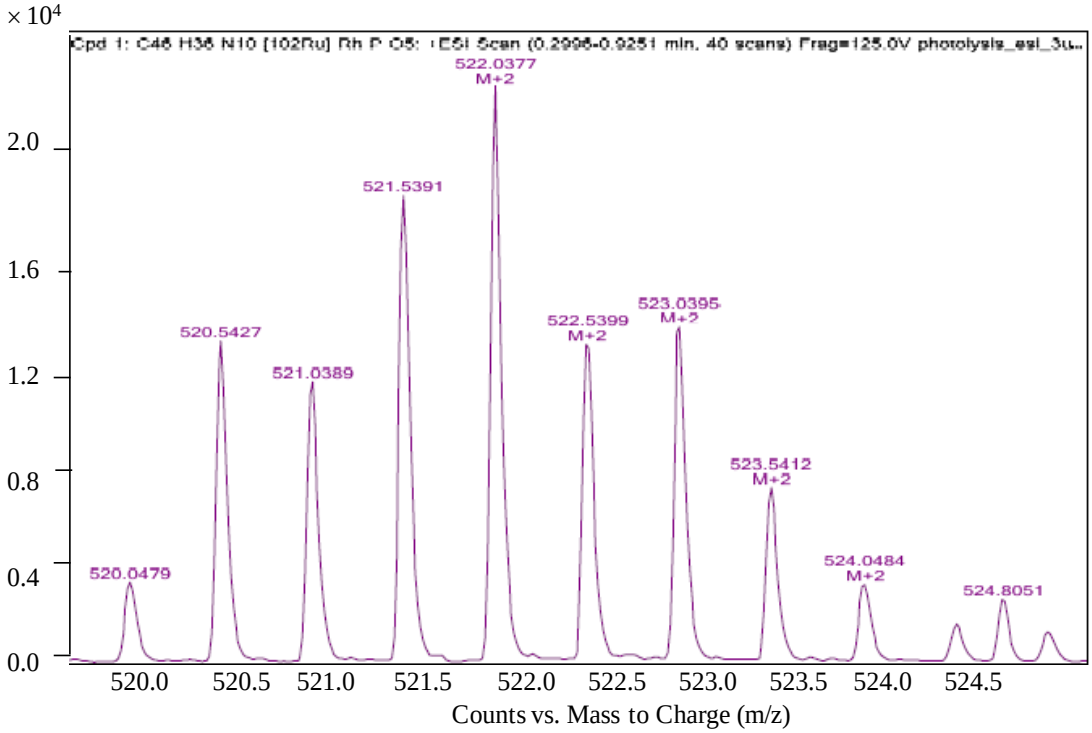

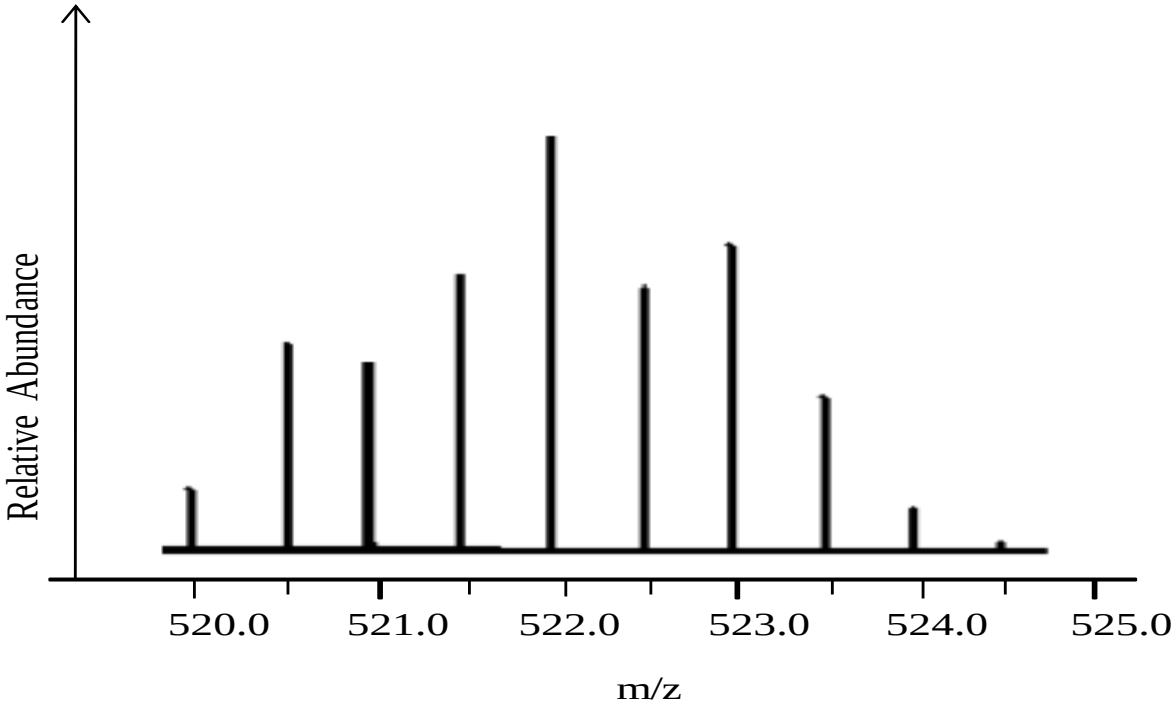

C) $[(bpy)_2Ru(dpp)Rh(H_2O)(HPO_4)(phen)]^{3+}$

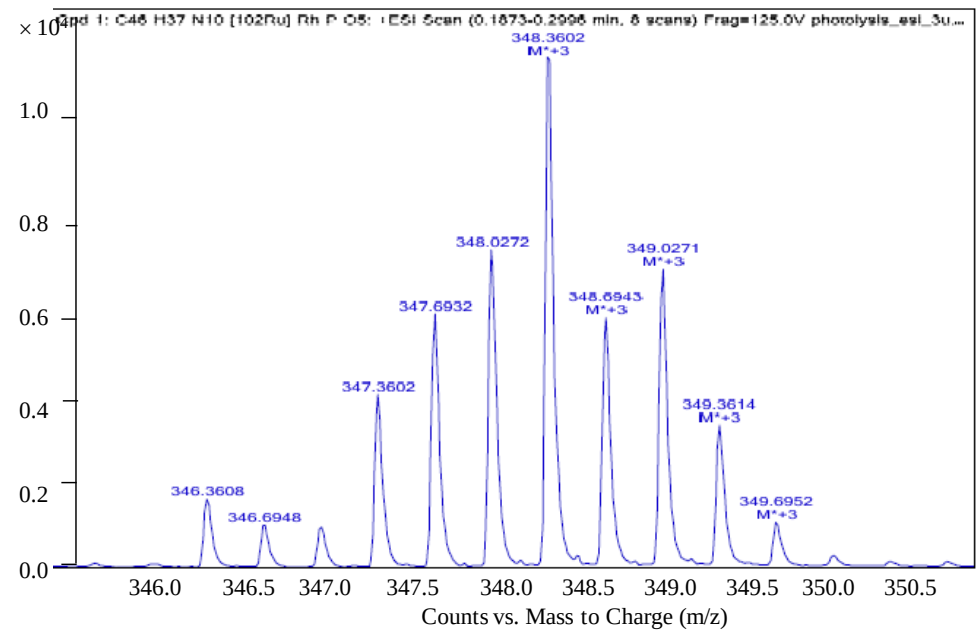

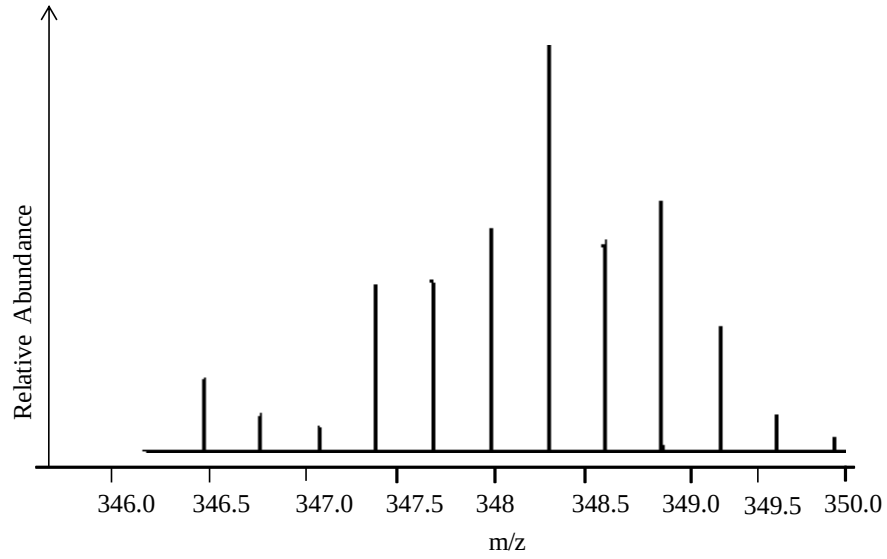

Figure 3.31. Mass spectrum of $[(bpy)_2Ru(dpp)Rh(HPO_4)(phen)]^{3+}$ (A), $[(bpy)_2Ru(dpp)Rh(OH)(HPO_4)(phen)]^{2+}$ (B) and $[(bpy)_2Ru(dpp)Rh(H_2O)(HPO_4)(phen)]^{3+}$ (C) showing isotopic distribution pattern as detected and showing isotopic distribution pattern as calculated with the ChemCalc, where bpy = 2,2′-bipyridine, phen = 1,10-phenanthroline and dpp = 2,3-bis(2-pyridyl)pyrazine.

These molecules (detected by ESI-mass spectrometry) suggest that the bimetallic complex loses chloride upon visible light excitation, and then coordinates through the newly unsaturated Rh

center which binds to available Lewis bases such as H_2O, HPO_4^- and OH^-,[139] or the Lewis base sites of DNA.

A second set of studies was designed to investigate the photoreactivity of $[(bpy)_2Ru(dpp)RhCl_2(phen)]^{3+}$ in buffer solution photolyzed first in the absence of DNA, then DNA was added into the photolysis solution as opposed to being photolyzed in the presence of DNA. This tried to test the hypothesis that ligand loss at Rh can occur in the absence of DNA and may permit subsequent thermal binding to DNA.

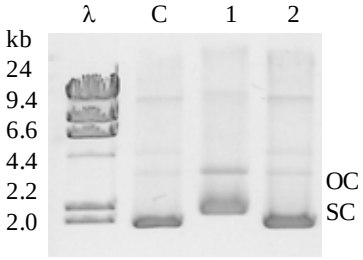

Figure 3.32. Imaged gel showing the photo-induced binding activity by $[(bpy)_2Ru(dpp)RhCl_2(phen)]^{3+}$ to pUC18 DNA under visible light ($\lambda = 455$ nm) irradiation from a 5 W LED with average flux of $2.0 \pm 0.1 \times 10^{19}$ photons/min under argon flow. λ lane is molecular weight marker, C lane is pUC18 plasmid DNA control, lane 1 is metal complex photolyzed for 20 min in the presence of pUC18 plasmid DNA, lane 2 is metal complex photolyzed for 20 min in 10 mM phosphate buffer with pUC18 plasmid DNA added following photolysis.

As shown in the gel shift assay (Figure 3.32), λ lane is molecular weight marker. C lane is pUC18 plasmid DNA control having most of DNA in the supercoiled form (SC) with a small amount of the open circular form (OC). Lane 1 is metal complex in the presence of pUC18 plasmid DNA at 1:5 MC:BP ratio photolyzed for 20 min as same as lane 20 in Figure 3.28 C. Lane 2 is the same concentration metal complex in 10 mM NaH_2PO_4 buffer solution with pUC18 DNA added following 20 min photolysis. Lane 2 is similar to lane C and does not show $[(bpy)_2Ru(dpp)RhCl_2(phen)]^{3+}$ complex photobinding or photocleaving DNA, indicating that

when Rh center was already coordinated with H_2O, HPO_4^- and OH^-, subsequent dark binding to DNA is not seen, consistent with the thermally stable Rh-ligand bonds.

The Ru,Rh bimetallics display interesting and efficient photo-reactivity with DNA activated by visible light. Through DNA gel shift assay, selective precipitation and ESI-mass spectrometry studies, Ru,Rh bimetallic complexes are demonstrated to photobind to DNA following visible light excitation via ^{3}MMCT facilitated Rh-Cl bond cleavage. This reactivity is not seen for analogous Ru,Rh,Ru trimetallics due to the steric protection of the Rh site in that motif. This study shows that the bimetallic complexes with only one Ru light absorber can efficiently photo-modify DNA and display varied photo-reactivity compared to the previously reported Ru,Rh,Ru trimetallics.[68,72] The photobinding of the bimetallic complexes $[(TL)_2Ru(dpp)RhCl_2(TL')]^{3+}$ (TL = phen, Ph_2phen, Me_2phen and bpy, TL′ = phen, bpy, Me_2bpy) with DNA could be the electrons from the Ru(II) center transferring through dpp to the Rh center under visible light irradiation, facilitating chloride ligand loss, and promoting Rh center bind to DNA. The DNA photocleavage could be the bimetallic complexes at the ^{3}MMCT excited state abstracting hydrogen from DNA sugar phosphate backbone through reactive Rh center.[68] The $[(TL)_2Ru(dpp)RhCl_2(TL')]^{3+}$ system has Ru ($d\pi$) based HOMO and Rh ($d\sigma^*$) based LUMO, and can photobind and photocleave DNA through the low-lying ^{3}MMCT excited state when excited by low energy visible light, with or without molecular oxygen. The efficiency of DNA photocleavage with $[(TL)_2Ru(dpp)RhCl_2(TL')]^{3+}$ is significantly enhanced by substituting bpy with phen attached to the Rh center and is decreased with Me_2bpy attached to the Rh center. The variation of terminal ligand on the Ru light absorbers does not have as much impact on the interactions of $[(TL)_2Ru(dpp)RhCl_2(TL')]^{3+}$ with DNA as the variation of TL′ attached to the Rh center. The

results are consistent with the fact that $[(TL)_2Ru(dpp)RhCl_2(TL')]^{3+}$ systems photobind and photocleave DNA through Rh center.[139]

3.5.4. Photobinding and Photocleavage of DNA with Bimetallic Complex $[(bpy)_2Os(dpp)RhCl_2(phen)]^{3+}$ in PDT Therapeutic Window

The Os,Rh bimetallic complex $[(bpy)_2Os(dpp)RhCl_2(phen)]^{3+}$ couples one Os polyazine light absorber to a *cis*-$Rh^{III}Cl_2$ center through a bridging ligand dpp. The Os,Rh bimetallic is an efficient light absorber through the UV and visible region of the spectrum.[119] The visible region is dominated by MLCT transitions. The Os(dπ)→bpy(π*) CT transition occurs at 413 nm and the Os(dπ)→dpp(π*) CT occurs at 521 nm. In the lower-energy visible region, the complex exhibits a weaker transition centered at 750 nm ($\varepsilon = 2.9 \times 10^3$ $M^{-1}cm^{-1}$), which is assigned as a $^1GS \rightarrow {}^3MLCT$ transition due to Os displaying significant spin orbit coupling providing enhanced absorptivity to the formally spin forbidden transtion (Figure 3.33). This transition can be utilized for therapeutic window (600-900 nm) excitation of this complex. This is a broad transition providing even more integrated absorptivity than expected based on the ε value. The electrochemical properties coupled with the light absorbing properties of $[(bpy)_2Os(dpp)RhCl_2(phen)]^{3+}$ suggest that this complex possesses an optically accessible low lying Os→dpp MLCT excited state and as a result of the Rh(dσ*) LUMO, a lower-lying ^{3}MMCT excited state. The ^{3}MMCT excited state has previously been shown to provide for oxygen-independent DNA photocleavage.[68,72] The ability to populate the reactive ^{3}MMCT excited state via direct ^{3}MLCT excitation with low energy visible light should allow this complex to be activated in the therapeutic window and function as an oxygen independent DNA photocleavage agent.

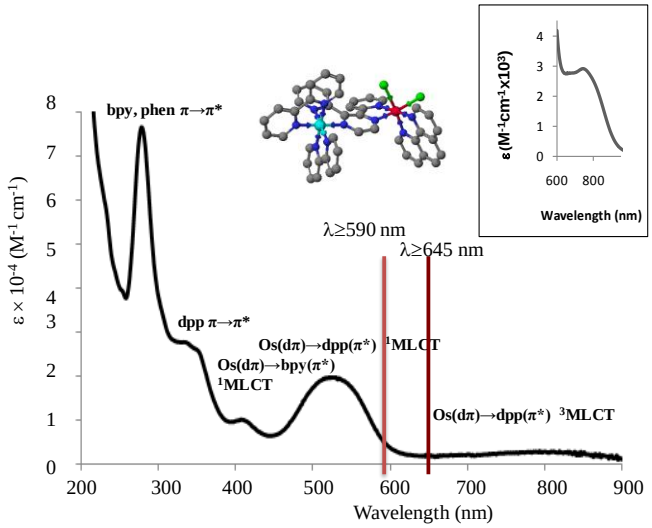

Figure 3.33. Electronic absorption spectrum of $[(bpy)_2Os(dpp)RhCl_2(phen)]^{3+}$ in the phosphate buffer solution at RT (black line), and 590 nm cuton filter (red line) and 645 nm cuton filter (dark red line) where bpy = 2,2′- bipyridine, phen = 1, 10-phenanthroline and dpp = 2,3-bis(2-pyridyl)pyrazine, ^{1}MLCT = singlet metal-to-ligand transition and ^{3}MLCT = triplet metal-to-ligand transition.

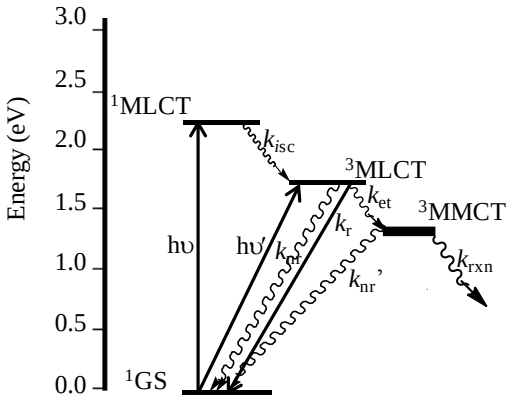

Figure 3.34. State diagram of $[(bpy)_2Os(dpp)RhCl_2(phen)]^{3+}$ photobinding to and photocleavage DNA. ^{1}GS = singlet ground state, ^{1}MLCT = singlet metal-to-ligand charge transfer excited state, ^{3}MLCT = triplet metal-to-ligand charge transfer excited state, k_r = rate constant for radiative decay, k_{nr} = rate constant for non-radiative decay, k_{isc} = rate constant for intersystem crossing non-radiative decay, k_{et} = rate constant for electron transfer and k_{rxn} = rate constant for reaction decay, bpy = 2,2′-bipyridine, dpp = 2,3-bis(2-pyridyl)pyrazine and phen = 1,10-phenanthroline.

The photobinding and photocleavage of DNA by bimetallic complex $[(bpy)_2Os(dpp)RhCl_2(phen)]^{3+}$ under red light irradiation through ^{3}MMCT excitation without

molecular oxygen are unprecedented investigated via a gel shift assay of the photolyzed DNA/metal complex solutions. This report is featured on the inside front cover of Chemical Communications (Figure 3.35).

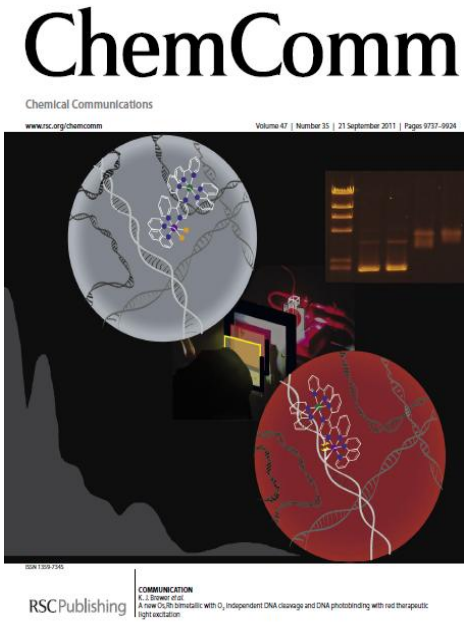

Figure 3.35. Inside front cover Chemical Communications. Reproduced from Wang, J.; Higgins, S. L. H.; Winkel, B. S. J.; Brewer, K. J. Chem. Comm. **2011**, *47*, 9786-9788 by permission from The Royal Society of Chemistry.[119]

The DNA/ metal complex sample was photolyzed using a 1000 W xenon arc lamp purchased from Oriel Light Source and Spectroscopy Instruments using the experiment apparatus shown in Figure 2.6. The light from the 1000 W xenon arc lamp was passed through a water filter which absorbs IR light between 1000-3000 nm, a 455 nm cuton filter from Newport Optics to remove the light $\lambda < 455$ nm and a $\lambda \geq 590$ or $\lambda \geq 645$ nm cuton filter for red light irradiation of the sample. The spectral output of xenon arc lamp and the measured spectra of each filter were shown in Figure 2.7. The photolyzed DNA/metal complex sample was investigated via a gel shift assay (Figure 3.36).

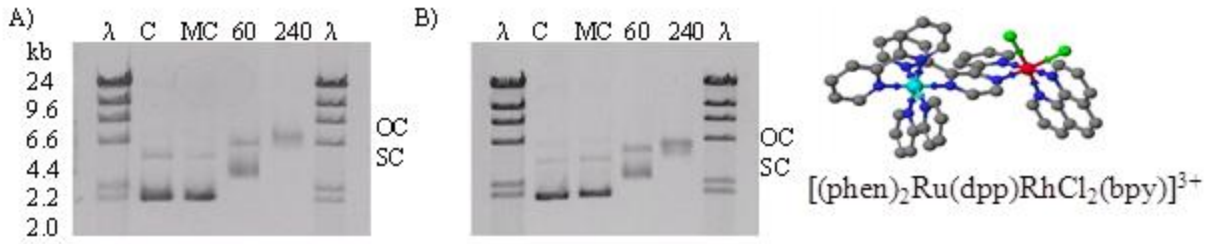

Figure 3.36. The imaged gels showing the complex $[(bpy)_2Os(dpp)RhCl_2(phen)]^{3+}$ photobinding and photocleavage of pUC18 DNA in the absence of molecular oxygen under red light at either $\lambda_{irr} \geq 590$ nm (A) or $\lambda_{irr} \geq 645$ nm (B). λ lanes are λ molecular weight markers, C lanes are pUC18 DNA controls, MC lanes are solutions containing pUC18 DNA and $[(bpy)_2Os(dpp)RhCl_2(phen)]^{3+}$ at a 1:5 metal complex:base pairs ratio incubated for 120 min in the dark without molecular oxygen, and the 60 and 240 lanes are complex $[(bpy)_2Os(dpp)RhCl_2(phen)]^{3+}$ and pUC18 DNA solutions at 1:5 metal complex:base pairs ratio under irradiation for 60 min and 240 min respectively under argon.

The images of agarose gel electrophoresis show: a molecular weight marker (lane λ), a pUC18 DNA control (lane C), a metal complex/DNA solution at 1:5 MC:BP ratio incubated in the dark at RT for 120 min (lane MC), a metal complex/DNA solution at 1:5 MC:BP ratio irradiated for 60 min under argon (lane 60) and a metal complex/DNA solution at 1:5 MC:BP ratio irradiated for 240 min under argon (lane 240). Figure 3.36 A shows the photocleavage study at $\lambda_{irr} \geq 590$ nm with Figure 3.36 B showing at $\lambda_{irr} \geq 645$ nm. The pUC18 DNA exists in supercoiled form (SC) with a minor fraction presented in the relaxed circular form (OC). Incubation of the pUC18 DNA with the complex in dark without molecular oxygen does not influence the DNA migration through the gel (lane MC). The retarded DNA migration was observed in lanes 60 in both gels (Figure 3.36, A and B), indicative of photobinding to DNA following exposure to red light ($\lambda_{irr} \geq 590$ nm (Figure 3.36 A), or $\lambda_{irr} \geq 645$ nm (Figure 3.36 B)) in the absence of oxygen.[140] Binding of the metal complex to supercoiled DNA slows migration, presumably due to the unwinding of the supercoiled DNA and partial neutralization of the negative charge on the DNA molecule by the cationic metal complex. Photocleavage of DNA was observed following 240 min of exposure

to red light, lanes 240 of both gels (Figure 3.36 A and B), with all SC pUC18 DNA converted to OC DNA.[72,113] These results indicate that the bimetallic $[(bpy)_2Os(dpp)RhCl_2(phen)]^{3+}$ complex photobinds to pUC18 DNA under red light irradiation for 60 min ($\lambda \geq 645$ nm) and photocleaves pUC18 DNA through an oxygen-independent mechanism.

The photoreactivity of the $[(bpy)_2Os(dpp)RhCl_2(phen)]^{3+}$ complex is unique representing the first system shown to undergo therapeutic light DNA cleavage in the absence of O_2. In addition, the system is unique as a new reactivity from the ^{3}MMCT state is observed. The bimetallic complex $[(bpy)_2Os(dpp)RhCl_2(phen)]^{3+}$ photobinds to DNA via the Rh site which is sterically accessible in this motif unlike in previously reported trimetallic systems.[68] Only one large $[(bpy)_2Os^{II}(dpp)]^{2+}$ sub-unit is bound to the Rh center instead of two large $[(TL)_2M^{II}(dpp)]^{2+}$ sub-units in the trimetallic motif. Photobinding with red therapeutic light was also not known prior to our report. The complex $[(bpy)_2Os(dpp)RhCl_2(phen)]^{3+}$ is activated to photobind and photocleave pUC18 DNA by low energy red light in the "phototherapeutic window" without molecular oxygen. This is made possible by direct photo-excitation to the Os→dpp ^{3}MLCT state, which covers the 600-900 nm region of the spectrum. This excited state is well coupled to the lower lying ^{3}MMCT state, which is typically populated with high efficiency in related emissive Ru analogs.[72] The photobinding of this bimetallic to DNA with therapeutic excitation is an exciting result as the drug locates the damage to the DNA target providing enhanced therapeutic light DNA photocleavage efficiency.

3.5.5. PCR Method Evaluate the Effect of DNA Photo-damage by Bimetallic Complex $[(bpy)_2Os(dpp)RhCl_2(phen)]^{3+}$ on DNA Amplification

The polymerase chain reaction (PCR) is a technique that enables the rapid amplification of specific DNA fragments *in vitro* that has seen widespread application in research and since the discovery of thermo-stable polymerases in the mid-1980s.[141,142-144] PCR has been used as an *in vitro* method to assess DNA modification or damage in cases where there is significant thermal stability of DNA-metal complex adducts in a few cases.[145,146] Lippard reported the anticancer drug, [*cis*-$Pt(NH_3)_2Cl_2$] (cisplatin), predominantly binds to two adjacent guanine, inhibiting DNA synthesis.[147] Eastman reported PCR detects DNA modification by cisplatin with inhibition sensitivity in PCR proportional to the size of DNA fragments amplified and the efficiency of the drug's modification of DNA, requiring 35:1 base pair:metal complex (BP:MC) ratio for 150 bp DNA replication inhibition.[148-150] The inhibition of amplification of a 148 bp fragment of DNA by [$(Rh_2(O_2CCH_3)_4$] requires a 1:50 bp:mc ratio incubated at 37 °C for 24 h and amplified 1450 bp DNA with a 1:5 bp:mc ratio at the same condition.[151]

In order to evaluate the effect of DNA photo-damage by $[(bpy)_2Os(dpp)RhCl_2(phen)]^{3+}$ under red therapeutic light irradiation on the DNA replication needed for cancer proliferation, the PCR experiments were conducted with 670 bp DNA daughter strand amplification and analyzed using agarose gel shift assay. The PCR samples were prepared by using the pUC18 DNA and $[(bpy)_2Os(dpp)RhCl_2(phen)]^{3+}$ complex solutions at a 1:5 MC:BP ratio as templates irradiated for 60 and 240 min under argon using red light $\lambda \geq 590$ and 645 nm. Following photolysis, 35 thermal cycles of PCR were conducted and the products were studied by the agarose gel shift assays. Mr. Jerry Newman, Jr conducted the PCR experiments under Ms. Jing Wang's supervision.

The images of the agarose gel shift assay of the complex $[(bpy)_2Os(dpp)RhCl_2(phen)]^{3+}$ DNA photolysis samples (Figure 3.37 A and Figure 3.38 A) show that $[(bpy)_2Os(dpp)RhCl_2(phen)]^{3+}$

photobinds to pUC18 DNA after 60 min under red light irradiation and photocleaves DNA with most of supercoiled form pUC18 DNA converted to open circular form DNA after 240 min exposure to the light ($\lambda \geq 590$ and 645 nm).

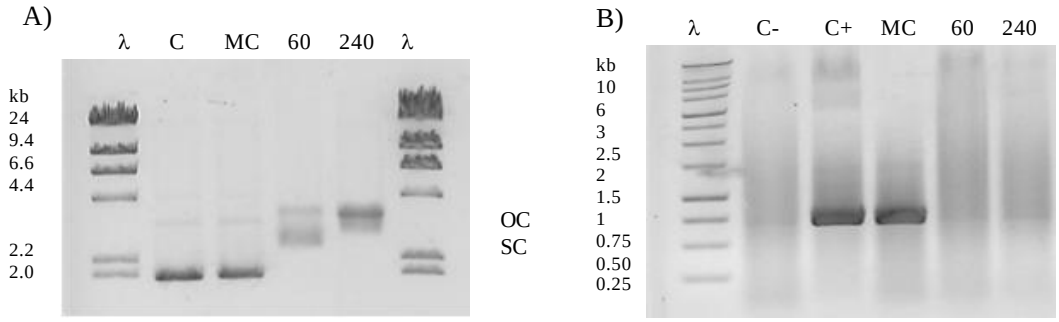

Figure 3.37. The imaged agarose gel of DNA photolysis samples under red light $\lambda \geq 590$ nm (A), and imaged gel of the amplified 670 bp DNA PCR samples (B). In gel A, λ lanes are λ molecular weight markers, C lane is pUC18 plasmid DNA control, MC lane is the solution containing pUC18 plasmid DNA and $[(bpy)_2Os(dpp)RhCl_2(phen)]^{3+}$ at a 1:5 MC:BP ratio incubated for 240 min in the dark without molecular oxygen, and the 60 and 240 lanes are complex $[(bpy)_2Os(dpp)RhCl_2(phen)]^{3+}$ and pUC18 DNA solutions at a 1:5 MC:BP ratio under red light $\lambda \geq 590$ nm irradiation for 60 min and 240 min respectively under argon. In gel B, λ lane is λ DNA ladder, lane C– is a negative control with de-ionized H_2O as a template, lane C+ is a positive control with pUC18 plasmid DNA as a template, lane MC is a PCR sample using the pUC18 plasmid DNA and $[(bpy)_2Os(dpp)RhCl_2(phen)]^{3+}$ complex solution at a 1:5 MC:BP ratio incubated for 240 min in dark as a template. Lane 60 and 240 are PCR samples using the pUC18 plasmid DNA and $[(bpy)_2Os(dpp)RhCl_2(phen)]^{3+}$ complex solutions at a 1:5 MC:BP ratio irradiation for 60 and 240 min with red light $\lambda \geq 590$ nm under argon.

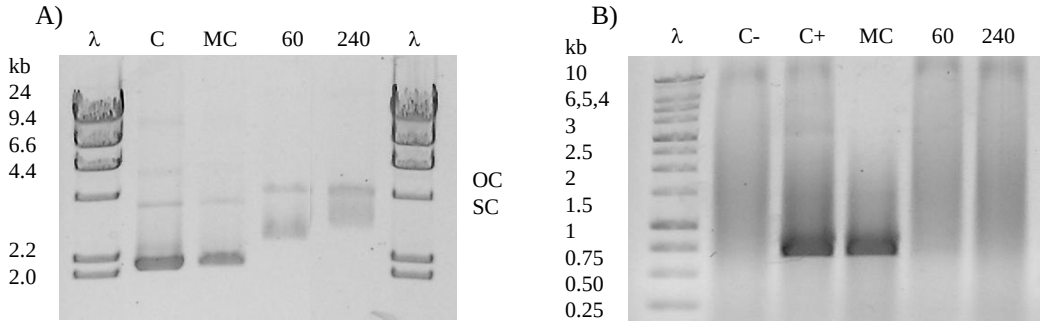

Figure 3.38. Imaged gel of DNA photolysis samples under red light $\lambda \geq 645$ nm (A), and imaged gel of the amplified 670 bp DNA PCR samples (B). In gel A, λ lanes are λ molecular weight markers, C lane is pUC18 plasmid DNA control, MC lane is the solution containing pUC18 plasmid DNA and $[(bpy)_2Os(dpp)RhCl_2(phen)]^{3+}$ at a 1:5 MC:BP ratio incubated for 240 min in the dark without molecular oxygen, and the 60 and 240 lanes are complex $[(bpy)_2Os(dpp)RhCl_2(phen)]^{3+}$ and pUC18 plasmid DNA solutions at a 1:5 MC:BP ratio under red light $\lambda \geq 645$ nm irradiation for 60 min and 240 min, under argon. In gel B, λ lane is λ DNA ladder, lane C– is a negative control with de-ionized H_2O as a template, lane C+ is a positive control with pUC18 plasmid DNA as a template, lane MC is a PCR sample using the pUC18 DNA and $[(bpy)_2Os(dpp)RhCl_2(phen)]^{3+}$ complex solution at a 1:5 MC:BP ratio incubated for 240 min in dark as a template. Lane 60 and 240 are PCR samples using the pUC18 plasmid DNA and $[(bpy)_2Os(dpp)RhCl_2(phen)]^{3+}$ complex solutions at a 1:5 MC:BP ratio irradiation for 60 and 240 min with red light $\lambda \geq 645$ nm under argon.

The PCR sample agarose gel images, Figure 3.37 B and 3.38 B represent the analysis of the impact of metal complex DNA photomodification on DNA amplification, include: a λ DNA molecular ladder (lane λ), a negative control with de-ionized H_2O as a template (lane C–), a positive control with pUC18 plasmid DNA as a template containing the amplified 670 bp DNA (lane C+), a PCR sample using the pUC18 plasmid DNA and $[(bpy)_2Os(dpp)RhCl_2(phen)]^{3+}$ complex solution at a 1:5 MC:BP ratio incubated for 240 min in the dark as a template (lane MC). The PCR samples use the pUC18 plasmid DNA and $[(bpy)_2Os(dpp)RhCl_2(phen)]^{3+}$ complex solutions at a 1:5 MC:BP ratio irradiation for 60 min with red light $\lambda \geq 590$ and 645 nm under argon as templates (lane 60), or irradiation for 240 min with red light $\lambda \geq 590$ and 645 nm under argon as templates (lane 240). Figure 3.37 B and 3.38 B show no DNA band in lane C–

due to the absence of DNA template in the PCR process. Intense dark bands are observed in the positive control C+, as well as in the dark control (lane MC) where the pUC18 plasmid DNA and $[(bpy)_2Os(dpp)RhCl_2(phen)]^{3+}$ complex solution at 1:5 MC:BP ratio was incubated for 240 min in the dark. As observed through gel electrophoresis, the complete amplification of the plasmid results in very dark bands on the gel, lane C+. Addition of the metal complex in the dark does not impede DNA amplification as seen in lanes MC in the Figure 3.37 B and 3.38 B. The intense dark bands indicate that a large amount of DNA amplification occurred during the PCR experiment and the DNA amplification was not influenced by metal complexes in the dark. No DNA bands are found in lanes containing the pUC18 plasmid DNA and $[(bpy)_2Os(dpp)RhCl_2(phen)]^{3+}$ complex solutions at a 1:5 MC:BP ratio under irradiation for 60 min with red light $\lambda \geq 590$ and 645 nm under argon (lane 60), and the pUC18 plasmid DNA and $[(bpy)_2Os(dpp)RhCl_2(phen)]^{3+}$ complex solutions at a 1:5 MC:BP ratio under irradiation for 240 min with red light $\lambda \geq 590$ and 645 nm under argon (lane 240). This unique result shows complete inhibition of DNA amplification after red light excitation of $[(bpy)_2Os(dpp)RhCl_2(phen)]^{3+}$ with DNA in the absence of oxygen.

In order to further investigate the DNA photo-damage by $[(bpy)_2Os(dpp)RhCl_2(phen)]^{3+}$ at low DNA metal complex:base pairs ratio, a solution of the pUC18 plasmid DNA and $[(bpy)_2Os(dpp)RhCl_2(phen)]^{3+}$ complex at a 1:50 MC:BP ratio was prepared and kept in the dark for 240 min and another solution at the same ratio was irradiated with red light $\lambda \geq 590$ under argon for 60 and 240 min (Figure 3.39). This study reduces the metal complex ratio to DNA base pairs by one order of magnitude now 1:50 MC:BP.

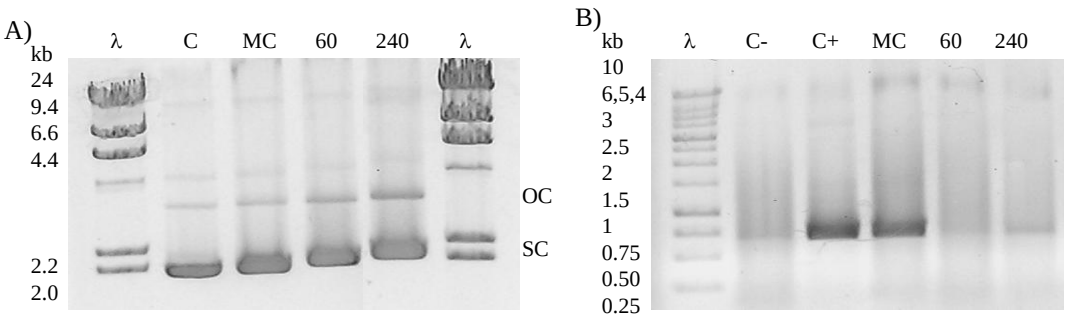

Figure 3.39. The imaged agarose gel of DNA photolysis samples under red light $\lambda \geq 590$ nm (A), and imaged gel of the amplified 670 bp DNA PCR samples (B). In gel A, λ lanes are λ molecular weight markers, C lane is pUC18 plasmid DNA control, MC lane is the solution containing pUC18 plasmid DNA and $[(bpy)_2Os(dpp)RhCl_2(phen)]^{3+}$ at a 1:50 MC:BP ratio incubated for 240 min in the dark without molecular oxygen, and the 60 and 240 lanes are complex $[(bpy)_2Os(dpp)RhCl_2(phen)]^{3+}$ and pUC18 plasmid DNA solutions at a 1:50 MC:BP ratio under red light $\lambda \geq 590$ nm irradiation for 60 min and 240 min, respectively, under argon. In gel B, λ lane is λ DNA ladder, lane C– is a negative control with de-ionized H_2O as a template, lane C+ is a positive control with pUC18 plasmid DNA as a template, lane MC is a PCR sample using the pUC18 plasmid DNA and $[(bpy)_2Os(dpp)RhCl_2(phen)]^{3+}$ complex solution at a 1:50 MC:BP ratio incubated for 240 min in dark as a template. Lane 60 and 240 are PCR samples using the pUC18 plasmid DNA and $[(bpy)_2Os(dpp)RhCl_2(phen)]^{3+}$ complex solutions at a 1:50 MC:BP ratio irradiation for 60 and 240 min with red light $\lambda \geq 590$ nm under argon.

Figure 3.39 A shows $[(bpy)_2Os(dpp)RhCl_2(phen)]^{3+}$ complex photobinds to pUC18 plasmid DNA after 60 min under red light irradiation, with minor cleavage evidenced by minor conversion of supercoiled form pUC18 DNA to open circular form DNA after 240 min exposure at the 1:50 MC:BP ratio. The PCR analysis shows complete inhibition of DNA amplification after photolysis of the metal complex DNA solution for 60 and 240 min with red light $\lambda \geq 590$ nm in the absence of oxygen even at this low metal complex concentration of 1:50 MC:BP ratio. Given the daughter DNA being amplified is 670 BP, this degree of DNA amplification with 1:50 MC:BP ratio demonstrates the large impact of DNA modification by $[(bpy)_2Os(dpp)RhCl_2(phen)]^{3+}$ on DNA amplification desirable for the application of this motif as a PDT drug.

This study shows that $[(bpy)_2Os(dpp)RhCl_2(phen)]^{3+}$ can act as a very specifically light activated agent to impede DNA amplification showing promise as a PDT drug for clinical applications. The red light induced inhibition of DNA amplification by a metal complex is unprecedented in the literature. This complex can photo-modify DNA under red therapeutic light excitation resulting in sufficient DNA modification and damage to inhibit DNA amplification even at low metal complex loading. In addition, there is no impact in the dark upon the incubation of this complex with DNA on amplification, making activity very specific for light exposure. The bimetallic $[(bpy)_2Os(dpp)RhCl_2(phen)]^{3+}$ is designed to provide an Os chromophore for therapeutic light excitation and a *cis*-$RhCl_2$ site for DNA photobinding and oxygen independent cleavage. Short time photolysis shows both DNA photobinding and photocleavage impede DNA amplification with low energy $\lambda \geq 645$ nm light with low metal complex loading. Different from normal cells, cancer cells exhibit higher rates of division and cell replications. The DNA photo-modification and photodamage induced by $[(bpy)_2Os(dpp)RhCl_2(phen)]^{3+}$ under red light irradiation will inhibit DNA replication and should disrupt the cell division cycle and prevent cancer cell DNA passing to the daughter cells through cell division, making $[(bpy)_2Os(dpp)RhCl_2(phen)]^{3+}$ a promising PDT agent.

Chapter 4. Conclusions and Future Directions

4.1. Conclusions

A series of mixed-metal bimetallic complexes $[(TL)_2M(dpp)RhCl_2(TL')]^{3+}$ (M = Ru and Os, TL = phen, Ph_2phen, Me_2phen and bpy, TL′ = phen, bpy and Me_2bpy), which couple one Ru or Os polyazine light absorber to a *cis*-$Rh^{III}Cl_2$ center through a dpp bridging ligand, were synthesized using a building block method with a variety of terminal ligands on light absorbers, light absorber's metal centers and terminal ligands attached to the rhodium center. These complexes were characterized and studied by electrochemistry, electronic absorption spectroscopy, ESI-mass spectrometry, steady-state and time-resolved emission spectroscopy and DNA photolysis experiments. These systems maintained some properties of the related Ru,Rh,Ru and Os,Rh,Os trimetallics but displayed other properties that varied unexpectedly from the well studied trimetallic systems.

The electrochemical properties of bimetallic complexes with polyazine ligands consist of a reversible one-electron metal-based oxidation, and a quasi-reversible $Rh^{III/II}Cl_2$ couple overlapped with a small amount of $Rh^{II/I}Cl$ reduction and an irreverisble $Rh^{II/I}Cl_2$ reduction prior to the reversible bridging ligand $dpp^{0/-}$ reduction. The energy of Rh ($d\sigma^*$) orbital and the bridging ligand dpp (π^*) orbital are very close. The structural differences between bimetallic and trimetallic complexes cause differences in electrochemical properties. The oxidative electrochemistry of trimetallic complexes $[\{(TL)_2M(dpp)\}_2RhCl_2]^{5+}$ shows two overlapping, one-electron reversible $M^{II/III}$ couples due to the nearly simultaneous oxidation of the two light absorbers. The reductive electrochemistry of trimetallic complexes shows irreversible two overlapping one-electron $Rh^{III/II/I}$ reductions, followed by two bridging ligand $dpp^{0/-}$ reductions.

The first and second one-electron reductions of trimetallic complexes are followed by a very fast chemical reaction of a chloride ligand loss. The third and forth reductions of trimetallic complexes are reversible dpp-based one-electron reductions. The electrochemical mechanisms of bimetallic complexes are different from those of trimetallic complexes due to slower halide loss after the first reduction compared to that of trimetallic complexes. The trimetallics are sterically crowded and the *cis*-$Rh^{III}Cl_2$ is bound to two withdrawing μ-dpp ligands, which makes the first chloride ligand easy to lose following the first rhodium reduction. However, for the bimetallic system, the order of the Rh (dσ*) and BL dpp (π*) orbitals is modulated by the electronic property of the terminal ligand TL′ attached to the *cis*-$Rh^{III}Cl_2$. Since the *cis*-$Rh^{III}Cl_2$ is bound to a μ-dpp ligand and a terminal ligand, the electronic and sterical properties of bimetallic complexes depend on the terminal ligand attached to the *cis*-$Rh^{III}Cl_2$ center. These factors make the reductive electrochemistry of bimetallic complexes complicated with two mechanisms each with two branches modified by the scan rate. The electrochemical properties of bimetallic complexes are modulated by variations of the light absorber's metal center, the terminal ligand on light absorbers and the terminal ligand attached to the rhodium center. The $Os^{II/III}$ oxidation couple of $[(bpy)_2Os(dpp)RhCl_2(phen)]^{3+}$ occurs at 1.20 V vs. Ag/AgCl, ca. 0.40 V less positive than the $Ru^{II/III}$ oxidation of Ru,Rh bimetallic complexes $[(TL)_2Ru(dpp)RhCl_2(TL')]^{3+}$ due to the energy of the Os(dπ) orbital that is higher than that of Ru (dπ) orbital. The $Ru^{II/III}$ oxidation couple of $[(Me_2phen)_2Ru(dpp)RhCl_2(phen)]^{3+}$ occurs at a less positive potential compared to the bimetallic complexes with TL = phen or Ph_2phen on LAs attributed to the electron donating character of Me_2phen. The first reduction of $[(bpy)_2Ru(dpp)RhCl_2(Me_2bpy)]^{3+}$ appears more reversible than the same reductive wave of $[(bpy)_2Ru(dpp)RhCl_2(bpy)]^{3+}$, indicating that the Rh(dσ*) orbital is modulated by terminal ligand attached to the rhodium center.[91]

The electronic absorption spectroscopic properties of bimetallic complexes are similar to their trimetallic analogues, with extinction coefficient values approximately half those of the trimetallics both in the UV and visible regions of the spectrum. These complexes are efficient light absorbers and display ligand-based $\pi \rightarrow \pi^*$ transitions in the UV region of the spectrum and metal-to-ligand charge transfer (MLCT) transitions in the visible region of the spectrum. The Os,Rh bimetallic complex, $[(bpy)_2Os(dpp)RhCl_2(phen)]^{3+}$, displays a more intense low energy absorption band in the low energy visible region than the Ru analogs with enhanced ε due to increased spin orbital coupling. The bimetallic complex, $[(Ph_2phen)_2Ru(dpp)RhCl_2(phen)]^{3+}$ with TL = Ph_2phen, on LA displays enhanced absorption in the UV and visible regions without the absorption dropping between 350 nm and 450 nm which is typical for the bpy and phen systems.[129,130]

The photophysical properties of Ru,Rh bimetallics are close to those of trimetallic analogues. At room temperature, both bimetallic and trimetallic complexes display a weak and short-lived emission from the $Ru(d\pi) \rightarrow dpp(\pi^*)$ ^{3}MLCT excited state in acetonitrile solution. At 77 K, the bimetallics as well as trimetallics exhibit a more intense blue-shifted emission with a longer lifetime, which is from $Ru(d\pi) \rightarrow dpp(\pi^*)$ ^{3}MLCT excited state in 4:1 ethanol/methanol glass with similar energy, structure, and τ as the Ru,Ru bimetallic motifs $[\{(TL)_2Ru\}_2(dpp)]^{4+}$. The Ru,Rh complexes in the ^{3}MLCT excited state can populate $Ru(d\pi) \rightarrow Rh(d\sigma^*)$ ^{3}MMCT excited state through the intramolecular electron transfer at room temperature which is inhibited in the rigid matrix at 77 K due to the large reorganizational energy. The variation of terminal ligands on the light absorbers influences the Ru,Rh bimetallic and trimetallic photophysical properties due to the terminal ligand impacting the energy of the $Ru(d\pi)$ orbital which is the donor orbital in ^{3}MLCT excited state. The variation of terminal ligand attached to the Rh metal center also

impacts photophysical properties, attributed to the terminal ligand affecting the energy of Rh(dσ*) orbital. The photophysical studies of Ru,Rh bimetallic complexes are important, and the results provide a clear direction of tuning the complexes excited state properties for the photochemical applications by changing the structural subunits.

The Ru,Rh bimetallics display interesting and efficient photoreactivity with DNA activated by visible light. The DNA gel shift assay, selective precipitation and ESI-mass spectrometry studies suggest that Ru,Rh bimetallic complexes photolabilize chlorides[139] and photobind to DNA following visible light excitation. This reactivity is not seen for analogous Ru,Rh,Ru trimetallics due to the steric protection of the Rh site in that motif. The bimetallic $[(TL)_2Ru(dpp)RhCl_2(TL')]^{3+}$ systems have Ru (dπ) based HOMOs and Rh (dσ*) based LUMOs, and can photobind and photocleave DNA through low-lying ^{3}MMCT excited state when excited by the low energy visible light, with or without molecular oxygen. The efficiency of DNA photocleavage by the bimetallic complexes $[(TL)_2Ru(dpp)RhCl_2(TL')]^{3+}$ is significantly enhanced by substituting bpy with phen attached to the Rh center, and is decreased with Me_2bpy attached to the Rh center. The variation of terminal ligand on the Ru light absorbers does not have as much impact on the photoreactions of bimetallics with DNA as the variation of terminal ligand attached to the Rh center. The results are consistent with the fact that $[(TL)_2Ru(dpp)RhCl_2(TL')]^{3+}$ systems photobind and photocleave DNA through Rh center.[139] Coupling Os light absorber to the Rh center provides $[(bpy)_2Os(dpp)RhCl_2(phen)]^{3+}$, a new system that has unprecedented reactivity with DNA. This complex, $[(bpy)_2Os(dpp)RhCl_2(phen)]^{3+}$, photobinds and photocleaves DNA under the red therapeutic light excitation without the presence of molecular oxygen. The PCR results show that the DNA

photo-modification and photo-damage induced by $[(bpy)_2Os(dpp)RhCl_2(phen)]^{3+}$ under red light irradiation inhibit DNA amplification even at low 1:50 MC:BP loading of the complex.

4.2. Future Directions

The mixed-metal bimetallic complexes $[(TL)_2M(dpp)RhCl_2(TL')]^{3+}$ (M = Ru and Os, TL = phen, Ph_2phen, Me_2phen and bpy, TL′ = phen, bpy and Me_2bpy) were characterized and studied by electrochemistry, electronic absorption spectroscopy, ESI-mass spectrometry, steady-state and time-resolved emission spectroscopy, and DNA photolysis experiments and presented in this dissertation. However, several questions remain related to the photochemical functions of these bimetallic complexes. Future directions are aimed to understand the photochemical reactivities of structurally diverse bimetallic complexes.

The research presented in this dissertation answered many questions. It revealed that bimetallic complexes display interactions with DNA under visible light irradiation in the absence of molecular oxygen. The photochemical reaction process leading to DNA cleavage of bimetallic complexes $[(TL)_2Ru(dpp)RhCl_2(TL')]^{3+}$ (TL = phen, Ph_2phen, Me_2phen and bpy, TL′ = phen, bpy, Me_2bpy) with DNA could be the electrons from the Ru(II) center transferring through dpp to the Rh center under visible light irradiation, facilitating chloride ligand's loss and promoting Rh center binding to DNA, and abstracting hydrogen from DNA phosphate backbone through Rh center causes DNA cleavage. The variation of terminal ligand attached to the Rh center has significant impact on the interactions of bimetallic complexes with DNA. The efficiency of DNA photocleavage is significantly enhanced by substituting bpy with phen attached to the Rh center and decreased with Me_2bpy attached to the Rh center. We can further study the effect of the Rh center by substituting terminal ligands with other ligands such as Me_2phen, Ph_2phen, and

$^{t}Bu_2bpy$ and investigate the new bimetallic complexes' electrochemical, photophysical and photochemical properties and find out why the Rh center has such significant impact on DNA interactions. Furthermore, an attempt to understand the orbital energetics of the bimetallic complexes can be made by keeping the terminal ligands' structure and changing the bridging ligands.[15,152]

This dissertation also reveals that the $[(bpy)_2Os(dpp)RhCl_2(phen)]^{3+}$ complex photobinds and photocleaves DNA under red therapeutic light excitation without molecular oxygen. The PCR results show that the DNA photo-modification and photo-damage induced by $[(bpy)_2Os(dpp)RhCl_2(phen)]^{3+}$ under red light irradiation inhibit DNA amplification. Since the Ru bimetallic complex $[(Ph_2phen)_2Ru(dpp)RhCl_2(phen)]^{3+}$ displays enhanced electronic absorption properties, it will be useful to design and synthesize Os,Rh bimetallic complexes with $[(Ph_2phen)_2Os(dpp)]^{2+}$ light absorber for the photodynamic applications. Furthermore, the bimetallic complexes with ruthenium light absorbers display similar photochemical properties under the visible light excitation without molecular oxygen. We can use PCR experiments to evaluate the ruthenium bimetallic complexes DNA photo-modification effect and the stability of the metal complex-DNA adducts. However, PCR cannot provide the specificity of metal complexes DNA interactions. The DNA sequencing experiment will provide the information about both the frequency and specificity of metal complexes DNA interaction and help to answer the question of which part of DNA is photocleaved by the excited metal complexes. In addition, in order to fulfill the PDT applications, we can use other biological targets in addition to DNA. The study of bimetallic complex treated cell cultures will provide information about bimetallic complexes' dark toxicities and photo-toxicities. Attaching the flourescent tags to the component of the bimetallics will provide a way to observe the location of the complex in the cell via

confocal microscopy[153] and the result is useful to further design the complex to reach the nuclei in live cancer cells. The investigation of bimetallic complexes interaction with proteins[154,155] and RNAs[156,157] will lead to the design and synthesis of multifunctional bimetallic complexes,[158] which is important for the application of photochemotherapy.

Finally, the future work in this PDT field will focus on how to target the photosensitizers specifically to cancer cells and protect normal cells. There are at least two ways to fulfill this goal. The first one is according to the specificity of the certain cell lines and makes the photosensitizers only accumulate in the cancer cells by modifying photosensitizers with selective targeting moieties such as the transporter-, antigen-, and receptor-based conjugate[159] or by modulating the hydrophobicity and hydrophilicity of photosensitizers by choosing suitable subunits in the photosensitizers.[160,161] Another possibility is to encapsulate photosensitizers in molecular carriers such as polymers and nanparticles to overcome the delivery limitation and release the photosensitizers when they reach the cell targets.[162,163,164]

References

(1) *The Nature of Cancer*; Cooper, G. M., Ed.; Jones and Bartlett: Boston, **1993**.

(2) *Cancer: The misguided cell*; Prescott, D. M.; Flexer, A. S., Ed.; SINAUER ASSOCIATES INC.: Massachusetts, 1986.

(3) Siegel, R.; Ward, E.; Brawley, O.; Jemal, A. "Cancer statistics, 2011" *CA: A Cancer Journal for Clinicians* **2011**, *61*, 212-236.

(4) Hanahan, D.; Weinberg, R. A. "The hallmarks of cancer" *Cell* **2000**, *100*, 57-70.

(5) Farber, E. "The multistep nature of cancer development" *Cancer Research* **1984**, *44*, 4217-4223.

(6) Beckmann, M. W.; Niederacher, D.; Schnürch, H.-G.; Gusterson, B. A.; Bender, H. G. "Multistep carcinogenesis of breast cancer and tumour heterogeneity" *Journal of Molecular Medicine* **1997**, *75*, 429-439.

(7) Columbano, A.; Rajalakshmi, S.; Sarma, D. S. R. "Requirement of cell proliferation for the initiation of liver carcinogenesis as assayed by three different procedures" *Cancer Research* **1981**, *41*, 2079-2083.

(8) Goth, R.; Rajewsky, M. F. "Persistence of O6-ethylguanine in rat-brain DNA: correlation with nervous system-specific carcinogenesis by ethylnitrosourea" *Proceedings of the National Academy of Sciences* **1974**, *71*, 639-643.

(9) Pegg, A. E. In *Advances in cancer research*; George, K., Sidney, W., Eds.; Academic Press, **1977**; Vol. Volume 25; pp 195-269.

(10) Upton, A. C. "The question of thresholds for radiation and chemical carcinogenesis" *Cancer Investigation* **1989**, *7*, 267-276.

(11) Cohen, S. M.; Ellwein, L. B. "Genetic errors, cell proliferation, and carcinogenesis" *Cancer Research* **1991**, *51*, 6493-6505.

(12) Klezovitch, O.; Chevillet, J.; Mirosevich, J.; Roberts, R. L.; Matusik, R. J.; Vasioukhin, V. "Hepsin promotes prostate cancer progression and metastasis" *Cancer Cell* **2004**, *6*, 185-195.

(13) Kang, Y.; Siegel, P. M.; Shu, W.; Drobnjak, M.; Kakonen, S. M.; Cordón-Cardo, C.; Guise, T. A.; Massagué, J. "A multigenic program mediating breast cancer metastasis to bone" *Cancer Cell* **2003**, *3*, 537-549.

(14) Gupta, G. P.; Massagué, J. "Cancer metastasis: building a framework" *Cell* **2006**, *127*, 679-695.

(15) Zigler, D. F.; Wang, J.; Brewer, K. J. "Ruthenium(II)-polyazine light absorbers bridged to reactive cis-dichlororhodium(III) centers in a bimetallic molecular architecture" *Inorganic Chemistry* **2008**, *47*, 11342-11350.

(16) Goodman, L. S.; Wintrobe, M. M.; Dameshek, W.; Goodman, M. J.; Gilman, A.; Mclennan, M. T. "Nitrogen mustard therapy use of methyl-bis(beta-chloroethyl)amine hydrochloride and tris(beta-chloroethyl)amine hydrochloride for Hodgkin's disease, lymphosarcoma, leukemia and certain allied and miscellaneous disorders " *Journal of American Medical Association* **1946**, *132*, 126-132.

(17) *Principles of Combination Chemotherapy*; Hellmann, K.; Carter, S. K., Eds.; McGraw-Hill, Inc.: New York, 1987.

(18) Bonadonna, G.; Valagussa, P.; Moliterni, A.; Zambetti, M.; Brambilla, C. "Adjuvant cyclophosphamide, methotrexate, and fluorouracil in node-positive breast cancer — the results of 20 years of follow-up" *New England Journal of Medicine* **1995**, *332*, 901-906.

(19) Ortega, J. A.; Douglass, E. C.; Feusner, J. H.; Reynolds, M.; Quinn, J. J.; Finegold, M. J.; Haas, J. E.; King, D. R.; Liu-Mares, W.; Sensel, M. G.; Krailo, M. D. "Randomized comparison of cisplatin/vincristine/fluorouracil and cisplatin/continuous infusion doxorubicin for treatment of pediatric hepatoblastoma: A report from the children's cancer group and the pediatric oncology group" *Journal of Clinical Oncology* **2000**, *18*, 2665-2675.

(20) Dalton, W. S.; Grogan, T. M.; Meltzer, P. S.; Scheper, R. J.; Durie, B. G.; Taylor, C. W.; Miller, T. P.; Salmon, S. E. "Drug-resistance in multiple myeloma and non-Hodgkin's lymphoma: detection of P-glycoprotein and potential circumvention by addition of verapamil to chemotherapy" *Journal of Clinical Oncology* **1989**, *7*, 415-424.

(21) Ackroyd, R.; Kelty, C.; Brown, N.; Reed, M. "The history of photodetection and photodynamic therapy¶" *Photochemistry and Photobiology* **2001**, *74*, 656-669.

(22) Celli, J. P.; Spring, B. Q.; Rizvi, I.; Evans, C. L.; Samkoe, K. S.; Verma, S.; Pogue, B. W.; Hasan, T. "Imaging and photodynamic therapy: mechanisms, monitoring, and 0ptimization" *Chemical Reviews* **2010**, *110*, 2795-2838.

(23) Henderson, B. W.; Dougherty, T. J. "How does photodynamic therapy work?" *Photochemistry and Photobiology* **1992**, *55*, 145-157.

(24) Allison, R. R.; Mota, H. C.; Sibata, C. H. "Clinical PD/PDT in north America: An historical review" *Photodiagnosis and Photodynamic Therapy* **2004**, *1*, 263-277.

(25) Lipson, R. L.; Baldes, E. J.; Olsen, A. M. "The use of a derivative of hematoporphyrin in tumor detection" *Journal of the National Cancer Institute* **1961**, *26*, 1-11.

(26) Schwartz, S. K.; Absolon, K.; Vermund, H. "Some relationships of porphyrins, X-rays, and tumors" *Univ. Minnesota Med. Bull.* **1955**, *27*, 7-13.

(27) Dougherty, T. J.; Grindey, G. B.; Fiel, R.; Weishaupt, K. R.; Boyle, D. G. "Photoradiation therapy. II. cure of animal tumors with hematoporphyrin and light" *Journal of the National Cancer Institute* **1975**, *55*, 115-121.

(28) Kelly, J. F.; Snell, M. E. "Hematoporphyrin derivative: a possible aid in the diagnosis and therapy of carcinoma of bladder" *Journal of Urology* **1976**, *115*, 150-151.

(29) Sibille, A.; Lambert, R.; Souquet, J.-C.; Sabben, G.; Descos, F. "Long-term survival after photodynamic therapy for esophageal cancer" *Gastroenterology* **1995**, *108*, 337-344.

(30) Alexiades-Armenakas, M. "Laser-mediated photodynamic therapy" *Clin. Dermatol* **2006**, *24*, 16-25.

(31) Lovell, J. F.; Liu, T. W. B.; Chen, J.; Zheng, G. "Activatable photosensitizers for imaging and therapy" *Chemical Reviews (Washington, DC, United States)* **2010**, *110*, 2839-2857.

(32) Allison, R.; Moghissi, K.; Downie, G.; Dixon, K. "Photodynamic therapy (PDT) for lung cancer" *Photodiagnosis and Photodynamic Therapy* **2011**, *8*, 231-239.

(33) Castano, A. P.; Demidova, T. N.; Hamblin, M. R. "Mechanisms in photodynamic therapy: part one—photosensitizers, photochemistry and cellular localization" *Photodiagnosis and Photodynamic Therapy* **2004**, *1*, 279-293.

(34) Dougherty, T. J.; Marcus, S. L. "Photodynamic therapy" *European Journal of Cancer* **1992**, *28*, 1734-1742.

(35) Mroz, P.; Yaroslavsky, A.; Kharkwal, G. B.; Hamblin, M. R. "Cell death Pathways in photodynamic therapy of cancer" *Cancers* **2011**, *3*, 2516-2539.

(36) Dequeant, M. Q.; Bradley, P. M.; Xu, G.-L.; Lutterman, D. A.; Turro, C.; Ren, T. "Dirhenium paddlewheel compounds supported by N,N‘-dialkylbenzamidinates:

synthesis, structures, and photophysical properties" *Inorganic Chemistry* **2004**, *43*, 7887-7892.
(37) *Biomolecules, mechanisms of enzyme action, and metabolism*; Voet, D.; Voet, J. G., Eds.; John Wiley & Sons, Inc, 2003.
(38) Várnai, P.; Zakrzewska, K. "DNA and its counterions: a molecular dynamics study" *Nucleic Acids Research* **2004**, *32*, 4269-4280.
(39) *Molecular biology of cancer: Mechanisms, Targets, and Therapeutics*; 2nd ed.; Pecorino, L., Ed.; Oxford University Press Inc.,: New York, 2008.
(40) Kirsch-De Mesmaeker, A.; Lecomte, J.-P.; Kelly, J. M. "Photoreactions of metal complexes with DNA, especially those involving a primary photo-electron transfer;" *Top. Curr. Chem.* **1996**, *177*, 25-76.
(41) Boerner, L. J. K.; Zaleski, J. M. "Metal complex–DNA interactions: from transcription inhibition to photoactivated cleavage" *Current Opinion in Chemical Biology* **2005**, *9*, 135-144.
(42) Caradonna, J. P.; Lippard, S. J.; Gait, M. J.; Singh, M. "The antitumor drug *cis*-dichlorodiammineplatinum forms an intrastrand d(GpG) crosslink upon reaction with $[d(ApGpGpCpCpT)]_2$" *Journal of the American Chemical Society* **1982**, *104*, 5793-5795.
(43) Girault, J. P.; Chottard, G.; Lallemand, J. Y.; Chottard, J. C. "Interaction of *cis*-$[Pt(NH_3)_2(H_2O)_2](NO_3)_2$ with ribose and deoxyribose diguanosine phosphates" *Biochemistry* **1982**, *21*, 1352-1356.
(44) Smith, J. A.; Collins, J. G.; Keene, F. R. In *Metal Complex–DNA Interactions*; John Wiley & Sons, Ltd, **2009**; pp 317-346.
(45) Nafisi, S.; Saboury, A. A.; Keramat, N.; Neault, J.-F.; Tajmir-Riahi, H.-A. "Stability and structural features of DNA intercalation with ethidium bromide, acridine orange and methylene blue" *Journal of Molecular Structure* **2007**, *827*, 35-43.
(46) Szaciłowski, K.; Macyk, W.; Drzewiecka-Matuszek, A.; Brindell, M.; Stochel, G. "Bioinorganic photochemistry: frontiers and mechanisms" *Chemical Reviews* **2005**, *105*, 2647-2694.
(47) Stochel, G.; Wanat, A.; Kulis, E.; Stasicka, Z. "Light and metal complexes in medicine" *Coordination Chemistry Reviews* **1998**, *171*, 203-220.
(48) Huang, Z. "A review of progress in clinical photodynamic therapy" *Technology in Cancer Research& Treatment* **2005**, *4*, 283-294.
(49) Wyss, P.; Schwarz, V.; Dobler-Girdziunaite, D.; Hornung, R.; Walt, H.; Degen, A.; Fehr, M. "Photodynamic therapy of locoregional breast cancer recurrences using a chlorin-type photosensitizer" *International Journal of Cancer* **2001**, *93*, 720-724.
(50) Teiten, M. H.; Bezdetnaya, L.; Merlin, J. L.; Bour-Dill, C.; Pauly, M. E.; Dicato, M.; Guillemin, F. "Effect of meta-tetra(hydroxyphenyl)chlorin (mTHPC)-mediated photodynamic therapy on sensitive and multidrug-resistant human breast cancer cells" *Journal of Photochemistry and Photobiology B: Biology* **2001**, *62*, 146-152.
(51) Fan, K. F. M.; Hopper, C.; Speight, P. M.; Buonaccorsi, G. A.; Bown, S. G. "Photodynamic therapy using mTHPC for malignant disease in the oral cavity" *International Journal of Cancer* **1997**, *73*, 25-32.
(52) Detty, M. R.; Gibson, S. L.; Wagner, S. J. "Current clinical and preclinical photosensitizers for use in photodynamic therapy" *Journal of Medicinal Chemistry* **2004**, *47*, 3897-3915.

(53) Pandey, R. K.; Bellnier, D. A.; Smith, K. M.; Dougherty, T. J. "Chlorin and porphrin derivatives as potential photosensitizers in photodynamic therapy" *Photochemistry and Photobiology* **1991**, *53*, 65-72.
(54) Brasseur, N.; Ali, H.; Langlois, R.; Van Lier, J. E. "Biological activities of phthalocyanines-IX. photosensitization OFV–79 Chinese hamster cells ANDEMT–6 mouse mammary tumor by selectively sulfonated zinc phthalocyanines" *Photochemistry and Photobiology* **1988**, *47*, 705-711.
(55) Firey, P. A.; Rodgers, M. A. J. "Photo-properties of a silicon naphthalocyanine: A potential photosensitizer for photodynamic therapy *" *Photochemistry and Photobiology* **1987**, *45*, 535-538.
(56) Ali, H.; van Lier, J. E. "Metal complexes as photo- and radiosensitizers" *Chemical Reviews* **1999**, *99*, 2379-2450.
(57) Nyman, E. S.; Hynninen, P. H. "Research advances in the use of tetrapyrrolic photosensitizers for photodynamic therapy" *Journal of Photochemistry and Photobiology B: Biology* **2004**, *73*, 1-28.
(58) Lin, C. T.; Boettcher, W.; Chou, M.; Creutz, C.; Sutin, N. "Mechanism of the quenching of the emission of substituted polypyridineruthenium(II) complexes by iron(III), chromium(III), and europium(III) ions" *Journal of the American Chemical Society* **1976**, *98*, 6536-6544.
(59) Demas, J. N.; Diemente, D.; Harris, E. W. "Oxygen quenching of charge-transfer excited states of ruthenium(II) complexes. Evidence for singlet oxygen production" *Journal of the American Chemical Society* **1973**, *95*, 6864-6865.
(60) Durham, B.; Caspar, J. V.; Nagle, J. K.; Meyer, T. J. "Photochemistry of tris(2,2'-bipyridine)ruthenium(2+) ion" *Journal of the American Chemical Society* **1982**, *104*, 4803-4810.
(61) Harris, A. L. "Hypoxia a key regulatory factor in tumour growth" *Nat Rev Cancer* **2002**, *2*, 38-47.
(62) Bradley, P. M.; Angeles-Boza, A. M.; Dunbar, K. R.; Turro, C. "Direct DNA photocleavage by a new intercalating dirhodium(II/II) complex: Comparison to $Rh_2(\mu\text{-}O_2CCH_3)_4$" *Inorganic Chemistry* **2004**, *43*, 2450-2452.
(63) Fu, P. K. L.; Bradley, P. M.; Turro, C. "DNA cleavage by photogenerated $Rh_2(O_2CCH_3)_4(H_2O)^{2+}$" *Inorganic Chemistry* **2001**, *40*, 2476-2477.
(64) Angeles-Boza, A. M.; Bradley, P. M.; Fu, P. K. L.; Wicke, S. E.; Bacsa, J.; Dunbar, K. R.; Turro, C. "DNA binding and photocleavage in vitro by new dirhodium(II) dppz complexes: Correlation to cytotoxicity and photocytotoxicity" *Inorganic Chemistry* **2004**, *43*, 8510-8519.
(65) Angeles-Boza, A. M.; Bradley, P. M.; Fu, P. K. L.; Shatruk, M.; Hilfiger, M. G.; Dunbar, K. R.; Turro, C. "Photocytotoxicity of a new Rh_2(II,II) complex: Increase in cytotoxicity upon irradiation similar to that of PDT agent hematoporphyrin" *Inorganic Chemistry* **2005**, *44*, 7262-7264.
(66) *Supramolecular Photochemistry*; Balzani, V.; Moggi, L.; Scandola, F., Eds.: Reidel, Dordrecht, **1987**, pp 1.
(67) Juris, A.; Balzani, V.; Barigelletti, F.; Campagna, S.; Belser, P.; von Zelewsky, A. "Ru(II) polypyridine complexes: photophysics, photochemistry, eletrochemistry, and chemiluminescence" *Coordination Chemistry Reviews* **1988**, *84*, 85-277.

(68) Holder, A. A.; Swavey, S.; Brewer, K. J. "Design aspects for the development of mixed-metal supramolecular complexes capable of visible light induced photocleavage of DNA" *Inorganic Chemistry* **2004**, *43*, 303-308.
(69) Holder, A. A.; Zigler, D. F.; Tarrago-Trani, M. T.; Storrie, B.; Brewer, K. J. "Photobiological impact of $[\{(bpy)_2Ru(dpp)\}_2RhCl_2]Cl_5$ and $[\{(bpy)_2Os(dpp)\}_2RhCl_2]Cl_5$ [bpy = 2,2′-Bipyridine; dpp = 2,3-Bis(2-pyridyl)pyrazine] on Vero cells" *Inorganic Chemistry* **2007**, *46*, 4760-4762.
(70) Molnar, S. M.; Jensen, G. E.; Vogler, L. M.; Jones, S. W.; Laverman, L.; Bridgewater, J. S.; Richter, M. M.; Brewer, K. J. "Photochemical properties of mixed-metal supramolecular complexes" *Journal of Photochemistry and Photobiology A: Chemistry* **1994**, *80*, 315-322.
(71) Swavey, S.; Brewer, K. J. "Synthesis and study of Ru,Rh,Ru triads: Modulation of orbital energies in a supramolecular architecture" *Inorganic Chemistry* **2002**, *41*, 4044-4050.
(72) Swavey, S.; Brewer, K. J. "Visible light induced photocleavage of DNA by a mixed-metal supramolecular complex: $[\{(bpy)_2Ru(dpp)\}_2RhCl_2]^{5+}$" *Inorganic Chemistry* **2002**, *41*, 6196-6198.
(73) Elvington, M.; Brewer, K. J. "Photoinitiated electron collection at a metal in a rhodium-centered mixed-metal supramolecular complex" *Inorganic Chemistry* **2006**, *45*, 5242-5244.
(74) Allen J. Bard; Faulkner, L. R. "Electrochemical methods: fundamentals and applications." 2nd ed.; John Wiley & Sons: New York, 2000.
(75) Kissinger, P. T.; Heineman, W. R. "Cyclic voltammetry" *Journal of Chemical Education* **1983**, *60*, 702.
(76) Kissinger, P. T.; Helneman, W. H. "Laboratory techniques in electroanalytical chemistry" 2 ed.; Marcel Dekker: New York, 1996.
(77) Harris, D. C. "Quantitative chemical analysis" 8 ed.; W. H. Freeman and Company: New York, 2010.
(78) Fuchs, Y.; Lofters, S.; Dieter, T.; Shi, W.; Morgan, R.; Strekas, T. C.; Gafney, H. D.; Baker, A. D. "Spectroscopic and electrochemical properties of dimeric Ruthenium(II) diimine complexes and determination of their excited state redox properties" *Journal of the American Chemical Society* **1987**, *109*, 2691-2697.
(79) Brewer, K. J.; Murphy, W. R.; Spurlin, S. R.; Petersen, J. D. "The next generation of (polyazine)ruthenium(II) complexes" *Inorganic Chemistry* **1986**, *25*, 882-884.
(80) Wallace, A. W.; Rorer Murphy Jr, W.; Petersen, J. D. "Electrochemical and photophysical properties of mono- and bimetallic ruthenium(II) complexes" *Inorganica Chimica Acta* **1989**, *166*, 47-54.
(81) White, T. A.; Rangan, K.; Brewer, K. J. "Synthesis, characterization, and study of the photophysics and photocatalytic properties of the photoinitiated electron collector $[\{(phen)_2Ru(dpp)\}_2RhBr_2](PF_6)_5$" *Journal of Photochemistry and Photobiology A: Chemistry* **2010**, *209*, 203-209.
(82) Mongelli, M. T.; Brewer, K. J. "Synthesis and study of the light absorbing, redox and photophysical properties of Ru(II) and Os(II) complexes of 4,7-diphenyl-1,10-phenanthroline containing the polyazine bridging ligand 2,3-bis(2-pyridyl)pyrazine" *Inorganic Chemistry Communications* **2006**, *9*, 877-881.
(83) Braunstein, C. H.; Baker, A. D.; Strekas, T. C.; Gafney, H. D. "Spectroscopic and electrochemical properties of the dimer tetrakis(2,2'-bipyridine)(2,3-bis(2-

pyridyl)pyrazine)diruthenium(II) and its monomeric analog" *Inorganic Chemistry* **1984**, *23*, 857-864.
(84) Murphy, W. R.; Brewer, K. J.; Gettliffe, G.; Petersen, J. D. "Luminescent tetrametallic complexes of ruthenium" *Inorganic Chemistry* **1989**, *28*, 81-84.
(85) Richter, M. M.; Brewer, K. J. "Synthesis and characterization of osmium(II) complexes incorporating polypyridyl bridging ligands" *Inorganica Chimica Acta* **1991**, *180*, 125-131.
(86) Kober, E. M.; Caspar, J. V.; Sullivan, B. P.; Meyer, T. J. "Synthetic routes to new polypyridyl complexes of osmium(II)" *Inorganic Chemistry* **1988**, *27*, 4587-4598.
(87) Kew, G.; DeArmond, K.; Hanck, K. "Electrochemistry of rhodium-dipyridyl complexes" *The Journal of Physical Chemistry* **1974**, *78*, 727-734.
(88) Kew, G.; Hanck, K.; DeArmond, K. "Voltammetry of rhodium-1,10-phenanthroline complexes" *The Journal of Physical Chemistry* **1975**, *79*, 1828-1835.
(89) Nicholson, R. S. "Semiempirical procedure for measuring with stationary electrode polarography rates of chemical reactions involving the product of electron transfer" *Analytical Chemistry* **1966**, *38*, 1406-1406.
(90) Nicholson, R. S.; Shain, I. "Theory of stationary electrode polarography. single scan and cyclic methods applied to reversible, irreversible, and kinetic systems" *Analytical Chemistry* **1964**, *36*, 706-723.
(91) Rasmussen, S. C.; Richter, M. M.; Yi, E.; Place, H.; Brewer, K. J. "Synthesis and characterization of a series of novel rhodium and iridium complexes containing polypyridyl bridging ligands: potential uses in the development of multimetal catalysts for carbon dioxide reduction" *Inorganic Chemistry* **1990**, *29*, 3926-3932.
(92) Kalyanasundaram, K.; Graetzel, M.; Nazeeruddin, M. K. "Excited-state interactions in ligand-bridged chromophore-quencher complexes containing rhodium(III) and ruthenium(II) polypyridyl units" *The Journal of Physical Chemistry* **1992**, *96*, 5865-5872.
(93) *Physical Chemistry*; Atkins, P.; de Paula, J., Eds.; W. H. Freeman & Co.: New Year, **2002**, pp 540-578, 686-718.
(94) *Metal Complex-DNA Interactions*; Hadjiliadis, N.; Sletten, E., Eds.; John Wiley & Sons: West Sussex, United Kingdom, 2009.
(95) Kalyanasundaram, K.; Nazeeruddin, M. K. "Photophysics and photoredox reactions of ligand-bridged binuclear polypyridyl complexes of ruthenium(II) and of their monomeric analogs" *Inorganic Chemistry* **1990**, *29*, 1888-1897.
(96) Mongelli, M. T.; Heinecke, J.; Mayfield, S.; Okyere, B.; Winkel, B. S. J.; Brewer, K. J. "Variation of DNA photocleavage efficiency for $[(TL)_2Ru(dpp)]Cl_2$ complexes where TL = 2,2′-bipyridine, 1,10-phenanthroline, or 4,7-diphenyl-1,10-phenanthroline" *Journal of Inorganic Biochemistry* **2006**, *100*, 1983-1987.
(97) Rillema, D. P.; Mack, K. B. "The low-lying excited state in ligand .pi.-donor complexes of ruthenium(II): mononuclear and binuclear species" *Inorganic Chemistry* **1982**, *21*, 3849-3854.
(98) Rillema, D. P.; Taghdiri, D. G.; Jones, D. S.; Worl, L. A.; Meyer, T. J.; Levy, H. A.; Keller, C. D. "Structure and redox and photophysical properties of a series of ruthenium heterocycles based on the ligand 2,3-bis(2-pyridyl)quinoxaline" *Inorganic Chemistry* **1987**, *26*, 578-585.
(99) Higgins, S. L. H.; White, T. A.; Winkel, B. S. J.; Brewer, K. J. "Redox, spectroscopic, and photophysical properties of Ru−Pt mixed-metal complexes incorporating 4,7-

diphenyl-1,10-phenanthroline as efficient DNA binding and photocleaving agents" *Inorganic Chemistry* **2011**, *50*, 463-470.
(100) Kalyanasundaram, K.; Nazeeruddin, M. K. "Photophysical and redox properties of mono- and bi-nuclear complexes of osmium(II) with 2,3-bis(2-pyridyl)pyrazine as bridging ligand" *Chemical Physics Letters* **1989**, *158*, 45-50.
(101) Armitage, B. "Photocleavage of nucleic acids" *Chemical Reviews* **1998**, *98*, 1171-1200.
(102) DeRosa, M. C.; Crutchley, R. J. "Photosensitized singlet oxygen and its applications" *Coordination Chemistry Reviews* **2002**, *233–234*, 351-371.
(103) Abdel-Shafi, A. A.; Worrall, D. R.; Ershov, A. Y. "Photosensitized generation of singlet oxygen from ruthenium(ii) and osmium(ii) bipyridyl complexes" *Dalton Transactions* **2004**, 30-36.
(104) Nishizawa, M.; Suzuki, T. M.; Sprouse, S.; Watts, R. J.; Ford, P. C. "Ligand steric effects on the photophysics of bis- and tris(2,2'-bipyridine) complexes of rhodium(III)" *Inorganic Chemistry* **1984**, *23*, 1837-1841.
(105) DeArmond, M. K.; Hillis, J. E. "Luminescence of transition metal d6 Chelates" *The Journal of Chemical Physics* **1971**, *54*, 2247-2253.
(106) Muir, M. M.; Huang, W.-L. "Photoaquation of some complexes of rhodium(III)" *Inorganic Chemistry* **1973**, *12*, 1831-1835.
(107) Mahnken, R. E.; Billadeau, M. A.; Nikonowicz, E. P.; Morrison, H. "Toward the development of photo cis-platinum reagents. Reaction of cis-dichlorobis(1,10-phenanthroline)rhodium(III) with calf thymus DNA, nucleotides and nucleosides" *Journal of the American Chemical Society* **1992**, *114*, 9253-9265.
(108) Menon, E. L.; Perera, R.; Navarro, M.; Kuhn, R. J.; Morrison, H. "Phototoxicity against tumor cells and Sindbis Virus by an octahedral rhodium bisbipyridyl complex and evidence for the genome as a target in viral photoinactivation" *Inorganic Chemistry* **2004**, *43*, 5373-5381.
(109) Billadeau, M. A.; Wood, K. V.; Morrison, H. "Reductive photochemistry of cis-dichlorobis(1,10-phenanthroline)rhodium(III) chloride" *Inorganic Chemistry* **1994**, *33*, 5780-5784.
(110) Harmon, H. L.; Morrison, H. "Anaerobic photoinduced N7-binding of cis-dichlorobis(1,10-phenanthroline)rhodium(III) chloride to 2'-deoxyguanosine: A one-electron-transfer chain process" *Inorganic Chemistry* **1995**, *34*, 4937-4938.
(111) Curtis, J. C.; Bernstein, J. S.; Meyer, T. J. "Directed, intramolecular electron transfer in mixed-valence dimers" *Inorganic Chemistry* **1985**, *24*, 385-397.
(112) White, T. A.; Arachchige, S. M.; Sedai, B.; Brewer, K. J. "Emission spectroscopy as a probe into photoinduced intramolecular electron transfer in polyazine bridged Ru(II), Rh(III) supramolecular complexe" *Materials* **2010**, *3*, 4328-4354
(113) Vinograd, J.; Lebowitz', J. "Physical and Topological Properties of Circular DNA" *J. Gen. Physiol.* **1966**, *49*, 103-125.
(114) Sullivan, B. P.; Salmon, D. J.; Meyer, T. J. "Mixed phosphine 2,2'-bipyridine complexes of ruthenium" *Inorganic Chemistry* **1978**, *17*, 3334-3341.
(115) McKenzie, E. D.; Plowman, R. A. "Rhodium(III) compounds with 1,10-phenanthroline and 2,2'-bipyridyl" *J. Inorg. Nucl. Chem.* **1970**, *32*, 199-212.
(116) Bieda, R.; Ott, I.; Dobroschke, M.; Prokop, A.; Gust, R.; Sheldrick, W. S. "Structure–activity relationships and DNA binding properties of apoptosis inducing cytotoxic

rhodium(III) polypyridyl complexes containing the cyclic thioether [9]aneS3" *Journal of Inorganic Biochemistry* **2009**, *103*, 698-708.

(117) Bieda, R.; Ott, I.; Gust, R.; Sheldrick, W. S. "Cytotoxic rhodium(III) polypyridyl complexes containing the tris(pyrazolyl)methane coligand: synthesis, DNA binding properties and structure–activity relationships" *European Journal of Inorganic Chemistry* **2009**, *2009*, 3821-3831.

(118) Wang, J.; White, T. A.; Arachchige, S. M.; Brewer, K. J. "A new structural motif for photoinitiated electron collection: Ru,Rh bimetallics providing insight into H_2 production via photocatalysis of water reduction by Ru,Rh,Ru supramolecules" *Chemical Communications (Cambridge, United Kingdom)* **2011**, *47*, 4451-4453.

(119) Wang, J.; Higgins, S. L. H.; Winkel, B. S. J.; Brewer, K. J. "A new Os,Rh bimetallic with O_2 independent DNA cleavage and DNA photobinding with red therapeutic light excitation" *Chemical Communications (Cambridge, United Kingdom)* **2011**, *47*, 9786-9788.

(120) Arachchige, S. M.; Brown, J. R.; Chang, E.; Jain, A.; Zigler, D. F.; Rangan, K.; Brewer, K. J. "Design considerations for a system for photocatalytic hydrogen production from water employing mixed-metal photochemical molecular devices for photoinitiated electron collection" *Inorganic Chemistry* **2009**, *48*, 1989-2000.

(121) *Electrochemical methods: fundamentals and applications* 2nd ed.; Allen J. Bard; Faulkner, L. R., Eds.; John Wiley & Sons, Inc,: New York, **2001**.

(122) Gennett, T.; Milner, D. F.; Weaver, M. J. "Role of solvent reorganization dynamics in electron-transfer processes. Theory-experiment comparisons for electrochemical and homogeneous electron exchange involving metallocene redox couples" *The Journal of Physical Chemistry* **1985**, *89*, 2787-2794.

(123) Caspar, J. V.; Kober, E. M.; Sullivan, B. P.; Meyer, T. J. "Application of the energy gap law to the decay of charge-transfer excited states" *Journal of the American Chemical Society* **1982**, *104*, 630-632.

(124) Prussin Ii, A. J.; Zigler, D. F.; Jain, A.; Brown, J. R.; Winkel, B. S. J.; Brewer, K. J. "Photochemical methods to assay DNA photocleavage using supercoiled pUC18 DNA and LED or xenon arc lamp excitation" *Journal of Inorganic Biochemistry* **2008**, *102*, 731-739.

(125) Williams, R. L.; Toft, H. N.; Winkel, B.; Brewer, K. J. "Synthesis, characterization, and DNA binding Properties of a series of Ru, Pt mixed-metal complexes" *Inorganic Chemistry* **2003**, *42*, 4394-4400.

(126) Broomhead, J. A.; Grumley, W. "Iridium(III) and rhodium(III) mono-and bis(1,10-phenanthroline) complexes and the optical isomers of iridium(III), rhodium(III), chromium(III), and cobalt(III) dihalobis(1-10-phenanthroline) complex cations" *Inorganic Chemistry* **1971**, *10*, 2002-2009.

(127) Smieja, J. M.; Kubiak, C. P. "Re(bipy-tBu)$(CO)_3$Cl−improved catalytic activity for reduction of carbon dioxide: IR-spectroelectrochemical and mechanistic studies" *Inorganic Chemistry* **2010**, *49*, 9283-9289.

(128) Arachchige, S. M.; Brown, J.; Brewer, K. J. "Photochemical hydrogen production from water using the new photocatalyst $[\{(bpy)_2Ru(dpp)\}_2RhBr_2](PF_6)^5$" *Journal of Photochemistry and Photobiology A: Chemistry* **2008**, *197*, 13-17.

(129) Herman, A.; Tanski, J. M.; Tibbetts, M. F.; Anderson, C. M. "Synthesis, characterization, and in vitro evaluation of a potentially selective anticancer, mixed-metal

[Ruthenium(III)−Platinum(II)] trinuclear complex" *Inorganic Chemistry* **2007**, *47*, 274-280.
(130) Still, B. M.; Kumar, P. G. A.; Aldrich-Wright, J. R.; Price, W. S. "195Pt NMR-theory and application" *Chemical Society Reviews* **2007**, *36*, 665-686.
(131) Crosby, G. A. "Spectroscopic investigations of excited states of transition-metal complexes" *Accounts of Chemical Research* **1975**, *8*, 231-238.
(132) Treadway, J. A.; Loeb, B.; Lopez, R.; Anderson, P. A.; Keene, F. R.; Meyer, T. J. "Effect of delocalization and rigidity in the acceptor ligand on MLCT excited-state decay" *Inorganic Chemistry* **1996**, *35*, 2242-2246.
(133) Marcus, R. A.; Sutin, N. "Electron transfers in chemistry and biology" *Biochimica et Biophysica Acta (BBA) - Reviews on Bioenergetics* **1985**, *811*, 265-322.
(134) Marcus, R. A. "Chemical and electrochemical electron-transfer theory" *Annual Review of Physical Chemistry* **1964**, *15*, 155-196.
(135) Indelli, M. T.; Bignozzi, C. A.; Harriman, A.; Schoonover, J. R.; Scandola, F. "Four intercomponent processes in a Ru(II)-Rh(III) polypyridine dyad: Electron transfer from excited donor, electron transfer to excited acceptor, charge recombination, and electronic energy transfer" *Journal of the American Chemical Society* **1994**, *116*, 3768-3779.
(136) Indelli, M. T.; Chiorboli, C.; Scandola, F. "Photochemistry and photophysics of coordination compound: Rhodium" *Top Curr. Chem.* **2007**, *280*, 215-255.
(137) Keck, M. V.; Lippard, S. J. "Unwinding of supercoiled DNA by platinum-ethidium and related complexes" *Journal of the American Chemical Society* **1992**, *114*, 3386-3390.
(138) Barton, J. K.; Lolis, E. "Chiral discrimination in the covalent binding of bis(phenanthroline)dichlororuthenium(II) to B-DNA" *Journal of the American Chemical Society* **1985**, *107*, 708-709.
(139) Wang, J.; Zigler, D. F.; Hurst, N.; Othee, H.; Winkel, B. S. J.; Brewer, K. J. "A new, bioactive structural motif: Visible light induced DNA photobinding and oxygen independent photocleaveage by Ru^{II},Rh^{II} bimetallics" *J. Inorg. Biochem.* **2012**, *116*,135-139.
(140) Miao, R.; Mongelli, M. T.; Zigler, D. F.; Winkel, B. S. J.; Brewer, K. J. "A multifunctional tetrametallic Ru−Pt supramolecular complex exhibiting both DNA binding and photocleavage" *Inorganic Chemistry* **2006**, *45*, 10413-10415.
(141) Kleppe, K.; Ohtsuka, E.; Kleppe, R.; Molineux, I.; Khorana, H. G. "Studies on polynucleotides: XCVI. Repair replication of short synthetic DNA's as catalyzed by DNA polymerases" *Journal of Molecular Biology* **1971**, *56*, 341-361.
(142) Saiki, R.; Scharf, S.; Faloona, F.; Mullis, K.; Horn, G.; Erlich, H.; Arnheim, N. "Enzymatic amplification of beta-globin genomic sequences and restriction site analysis for diagnosis of sickle cell anemia" *Science* **1985**, *230*, 1350-1354.
(143) Saiki, R.; Gelfand, D.; Stoffel, S.; Scharf, S.; Higuchi, R.; Horn, G.; Mullis, K.; Erlich, H. "Primer-directed enzymatic amplification of DNA with a thermostable DNA polymerase" *Science* **1988**, *239*, 487-491.
(144) Baumforth, K. R. N.; Nelson, P. N.; Digby, J. E.; O'Neil, J. D.; Murray, P. G. "Demystified... The polymerase chain reaction" **1999**, *52*, 1-10.
(145) *In real time PCR: Current technology and applications* Logan, J., Edwards, K., Saunders, N., Eds.; Caister Academic Press: Norfolk, UK, **2009**.

(146) McMahon, G.; Davis, E.; Wogan, G. N. "Characterization of c-Ki-ras oncogene alleles by direct sequencing of enzymatically amplified DNA from carcinogen-induced tumors" *Proceedings of the National Academy of Sciences* **1987**, *84*, 4974-4978.
(147) Pinto, A. L.; Lippard, S. J. "Sequence-dependent termination of in vitro DNA synthesis by cis- and trans-diamminedichloroplatinum (II)" *Proceedings of the National Academy of Sciences* **1985**, *82*, 4616-4619.
(148) Jennerwein, M. M.; Eastman, A. "A polymerase chain reaction-based method to detect cisplatin adducts in specific genes" *Nucleic Acids Research* **1991**, *19*, 6209-6214.
(149) Bingham, J. P.; Hartley, J. A.; Souhami, R. L.; Grimaldi, K. A. "Strand-specific measurement of cisplatin-induced DNA damage and repair using quantitative PCR" *Nucleic Acids Research* **1996**, *24*, 987-989.
(150) Kalinowski, D. P.; Illenye, S.; Van Houten, B. "Analysis of DNA damage and repair in murine leukemia L1210 cells using a quantitative polymerase chain reaction assay" *Nucleic Acids Research* **1992**, *20*, 3485-3494.
(151) Rahman, M. M.; Yasuda, H.; Katsura, S.; Mizuno, A. "Inhibition of endonuclease cleavage and DNA replication of E. coli plasmid by the antitumor rhodium(II) complex" *Archives of Biochemistry and Biophysics* **2007**, *464*, 28-35.
(152) Balzani, V.; Juris, A.; Venturi, M.; Campagna, S.; Serroni, S. "Luminescent and redox-active polynuclear transition metal complexes†" *Chemical Reviews* **1996**, *96*, 759-834.
(153) Basu, U.; Khan, I.; Hussain, A.; Kondaiah, P.; Chakravarty, A. R. "Photodynamic effect in near-IR light by a photocytotoxic iron(III) cellular imaging agent" *Angewandte Chemie International Edition* **2012**, *51*, 2658-2661.
(154) Bocarsly, J. R.; Barton, J. K. "Protein surface recognition and covalent binding by chromium nitrilotriacetate complexes: elucidation using NMR and CD spectroscopies" *Inorganic Chemistry* **1992**, *31*, 2827-2834.
(155) Fazal, M. A.; Roy, B. C.; Sun, S.; Mallik, S.; Rodgers, K. R. "Surface recognition of a protein using designed transition metal complexes" *Journal of the American Chemical Society* **2001**, *123*, 6283-6290.
(156) Chen, C.-A.; Cowan, J. A. "In vivo cleavage of a target RNA by copper kanamycin A. Direct observation by a fluorescence assay" *Chemical Communications* **2002**, 196-197.
(157) Iranzo, O.; Kovalevsky, A. Y.; Morrow, J. R.; Richard, J. P. "Physical and kinetic analysis of the cooperative role of metal ions in catalysis of phosphodiester cleavage by a dinuclear Zn(II) complex" *Journal of the American Chemical Society* **2003**, *125*, 1988-1993.
(158) Morrow, J. R.; Iranzo, O. "Synthetic metallonucleases for RNA cleavage" *Current Opinion in Chemical Biology* **2004**, *8*, 192-200.
(159) Dancey, J. E.; Chen, H. X. "Strategies for optimizing combinations of molecularly targeted anticancer agents" *Nat Rev Drug Discov* **2006**, *5*, 649-659.
(160) Park, E. K.; Lee, S. B.; Lee, Y. M. "Preparation and characterization of methoxy poly(ethylene glycol)/poly(ε-caprolactone) amphiphilic block copolymeric nanospheres for tumor-specific folate-mediated targeting of anticancer drugs" *Biomaterials* **2005**, *26*, 1053-1061.
(161) Bonnett, R. "Photosensitizers of the porphyrin and phthalocyanine series for photodynamic therapy" *Chemical Society Reviews* **1995**, *24*, 19-33.

(162) Kojima, C.; Kono, K.; Maruyama, K.; Takagishi, T. "Synthesis of polyamidoamine dendrimers having poly(ethylene glycol) grafts and their ability to encapsulate anticancer drugs" *Bioconjugate Chemistry* **2000**, *11*, 910-917.
(163) Fabbro, C.; Ali-Boucetta, H.; Ros, T. D.; Kostarelos, K.; Bianco, A.; Prato, M. "Targeting carbon nanotubes against cancer" *Chemical Communications* **2012**, *48*, 3911-3926.
(164) Sun, C.; Lee, J. S. H.; Zhang, M. "Magnetic nanoparticles in MR imaging and drug delivery" *Advanced Drug Delivery Reviews* **2008**, *60*, 1252-1265.
(165) White, T.; Arachchige, S.; Sedai, B.; Brewer, K. "Emission spectroscopy as a probe into photoinduced intramolecular electron transfer in polyazine bridged Ru(II),Rh(III) supramolecular Complexes" *Materials* **2010**, *3*, 4328-4354.
(166) Richter, M. M.; Brewer, K. J. "Osmium(II)/ruthenium(II) trimetallics incorporating polyazine bridging ligands: isovalent near-IR absorbers with unique electrochemical behavior" *Inorganic Chemistry* **1993**, *32*, 5762-5768.

Appendix Table of Contents

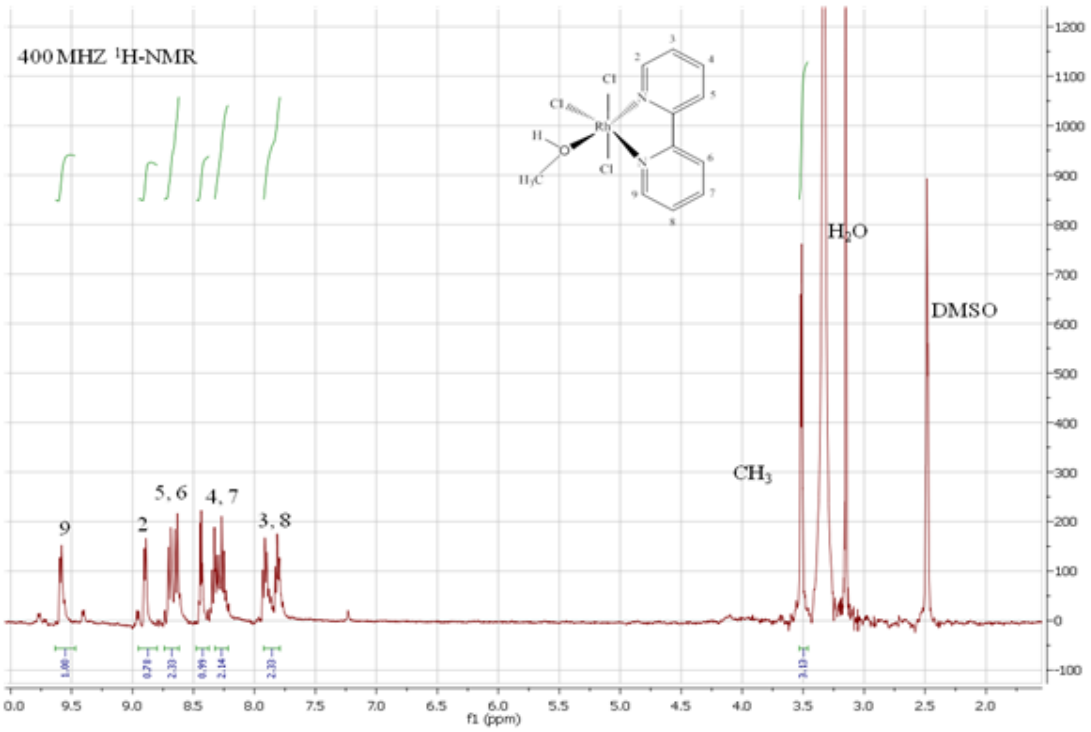

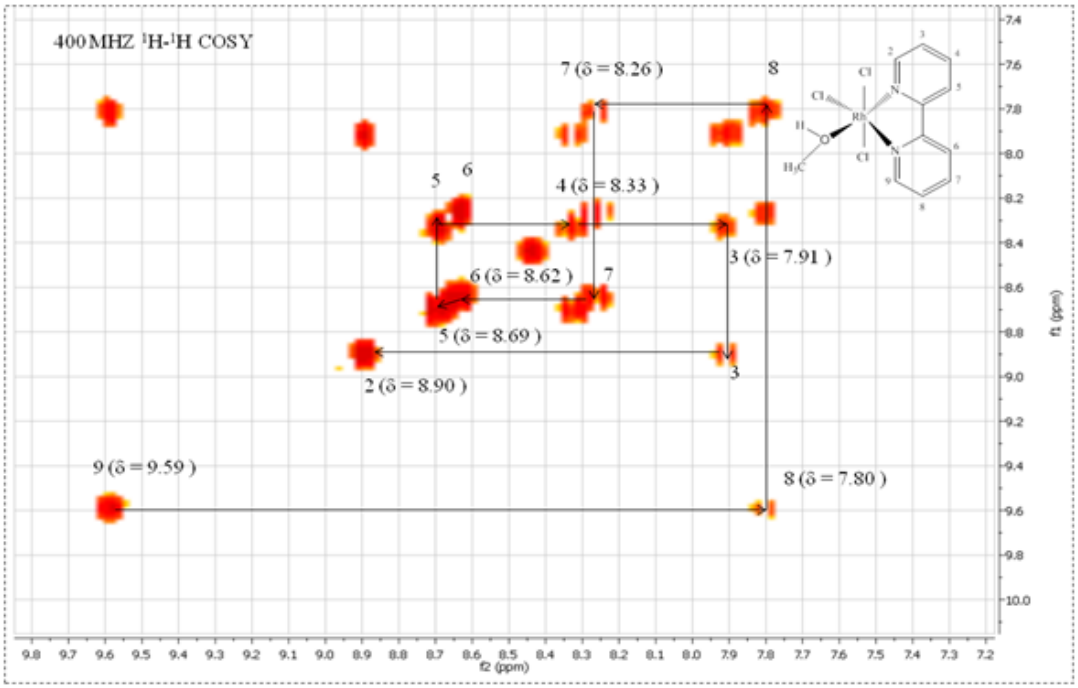

Appendix A. Proton and ^{1}H-^{1}H COSY NMR spectra of $[(bpy)RhCl_3(CH_3OH)] \cdot CH_3OH$ in DMSO-d_6 at 298 K, where bpy = 2,2′- bipyridine.

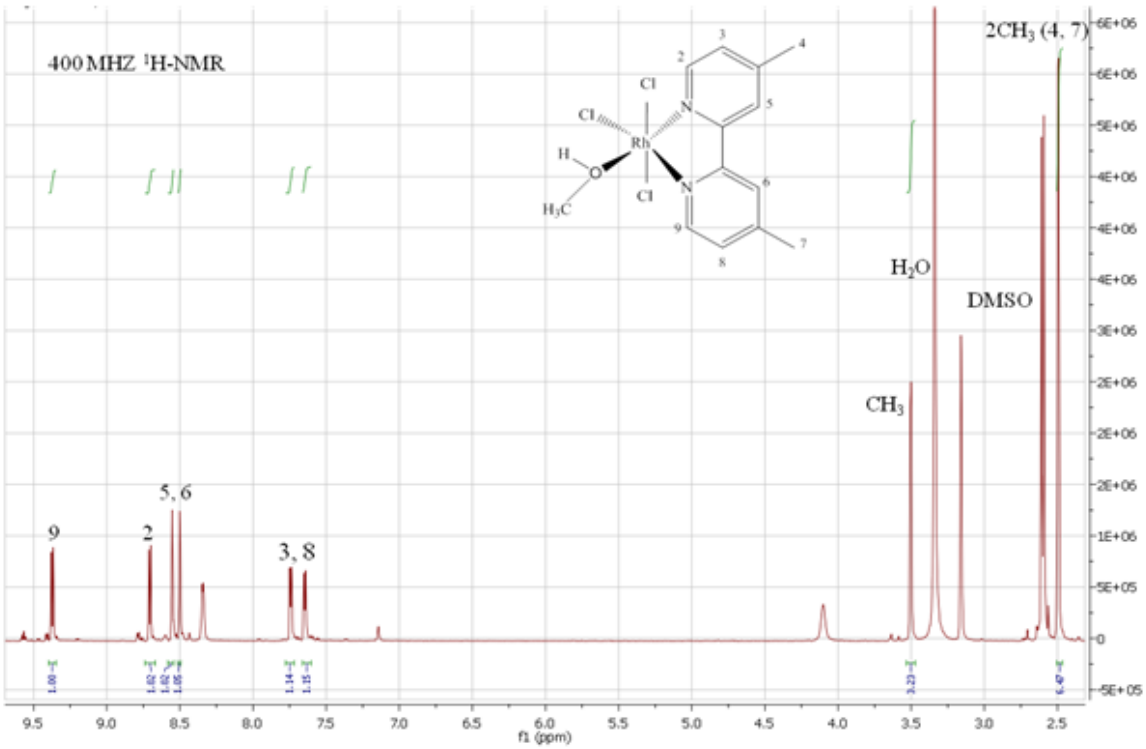

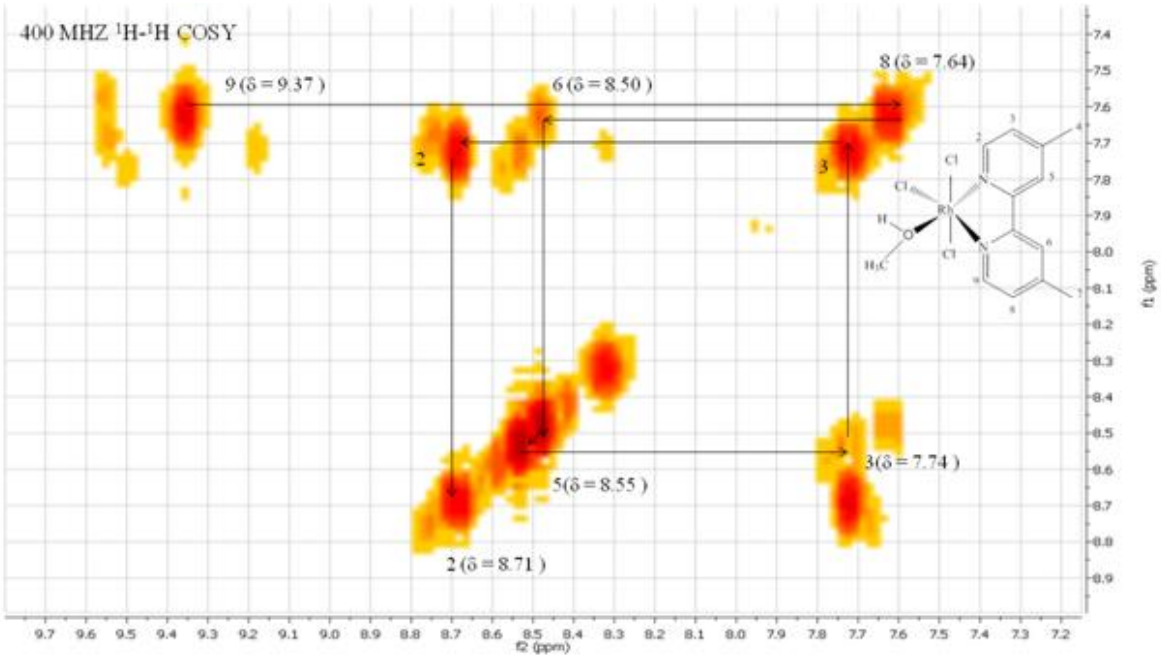

Appendix B. Proton and ^{1}H-^{1}H COSY NMR spectra of $[(Me_2bpy)RhCl_3(CH_3OH)] \cdot CH_3OH$. in DMSO-$d_6$ at 298 K, where Me_2bpy =4,4′-dimethyl- 2,2′- bipyridine.

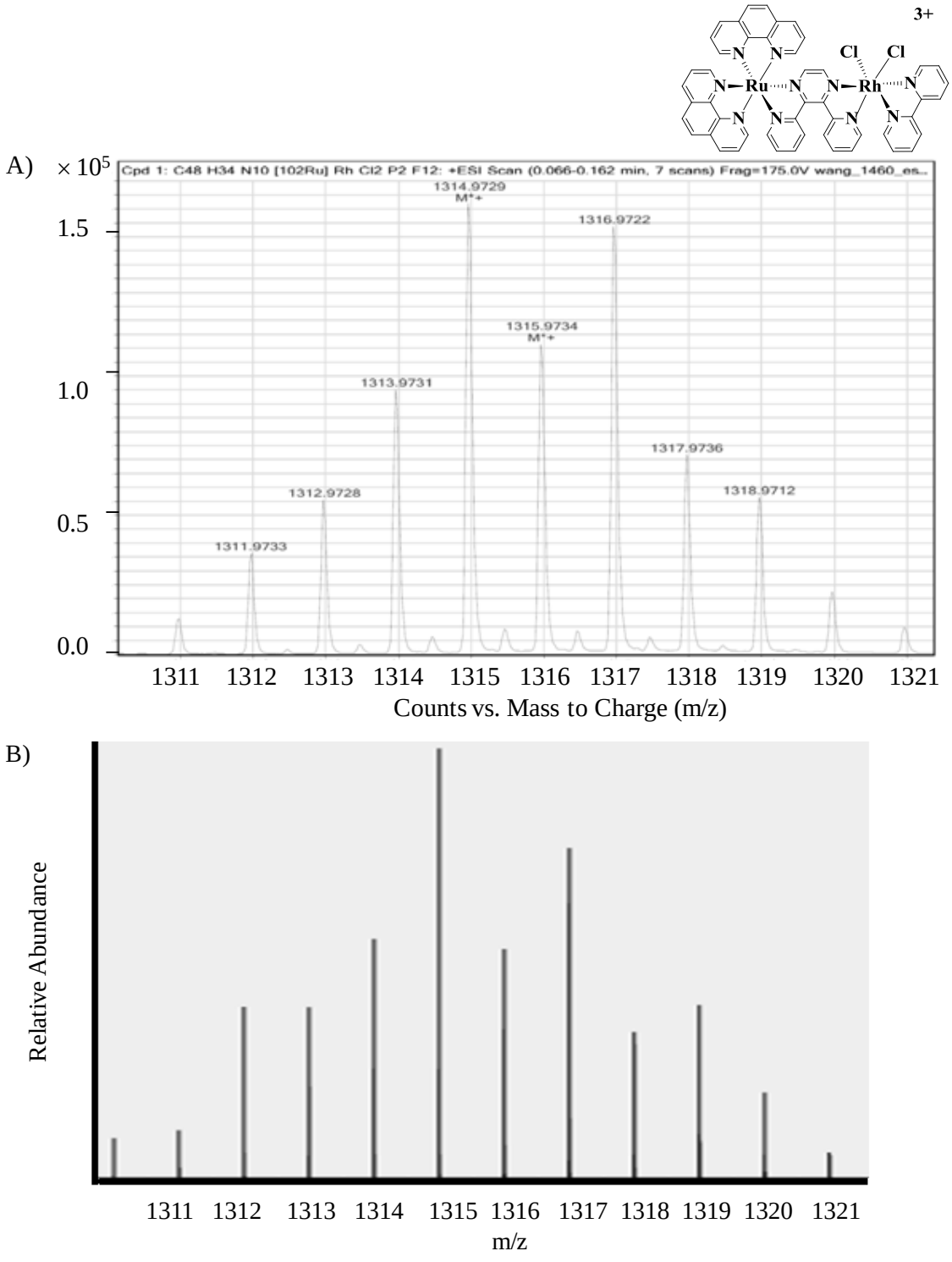

Appendix C. Mass spectrum of $[(phen)_2Ru(dpp)RhCl_2(bpy)](PF_6)^{2+}$ showing isotopic distribution pattern as detected (A) and showing isotopic distribution pattern as calculated with the ChemCalc (B), where bpy = 2,2′- bipyridine, phen = 1, 10-phenanthroline and dpp = 2,3-bis(2-pyridyl)pyrazine.

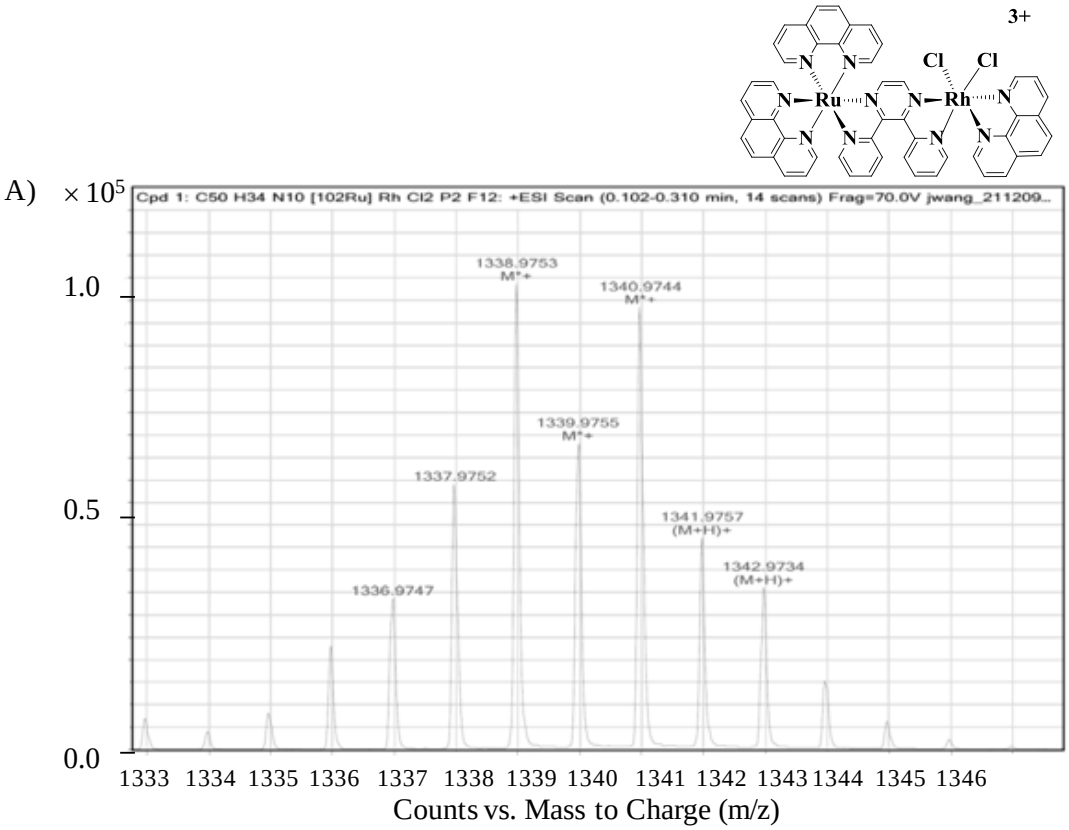

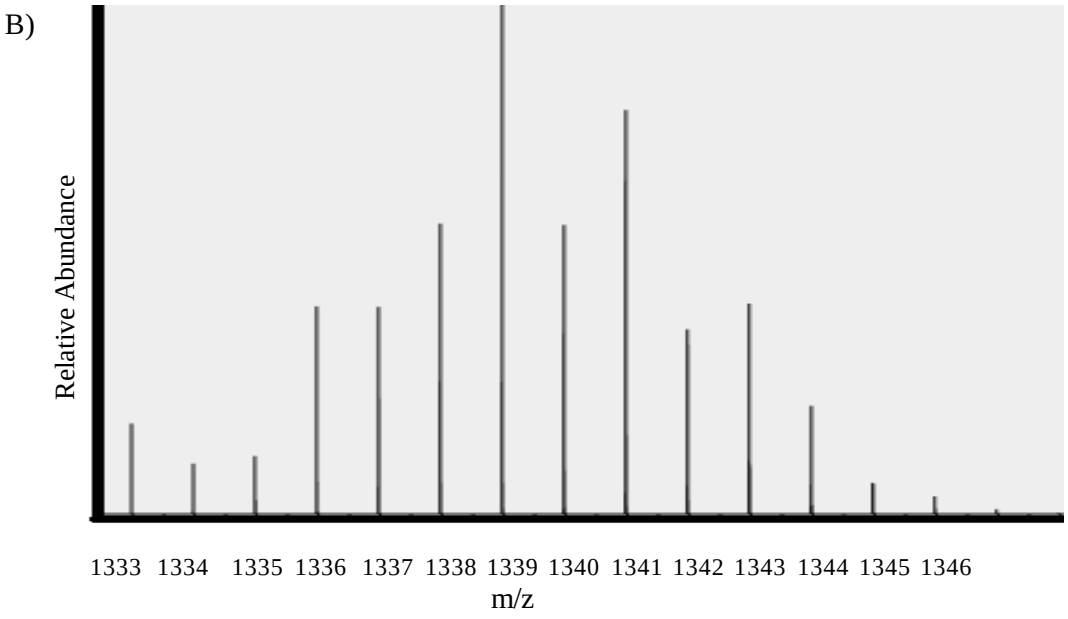

Appendix D. Mass spectrum of $[(phen)_2Ru(dpp)RhCl_2(phen)](PF_6)_2^+$ showing isotopic distribution pattern as detected (A) and showing isotopic distribution pattern as calculated with the ChemCalc (B), where phen = 1, 10-phenanthroline and dpp = 2,3-bis(2-pyridyl)pyrazine.

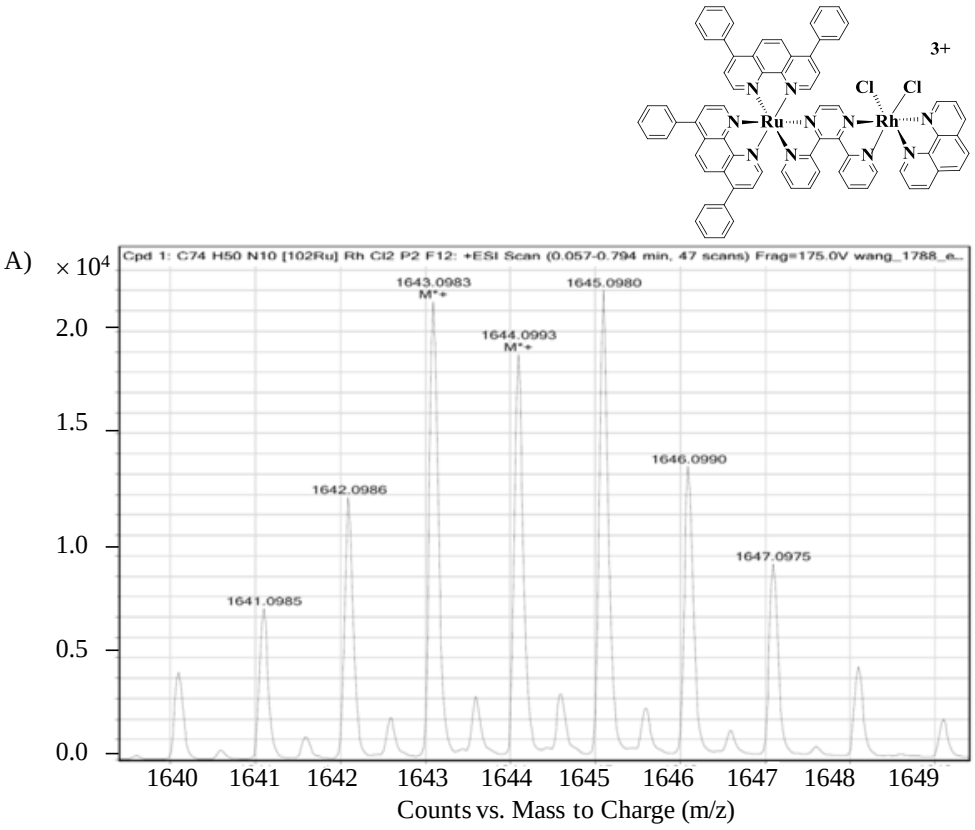

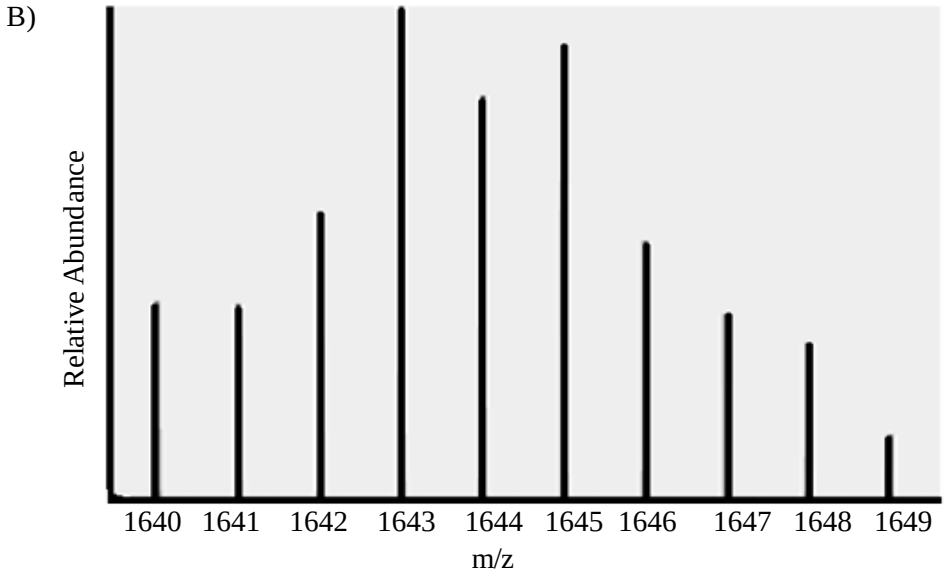

Appendix E. Mass spectrum of $[(Ph_2phen)_2Ru(dpp)RhCl_2(phen)](PF_6)^{2+}$ showing isotopic distribution pattern as detected (A) and showing isotopic distribution pattern as calculated with the ChemCalc (B), where Ph2phen = 4,7-diphenyl-1,10-phenanthroline, phen = 1, 10-phenanthroline and dpp = 2,3-bis(2-pyridyl)pyrazine.

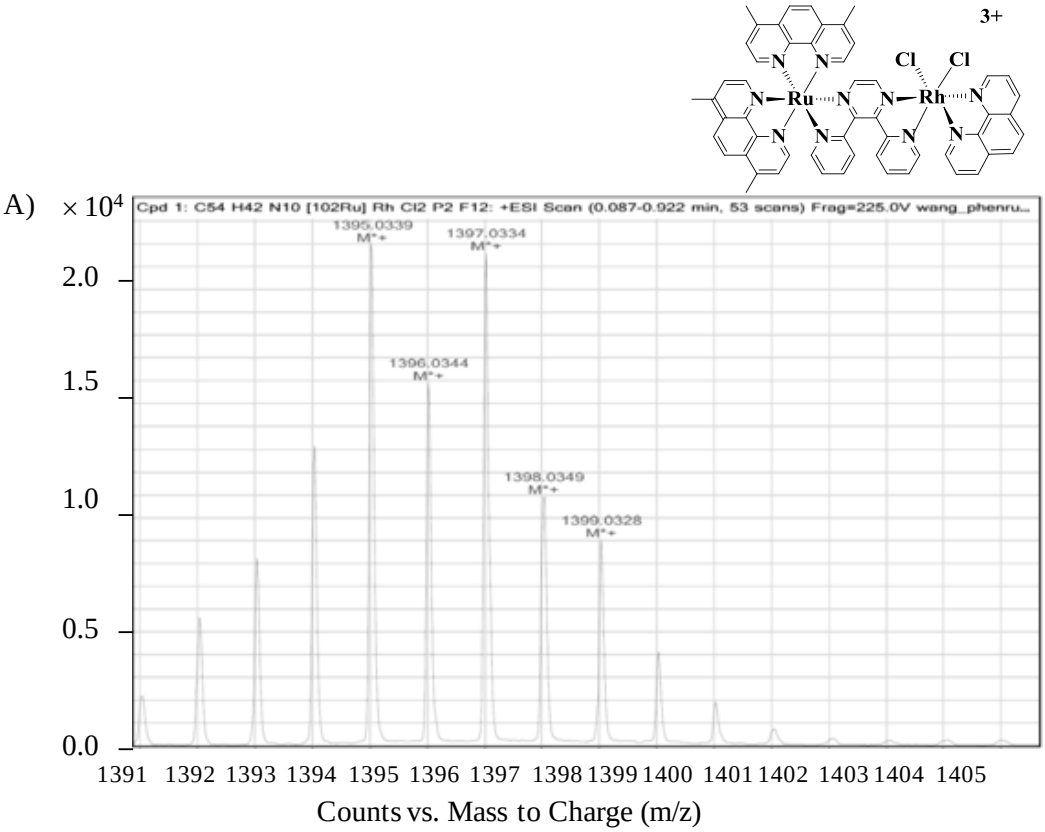

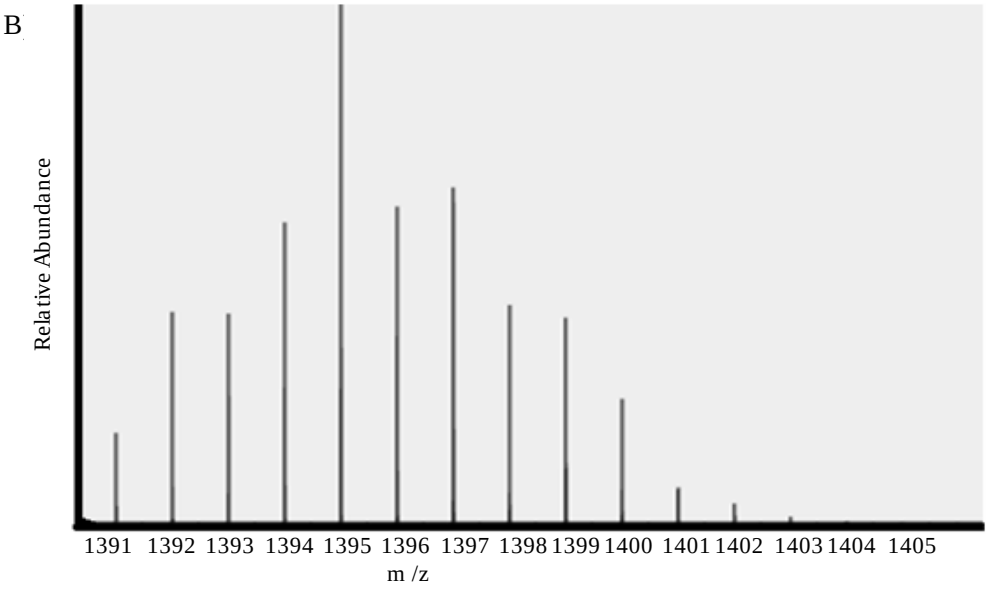

Appendix F. Mass spectrum of $[(Me_2phen)_2Ru(dpp)RhCl_2(phen)](PF_6)^{2+}$ showing isotopic distribution pattern as detected (A) and showing isotopic distribution pattern as calculated with the ChemCalc (B), where Me2phen = 4,7-methyl-1,10-phenanthroline, phen = 1, 10-phenanthroline and dpp = 2,3-bis(2-pyridyl)pyrazine.

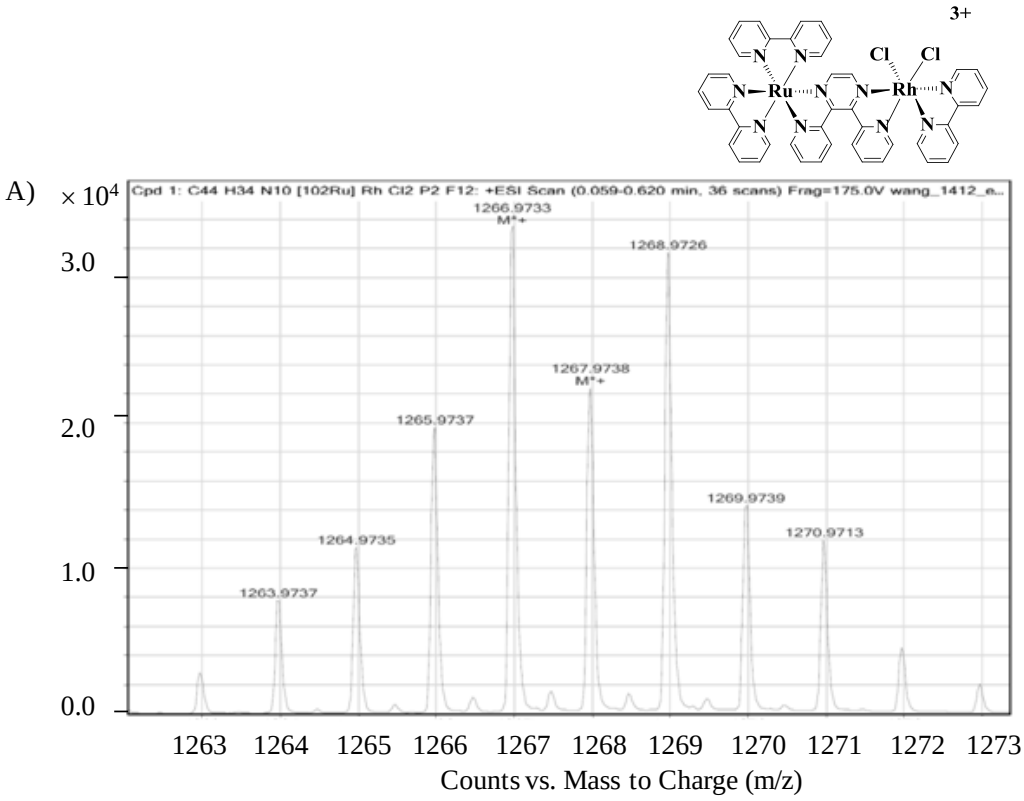

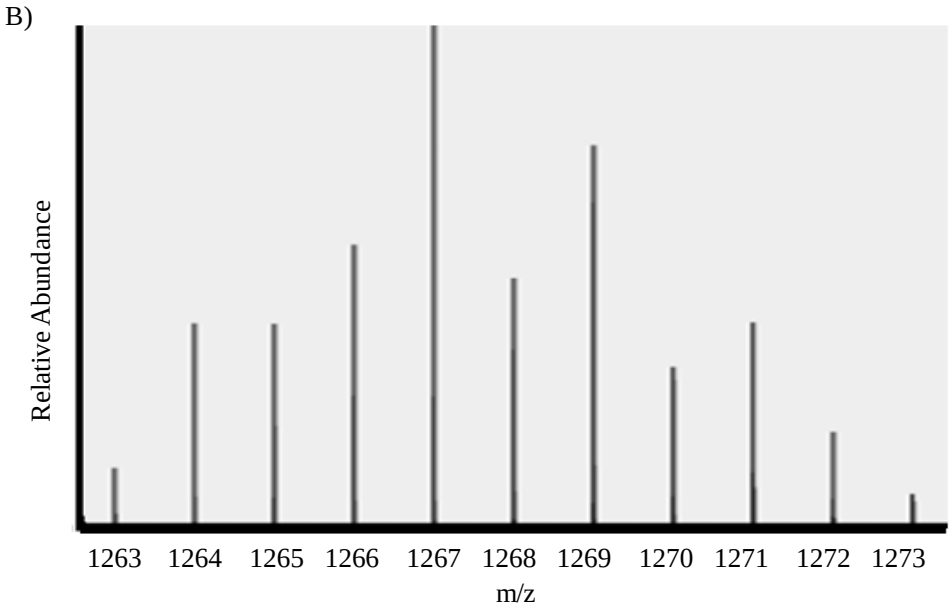

Appendix G. Mass spectrum of $[(bpy)_2Ru(dpp)RhCl_2(bpy)](PF_6)^{2+}$ showing isotopic distribution pattern as detected (A) and showing isotopic distribution pattern as calculated with the ChemCalc (B), where bpy = 2,2′-bipyridine and dpp = 2,3-bis(2-pyridyl)pyrazine.

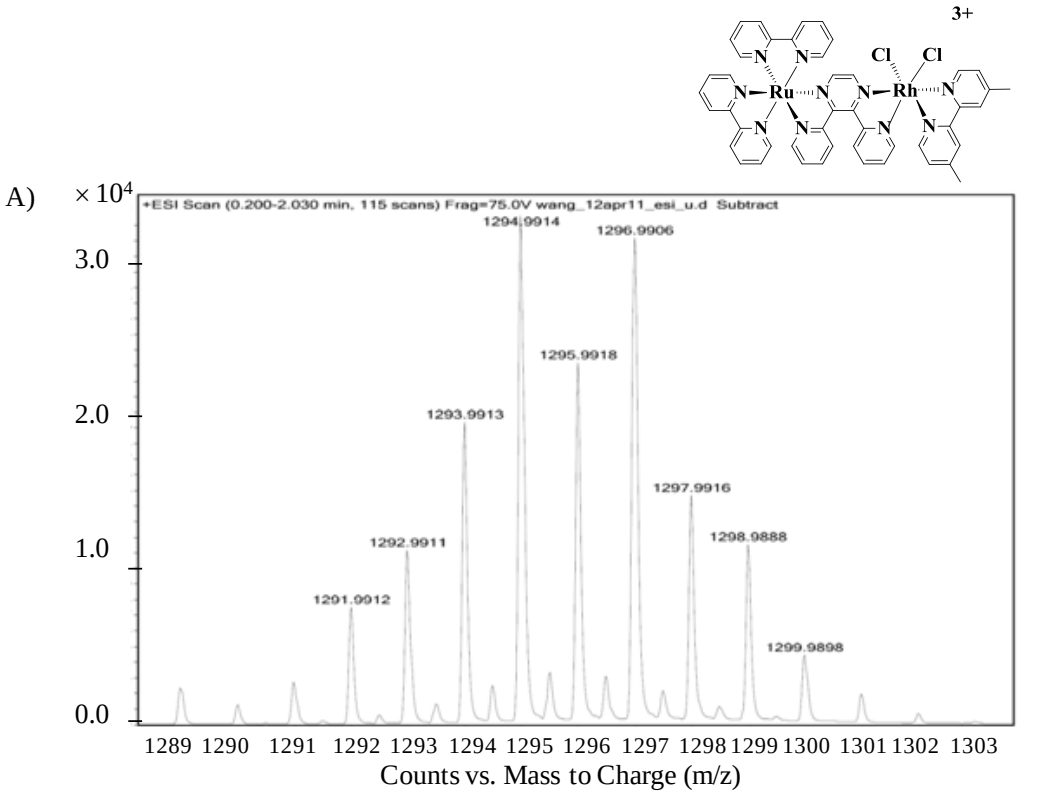

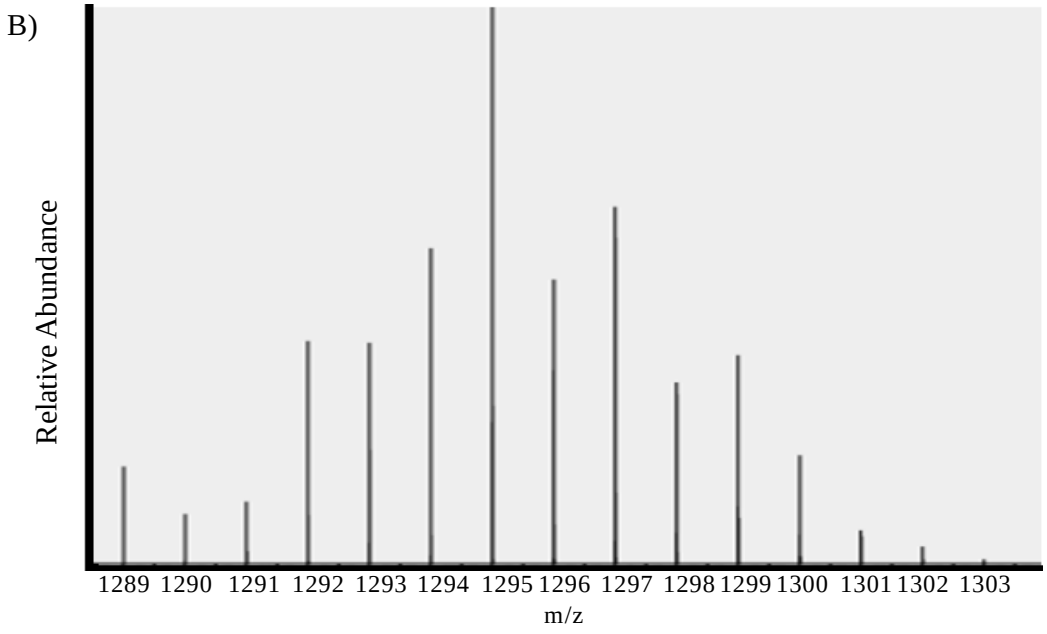

Appendix H. Mass spectrum of $[(bpy)_2Ru(dpp)RhCl_2(Me_2bpy)](PF_6)_2^+$ showing isotopic distribution pattern as detected (A) and showing isotopic distribution pattern as calculated with the ChemCalc (B), where bpy = 2,2′-bipyridine, Me_2bpy =4,4′-dimethyl-2,2′-bipyridine and dpp = 2,3-bis(2-pyridyl)pyrazine.

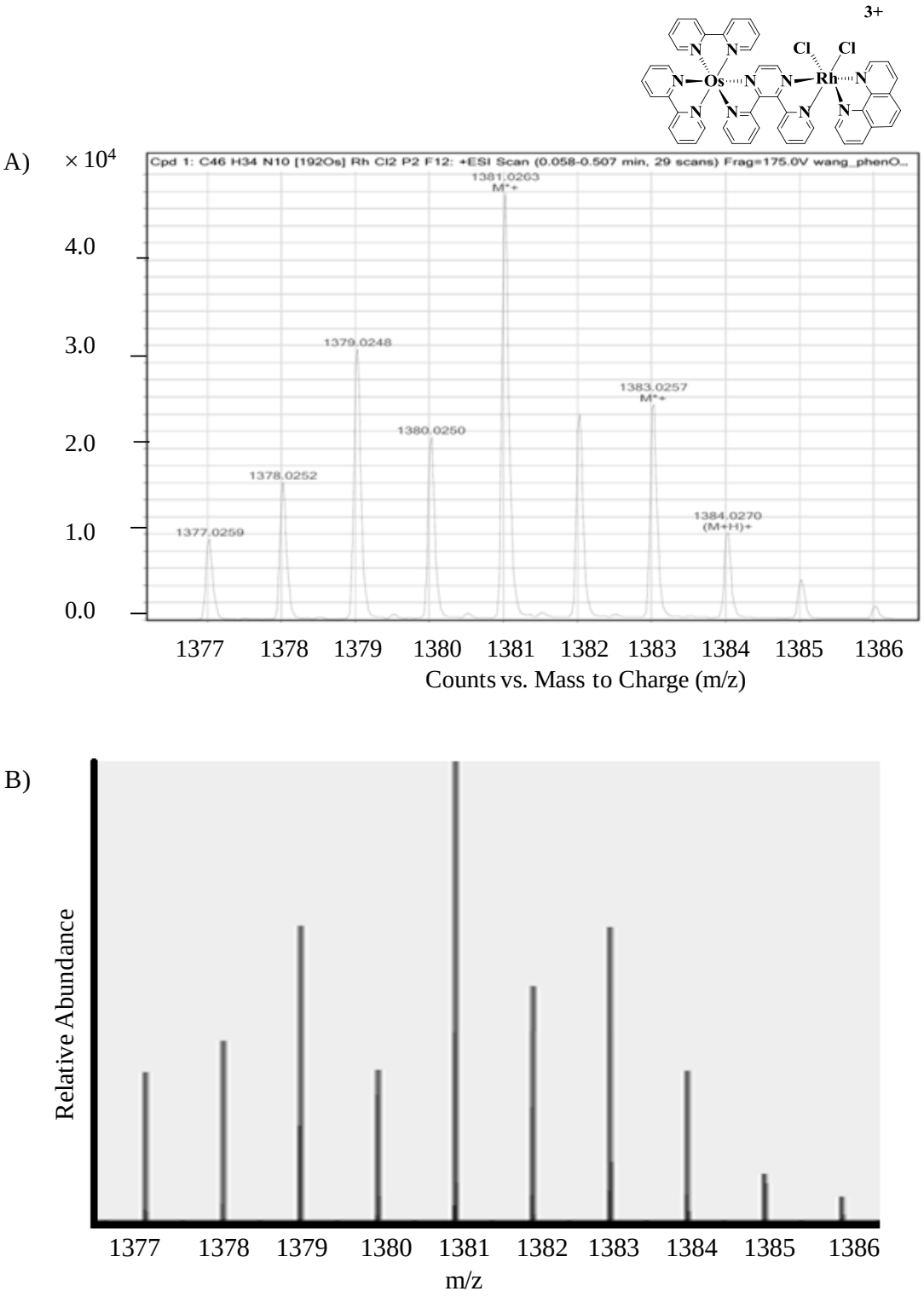

Appendix I. Mass spectrum of $[(bpy)_2Os(dpp)RhCl_2(phen)](PF_6)^{2+}$ showing isotopic distribution pattern as detected (A) and showing isotopic distribution pattern as calculated with the ChemCalc (B), where bpy = 2,2′-bipyridine, phen = 1,10-phenanthroline and dpp = 2,3-bis(2-pyridyl)pyrazine.

Appendix J. Electrochemical and photophysical data for Ru and Os-based monometallic complexes, homobimetallic, mixed-metal bimetallic and trimetallic complexes.

Complex[a]	$E_{1/2}^{ox}$ (V vs. Ag/AgCl)[b]		$E_{1/2}^{ox}$ (V vs. Ag/AgCl)[b]		λ_{max}^{abs} (nm)[c]	λ_{max}^{em} (nm)[d]	$\Phi^{em\ e}$	τ (ns)[d]	reference
$[Ru(bpy)_3]^{2+}$	1.27	$Ru^{II/III}$	−1.24	$bpy^{0/-}$	452	605	0.062	860	[60]
			−1.43	$bpy^{0/-}$					
			−1.67	$bpy^{0/-}$					
$[Os(bpy)_3]^{2+}$	0.82	$Os^{II/III}$	−1.26	$bpy^{0/-}$	480	723	4.6×10^{-3}	60	[85]
			−1.44	$bpy^{0/-}$					
			−1.74	$bpy^{0/-}$					
$[(bpy)_2Ru(dpp)]^{2+}$	1.38	$Ru^{II/III}$	−1.02	$dpp^{0/-}$	464	680	0.012	380	[80,82,95,165]
			−1.44	$bpy^{0/-}$					
			−1.76	$bpy^{0/-}$					
$[(phen)_2Ru(dpp)]^{2+}$	1.45	$Ru^{II/III}$	−1.02	$dpp^{0/-}$	465	660	0.027	460	[80,82,95,165]
			−1.45	$phen^{0/-}$					

$[(Ph_2phen)_2Ru(dpp)]^{2+}$	1.39	$Ru^{II/III}$	−1.04	$dpp^{0/-}$	474	697	0.032	1000	80,82,95,165
			−1.39	$Ph_2phen^{0/-}$					
$[(bpy)_2Os(dpp)]^{2+}$	0.94	$Os^{II/III}$	−1.02	$dpp^{0/-}$	486	778		60	166
			−1.38	$bpy^{0/-}$					
			−1.58	$bpy^{0/-}$					
$[(bpy)_2Ru(dpp)Ru(bpy)_2]^{4+}$	1.51	$Ru^{II/III}$	−0.58	$dpp^{0/-}$	526	758	$9.8 \times$	126	81,92
	1.71	$Ru^{II/II}$	−1.09	$dpp^{0/-}$			10^{-4}		
			−1.45	$bpy^{0/-}$					
$[(phen)_2Ru(dpp)Ru(phen)_2]^{4+}$	1.50	$Ru^{II/III}$	−0.62	$dpp^{0/-}$	524	750	$1.6 \times$	170	81
	1.69	$Ru^{II/II}$	−1.12	$dpp^{0/-}$			10^{-3}		
			−1.41	$phen^{0/-}$					
$[(Ph_2phen)_2Ru(dpp)Ru(Ph_2phen)_2]^{4+}$	1.45	$Ru^{II/III}$	−0.61	$dpp^{0/-}$	540	754	$1.7 \times$	192	165
	1.64	$Ru^{II/II}$	−1.11	$dpp^{0/-}$			10^{-3}		
			−1.35	$phen^{0/-}$					
$[(phen)_2Ru(dpp)RhCl_2(bpy)]^{3+}$	1.62	$Ru^{II/III}$	−0.44[f]	$Rh^{III/II}Cl_2$,RhII/ICl	505	766	$1.5 \times$	42	118
				$Rh^{II/I}Cl$					

			–0.79[g]	dpp$^{0/-}$			10^{-4}	
			–1.03					
[(phen)$_2$Ru(dpp)RhCl$_2$(phen)]$^{3+}$	1.62	Ru$^{II/III}$	–0.44[f]	Rh$^{III/II}$Cl$_2$,RhII$^{/I}$Cl	508	770	2.4 ×	64
			–0.81[g]	Rh$^{II/I}$Cl			10^{-4}	
			–1.03	dpp$^{0/-}$				
[(Ph$_2$phen)$_2$Ru(dpp)RhCl$_2$(phen)]$^{3+}$	1.58	Ru$^{II/III}$	–0.42[f]	Rh$^{III/II}$Cl$_2$,Rh$^{II/I}$Cl	515	786	1.8 ×	46
			–0.79[g]	Rh$^{II/I}$Cl			10^{-4}	
			–1.02	dpp$^{0/-}$				
[(Me$_2$phen)$_2$Ru(dpp)RhCl$_2$(phen)]$^{3+}$	1.53	Ru$^{II/III}$	–0.44[f]	Rh$^{III/II}$Cl$_2$,Rh$^{II/I}$Cl	516	786	5.5 ×	27
			–0.79[g]	Rh$^{II/I}$Cl			10^{-5}	
			–1.02	dpp$^{0/-}$				
[(bpy)$_2$Ru(dpp)RhCl$_2$(bpy)]$^{3+}$	1.57	Ru$^{II/III}$	–0.45[f]	Rh$^{III/II}$Cl$_2$,Rh$^{II/I}$Cl	510	786	1.5 ×	42
			–0.74[g]	Rh$^{II/I}$Cl			10^{-4}	
			–1.02	dpp$^{0/-}$				
[(bpy)$_2$Ru(dpp)RhCl$_2$(Me$_2$bpy)]$^{3+}$	1.59	Ru$^{II/III}$	–0.46[f]	Rh$^{III/II}$	506	786	1.7 ×	44
				Rh$^{II/I}$				

			–0.74[g]	dpp$^{0/-}$			10^{-4}		
			–1.01						
[(bpy)$_2$Os(dpp)RhCl$_2$(phen)]$^{3+}$	1.20	Os$^{II/III}$	–0.46[f]	Rh$^{III/II}$Cl$_2$,Rh$^{II/I}$Cl	521				119
			–0.75[g]	Rh$^{II/I}$Cl					
			–0.98	dpp$^{0/-}$					
[{(bpy)$_2$Ru(dpp)}$_2$RhCl$_2$]$^{5+}$	1.60[h]	2Ru$^{II/III}$	–0.39[i]	Rh$^{III/II/I}$	518	776	2.6 ×	38	15
			–0.79	dpp$^{0/-}$			10^{-4}		
			–1.02	dpp$^{0/-}$					
[{(phen)$_2$Ru(dpp)}$_2$RhCl$_2$]$^{5+}$	1.61[h]	2Ru$^{II/III}$	–0.35[i]	Rh$^{III/II/I}$	512	760	2.2 ×	35	118
			–0.75	dpp$^{0/-}$			10^{-4}		
			–1.02	dpp$^{0/-}$					
[{(Ph$_2$phen)$_2$Ru(dpp)}$_2$RhCl$_2$]$^{5+}$	1.58[h]	2Ru$^{II/III}$	–0.36[i]	Rh$^{III/II/I}$	520	770	2.4 ×	52	165
			–0.75	dpp$^{0/-}$			10^{-4}		
			–1.01	dpp$^{0/-}$					

$[\{(bpy)_2Os(dpp)\}_2RhCl_2]^{5+}$	1.21[h]	$2Os^{II/III}$	–0.39[i]	$Rh^{III/II/I}$	534	119
			–0.76	$dpp^{0/-}$		
			–1.00	$dpp^{0/-}$		

[a]bpy = 2,2′-bipyridine, dpp = 2,3-bis(2-pyridyl)pyrazine and phen = 1,10-phenanthroline, Ph_2phen = 4,7-diphenyl-1,10-phenanthroline, Me_2phen = 4,7-dimethyl-1,10-phenanthroline and Me_2bpy =4,4′-dimethyl-2,2′-bipyridine.
[b]Measured against a Ag/AgCl (3 M NaCl) reference electrode, potential scan rate υ = 100 mV/s with a carbon glassy disk working electrode and a Pt wire counter electrode in 0.1 M Bu_4NPF_6 in CH_3CN at RT, unless otherwise indicated
[c] Measured at RT in CH_3CN , unless otherwise indicated
[d]Measured at RT in CH_3CN following deoxygenation, and error associated with lifetime measurements ± 5%
[e]Measured at RT in CH_3CN following deoxygenation, and error associated with lifetime measurements ± 5%
[f]Reported E_p^c of quasi-reversible process
[g]Reported E_p^c of irreversible process
[h]Two overlapping, one-electron reversible waves.
[i]Two overlapping, one-electron irreversible waves